NASA-CP-2395 19860012462

NASA Conference Publication 2395

FOR REFERENCE

NOT TO BE TAKEN FROM THIS ROOM

Full-Scale Transport Controlled Impact Demonstration



LIBRARY COPY

LANGLEY RESEARCH CENTER
LIBRARY, NASA
HAMPTON, VIRGINIA

Proceedings of a workshop held at
NASA Langley Research Center
Hampton, Virginia
April 10, 1985





NASA Technical Library
3 1176 01502 4582

NASA Conference Publication 2395

Full-Scale Transport Controlled Impact Demonstration

Robert J. Hayduk, *Compiler*
Langley Research Center

Proceedings of a workshop sponsored by NASA Langley Research Center, Hampton, Virginia, and the FAA Technical Center, Atlantic City, New Jersey, and held in Hampton, Virginia
April 10, 1985

NASA
National Aeronautics and Space Administration

Scientific and Technical Information Branch

1986

PREFACE

Prior to the FAA/NASA Full-Scale Transport Controlled Impact Demonstration (C.I.D.), the last test of a large transport was conducted in the mid-1960's. Tests of this magnitude require a tremendous commitment of resources, both money and manpower, by the sponsoring agencies. Consequently, a strong, compelling purpose must exist before such an undertaking can be initiated. For the C.I.D. this strong compelling purpose was a Congressional commitment to demonstrate the effectiveness of an antimisting fuel additive named FM-9.

The FAA had invested millions of dollars and perhaps 20 years of research into antimisting fuels before selecting FM-9 as the one to be demonstrated. The FAA initiated the program, acquired the aircraft, and invited NASA to cosponsor the project because of NASA LaRC's vast crash dynamics experience in full-scale crash testing of general aviation aircraft and NASA Ames/Dryden's expertise in remote piloting of drone aircraft. Thus, the partnership that evolved saw the FAA Technical Center with overall project management plus responsibility for the antimisting fuels aspects and seat crashworthiness research, NASA LaRC with responsbility for the structural loads measurement experiment, and NASA Ames/Dryden with the responsibility for the remote piloting of the aircraft and systems/experiments integration.

More than 4 years of effort were required before the project came to fruition. The C.I.D took place on December 1, 1984, crashing at a prepared site on Rogers Dry Lakebed, Edwards Air Force Base, California. The test was spectacular, receiving national press coverage that generally proclaimed the test a failure because a fireball enveloped the aircraft. The demonstration was a setback for the antimisting kerosene (AMK) researchers. The impact conditions, considerably different from the planned scenario, exposed large quantitites of degraded AMK and hydraulic fluid and caused unexpectedly hot ignition sources, bulk loss of fuel from the right wing, airflow patterns over the wings and fuselage that were untested on AMK, and fuel intrusion into the lower fuselage. The test was much more severe than planned and is generally considered to be unrepresentative of the type of survivable crash that would benefit from AMK.

There were other important and successful experiments on board the C.I.D which were initially ignored by the press. The structural crashworthiness researchers considered the loads measurement experiment to be of equal importance to the AMK demonstration. Ninety-seven percent of the sensors on the fuselage and wing structure, seats, dummies, restraint systems, galley, and bins were active at impact. A wealth of sensor data was collected from this once-in-a-lifetime research test. The flight data recorder experiments on board were also generally successful.

Because of the significance of the test to the crashworthiness of future aircraft, NASA Langley Research Center management initiated the idea of conducting a workshop to release the preliminary structural loads data to the industry, other government agencies, and academia. The idea was to foster discussions and expose the important questions before completion of the initial data analysis and reporting phase.

The NASA/FAA C.I.D. Workshop was held April 10, 1985, at NASA Langley Research Center, Hampton, Virginia. Seventy-four participants attended the 1-day workshop. The attendees were equally divided between industry and governmental agencies. Only one university researcher attended. Four foreign countries were represented among 13 foreign attendees.

This publication contains the technical presentations made at the workshop plus the ensuing discussions. Additional questions forwarded to the Chairman either before or after the workshop are also included in a separate section.

The use of trade names or names of manufacturers does not constitute endorsement, either express or implied, by the National Aeronautics and Space Administration.

CONTENTS

PREFACE iii

ATTENDEES vii

CID OVERVIEW 1
Robert J. Hayduk

CID FLIGHT/IMPACT 17
Russ Barber

NASA EXPERIMENTS ON THE B-720 STRUCTURE AND SEATS 29
Emilio Alfaro-Bou

CONTROLLED IMPACT DEMONSTRATION SEAT/CABIN RESTRAINT SYSTEMS - FAA 49
Richard A. Johnson

DATA REDUCTION, MANAGEMENT, AND ANALYSIS SOFTWARE FOR CID 61
Charles W. Davis

NASA SEAT EXPERIMENT AND OCCUPANT RESPONSES 79
E. L. Fasanella

STRUCTURAL LOADS PRELIMINARY RESULTS 91
Emilio Alfaro-Bou

DIGITAL FILTERING AND ACCELERATION PULSE INTERPRETATION 103
E. L. Fasanella

PRELIMINARY FLOOR, SEAT, AND DUMMY DATA 125
Mark R. Cannon and Richard E. Zimmerman

CONTROLLED IMPACT DEMONSTRATION AIRFRAME BENDING BRIDGES 157
Stephen J. Soltis

CONTROLLED IMPACT DEMONSTRATION FLIGHT DATA RECORDERS/COCKPIT VOICE RECORDERS 181
Leo J. Garodz

UNITED STATES NAVY - CANADIAN FORCES SOLID STATE FLIGHT DATA RECORDER/ CRASH POSITION LOCATOR EXPERIMENT ON THE B-720 CONTROLLED IMPACT DEMONSTRATION 195
D. M. Watters

CONTROLLED IMPACT DEMONSTRATION ON-BOARD (INTERIOR) PHOTOGRAPHIC SYSTEM . . . 209
Clyde J. May

CID-720 AIRCRAFT HIGH-ENVIRONMENT FLIGHT INSTRUMENTATION SYSTEM 241
R. S. Calloway

IMPACT DYNAMICS INSTRUMENTATION 289
Royce F. McCormick

CID-720 AIRCRAFT LaRC PREFLIGHT HARDWARE TESTS: DEVELOPMENT, FLIGHT ACCEPTANCE AND QUALIFICATION 303
J. D. Pride

QUESTIONS AND ANSWERS 329

ATTENDEES

Emilio Alfaro-Bou
NASA Langley Research Center
M.S. 495
Hampton, VA 23665
FTS 88-928-3795
(804) 865-3795

Arthur L. Asher
Cessna Aircraft Co.
P.O. Box 1521
Wichita, KS 67201
(316) 688-4029

Robert C. Auberg
System Development Corp.
3217 North Armistead Ave.
Hampton, VA 23666
(804) 865-1111

M. R. Barber
NASA Dryden Flight Research Facility
Edwards, CA 93523
FTS 88-961-3165

Donald S. Barrow
Sicma America, Inc.
6929 Northwest 46th St.
Miami, FL 33166
(305) 592-7428

John C. Berwick
Cessna Aircraft Co.
Pawnee Division
P.O. Box 1521
Wichita, KS 67201
(316) 688-4025

Vahe Bilezikjian
Weber Aircraft
Div. of Walter Kidde and Co.
2820 Ontario St.
Burbank, CA 91510
(818) 848-5543

Thomas M. Birdwell
Silicone Products Div.
General Electric Co.
9119 Gaither Road
Gaithersburg, MD 20877
(301) 840-3681

Charles P. Blankenship
NASA Langley Research Center
Mail Stop 118
Hampton, VA 23665
FTS 88-928-2042
(804) 865-2042

Edmond Boullay
Embassy of France
2164 Florida Ave., N.W.
Washington, DC 20008
FTS 88-202-944-6444

Caesar Caiafa
FAA Technical Center
Atlantic City Airport, NJ 08037
FTS 88-482-4285

Raymond S. Calloway
NASA Langley Research Center
Mail Stop 471
Hampton, VA 23665
FTS 88-928-3761
(804) 865-3761

Richard F. Chandler
FAA Aeronautical Center
Civil Aeromedical Institute
AAC-119
P.O. Box 25082
Oklahoma City, OK 73125
FTS 88-749-4851

Fernon J. Clark
American Airlines
3800 N. Mingo Road
Tulsa, OK 74151
(918) 832-3773

John Clark
NTSB
800 Independence Ave., S.W.
Washington, DC 20594
(202) 382-6626

George E. Clarke
Naval Air Test Center
Patuxent River, MD 20670
(301) 863-4537

Donald J. Collier
Air Transportation Assoc.
1709 New York Avenue, N.W.
Washington, DC 20006
(202) 626-4017

Jean Pierre Cornand
c/o Edmond Boullay
Embassy of France
2164 Florida Ave., N.W.
Washington, DC 20008
FTS 88-202-944-6444

Richard E. Coykendall
United Airlines, Eng. Dept.
San Francisco Int'l. Airport, CA 94128
(415) 876-3721

Charles W. Davis
System Development Corp.
3217 North Armistead Ave.
Hampton, VA 23666
(804) 865-1111

Jean Paul Deneuville
c/o Embassy of France
Embassy of France
2164 Florida Ave., N.W.
Washington, DC 20008
FTS 88-202-944-6444

Edwin Fasanella
Kentron International
NASA Langley Research Center
Mail Stop 495
Hampton, VA 23665
FTS 88-928-3795
(804) 865-3795

Erich Feldkirchner
c/o Embassy of France
2164 Florida Ave., N.W.
Washington, DC 20008
FTS 88-202-944-6444

Roy G. Fox
Bell Helicopter Textron
Dept. 81, Flight Technology
P.O. Box 482
Fort Worth, TX 76101

John L. Galligher
McDonnell Douglas Corp.
3855 Lakewood Blvd.
Long Beach, CA 90846
(213) 593-3861

Ramon Garcia
Naval Air Development Center
Code 6043
Warminster, PA 18974
(215) 441-1321

Leo J. Garodz
FAA Technical Center
Atlantic City Airport, NJ 08037
FTS 88-482-4280

David A. Godfrey
Leigh Instrument Ltd.
P.O. Box 532
Coronado, CA 92118
(619) 437-5631

Dayton L. Hartley
Beech Aircraft Corp.
9709 E. Central
Wichita, KS 67201
(316) 681-7878

Robert J. Hayduk
NASA Langley Research Center
Mail Stop 495
Hampton, VA 23665
FTS 88-928-3795
(804) 865-3795

Jean Hoeb
c/o Edmond Boullay
Embassy of France
2164 Florida Ave., N.W.
Washington, DC 20008
FTS 88-202-944-6444

Donald A. Holmes
USAir
Greater Pittsburgh Int'l. Airport
Eng. Dept. - Hangar #3 (Rm 221)
Pittsburg, PA 15231
(412) 262-7061

Richard Johnson
FAA Technical Center
Atlantic City Airport, NJ 08037
FTS 88-482-4280

Christof Kindervater
Wright Aeronautical Lab./MLBM
Wright-Patterson AFB
Dayton, OH 45433
(513) 255-4871

James G. Kline, Jr.
Naval Safety Center
Code 13
NAS Norfolk, VA 23511
(804) 444-3321

William G. Laynor
NTSB, Bureau of Tech.
800 Independence Ave., S.W.
Washington, DC 20594
(202) 382-6610

Roger M. Lloyd
RMS Technologies, Inc.
One Neshaminy Interplex
Suite 306
Trevose, PA 19047
(215) 638-9630

Dennis Manibusan
Ozark Airlines, Inc.
Box 10007-Lambert
St. Louis Int'l Airport
St. Louis, MO 63145
(314) 429-8502

Ralph G. Marrujo
Fairchild Burns Co.
1455 Fairchild Road
Winston-Salem, NC 27105
(919) 744-1040

Yves Martin-Siegfried
c/o Edmond Boullay
Embassy of France
2164 Florida Ave., N.W.
Washington, DC 20008
FTS 88-202-944-6444

Clyde J. May
NASA Langley Research Center
Mail Stop 433
Hampton, VA 23665
FTS 88-928-4621
(804) 865-4621

Harvey G. McComb, Jr.
NASA Langley Research Center
Mail Stop 244
Hampton, VA 23665
FTS 88-928-3121
(804) 865-3121

Royce F. McCormick
NASA Langley Research Center
Mail Stop 236
Hampton, VA 23665
FTS 88-928-3492
(804) 865-3492

Peter Meicklem
British Embassy
3100 Massachusetts Ave., N.W.
Washington, DC 20007
FTS 88-202-944-6444

Jacques Mens
c/o Edmond Boullay
Embassy of France
2164 Florida Ave., N. W.
Washington, DC 20008
FTS 88-202-944-6444

Dan M. Motley, Jr.
Lockheed-Georgia Co.
86 South Cobb Drive
Marietta, GA 30063
(404) 424-7688

Werner Muenster
Messerschmitt Bolkow-Blohm
Transport Aircraft Division
D2103 Hamburg 95
P.O. Box 950109
(40) 7437-5615

Charles H. Nixon
Avco Specialty Materials Div.
2 Industrial Avenue
Lowell, MA 01851
(617) 452-8961

Charles E. Nuckolls
Mechanical Eng. Dept.
Univ. of Central Florida
Box 25000
Orlando, FL 32751
(305) 275-2221

Robert R. Nunamaker
NASA Langley Research Center
Mail Stop 107
Hampton, VA 23665
FTS 88-928-2893

Thomas L. Partin
Naval Safety Center
NAS Norfolk, VA 23511
(804) 444-7926

Allan B. Pifko
Grumman Aerospace Corp.
Research & Development Center
Mail Stop A08-35
Bethpage, NY 11714
(516) 575-2212

David K. Pitman
USAF HQ SAC Safety
Offutt AFB, NE 68113-5001
(402) 294-4676

Mukunda Pramanik
Sikorsky Aircraft
North Main St.
Stratford, CN 06601
(203) 386-5001

Joseph D. Pride, Jr.
NASA Langley Research Center
Mail Stop 432
Hampton, VA 23665
FTS 88-928-4666
(804) 865-4666

Eric Raitch
System Development Corp.
3217 North Armistead Ave.
Hampton, VA 23665
(804) 865-1111

David Ramage
Air Canada
Montreal Int'l. Airport
Dorval Base 15
Dorval, Quebec H4y 1C2
CANADA
(514) 636-7560

Edgar T. Rawles
System Development Corp.
3217 North Armistead Ave.
Hampton, VA 23666
(804) 865-1111

John E. Reed
FAA Technical Center
ACT-300C
Atlantic City Airport, NJ 08037
FTS 88-482-5902
(609) 484-5902

Stephen Reimers
Strike Aircraft Test Directorate
Code SAO4A1
Patuxent River, MD 20670

Jackie L. Smith
System Development Corp.
3217 North Armistead Ave.
Hampton, VA 23666
(804) 865-1111

Richard Soloski
Cessna Aircraft Company
P.O. Box 7704
Wichita, KS 67217

Stephen Soltis
FAA Aircraft Certification Office
ANW-102N
Long Beach, CA 90808
FTS 88-796-2825

Robert G. Thomsom
NASA Langley Research Center
Mail Stop 497
Hampton, VA 23665
FTS 88-928-2796
(804) 865-2796

Richard A. Tobiason
Air Transportation Association
1709 New York Avenue, N.W.
Washington, DC 20006
(202) 626-4016

Jon Turner
Air Canada
Montreal International Airport
Dorval Base 15
Dorval, Quebec H4Y 1C2
CANADA
(514) 636-4323

Gerrit J. Walhout
NTSB
800 Independence Ave., S.W.
Washington, DC 20594
(202) 382-6626

Daniel M. Watters
Naval Air Test Center
Patuxent River, MD 20670-5304
(301) 863-4673

Donald W. Wells
Leigh Instruments, Ltd.
2680 Queensview Drive
Ottawa, Ontario
CANADA K2B8J9
(613) 820-9720

John J. White
FAA
800 Independence Ave., S.W.
Washington, DC 20591
(202) 426-3593

Edward Widmayer
Boeing Commercial Airplane Co.
P.O. Box 3707
Seattle, WA 98124
(206) 237-6042

Robert Winter
Grumman Aerospace Corp.
Research & Development Center
A08-35
Bethpage, NY 11714
(516) 575-2237

Gill Wittlin
Lockheed California Co.
Dept. 76-12
Building 63, Plant A-1
Burbank, CA 91503
FTS 88-213-847-3835

Richard Zimmerman
Simula, Inc.
2223 S. 48th Street
Tempe, AZ 85282
FTS 88-602-438-1446

CID OVERVIEW

Robert J. Hayduk
NASA Langley Research Center
Hampton, Virginia

NASA/FAA Government/Industry CID Workshop
NASA Langley Research Center
April 10, 1985

INTRODUCTION

On December 1, 1984, NASA and the Federal Aviation Administration (FAA) conducted the first remotely piloted air-to-ground crash test of a transport category aircraft. The Full-Scale Transport Controlled Impact Demonstration (CID) was the culmination of 4 years of effort by the two agencies. NASA and the FAA had many objectives during the joint planning and execution of the Controlled Impact Demonstration. NASA's interest was primarily structural crashworthiness. The FAA's primary interest was the demonstration of an antimisting fuel additive's performance. Demonstration of improved crashworthy design features was a secondary objective for the FAA.

This workshop is intended to provide results obtained to date on the performance of the airframe structure and the associated structural loads from the CID test to the industry/university/government community.

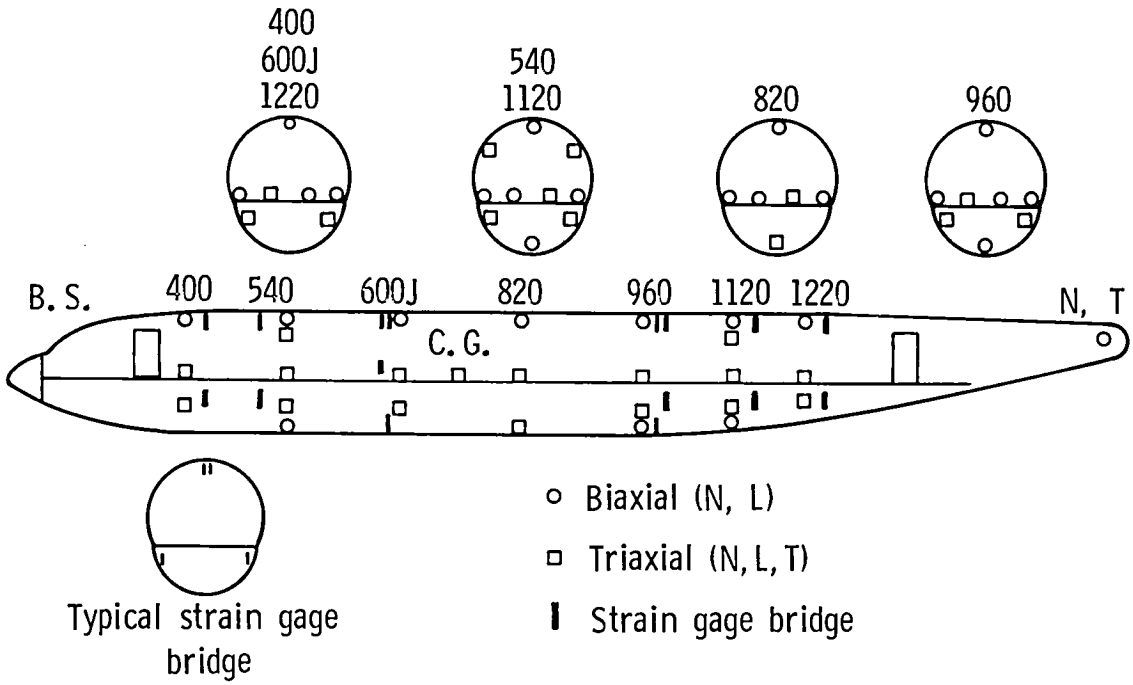
C.I.D. OBJECTIVES

The major C.I.D. objective for the FAA was the antimisting kerosene (AMK) experiment with the modified fuel system. The FAA had a great deal of success during the developmental tests of the AMK and spent a lot of effort at Dryden implementing the fuel degraders and cooler systems for the AMK. However, this workshop is not going to address the AMK experiment. We will concentrate on the NASA structural baseline data experiment that provides information for our future composite structure dynamics program. We are going to describe the crashworthy design features that both NASA and the FAA have onboard the aircraft.

- Verify antimisting fuel (AMK) performance
- Demonstrate operational AMK fuel/propulsion system capability
- Acquire structural baseline data for composite structures program
- Test improved crashworthy design features

C. I. D. FUSELAGE INSTRUMENTATION

This figure shows the instrumentation that we had on the fuselage for the structural loads experiment. The wings were also very heavily instrumented. The structural instrumentation details are presented in reference 1. This data, along with the data from the seats and dummies that were on the aircraft, will be the principal data presented at this workshop.



IMPACT SURVIVABLE SEATS

The majority of the seats onboard were FAA sponsored seats. Those seats are described in reference 2, and reference 3 presents the results of the FAA seat experiments. The two NASA seats onboard the aircraft are described in reference 1 and results are given.



OBJECTIVES

The primary objectives of the workshop are to release, in preliminary fashion, the results of the structural loads data that we obtained from the C.I.D., and also to release the data on the seats, dummies, restraint systems, galleys, bins, and flight data recorders.

The most important purpose of this meeting is to interact with the user community. This is just a preliminary release of data; we would like to make sure that when we complete our data reduction analysis and report that we address the important questions that you help us raise.

- Preliminary release of structural loads data from CID
- Preliminary release of data on seats, dummies, restraint systems, galley, bins, and flight data recorders
- Interaction with user community

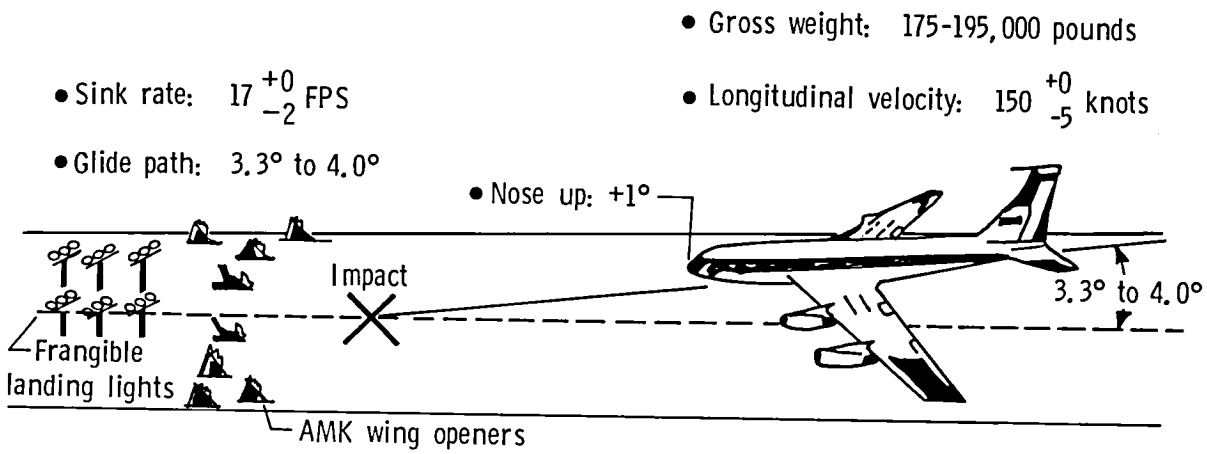
LANGLEY C.I.D. RESPONSIBILITIES

Langley C.I.D. responsibilities were primarily for the structural instrumentation experiment. Langley developed a data acquisition system and photographic system to cover the impact with both general data and photographic coverage of the interior of the aircraft. Langley was responsible for the acquisition of the impact loads, the data reduction and analysis, and correlation with the analytical models that have been developed using the DYCAST computer program.

- Structural instrumentation
- Data acquisition system - hardware/software
- Interior photo coverage
- Impact loads acquisition/analysis
- Aircraft analytical modelling

PLANNED C.I.D. IMPACT SCENARIO

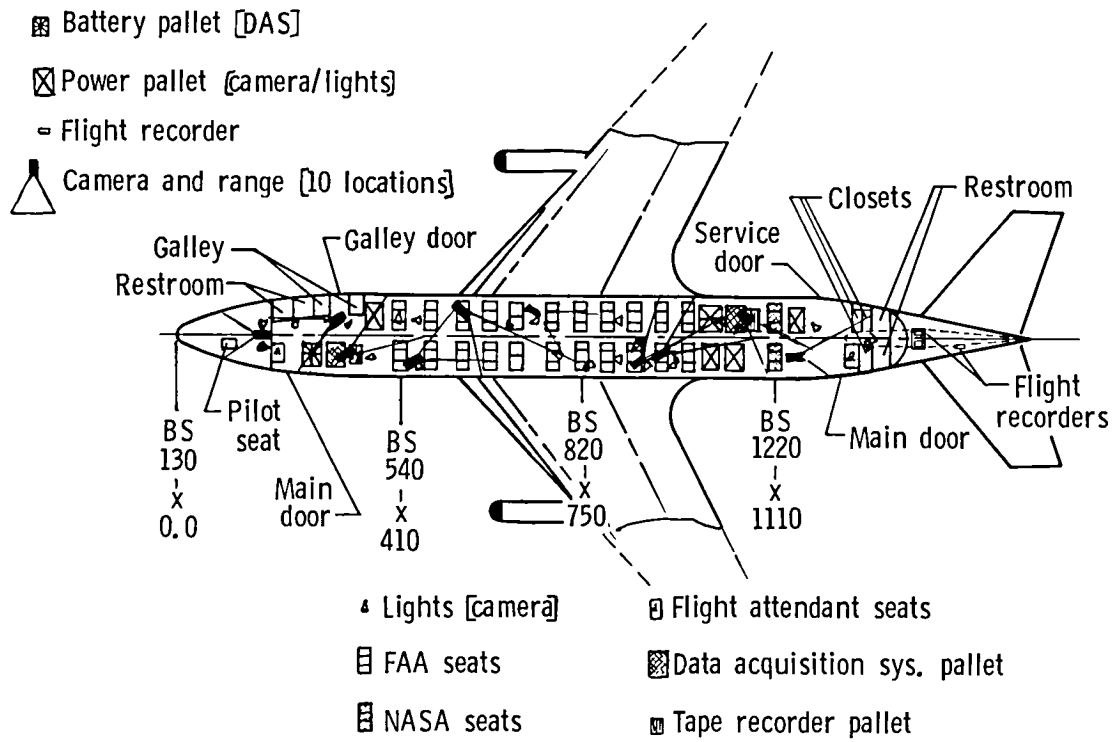
This is a brief description of the planned C.I.D. impact scenario. Barber (ref. 4) goes into more detail. Basically, we were trying to impact in front of the AMK wing openers so that the structural loads impact experiment would occur prior to impact with the wing cutters. We were expecting about 17 feet per second vertical sink rate and longitudinal velocity of 150 knots.



C.I.D. PLAN VIEW

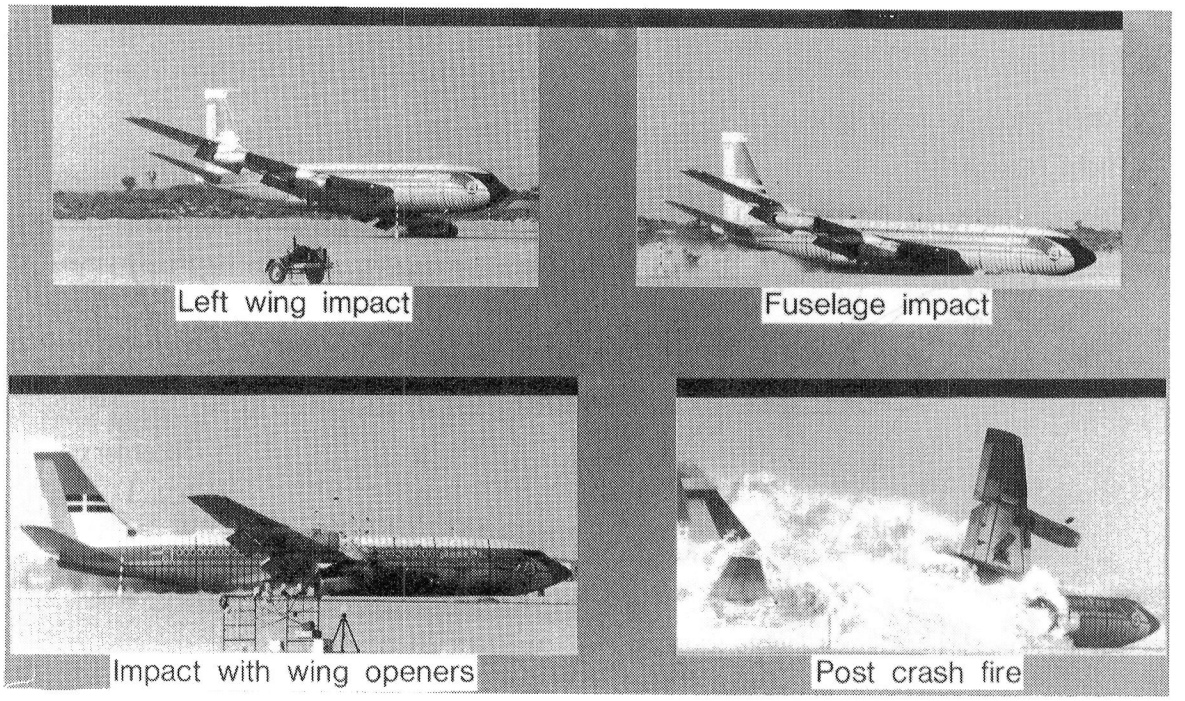
The interior of the aircraft had a large number of seats onboard with data acquisition systems fore and aft. Photographic coverage throughout the fuselage was provided by Langley (10 cameras) and JPL (1 camera). Two nose cameras were installed by Dryden to assist the ground-based pilot. JPL installed a camera on the vertical stabilizer looking down on the fuselage and wings. Ground-based and airborne photographic coverage was provided by JPL.

Note that two longitudinal location identifiers are marked on the plan view. The usual body station (BS) system is used, as well as a longitudinal X-coordinate measured in inches from the nose of the aircraft.



C.I.D. IMPACT SEQUENCE

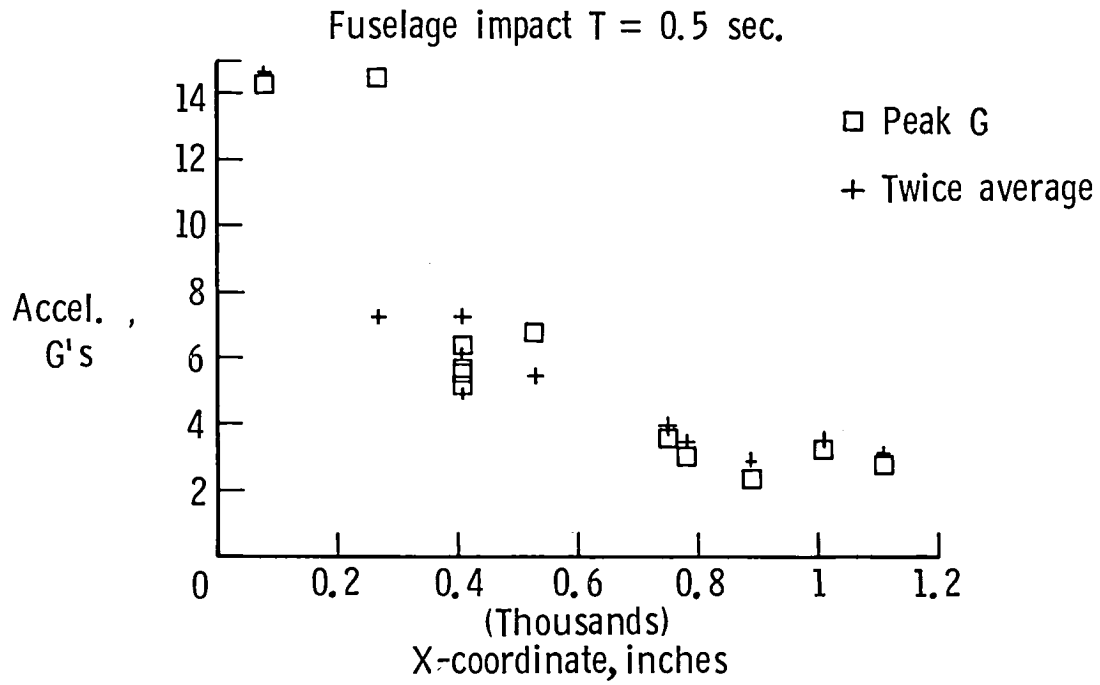
This sequence of four scenes from a Hulcher camera shows the sequence of events. The primary period of times that are of interest to this workshop are the left wing impact and the impact of the fuselage with the ground. By the time the aircraft impacted the wing cutter, the NASA structural loads experiment was essentially over. However, there were substantial loads that occurred during impact with the wing cutters that are of interest to the seat experimenters. After the aircraft came to rest and was engulfed by fire, the structural and seat loads experiment was over. However, there were some fire-resistant materials experiments onboard, such as seat fire-blocking layers and heat resistant window panes.



C.I.D. VERTICAL FLOOR ACCELERATIONS

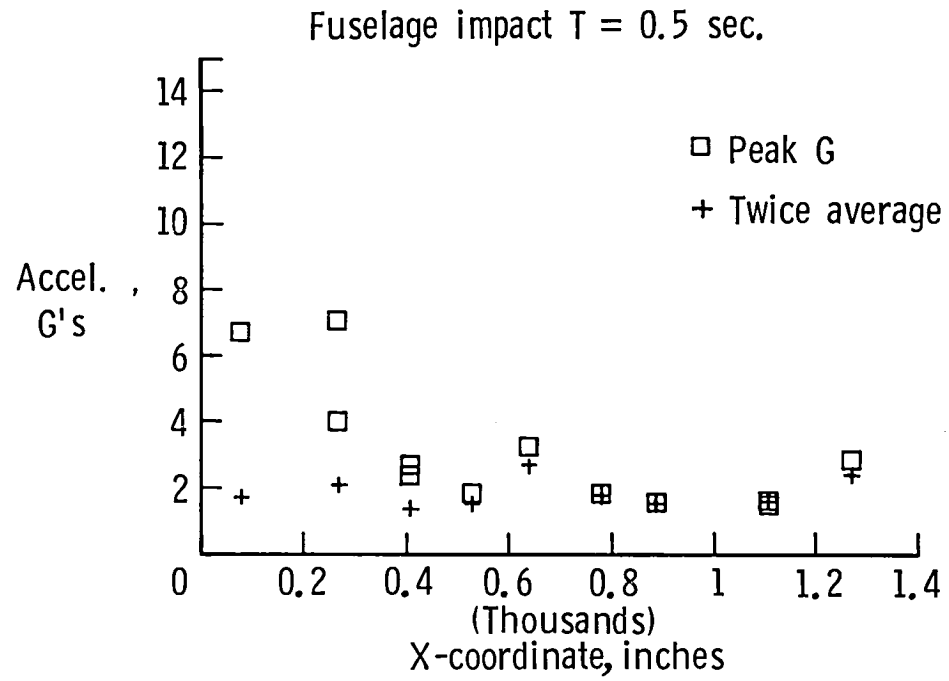
The next four figures give a very brief overview of the structural loads data. On these figures, acceleration (G's) is plotted as a function of an X coordinate, which is simply the distance measured from the nose aft in thousands of inches. Vertical acceleration peaks in the neighborhood of 14 to 15 G's occurred in the nose and forward cabin, substantially dropping off to levels of 7 to 2 G's in the remainder of the fuselage. It was a very, very mild impact from a human tolerance point of view. I believe a fit, young adult male could withstand upwards of 25 G's in a vertical direction for short durations. The C.I.D. aircraft had fairly low levels throughout, which would have been tolerable by a fit and well restrained human.

The peaks from the data are represented by the squares. The plus symbols represent an average peak which is determined by a triangularization technique described by Fasanella (ref. 5). These average peaks correlate very well with the peaks from the actual filtered data, except perhaps in a few instances where high frequency oscillation occurs.



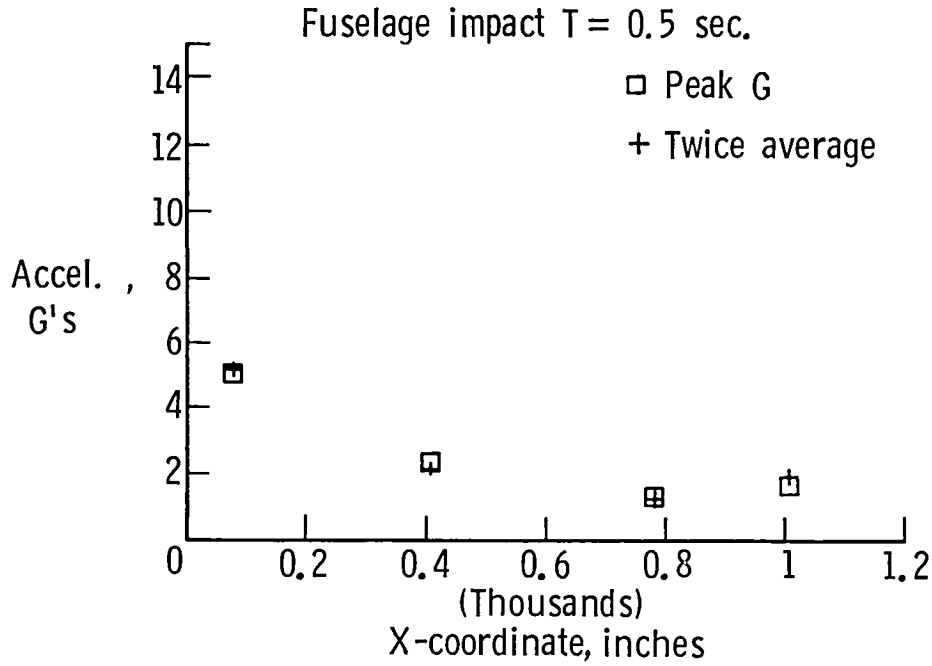
C.I.D. LONGITUDINAL FLOOR ACCELERATIONS

Longitudinally, the acceleration distribution throughout the aircraft was fairly low. Again, the highest levels occurred in the nose and forward cabin, dropping off substantially below 4 G's down around the 2 G-level for most of the aircraft.



C.I.D. TRANSVERSE FLOOR ACCELERATIONS

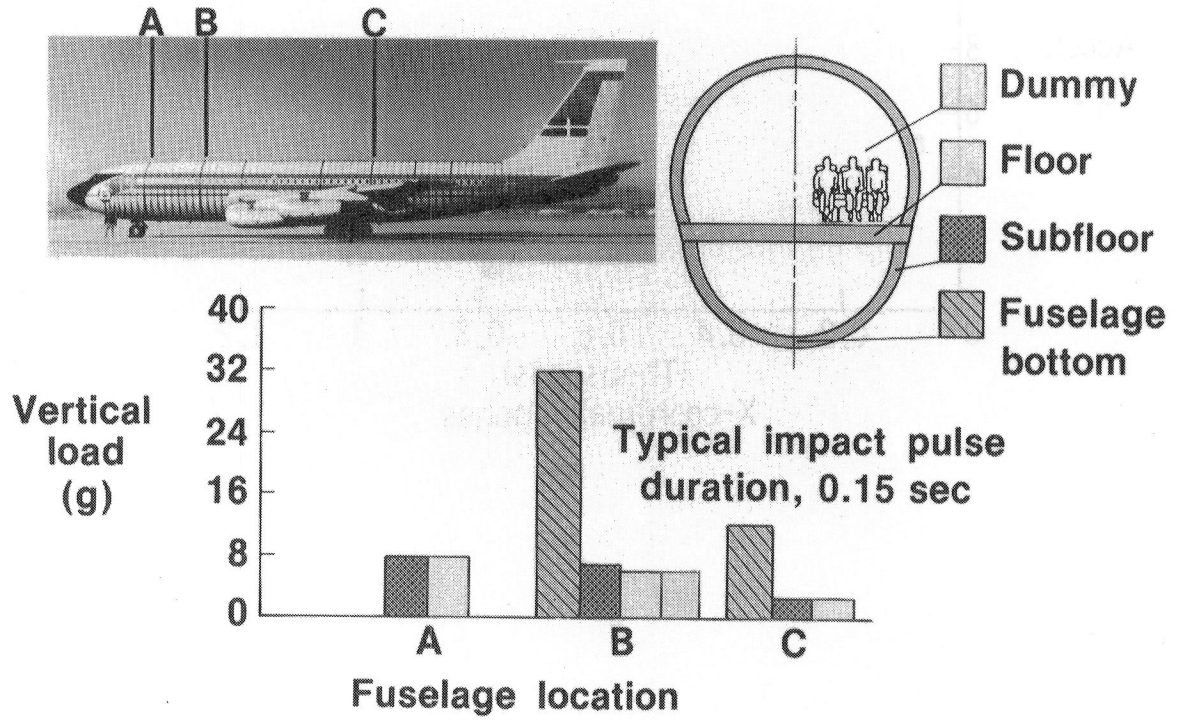
Transverse accelerations along the floor were also generally low -- 5 G's in the nose, down around 2 G's for the remainder of the aircraft.



AIRCRAFT STRUCTURAL RESPONSE

Load transmission from the fuselage bottom up to the dummy is discussed in reference 1. This figure introduces the levels at one particular body station.

Point B is body station 540, about 410 inches back from the nose. The fuselage bottom experienced about 32 G's at impact. By the time the load got up along the side wall and under the floor, the level was reduced to around 7 G's. On the floor and in the pelvis of the dummies, the vertical acceleration was down to 6 G's.



C.I.D. SUMMARY

In summary, the structural loads experiment was very successful. Ninety-seven percent of the channels were active at impact. The data is still being assessed. Only a portion of the data has been presented here; approximately 80 channels of data are available. Analysis of the remaining data is in progress.

Interior photography was also very successful. One hundred percent of the cameras functioned. The film contains unique information on the development of fire and smoke in the interior of the aircraft. From a human tolerance point of view, the C.I.D. was a simulation of a survivable crash.

1. Structural loads experiment was successful
   - 97% of channels active
   - Data being assessed

2. Interior photography successful
   - 100% of cameras functional
   - Significant information

3. CID survivable from impact loads point of view

REFERENCES

1. Alfaro-Bou, Emilio: NASA Experiments on the B-720 Structure and Seats. Full-Scale Transport Controlled Impact Demonstration, NASA CP-2395, 1986, pp. 29-47.

2. Johnson, Richard A.: Controlled Impact Demonstration Seat/Cabin Restraint Systems - FAA. Full-Scale Transport Controlled Impact Demonstration, NASA CP-2395, 1986, pp. 49-60.

3. Cannon, Mark R.; and Zimmerman, Richard E.: Preliminary Floor, Seat, and Dummy Data. Full-Scale Transport Controlled Impact Demonstration, NASA CP-2395, 1986, pp. 125-155.

4. Barber, Russ: CID Flight/Impact. Full-Scale Transport Controlled Impact Demonstration, NASA CP-2395, 1986, pp. 17-28.

5. Fasanella, E. L.: Digital Filtering and Acceleration Pulse Interpretation. Full-Scale Transport Controlled Impact Demonstration, NASA CP-2395, 1986, pp. 103-123.

CID FLIGHT/IMPACT

Russ Barber
Ames Dryden Flight Research Facility
Moffett Field, California

NASA/FAA Government/Industry CID Workshop
NASA Langley Research Center
April 10, 1985

I am going to describe as best I can what happened during the impact of the C.I.D., as well as discuss the planned versus the actual impact.

The scenario that we were attempting to conduct is identified on figure 1. The scenario here represents almost a year or year and a half of negotiations among the project participants. There was a lot of interest in how this impact would take place. The aircraft manufacturing industry and the participating government organizations all had input to the desired scenario. We were changing this right up to the last week prior to the C.I.D. mission. The FAA knew that they wanted a survivable accident. In order to do that it seemed clear that we needed to have the landing gear retracted so that the fuselage would not fracture aft of the wing because of the high sink rate. The longitudinal velocity and gross weight were relatively easy to achieve. The difficulty came with the longitudinal impact window. That was primarily driven by the crashworthiness people wanting to have 75 milliseconds of time after ground impact, but prior to impact with the wing openers. The AMK people did not want the airplane to land too long and therefore be going too slow by the time that it impacted the wing openers. So the last change that was made to the scenario was the addition of 50 feet on the longitudinal envelope. The concern was that we would not be able to impact the airplane that precisely with the control and guidance system we had. In fact, that did turn out to be the case.

The approach to accomplish the objectives was to remotely control the vehicle to an impact site prepared on the dry lakebed at Edwards as depicted in figure 2. We utiliized many of the systems that we had utilized in the remote control of the HiMAT, DAST, and spin research vehicles that we had flown remotely at Dryden previously. The control system that was developed is illustrated in figures 3 and 4. The airborne and the ground portions of the control system are respectively depicted. We primarily used the autopilot that was in the airplane (Bendix PB-20) to provide control of the airplane. In addition to the control functions that the autopilot performed it was necessary to mechanize several housekeeping functions to actuate things like flaps, landing gear, shutting the engines down, and so forth. The system had a separate and independent terminate system that had the capability of causing the airplane to dive into the ground if we were to lose control of the vehicle through the single string autopilot and airborne control system. The ground-based system had almost a totally dualized control capability. It had dual computational capability going into the ground-based cockpit. Several radars received the data and brought it into the ground computers so that it could be processed and displayed to the pilot. The system had a dual transmitting capability up to the airplane. Figure 4 also shows the independent ground-based terminate system. Basically the control concept was single string with the terminate safety relief in case of loss of control through the single string system.

Having a terminate system required a sterile area in which the airplane could be terminated and not impact any property or lives. Figure 5 depicts the sterile area. The photographers had to be located outside this sterile area, which made their task more difficult. The terminate profile was identified and we knew that if we terminated the airplane anywhere along the flight path, that it would impact in a sterile area. The airplane took off on lakebed runway 17 and flew the profile. There was no go-around accomplished on the C.I.D. mission so the flight profile was as shown. Figure 6 illistrates the crash site. A rockbed 1200 feet long and 300 feet wide of coarse railroad gravel was laid to provide a friction ignition source.

An aiming fence was prepared to enable the pilot to have better guidance longitudinally. Figure 7 depicts the wing openers that were installed to open the wings after impact.

Figure 8 summarizes the manned flight development of these systems. The airplane was flown 14 times with a crew on board. The development flights totaled about 30 hours of flight time. About 52 percent of that time was devoted to RPV control system development. The airplane accomplished 9 takeoffs and 13 landings under remote control and about 69 approaches to the C.I.D. site down to altitudes between 150 and 200 feet. That was the lowest altitude from which a safe go-around could be effected since the landing gear was retracted for the actual impact. The day of impact timeline is shown in figure 9. It looks like a 9:13 takeoff time is pretty leisurely, but we were actually out there about 4:00 in the morning preparing for this. The mission from brake release to impact was something on the order of 9 minutes with a very short interval of time between the initial impact of the no. 1 engine and the fuselage impact. The telemetered data stayed on for a significant period of time after the impact and total data failure occurred at 09:22:12.8.

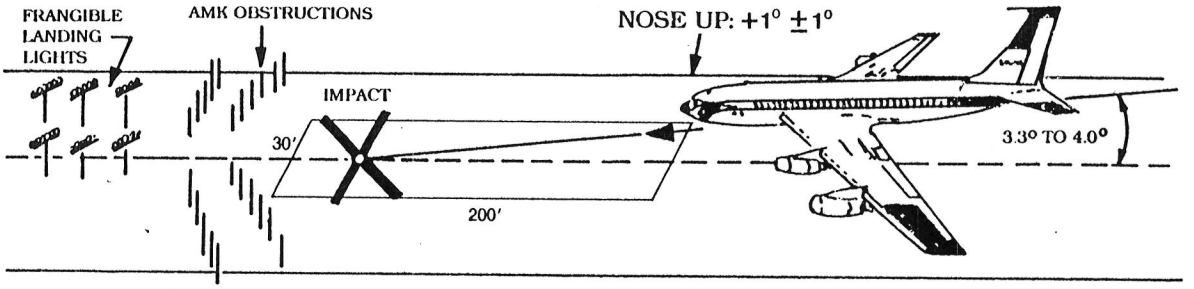
The weight and balance for the C.I.D. mission are shown in figure 10. The mission used 8000 pounds of fuel during the flight profile. The fuel used was obtained by integrating the fuel flow meters. All of that fuel came out of the center wing tank. All the fuel boost punps were on so the center wing override boost pump was predominant. The airplane had 76,000 pounds of AMK on for the final mission.

Figure 11 shows the wreckage distribution. This figure was provided by the FAA's Accident Investigation Team. It shows that the airplane impacted fairly close to the center line. Several areas of impact definition are still confusing and I will address that a little bit later. The airplane slid into the wing openers with a relatively large skew angle and then debris scattered throughout an area about 1500 feet long. The airplane came to rest with the right wing over the left side of the fuselage.

The data that has been obtained on impact is compared with the goals set out prior to the impact on figure 12. The actual sink rate was very close to the desired sink rate. The airspeed was right on. The fuselage hit 281 feet long of the impact envelope and the wing hit 410 feet long. The data showed the lateral deviation was 34 feet to the right of the centerline. The roll attitude was the variable that was probably the furthest off; it was -12^{o} rather than the desired wings-level attitude. The heading angle we have not totally defined yet. We are trying to get some additional photographs to enable us to evaluate this.

Figures 13a, 13b, 13c, and 13d are a sequence of photographs that show the airplane just prior to impact. They show the no. 1 engine impacting first and then the fuselage. It is interesting to note that the engines on the left wing are really distorted.

- REPRESENTATIVE OF: A SURVIVABLE ACCIDENT
- CRASH: AIR-TO-SURFACE; FINAL APPROACH/LANDING, MISSED APPROACH, AND/OR TAKEOFF ABORT
- AIRCRAFT CONFIGURATION: LANING GEAR RETRACTED, FLAPS, SPOILERS (AS REQUIRED), SYMMETRICAL/STABILIZED
- SINK RATE: 17^{+3}_{-2} FPS
- LONGITUDINAL VELOCITY: 150^{+5}_{-5} KNOTS
- GLIDE PATH: 3.3°TO 4.0°
- GROSS WEIGHT: 175-195,000 POUNDS



IMPACT GOALS: AMK--WING TANK RUPTURE, 20-100 GALLONS PER SECOND (SINGLE POINT RUPTURE), 4-5 SECONDS EXPOSURE WITH POSITIVE AMK IGNITION, SLIDE-OUT TO 100 KTS
CRASHWORTHINESS--SURVIVABLE IMPACT, MAINTAIN FUSELAGE INTEGRITY, VERICAL IMPACT PULSE (1 SECOND), LONGITUDINAL ACCELERATION DATA

Figure 1. Planned CID impact scenario.

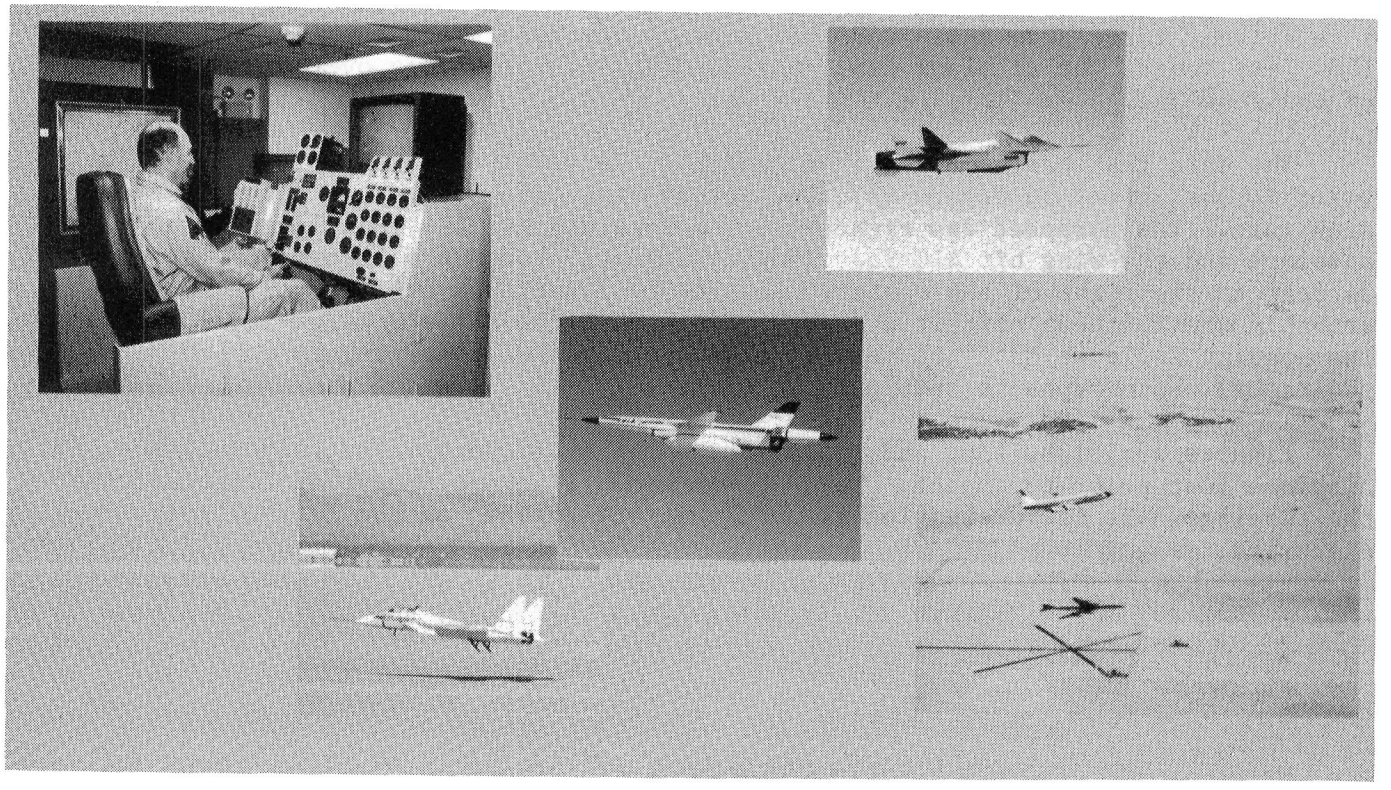


Figure 2. CID technical approach.

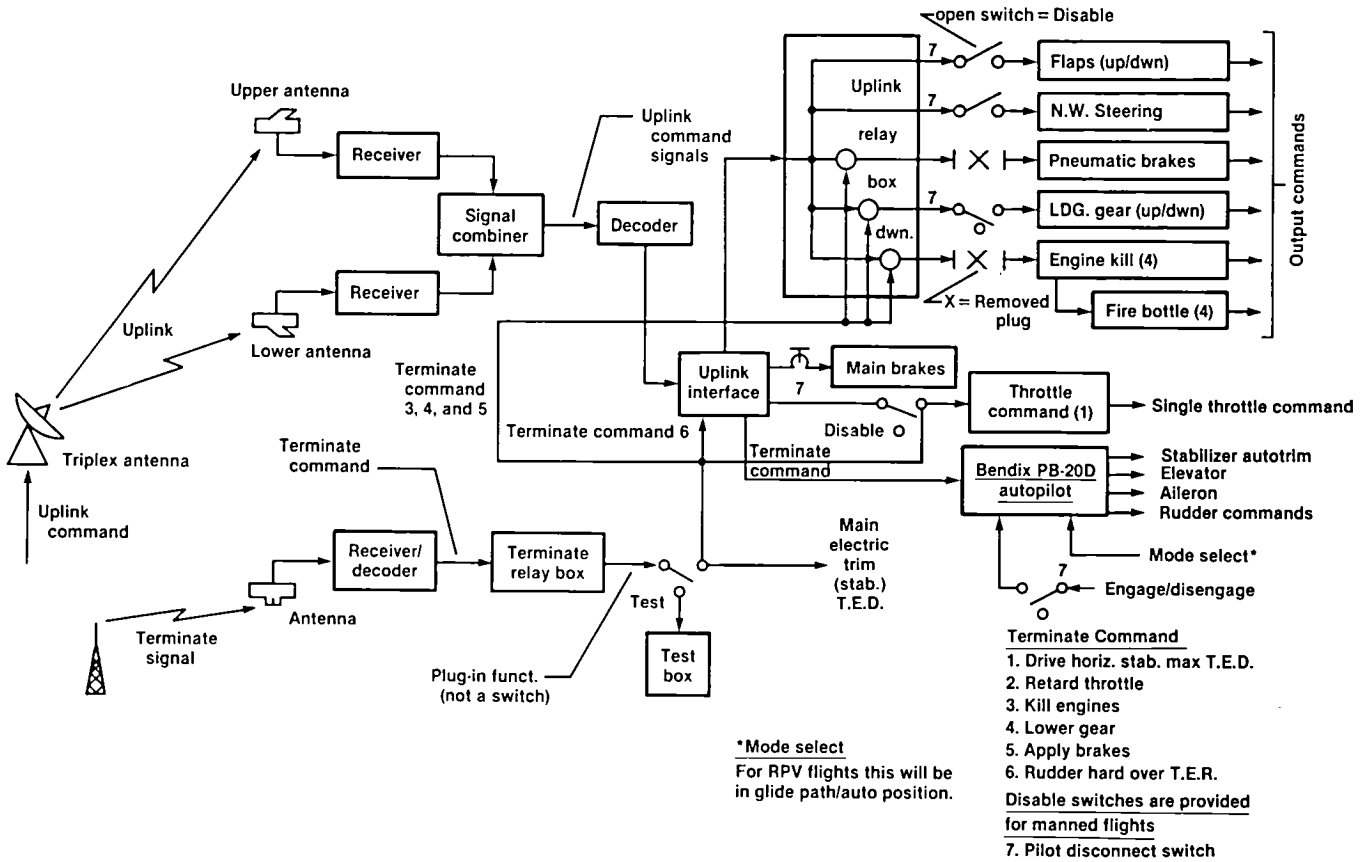


Figure 3. CID airborne RPV control system.

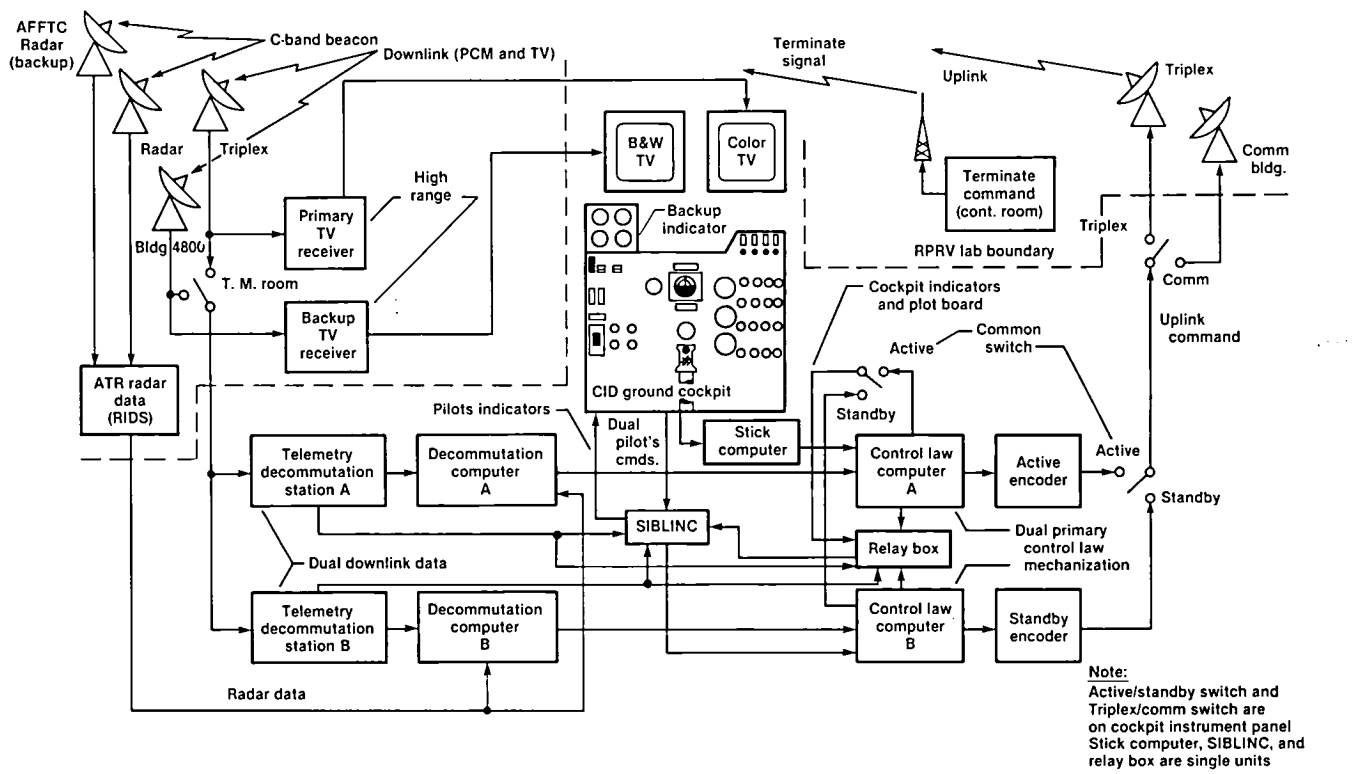


Figure 4. CID ground-based RPV control system.

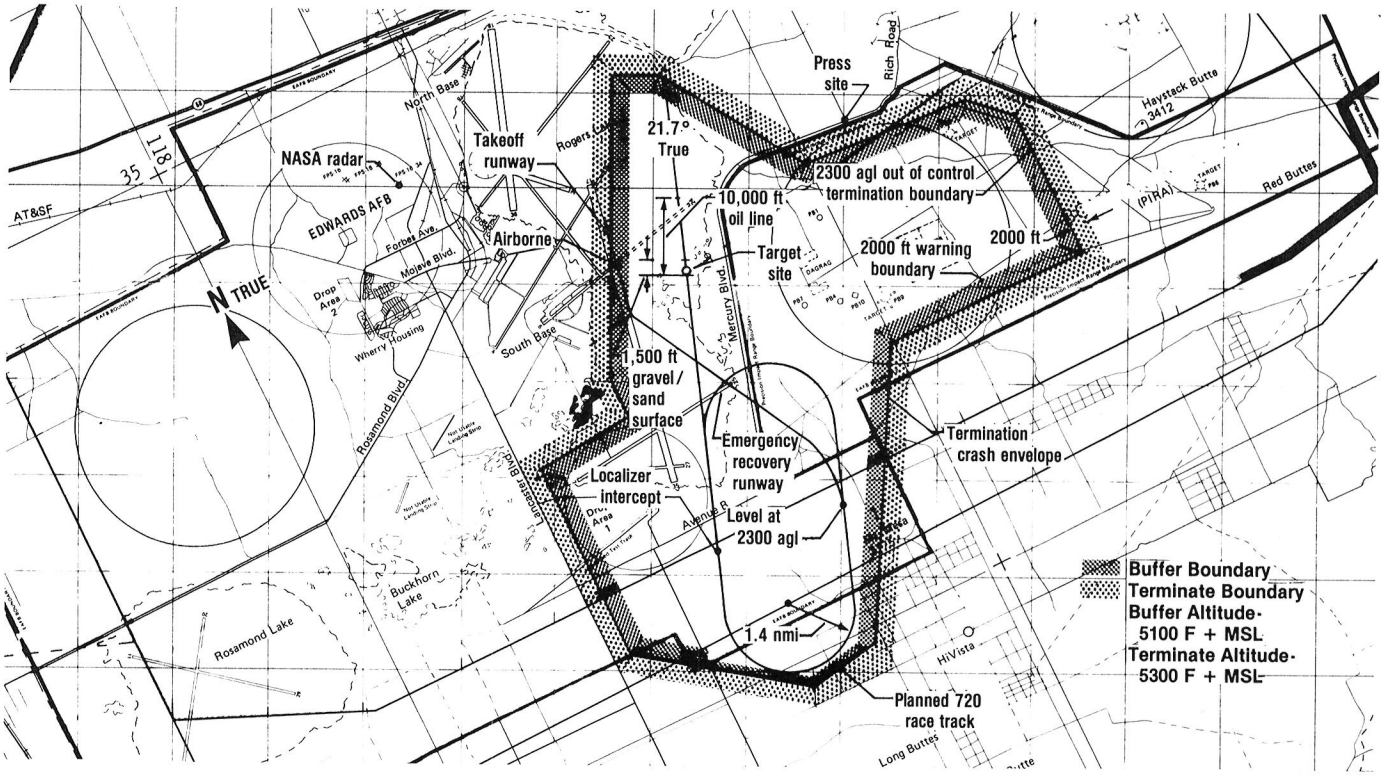


Figure 5. CID impact profile.

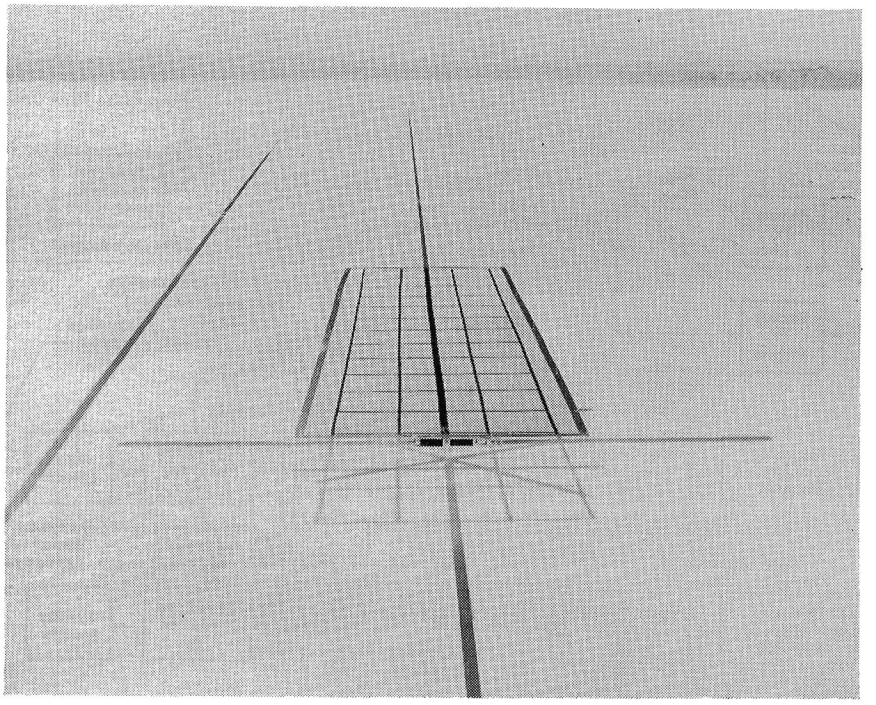


Figure 6. CID crash site.

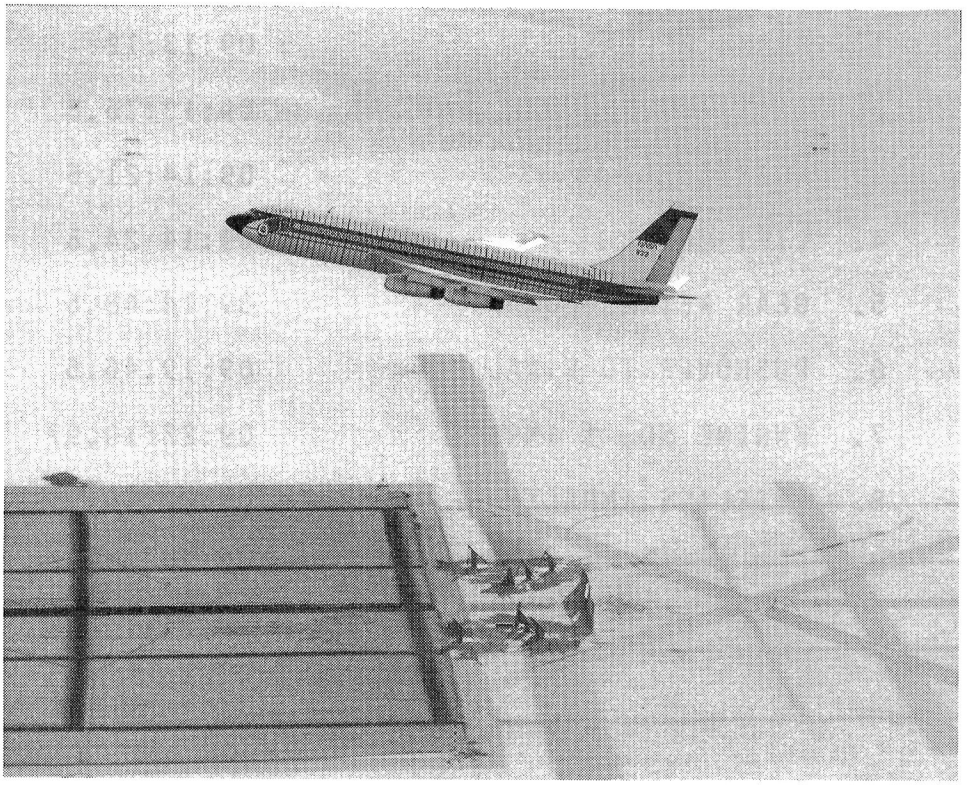


Figure 7. CID wing openers.

- **14 manned flights flown**
  - **Total flight time 31.4 h**
  - **Total RPV time was 52.2 percent of total**
  - **9 RPV takeoffs and 13 RPV landings**
  - **69 CID approaches to altitudes between 150 and 200 ft**

Figure 8. CID manned flight summary.

1.	BRAKE RELEASE	09:13:12
2.	INITIAL ROLL	09:13:16.8
3.	ROTATION	09:14:21.5
4.	LIFT OFF	09:14:24.5
5.	GEAR RETRACTED	09:14:48.5
6.	PUSHOVER TO FINAL	09:19:46.5
7.	ENGINE NO. 1 IMPACT	09:22:10.97
8.	FUSELAGE IMPACT	09:22:10.99
9.	PCM POWER FAIL	09:22:11.00
10.	TOTAL DATA FAIL	09:22:12.8

Figure 9. CID mission timeline.

PRE ENGINE START	GROSS WT 200,455 LBS C.G. 22.6% MAC
FUEL USED FROM C.W. TANK	8,072 LBS
IMPACT	GROSS WT 192,383 C.G. 24.2% MAC

76,058 LBS OF AMK WAS LOADED FOR THE CID MISSION

Figure 10. CID mission weight and balance.

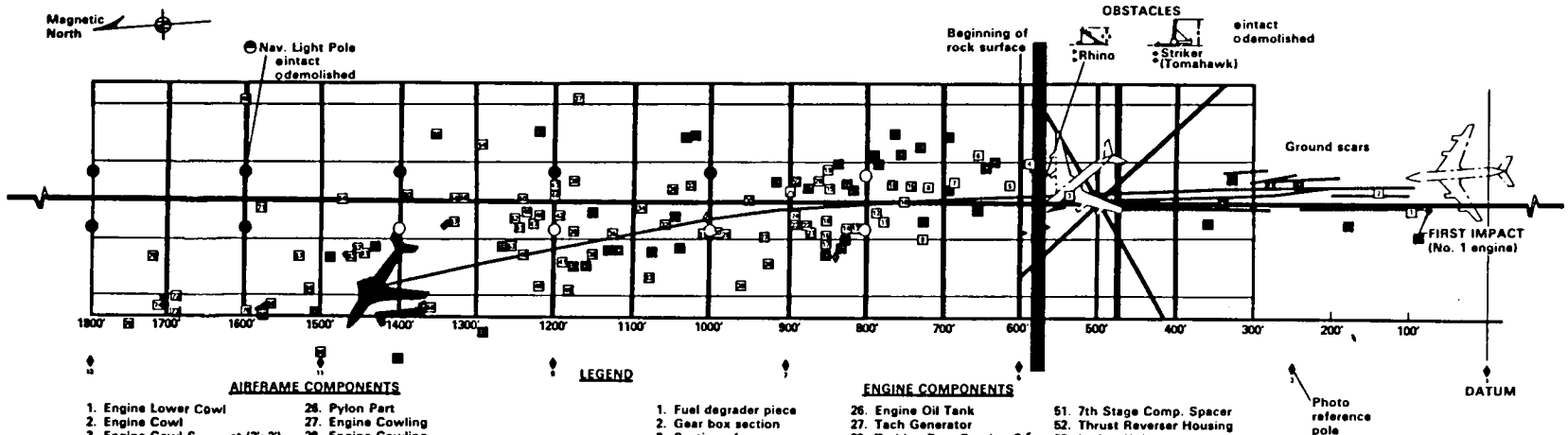


Figure 11. CID wreckage distribution.

THE TARGET CONDITIONS IN TERMS OF DESIRED AND ACCEPTABLE RANGES, TOGETHER WITH THE MEASURED VALUES, ARE AS FOLLOWS:

	DESIRED	ACCEPTABLE	MEASURED
SINK RATE (FPS)	15-17	15-20	17.3
LONGIT. VEL. (KTS)	150-155	145-155	151.5
PITCH ATTITUDE (DEG)	1	0-2	0
LONGIT. DEVIATION (FT)	-75 TO +75	-125 TO +75	-128 NOTE 1 OR -410 NOTE 2
LATERAL DEVIATION (FT)	-15 TO +15	-15 TO +15	+45 NOTE 1
ROLL ATTITUDE (DEG)	-1 TO +1	-1 TO +1	-12 NOTE 2
HEADING ANGLE (DEG)	-1 TO +1	-1 TO +1	NOTE 3

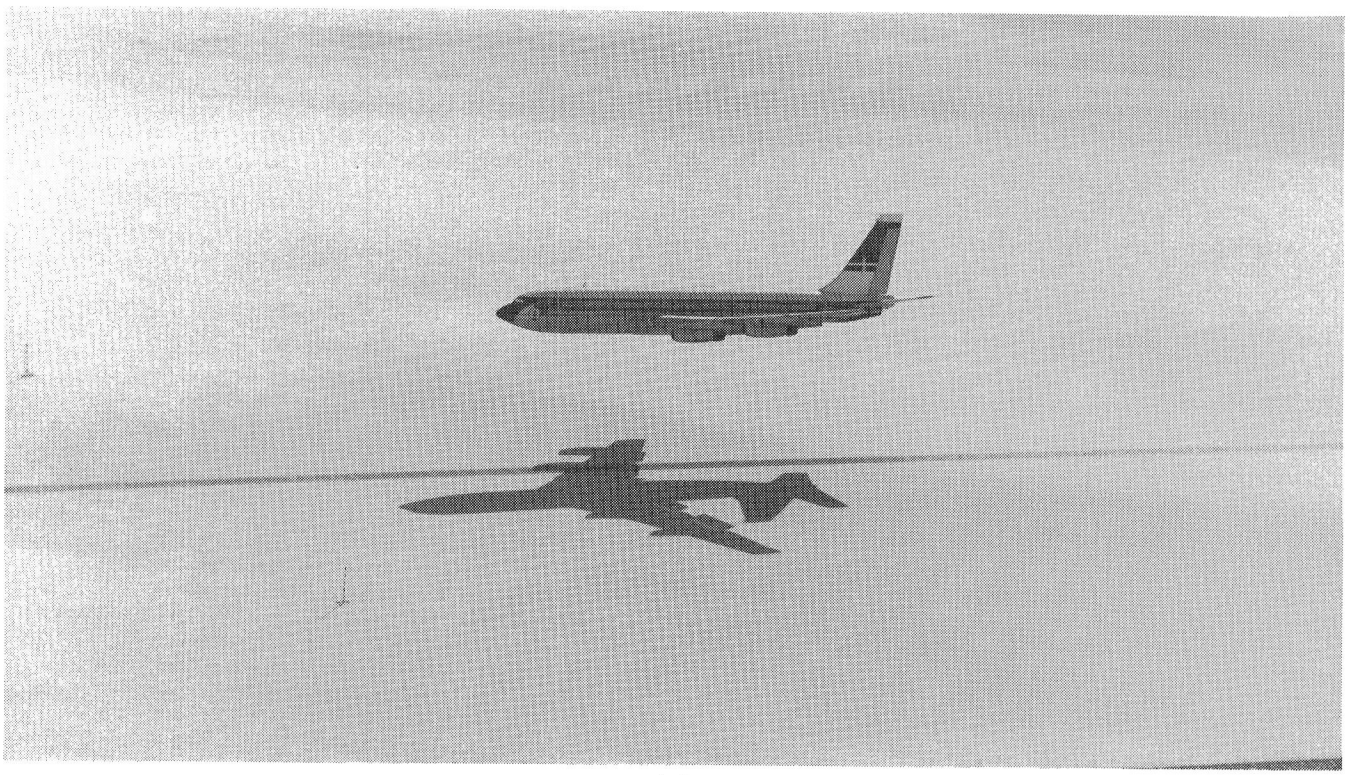
NOTE 1. MEASURED AT A POINT WHERE FUSELAGE MADE INITIAL CONTACT.

NOTE 2. MEASURED AT POINT OF INITIAL GROUND CONTACT (WHERE NUMBER 1 ENGINE IMPACTED THE GROUND).

NOTE 3. OVERHEAD PHOTOS ARE NEEDED TO DETERMINE VALUE. PHOTOS NOT YET RELEASED TO NASA.

- ASSUMED AIRCRAFT WOULD BE STABILIZED AT IMPACT.
- AT 200 FT THE CID PROFILE WAS NOMINAL LONGITUDINALLY, OFF NOMINAL LATERALLY.

Figure 12. CID actual impact scenario.

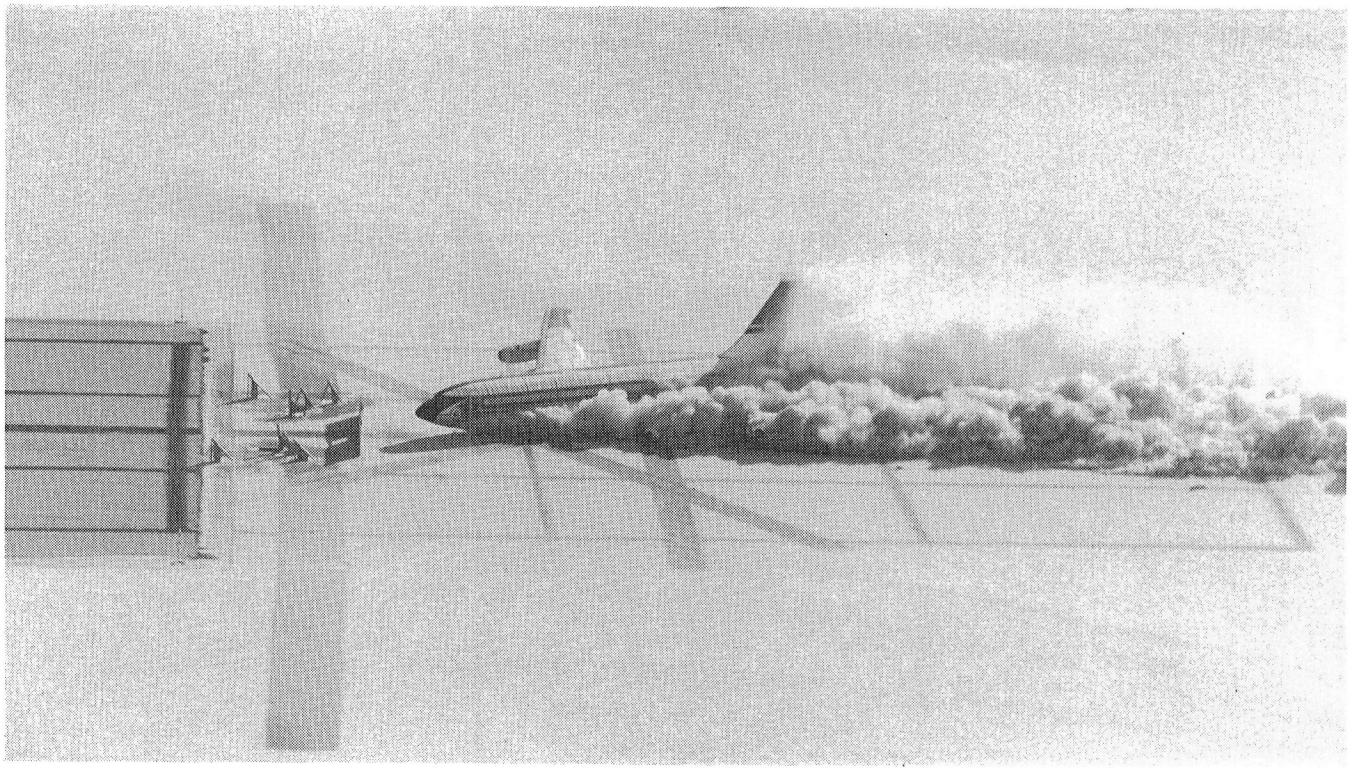


(a)

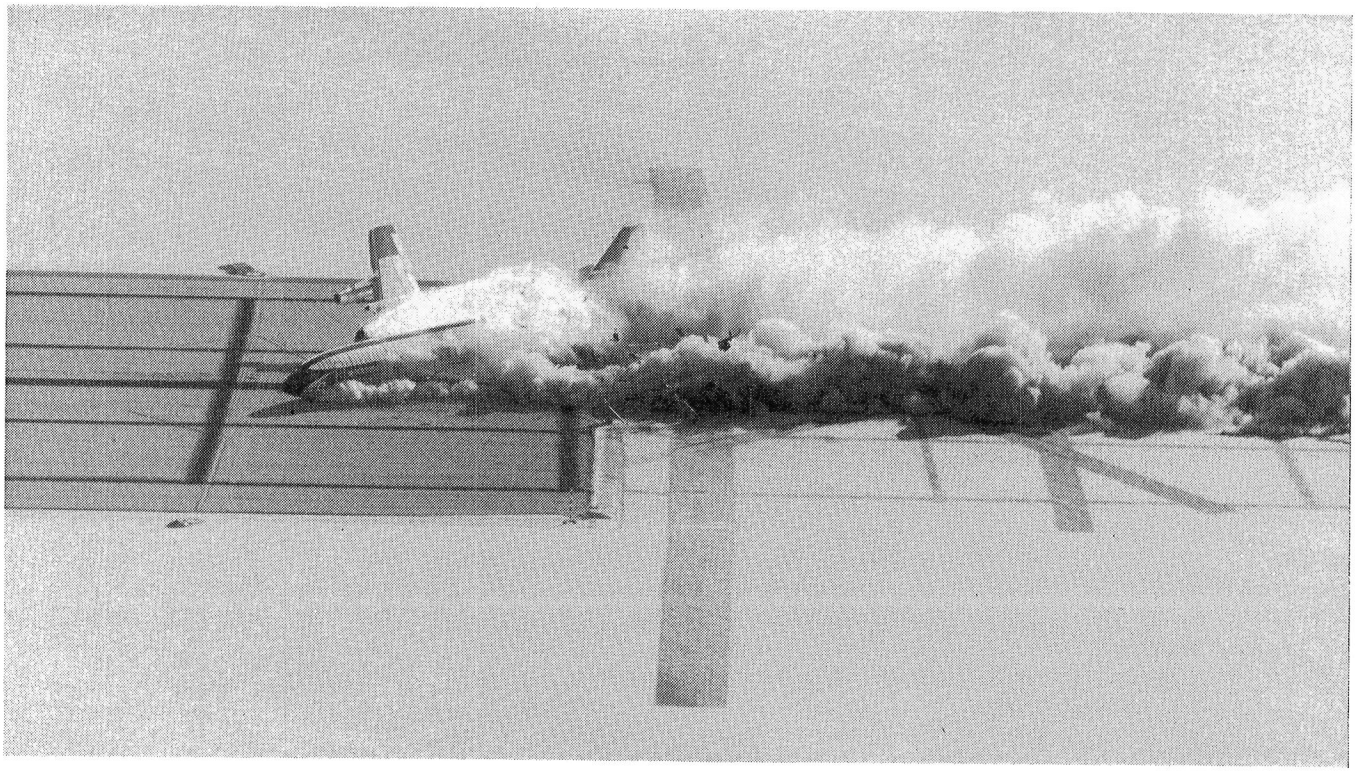


(b)

Figure 13. CID impact.



(c)



(d)

Figure 13. Concluded.

NASA EXPERIMENTS ON THE B-720 STRUCTURE AND SEATS

Emilio Alfaro-Bou
NASA Langley Research Center
Hampton, Virginia

NASA/FAA Government/Industry CID Workshop
NASA Langley Research Center
April 10, 1985

NASA EXPERIMENTS ON THE B720 STRUCTURE AND SEATS

This presentation addresses the two NASA LaRC experiments onboard: a structural experiment and a seat experiment.

The structural experiment deals with the location and distribution of the instrumentation throughout the airplane structure. In the seat experiment, the development and testing of an energy absorbing seat are discussed.

OBJECTIVES

STRUCTURAL EXPERIMENT

The objective of the structural experiment was to obtain a data base of structural crash loads for use in the advancement of crashworthy technology of materials (such as composites) in structural design and for use in the comparison between computer and experimental results.

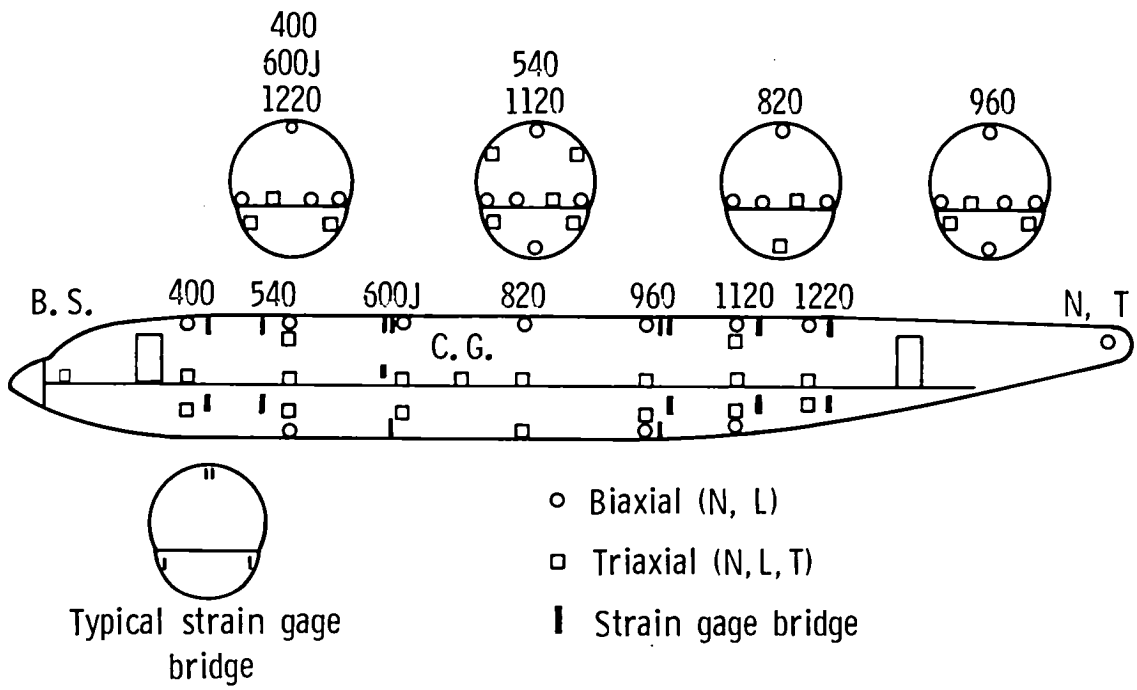
SEAT EXPERIMENT

The objective of the seat experiment was to compare the performance of an energy absorbing transport seat and a standard seat when subjected to similar crash pulses.

- To obtain a data base of structural crash loads for advancing the crashworthiness technology in materials and structural design
- To compare the performance of an energy absorbing seat to a standard transport seat

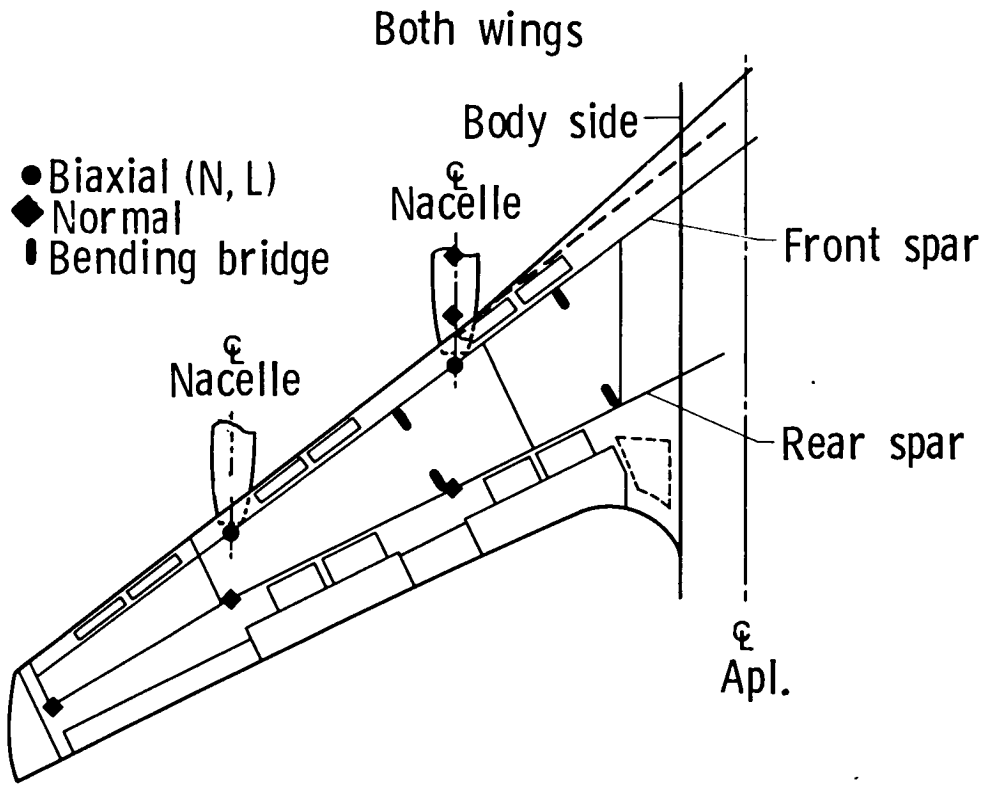
C.I.D. FUSELAGE INSTRUMENTATION

To measure acceleration time histories along the fuselage, distribution of accelerometers was concentrated in seven fuselage frames. Three frames were selected forward in the fuselage, three frames aft, and one frame in the center (wing box). The cross-section of the frames as viewed from the rear of the fuselage shows the placement of accelerometers to measure load transmission from bottom to crown. In addition to the accelerometers located in the seven frames there was a triaxial accelerometer mounted on the floor under the pilot's seat, a triaxial mounted at the center of gravity, and a biaxial mounted at the tail end of the fuselage. Also shown is the location of eight bending bridges to measure the vertical bending moment of the fuselage.



C.I.D. WING INSTRUMENTATION

On the wings, there were three normal accelerometers located on the rear spar. One accelerometer was located on the wing tip and the other two were located in line with the outboard and inboard engines respectively. Two biaxial accelerometers were located on the front wing spar in line with the engines. Two normal accelerometers were located on the inboard engine pylon, one in front and one in the rear. To measure spanwise bending moments in the wing, one strain gage bending bridge was located inboard on the wing and another outboard. The two wings were instrumented in a similar manner.



C.I.D. MEASUREMENTS

A total of 350 instruments were mounted throughout the airplane of which 187 were mounted on the fuselage structure and wings, 157 on the seats and dummies, and 6 on the overhead bins.

I Fuselage:
- Accelerometers 157
- Bending bridges 8

II Overhead bins:
- Accelerometers 3
- Load links 3

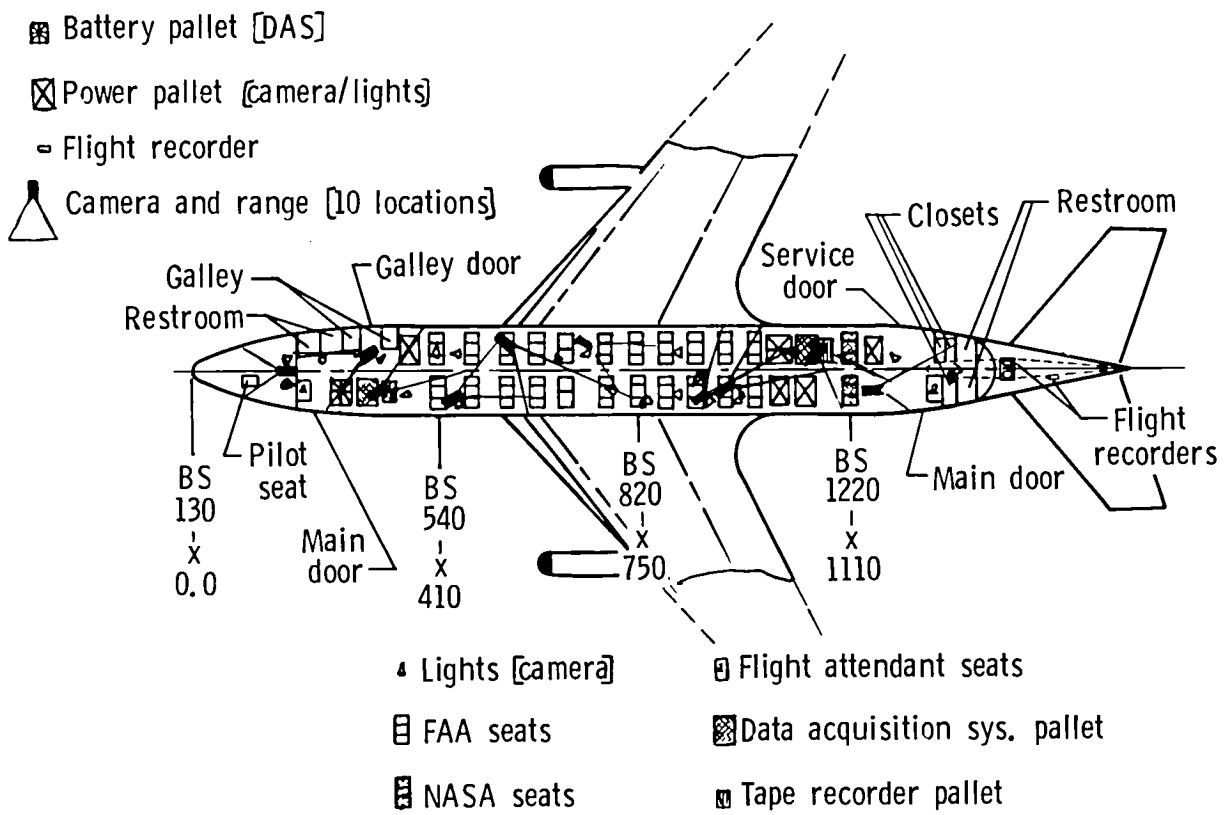
III Wings:
- Accelerometers 18
- Bending bridges 4

IV Seats:
- Accelerometers 75

V Dummies:
- Accelerometers 52
- Load cells 30

C.I.D. PLAN VIEW

This plan view of the cabin interior shows the location of the two NASA seats in Body Station 1220. The energy absorbing seat was located on the left and a standard commercial seat was located on the right. The other 25 seats were part of the FAA seat experiment. Also shown are the locations of the data acquisition system and its power supply, the photographic camera/lights and power pallet, and tape recorders.



B720 CABIN INTERIOR

In this view of the rear cabin interior some of the seats, anthropomorphic dummies and CPR dummies are shown. The two NASA seats are located in the rear. Also shown are some of the cameras and lights used in photographing the dummies and seats during the crash sequence.



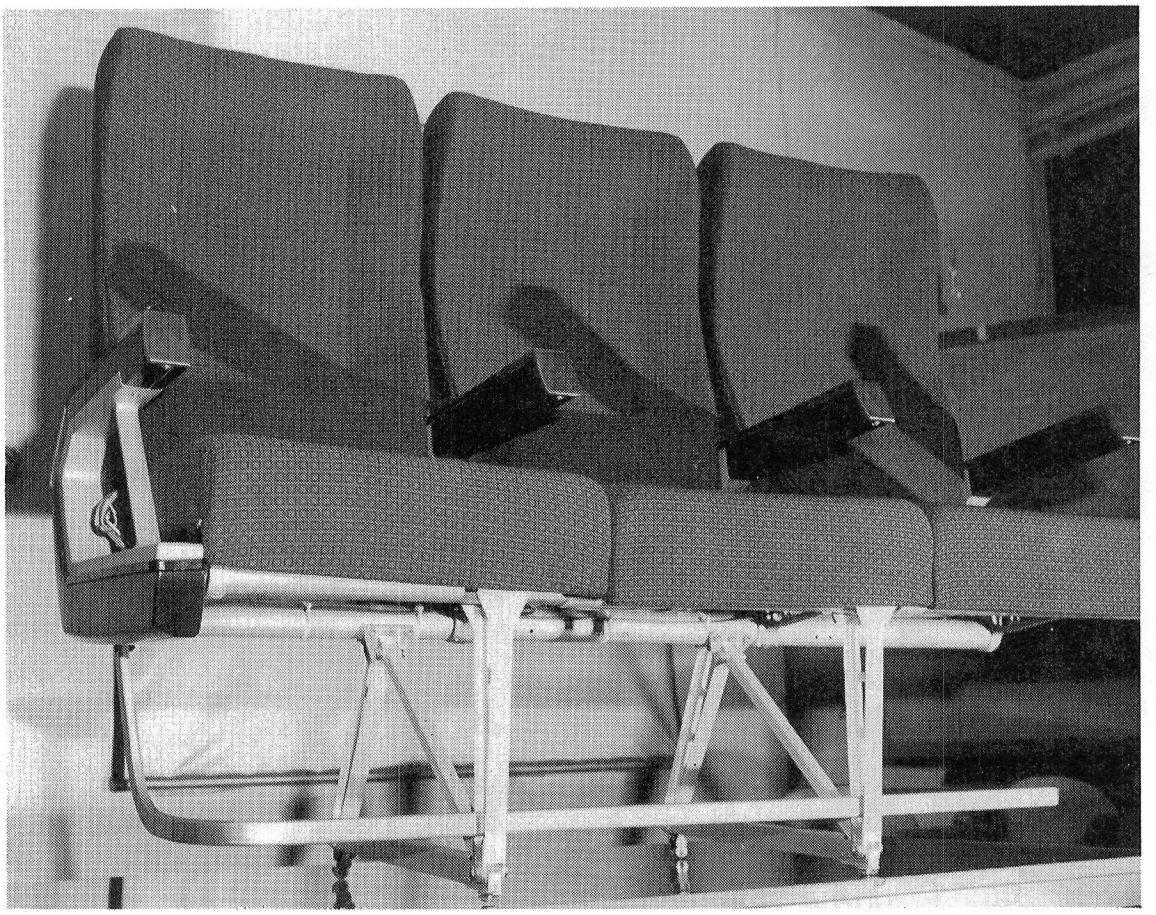
DUMMIES IN CRASH POSITION

In both NASA seats the dummies were placed bent down in an assumed crash position as shown here. The 50 percentile anthropomorphic dummy at the center in each seat was instrumented with a triaxial accelerometer at the pelvis and with a load cell at each side of the lap belt.



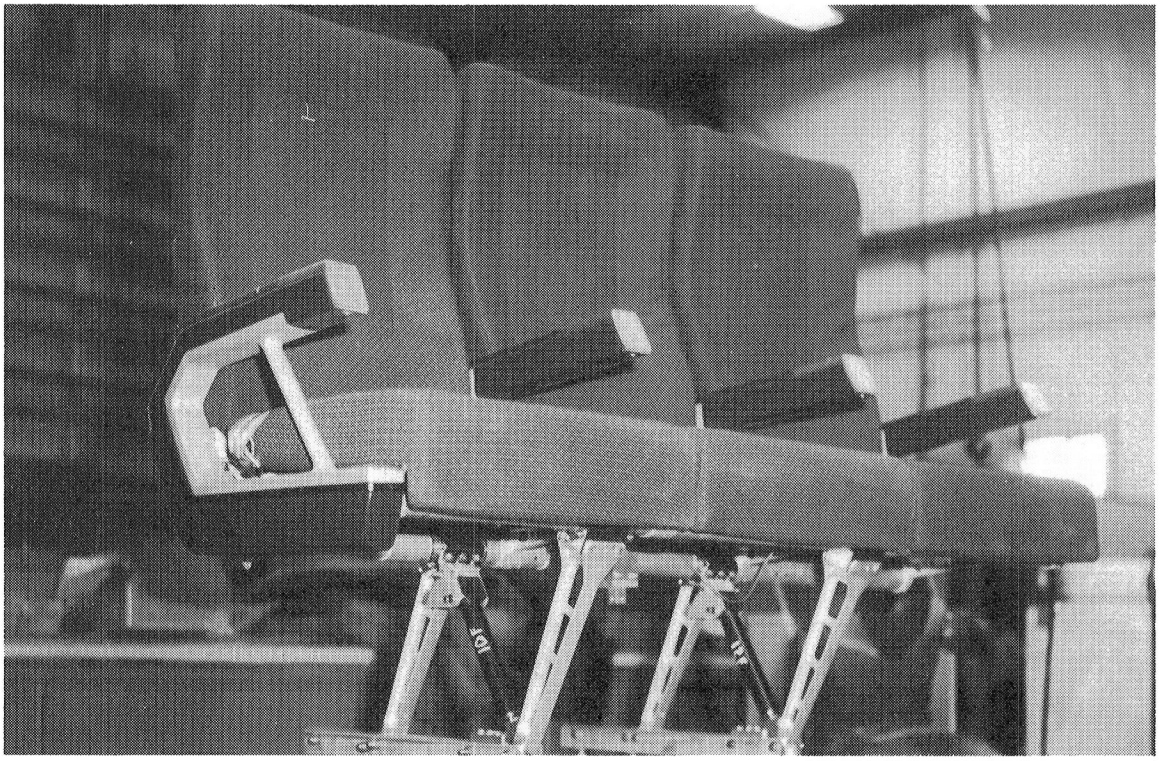
AIREST 2000 TRIPLE SEAT

The standard seat used in the NASA experiment at Body Station 1220 on the right side was a Fairchild Burns Airest 2000 in which the seat cushions were covered with heat blocking material. A similar seat was converted into an energy absorbing seat by replacing the two diagonal members with graphite epoxy energy absorbing tubes. To allow the energy absorbers to load during the crash impact the bolts that fastened the seat legs to the seat frame tubes were replaced with a bearing surface around the tubes.



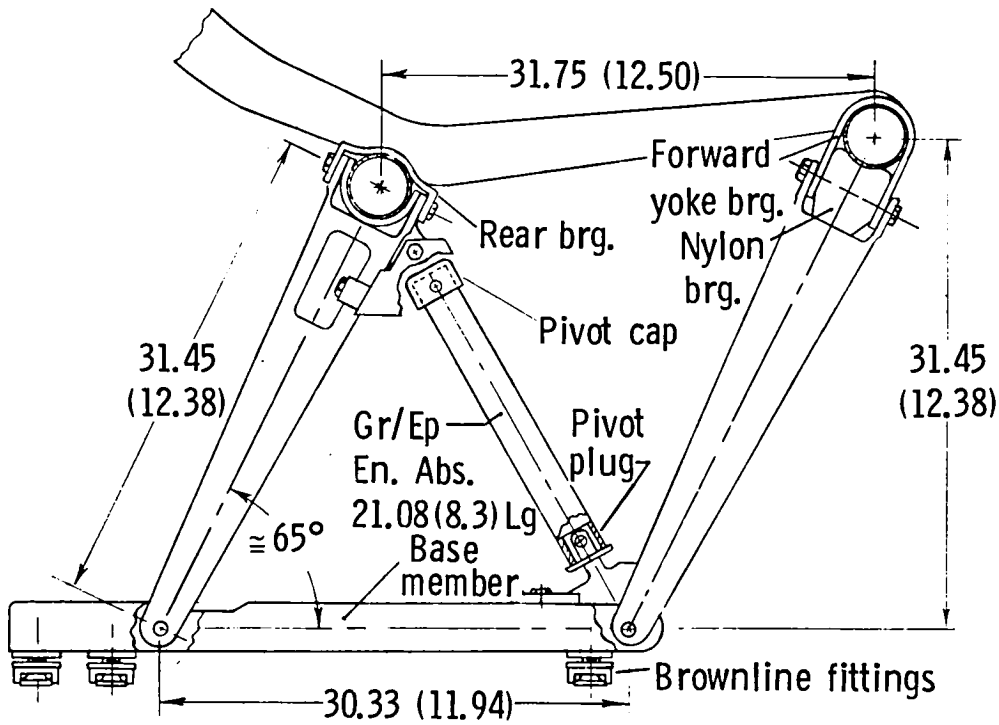
TRANSPORT ENERGY ABSORBING SEAT

The two diagonal energy absorbers and the four bearings attached to the upper portion of the seat legs are shown. The seat frame accelerometer block is shown mounted midway on the rear tube. On the airplane, a triaxial accelerometer was mounted on the floor seat track to determine load transmission from the floor to the seat. The seat cushions were covered with a heat blocking material to retard the propagation of fire.



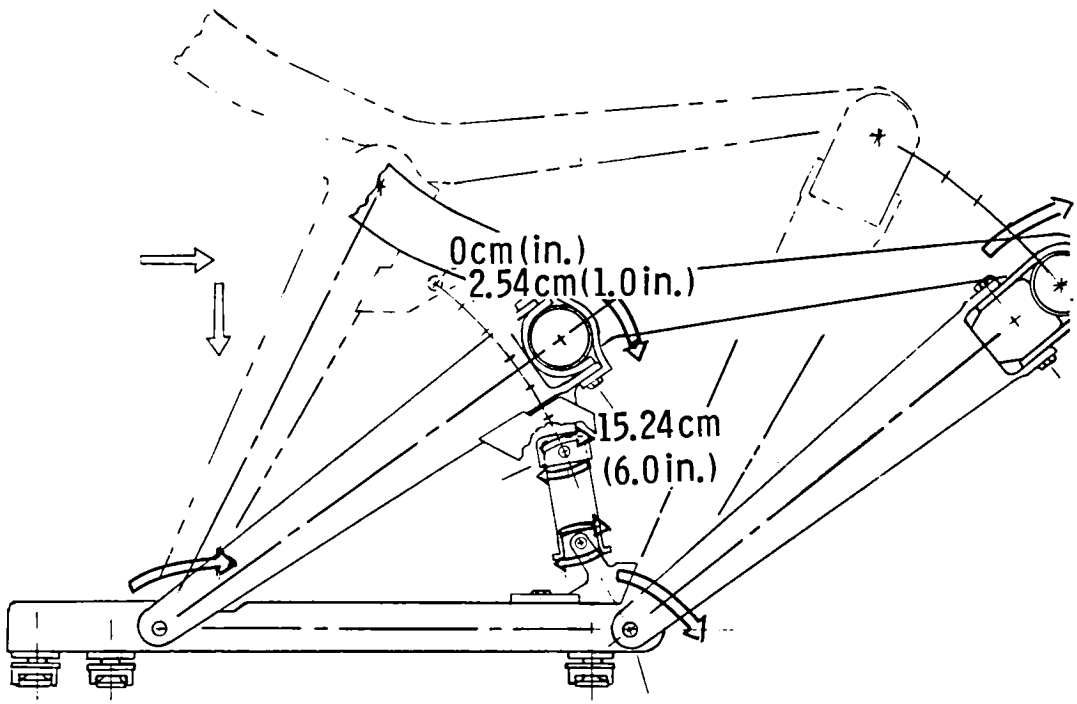
MODIFIED AIREST 2000

Modifications to the seat are shown in more detail. They include the front and rear leg bearings, the graphite epoxy energy absorber and its pivoting mechanism, and the base member with the brownline fittings.



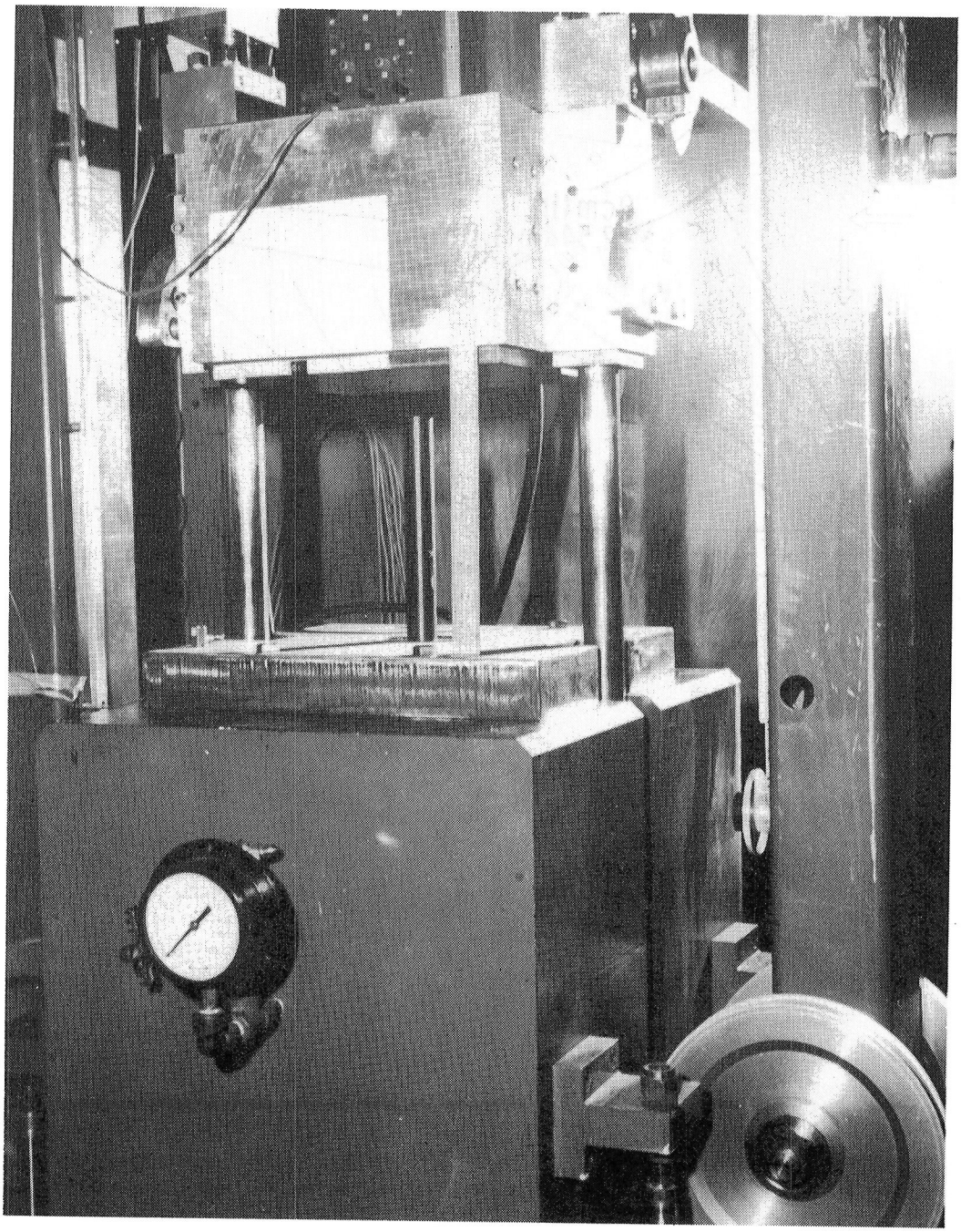
SEAT STROKE GEOMETRY

The stroking action of the energy absorbing seat is depicted in this view. Outlines of the seat in its normal and stroked positions are shown. During stroking, the seat, which is a four-bar linkage, moves downward and forward causing the energy absorber to stroke approximately 6 inches.



ENERGY ABSORBING TUBE IMPACT TEST

The energy absorbing graphite-epoxy tube was impact tested in this machine to investigate its dynamic response during collapse. Of particular interest were the mechanism by which gradual crushing of the walls occurred and the tube stability during stroking. In the test, the tube stroked 6 inches which is also the maximum stroke the tube is subjected to when installed in the seat.



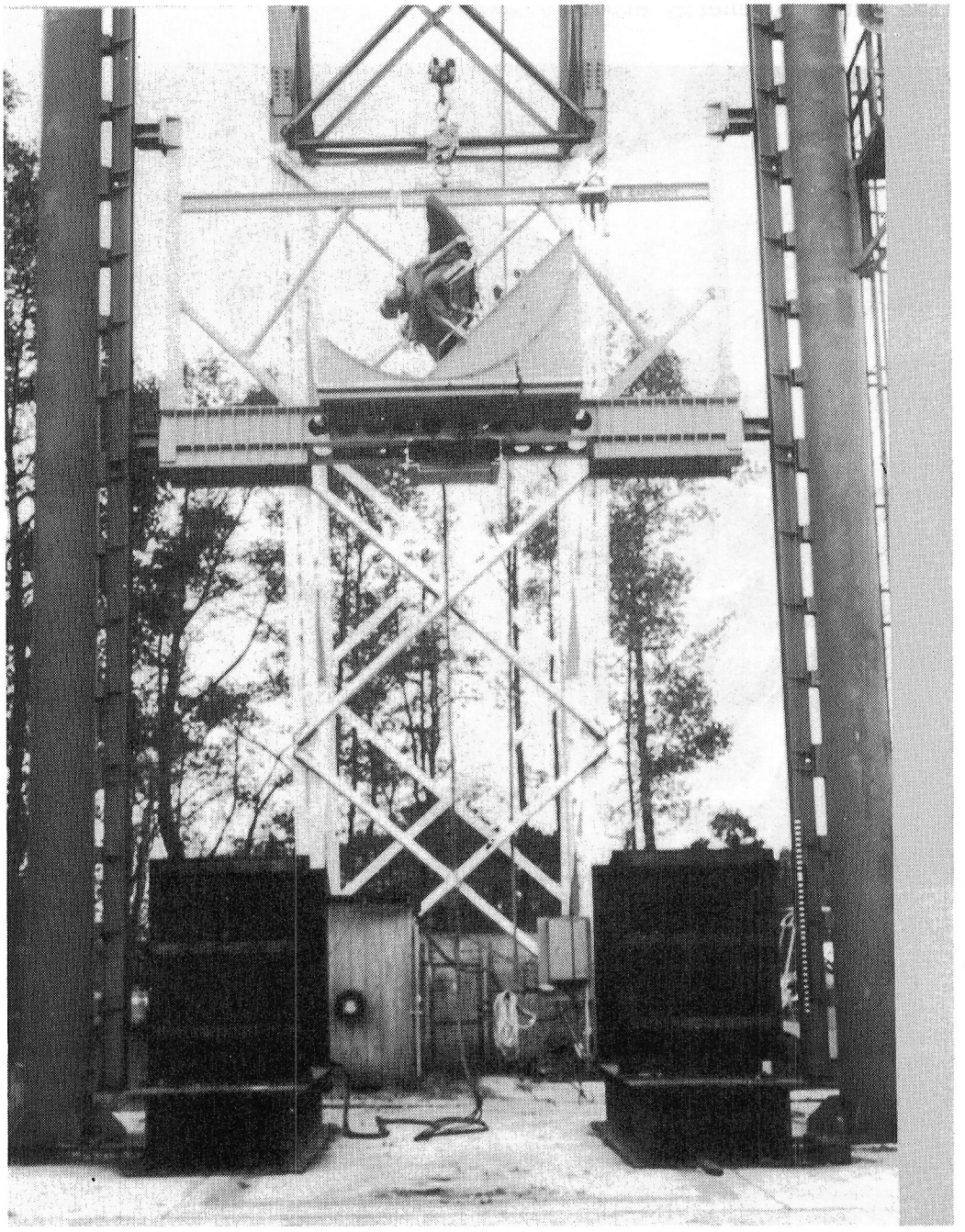
STATIC SEAT TEST

This is the static seat test configuration. It shows the seat mounted on 6-axis load cells under each seat leg. The load cells measure moments in 3 axes and triaxial forces. The seat was loaded in the vertical direction to check the operation of the stroking mechanism. In earlier static tests it was found that during stroking, the energy absorbers were subjected to bending loads and failed prematurely. This difficulty was corrected by installing a self aligning mechanism that held the energy absorbers in place and prevented transmission of bending loads to the energy absorbers by allowing only axial loads in line with the energy absorber axis.



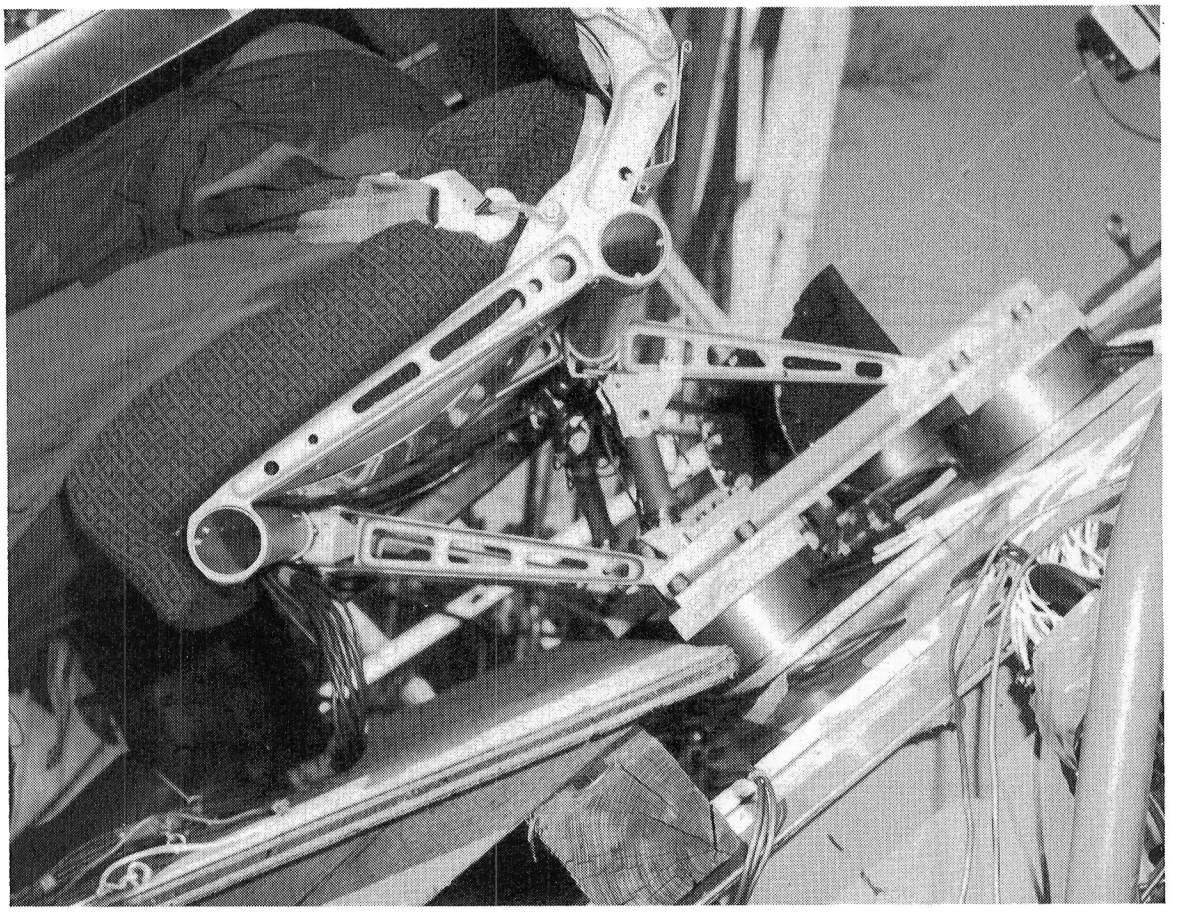
DYNAMIC SEAT TEST

To dynamic test the energy absorbing seat, the sled was raised to a height of 14 ft to achieve an impact velocity of 30 ft/sec and a peak acceleration of 14 g with a 120 ms pulse duration. The dummies were bent in a crash position to simulate the effects of a real crash. The drop tower is 75 ft high and impact velocities to 50 ft/sec are possible. Impact pulses can be obtained with up to 50 g peak acceleration and 50 to 150 ms pulse duration by varying the number of straps (2" wide x 3/8") in the pulse generating system.



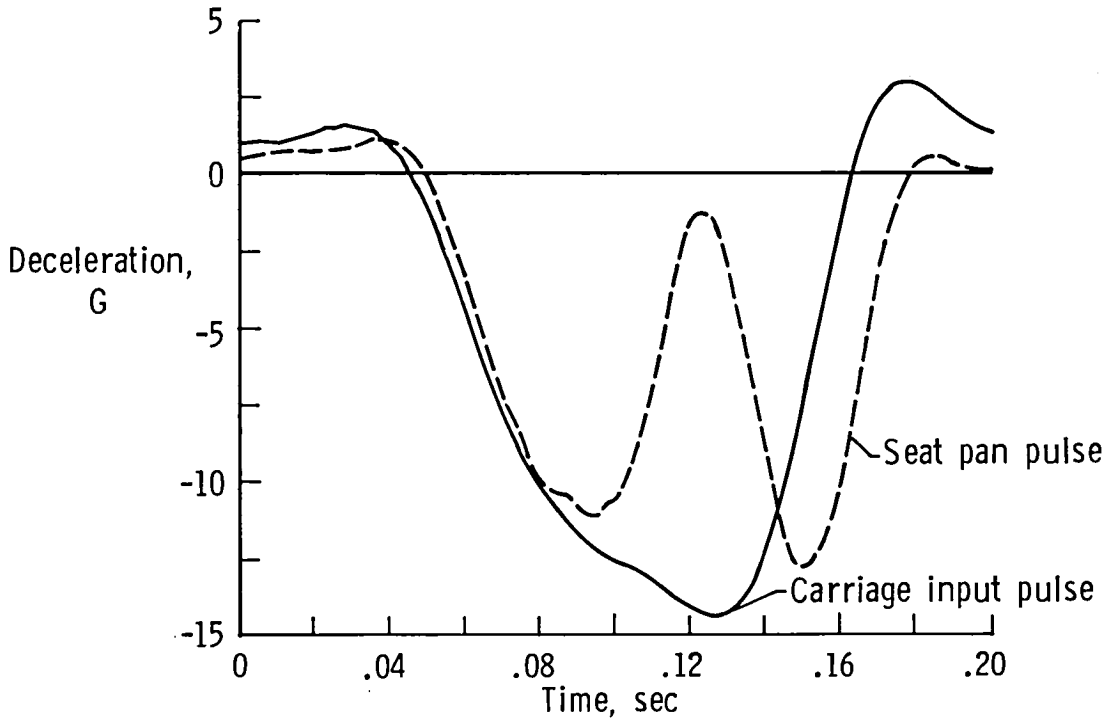
DYNAMIC IMPACT TEST - STROKED SEAT

The energy absorbing seat is shown in the stroked position after the drop test. The seat started to stroke at approximately 11 g's and the stroke length was about 5 inches. The seat and energy absorbing mechanism worked satisfactorily.



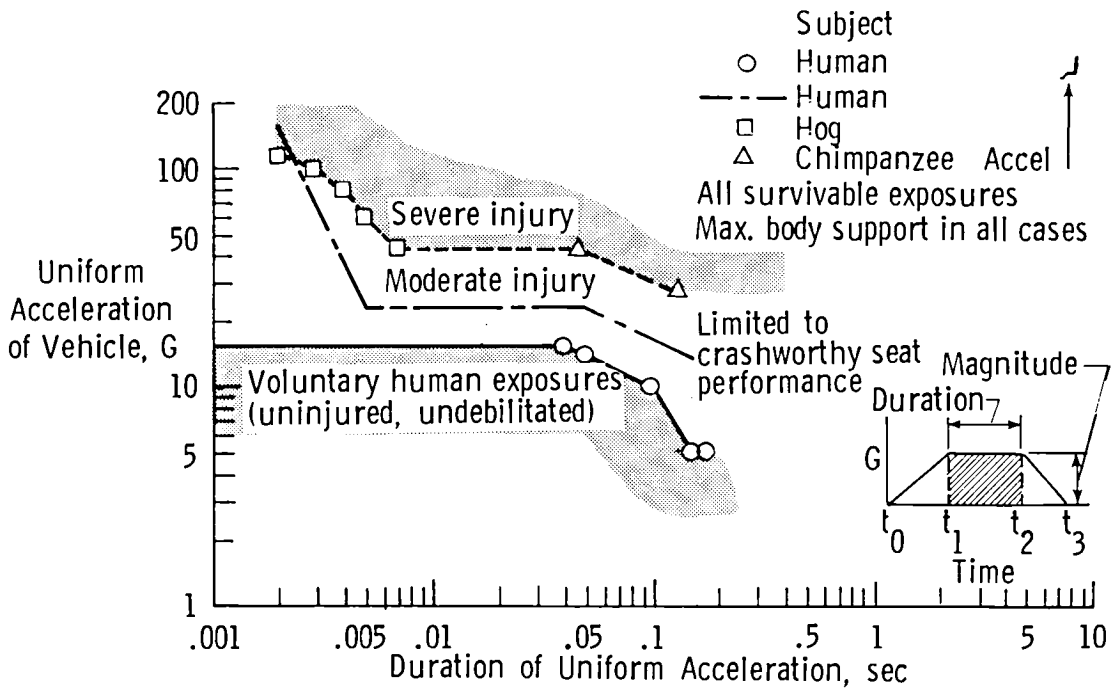
DYNAMIC SEAT TEST PULSE

The solid line represents the carriage impact pulse (vertical). A peak acceleration of 14 g's at 120 ms duration was obtained. The dashed line is the seat pan acceleration time history and the data was taken from an accelerometer at 45 degrees to the horizontal. The seat pan pulse duration at 10 g is approximately 25 ms and falls within the voluntary human exposure area in the EIBAND curve.



HEADWARD ACCELERATION LIMITS

It is desirable to design a seat to absorb the maximum energy possible during a crash without injuring the seat occupant. To accomplish this, the seat is designed to limit the maximum acceleration transmitted to the occupant to a value not to exceed the human tolerance level. The chart below gives tolerance levels below 15 g's that could be used to limit acceleration values in the vertical direction in seat design. Values of 10 g at 25 ms were measured in the transport seat and it can be seen that these values fall within the voluntary human exposure levels in the chart.



CONTROLLED IMPACT DEMONSTRATION
SEAT/CABIN RESTRAINT SYSTEMS - FAA

Richard A. Johnson
Federal Aviation Administration
Technical Center
Atlantic City Airport, New Jersey

NASA/FAA Government/Industry CID Workshop
NASA Langley Research Center
April 10, 1985

INTRODUCTION

Five years ago, the FAA initiated a program to determine the adequacy of existing occupant restraint system protection. This effort began with a contracted industry study of survivable accidents and extended to over 100 systems and full-scale aircraft drop tests performed at the FAA Civil Aeromedical Institute (CAMI) and the FAA Technical Center. These studies and related tests formed the basis for the development and selection of the FAA onboard experiments which concerned occupant seta restraint and the retention of mass items in the cabin. I will briefly discuss these experiments and related instrumentation as part of the overall pretest discussion.

SEAT/CABIN RESTRAINT SYSTEMS--FAA

- EXPERIMENTS
- INSTRUMENTATION

OBJECTIVE

The FAA restraint system experiments consisted of 24 standard and modified seats, 2 standard galleys and 2 standard overhead compartments. Under the CID program, the experimental objective was to demonstrate the effectiveness of individual restraint system designs when exposed to a survivable air-to-ground impact condition. What we were looking for was the performance exhibited by standard and modified designs, performance differences resulting from their installed cabin location, and interrelating performance demonstrated by test article and attaching floor and/or fuselage structure.

DEMONSTRATE THE EFFECTIVENESS OF EXISTING AND IMPROVED SEAT/CABIN RESTRAINT SYSTEM CONCEPTS

SEAT/RESTRAINT EXPERIMENT

Of the 24 seat experiments, 11 were standard inservice designs of single, dual and triple occupant configurations. The remaining 13 seats were modified versions featuring improved energy absorption, higher strength and increased floor track retention as [C] in which 4 different seat modifications were developed [C,G,I,K]. Also, in the case of 9 seat designs, there were 2 test articles each of which were arranged in two separate fore and aft groupings in the cabin.

STANDARD		MODIFIED	
A - TRIPLE PAX.	(2)	C′ - (C) W/FITTING	(1)
B - TRIPLE PAX.	(2)	E - (A) E/A LEG/BRACE	(2)
C - TRIPLE PAX.	(2)	F - (B) E/A BRACE	(2)
* D - DUAL PAX	(2)	G - (C) E/A BELT	(2)
J - TRIPLE PAX.	(1)	H - (B) E/A LEG	(2)
* A - DUAL F/A	(1)	I - (C) E/A LEG	(2)
D - SINGLE PILOT	(1)	* K - (C) E/A LEG	(1)
		A′ - (A) STRENGTHEN	(1)
	11		13

* AFT FACING

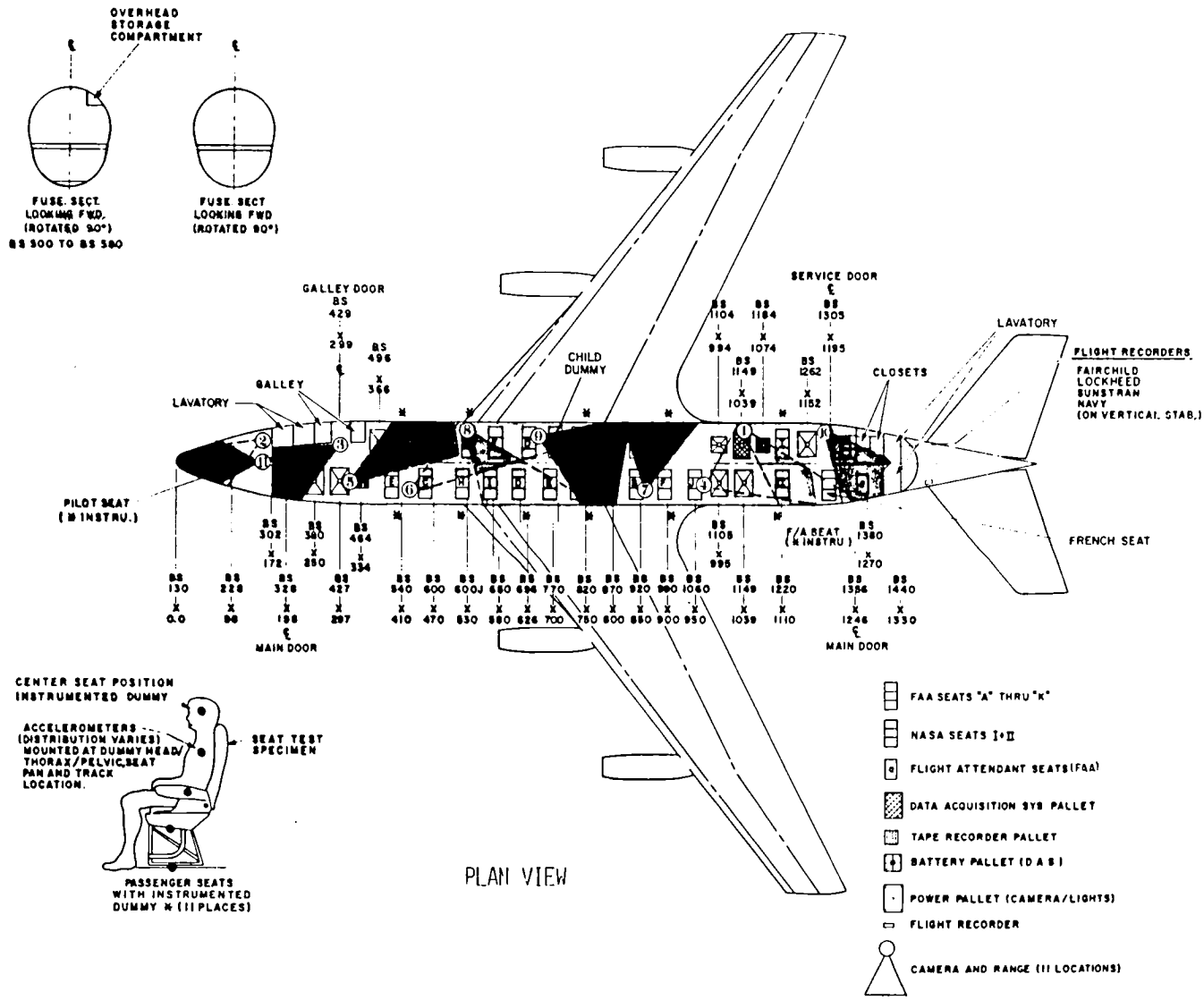
CABIN RESTRAINT EXPERIMENTS

The other restraint system experiment consisted of 2 standard overhead stowage compartments and 2 galley modules. Again, we are concerned with the retention of stowed equipment and carry-on articles. The overhead compartments were loaded with test weights up to their maximum capacity, and each of the galleys was filled with test articles: aft with normal galley equipment, forward with hazardous material test packages (an experiment sponsored by the DOT Office of Hazardous Materials).

- STOWAGE COMPARTMENTS: (2) STANDARD OVERHEAD COMPARTMENTS CONTAINING TEST WEIGHTS
- GALLEYS: (2) STANDARD FORE/AFT GALLEYS CONTAINING HAZARDOUS MATERIAL TEST PACKAGES/GALLEY EQUIPMENT

PLAN VIEW

This is a plan view of the aircraft showing the distribution of the FAA seat/cabin restraint system experiments in gray (beginning in the forward cabin section with the pilot seat, forward flight attendant seat, two groupings of standard and modified passenger seats and aft flight attendant seat). Also shown are the galleys and overhead compartments. The instrumentation varied between each of the test articles. This side view position shows a typical accelerometer installation involving floor, seat, and instrumented dummy. The 11 numbers identified throughout the cabin area represent camera positions from which high-speed movies were obtained during the test sequence.



INSTRUMENTATION

A breakdown of instrumentation and distribution is shown here beginning with 11 instrumented type anthropomorphic dummies and 185 sensors which provided for acceleration and load measurements at the various experiment and associated structure locations. The onboard cameras provided additional coverage of these experiments, including the areas of cabin which were not instrumented.

• DUMMIES: (TOTAL)	(66)
INSTRUMENTED	11
NON-INSTRUMENTED	55
• ACCELEROMETERS: (TOTAL)	(156)
DUMMY	46
SEAT	69
FLOOR (AT SEAT)	38
STOWAGE COMPARTMENT	3
• LOAD CELLS: (TOTAL)	(29)
LAP BELT	22
SHOULDER HARNESS	4
STOWAGE COMPARTMENT	3
• ONBOARD CAMERAS: (TOTAL)	(11)
COCKPIT	2
CABIN	9

SEAT/RESTRAINT MODIFICATIONS

As previously stated, seat modifications were aimed at improving the energy absorbing capability and floor track retention with consideration given to floor deformation. An emphasis was placed on the development of such improvements within acceptable cost/weight limits, while at the same time maintaining current practices relative to underseat stowage, seat pitch and overall accessibility.

- IMPROVED ENERGY ABSORPTION DESIGN
- IMPROVED FLOOR RETENTION DESIGN

SEAT DESIGN CRITERIA

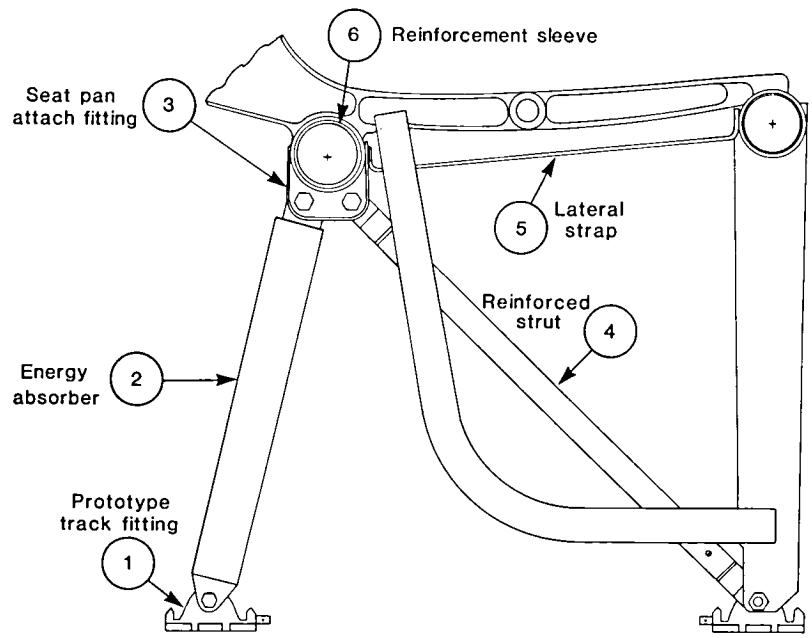
The criteria applied to the design of each of the seat modifications were established on the basis of previous accident studies and data obtained from current inservice seat tests, as well as full-scale tests, such as the L-1649. The selected criteria are shown next to current FAR 25 minimums, and include a triangular 18G peak dynamic pulse in the longitudinal direction and a 10G static load in the vertical and lateral directions.

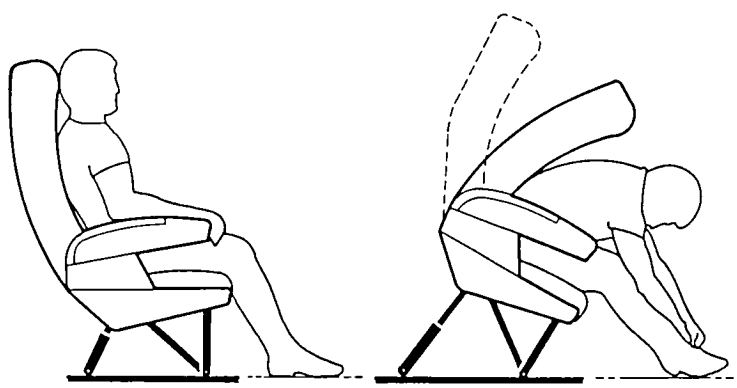
	STANDARD (FAR 25)	MODIFIED
FORWARD	9.0 G	18 G*
DOWNWARD	4.5 G	10 G
SIDEWARD	1.5 G	10 G

* DYNAMIC TRIANGULAR PULSE 35 FPS

TYPICAL SEAT RESTRAINT MODIFICATION

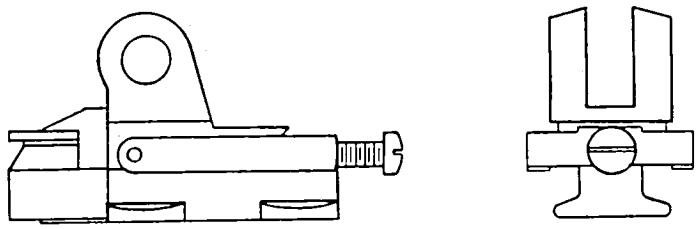
The concept of using energy absorption devices to limit the loads of both the occupant and floor attachment structure is not new. However, in many cases such devices developed in the past resulted in heavier, more complex seat configurations. This represents a typical CID seat modification which included the replacement of two aft legs with special energy absorber devices. As shown in the side view, other modification changes included strengthening various parts of the seat structure and increasing floor retention by adding improved track fittings to each of the four seat legs.



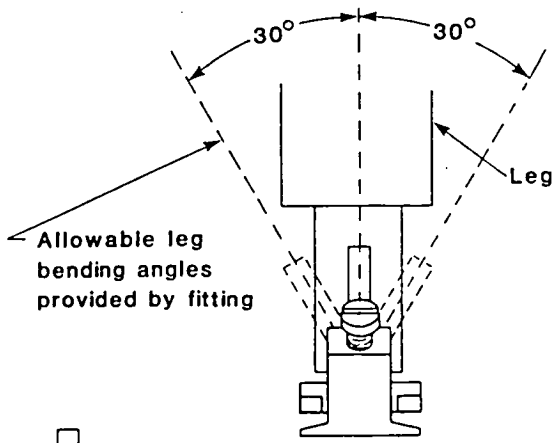


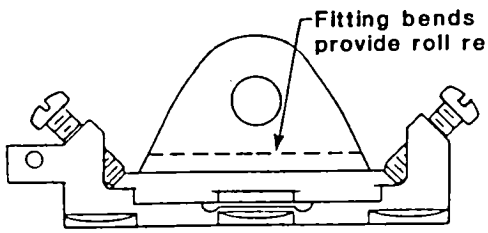
TRACK FITTINGS

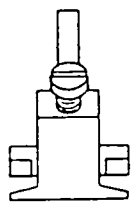
The fitting illustrated in the upper left hand corner is a standard rear leg type fitting which normally contains two interlocking track studs and a leg attachment point which allows release around the pitch axis. Unlike standard forward leg fittings which are represented by a single non-lock stud only, the standard rear leg fitting is designed to resist shear loads in the longitudinal direction. As shown below, the modified seats were fitted with these improved fittings on all four legs. These fittings featured a stronger triple lock stud design which included plastic hinges that allowed for release about both the pitch and roll axes. The combination of the multiple release type fitting and the aforementioned energy absorbing legs assured improved seat-track retention during realistic conditions of adverse floor deformation.



STANDARD TRACK FITTING



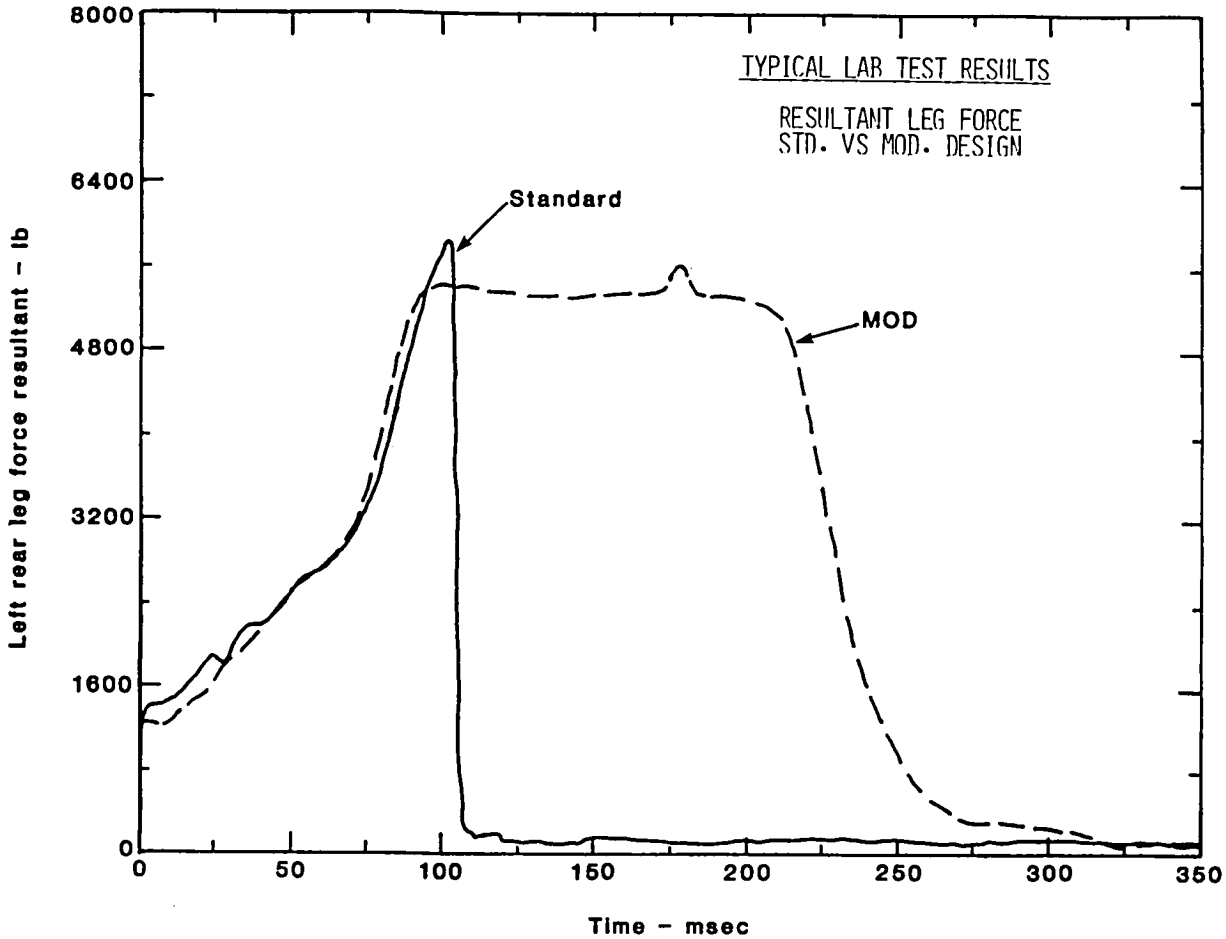




PROTOTYPE TRACK FITTING

TYPICAL LAB TEST RESULTS

This typifies the dynamic test results between one of the CID standards and a modified seat design. Shown are the window-side leg forces versus pulse duration. At a 9G 50-ft/sec dynamic pulse, the leg of the standard seat detached from the track fitting at 5900 lbs. The energy absorbing leg of the modified design stroked 3 inches and limited the load on the fitting to 5370 lb for 110 seconds. No failure was observed on the modified seate(weight increase due to the energy absorbers was 2 percent).



DATA REDUCTION, MANAGEMENT, AND ANALYSIS SOFTWARE FOR CID

Charles W. Davis
System Development Corporation
Hampton, Virginia

NASA/FAA Government/Industry CID Workshop
NASA Langley Research Center
April 10, 1985

OVERVIEW OF DATA REDUCTION SYSTEM

In an overview of the Data Reduction System, one must look at 3 major steps. First, the raw data tapes were selected from the onboard recorders. These tapes should provide the best quality data for the data reduction software system. These tapes contained 352 channels of data, plus the monitor channels recorded in 8 bit Pulse Coded Modulation (PCM) words. The next step consists of transcribing the PCM tapes from 8 bit serial digital data to 8 bit parallel digital data. This puts the data in the correct format for processing. The transcription process was accomplished here at LaRC in the Central Data Transcription Facility (CDTF). The last step in this 3 step process is to process the data through the reduction system (reference 1) developed for the Impact Dynamic Research Facility in the early part of 1980.

- PCM tapes (on board recorders)
  - 352 channels plus monitor channels
  - 8 bit words
- Digital transcription (central data transcription facility at LaRC)
  - Convert raw data from 8 bit serial digital data to parallel digital data
  - Conversions done for prefires and in flight data
- Data reduction processing system for experimental and analytical data
  - Developed for impact dynamics research facility

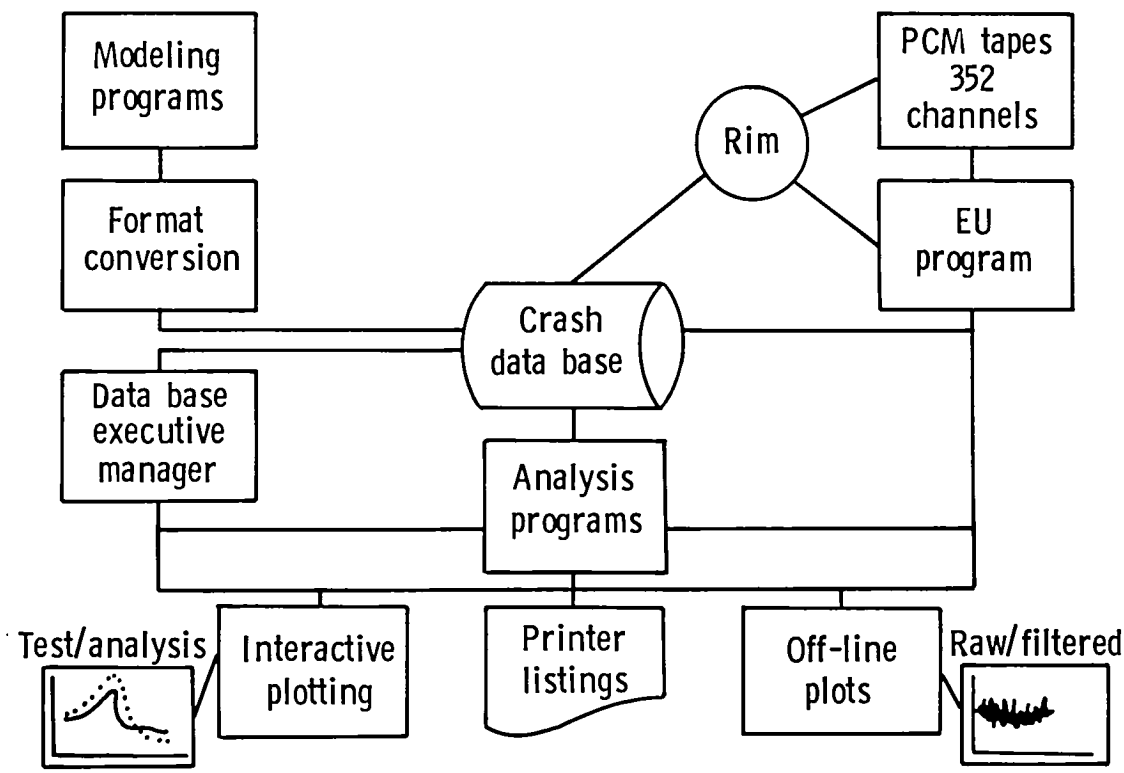
DATA REDUCTION PROCESSING SYSTEM DESIGN CRITERIA

In the design phase of the Data Reduction Processing System certain criteria were set forth to insure the processing system would be simple, fast, and give accurate results. The criteria set forth were: Program units perform one and ONLY one function. Each unit must be able to have interaction between any other program units. This makes multi program unit processing and job stepping possible. Program unit processing is order independent. Using these criteria the System was easy to design and implement, also making any modification to the processing system simplier. Before the new data reduction system was implemented it was taking approximately five weeks for turnaround, under the new system the same data can be processed in approximately one week. This means a 80 percent saving in time and personnel.

- Program unit performs one function
- Interaction between program units
- Multi program unit processing
- Independent processing order
- Simple, fast, and accurate results

DATA REDUCTION PROCESSING SYSTEM

This is the flowchart showing the Data Reduction Processing System. The flow from the top right shows the experimental data. The Raw Data PCM Tapes goes into the engineering units (EU) program. A listing of the calibrations was obtained from RIM database. These calibrations were applied to the raw data generating EU data. The output from the EU program is placed in the database. The flow from the top left shows the analytical data. This data is run through a modeling programs and the output goes through a format conversion programs to be put in the correct format before being placed in the database. The database can be accessed by the database executive program or any of the analysis programs. See reference 2 for information about the filter or analysis routines. By accessing the database the user can obtain listings, off-line plots, or interactive plots. The database is in a Time History Interface Tape (TIFT) format. This is a CDC internal binary code accessed by unformatted Reads and Writes.



SYSTEM INTERFACE ROUTINES

At present there are two system interface routines available for accessing the database. The first type converts analytical data, like output from the Dynamic Crash Analysis of Structures (DYCAST) program, into the TIFT format so it can be placed into the database. The second type converts the TIFT format into ASCII data for transmittal use. The ASCII data can be blocked at either 80 or 120 characters per record. The disadvantage to the ASCII format is its size. One 1600 BPI, TIFT formatted tape will produce five 1600 BPI, ASCII formatted tapes.

- Analytical data (dynamic crash analysis of structures)
  - Converts analytical modeling data to TIFT format
- Transmittal data (FAA)

  Converts TIFT formatted data to ASCII
  - 80 character blocking
  - 120 character blocking
- Ratio factor
  - 1 TIFT (1600 BPI tape)

    to
  - 5 ASCII (1600 BPI tapes)

ENGINEERING UNITS PROGRAM

The Engineering Units (EU) program, simply reads the digitized data from the tapes obtained from the onboard recorders, and applies the calibration and prefires to each channel. For the B720 CID test the EU program had to deal with 3 different sampling rates. The mainframe data was recorded at 1000 SPS, the subframe data was recorded at 500 SPS, and the voltage monitor channels were recorded at 100 SPS. The prefires or ambient conditions were recorded on the runway just prior to take-off. This would provide the best possible prefire conditions. The output from the EU program is in TIFT format so it can go directly into the database. During the processing of engineering units data the program also does a integration calculation on the accelerometers to produce velocities.

(PCM)

- On board tapes (352 data channels plus monitors
- Sample rates (1000 SPS, 500 SPS, 100 SPS)
- On board tapes digitalized
- Prefires and calibrations applied to raw data
- Engineering units output in TIFT format
- Integration calculations

The database executive program was designed to access the TIFT-formatted database. The database executive performs several functions, such as selecting a smaller subset by channels from the larger database, selecting a smaller time subset from a larger database, and performing some limited mathematical calculations on the data during the transfer function. The executive program was designed to run interactively. During execution it is capable of determining sample rate, number of channels, number of records, and the time segment (start and stop times).

(STRIPPR)

- **Selects channels** from larger data base (order independent)
- **Selects time segments** from larger data base
- **Performs limited calculations**
- Summarizes channel information per file
  - Sample rate
  - Number of channels
  - Number of records
  - Time segment

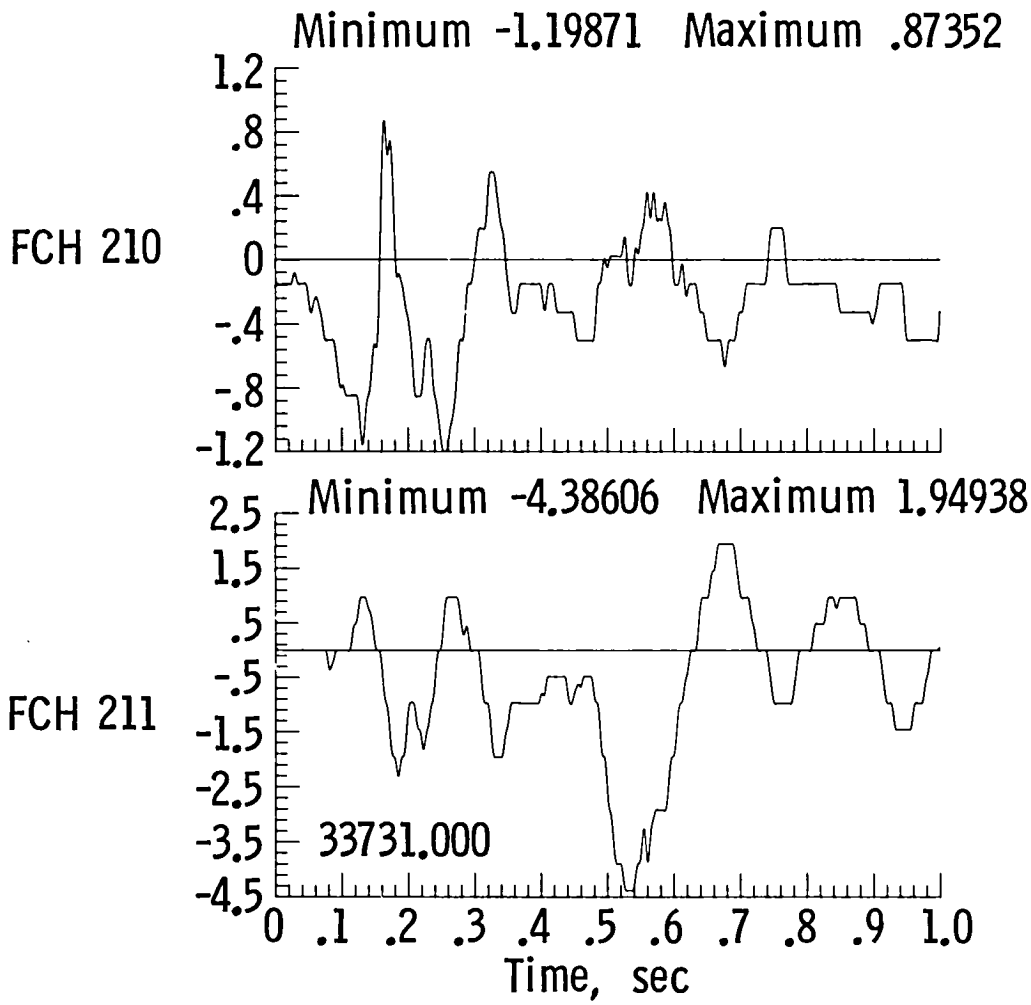
QUICK LOOK PLOTS

The varian fanfold quick look plotting program was designed for quick look working plots. This program has no input directives, it simply reads the database, determines the scales, and plots the data. The graphic output is on page size electrostatic paper processed on an off-line plotting device available at the computer center at LaRC.

- Quick look - working plots
- No input directives
- Page size graphic output (electrostatic)

QUICK LOOK EXAMPLE

Below is an example of the graphic output from the quick look plotting program.



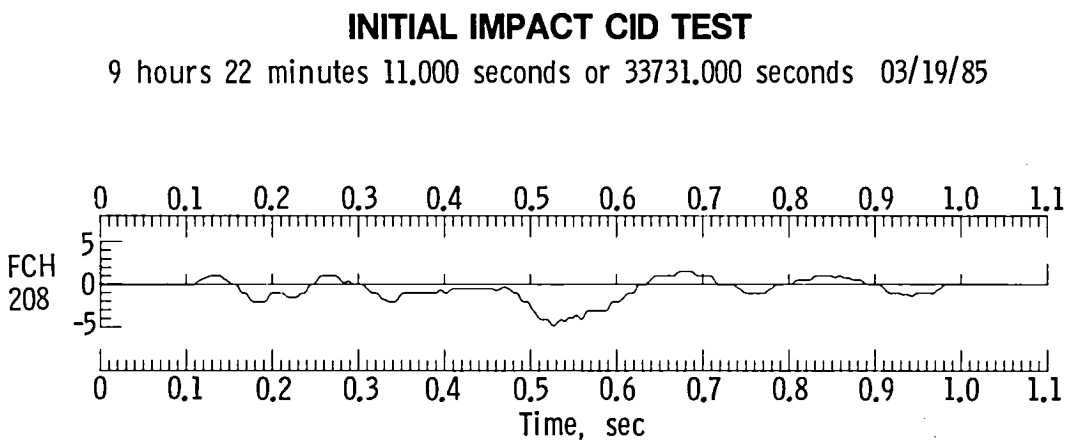
CALCOMP PLOTTING PROGRAM

The calcomp plotting program was designed for final report quality plots. This program permits the user to input the title and scales per inch for each channel. By having the channels plotted on the same scale it allows for a quick and easy comparison of different channels. The graphic output is on either 30 inch or 10 inch paper. The paper color can range from white to several selected grid patterns in red, blue or green.

- Report quality plots
- Input directives scale/inch, title
- Graphic output 30 inch paper - black ink

CALCOMP PLOTTING EXAMPLE

Below is an example of the graphic output from the Calcomp plotting program.



SYSTEM DEVELOPMENT CORPORATION INTERACTIVE GRAPHIC SYSTEM

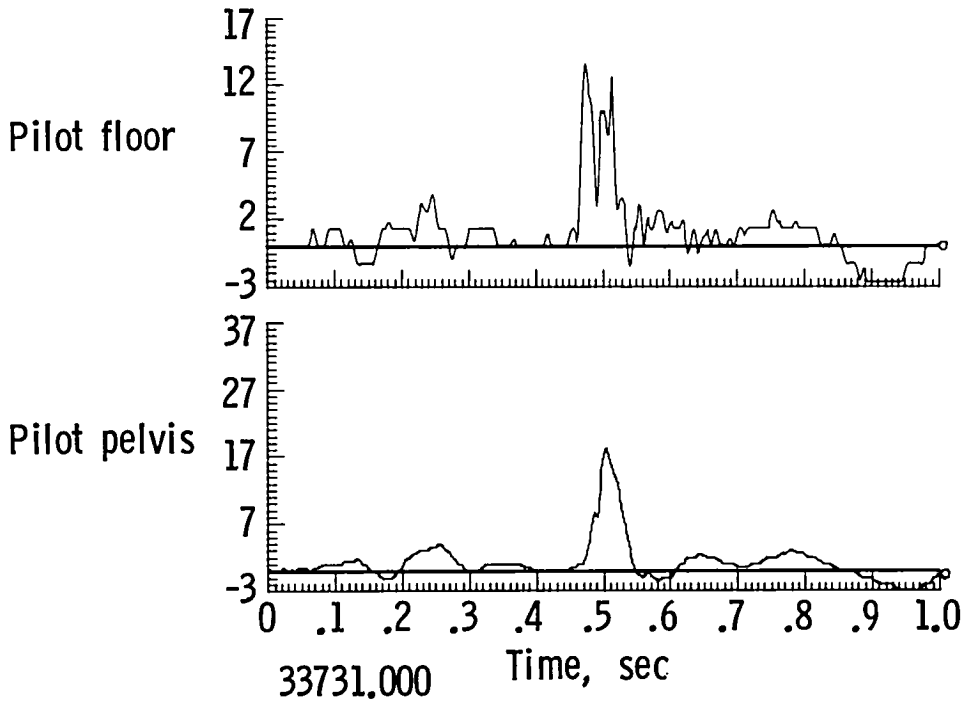
System Development Corporation Interactive Graphic System (SDCIGS) was developed primarily for interactive analysis and displaying of experimental and analytical data. SDCIGS was designed to handle multiple curves on one set of axes. These curves can be from the same test, different tests, analytical vs. experimental data, filter vs. raw data, or any combination the user chooses. SDCIGS also gives the user the option of splitting the screen and displaying data on 1 to 4 sets of independent axes. The multiple curve feature also works in the split screen mode. SDCIGS is great for designing graphic output for publications or reports. The graphic output is mainly an interactive device but the program writes an intermediate file which can be routed to off-line plotting devices.

(SDCIGS)

- Developed for interactive graphics support
- Plot related data on same frame
  - Same test
  - Different test
  - Experimental vs. analytical
  - Raw vs. filtered
- Graphic output - interactive or routed to NASA off-line plotting devices
- Great tool for designing final plots

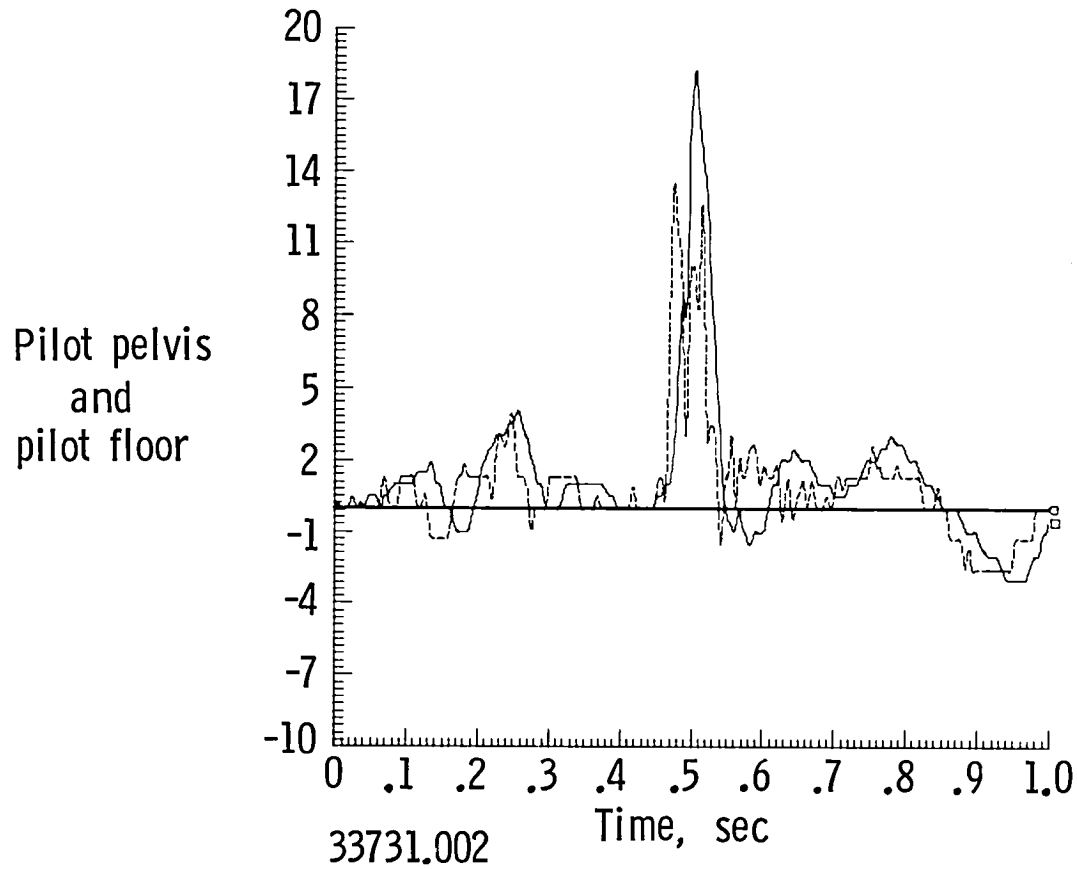
SDCIGS EXAMPLE 1

An example of SDCIGS graphic output comparing two related channels of information in the split screen mode is shown below.



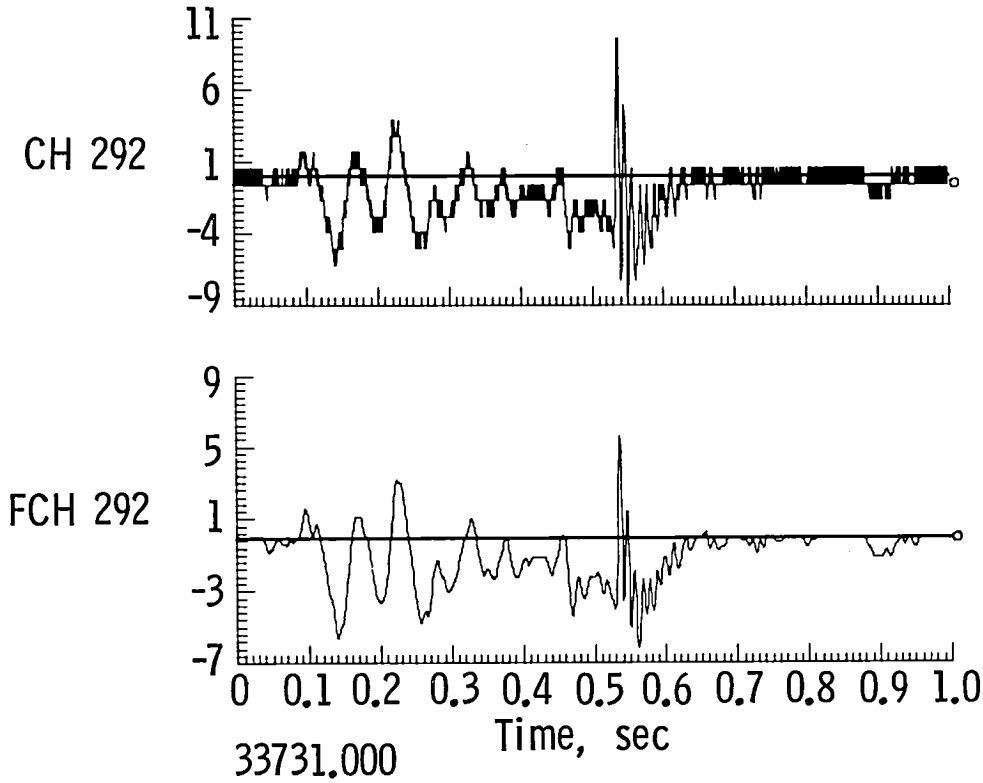
SDCIGS EXAMPLE 2

An example of SDCIGS graphic output comparing two related channels of information on the same axes appears below.



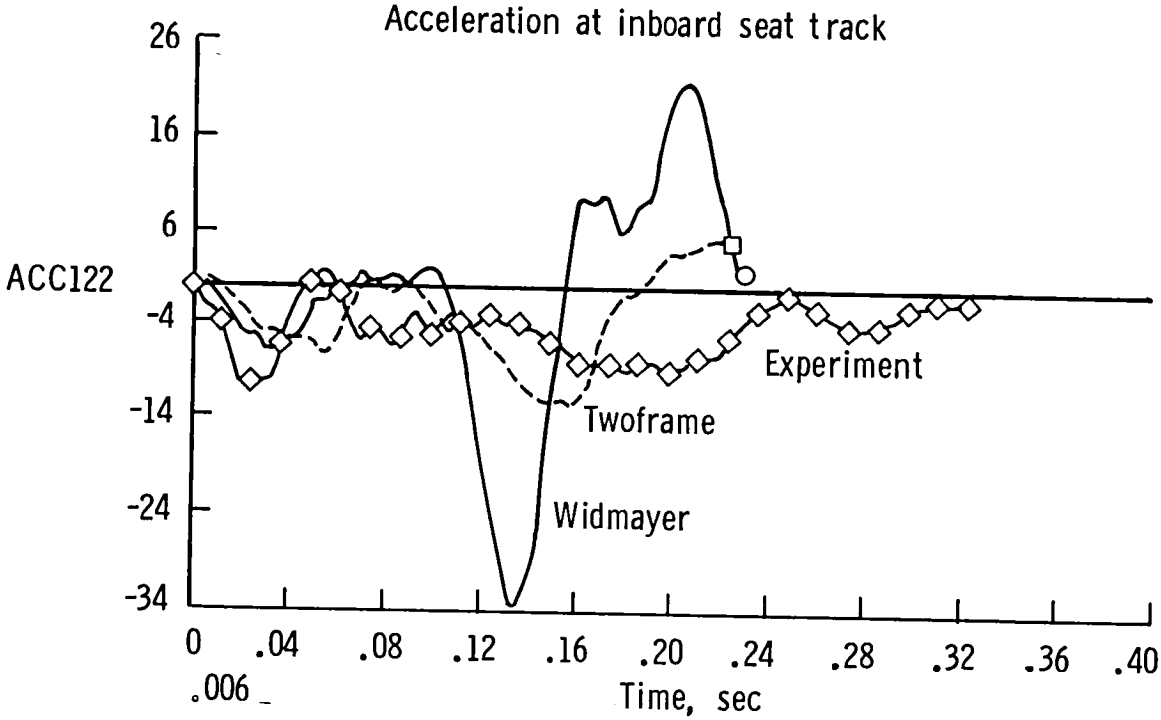
SDCIGS EXAMPLE 3

An example of SDCIGS graphic output comparing raw data vs. filter data in the split screen mode is shown here.



SDCIGS EXAMPLE 4

An example of SDCIGS graphic output comparing one experimental trace vs. two analytical traces is shown below.



REFERENCES

1. Davis, Charles W.: Impact Dynamic Research Processing Guide for Experimental and Analytical Data. NASA Contractor Report 172499, 1984.

2. Fasanella, E. L.: Digital Filtering and Acceleration Pulse Interpretation. Full-Scale Transport Controlled Impact Demonstration, NASA CP-2395, 1986, pp. 103-123.

NASA SEAT EXPERIMENT AND OCCUPANT RESPONSES

E. L. Fasanella
PRC Kentron, Inc.
Aerospace Technologies Division
Hampton, Virginia

NASA/FAA Government/Industry CID Workshop
NASA Langley Research Center
April 10, 1985

NASA EA-SEAT SHOWING INSTRUMENTATION

Figure 1 is a rear view of the NASA energy-absorbing transport seat showing longitudinal and normal (vertical) accelerometers attached to the rear tube of the seat structure. This seat was located on the left side of the aircraft in the rear (body station 1220) at what was designated row 14 in the instrumentation list. On the right side of the aircraft in the same row, there was placed for comparison an unmodified standard seat (NASA standard seat) of the same basic structure, but without an energy absorbing tube. Three dummies were placed in each NASA seat with each center dummy instrumented with accelerometers and lap belt load cells. The instrumented dummies in the EA- and standard seat were designated dummies 14B and 14E, respectively.

The planned crash scenario was for a 17 ft/s sink rate with attitude 1 degree nose up. For this scenario, the rear section of the aircraft near the two NASA seats would impact the ground first, generating a vertical pulse that was expected to cause the energy absorbers to stroke and to provide a comparison between an unmodified standard and an EA-seat.

Two unfortunate events prevented a good comparison: 1) The roll of the aircraft caused wing impact which reduced the vertical velocity and caused the nose to be the first part of the fuselage to impact the ground; 2) A pool fire developed in the rear of the aircraft and both seats were totally consumed by the fire.

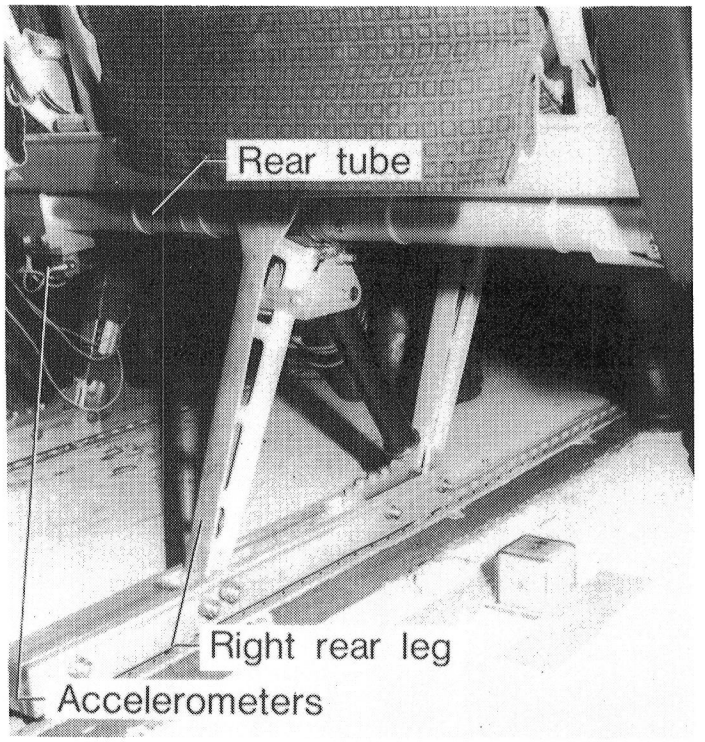


Figure 1

SEATED HUMAN TOLERANCE TO HEADWARD ACCELERATIONS

Figure 2 summarizes seated human tolerance limits to acceleration along the spinal direction with the stopping force pointed toward the head. Accelerations along the longitudinal direction will not be discussed because the CID accelerations were very low in the longitudinal direction. In addition, the human body can withstand greater acceleration in the longitudinal direction. Human tolerance is a subject that creates a lot of controversy, even among the experts. Human subjects cannot be used to determine permanent injury levels, and the accelerations and durations from accident data are only estimated. Well-restrained volunteers have mapped out non-injurious acceleration levels and durations as shown in the figure. Human surrogates such as hogs and chimpanzees have been used to establish estimated human severe injury levels.

In the CID crash, the acceleration levels were low but of relatively long duration. Many pulses exceeded 0.1 seconds and some were of nearly 0.2 second duration. Most of the voluntary exposure was for durations less than 0.1 seconds.

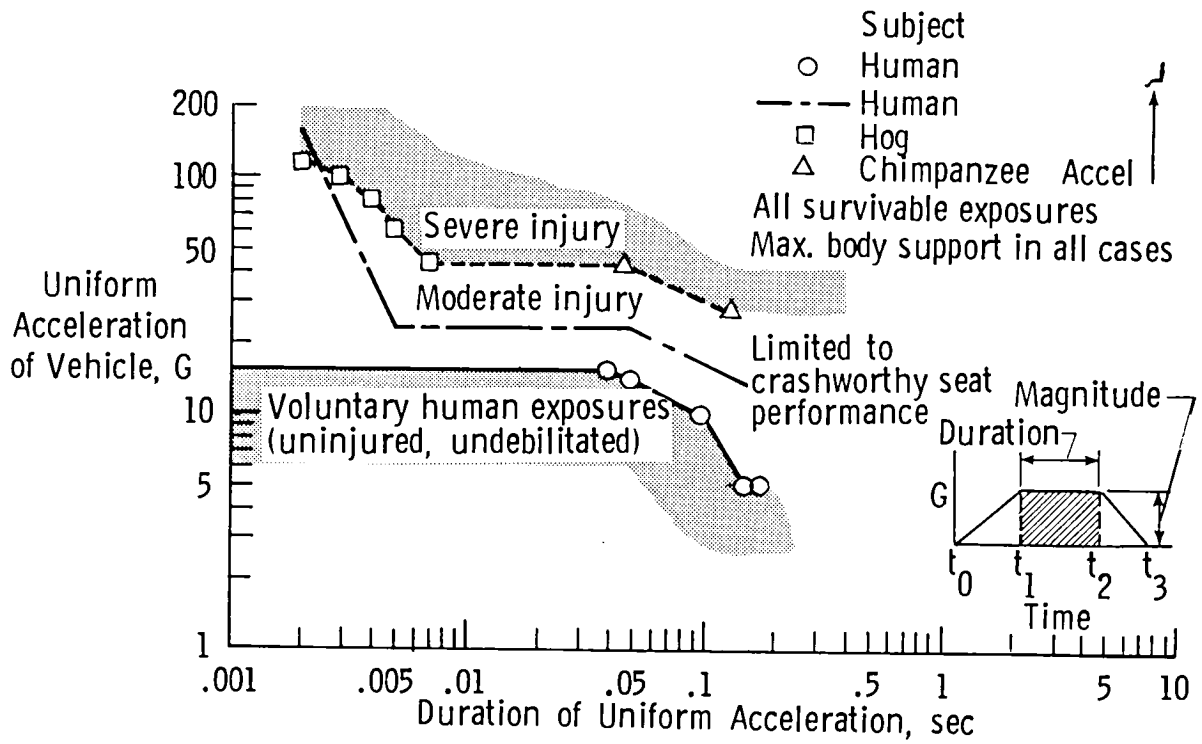


Figure 2

DRI MODEL

The Dynamic Response Index (DRI) model (ref. 1) was developed by the Air Force as an aid for studying injury to pilots who had ejected from high-speed aircraft and for specifying ejection seat performance. In this model, mass M is the upper torso mass, K is the spinal stiffness, and C is the spinal damping constant. The acceleration input (Z) forces the upper body and is generally taken to be the "vertical" seat pan acceleration for the Air Force ejection seat. For our purposes, the normal pelvis acceleration will be used since it is located directly above the seat pan and is the acceleration input that is forcing the upper body mass. Omega is 2 pi times the natural frequency. The equation in figure 3 is simply the equation for a forced simple harmonic oscillator. The DRI can be shown to be the maximum output acceleration of the mass M driven by forcing acceleration Z.

The plot on the left shows spinal injury rate as a function of DRI from cadaver (solid line) and from emergency ejections (dashed line).

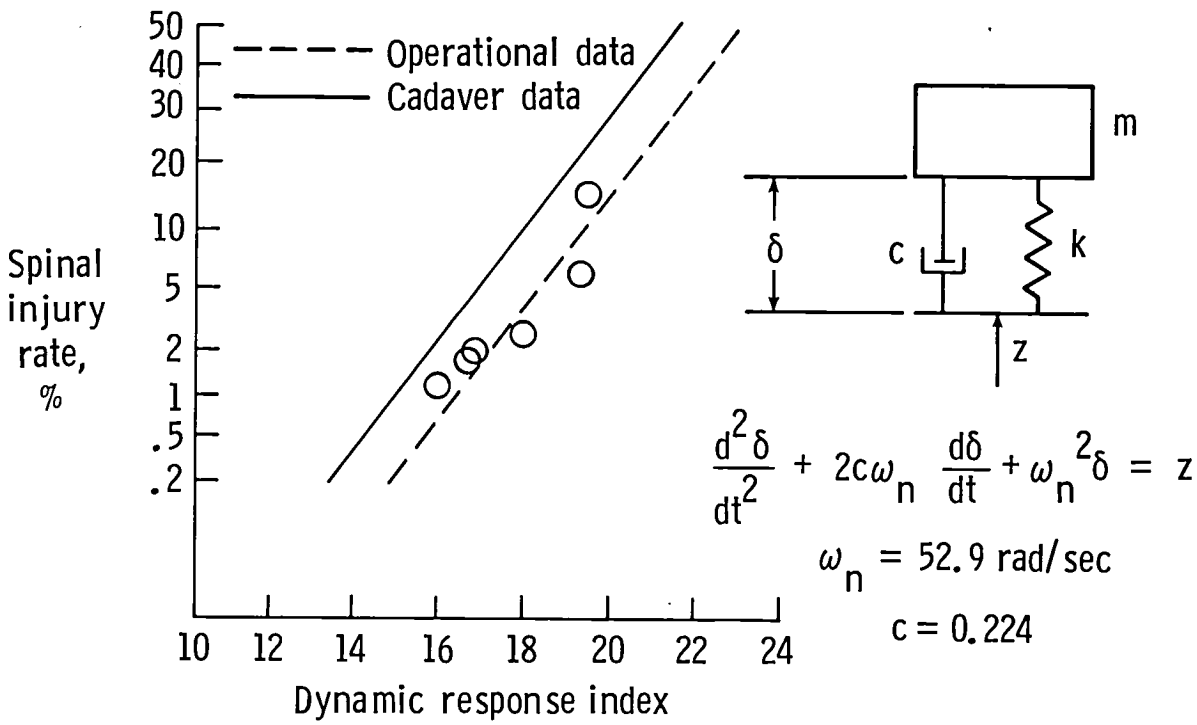


Figure 3

NASA EA-SEAT PERFORMANCE

In figure 4 the dummy (14B) pelvis normal acceleration (along the spine) for the primary ground impact (wing cutter data not considered) is compared to the EA-seat normal (to floor) acceleration. Notice that the dummy pelvis acceleration follows the EA-seat acceleration rather closely except that it lags slightly in time. Also note that the peak acceleration is less than four G's, with the average acceleration down in the 1 to 2 G range and with durations approaching 0.2 seconds. Referring to figure 2, one can see that these levels are quite low and in the non-injurious range. This seat was designed to begin stroking for a normal input acceleration of approximately 8-10 G's. Since the input acceleration is well below that value, the graphite/epoxy energy-absorber would act as a solid member with no stroking.

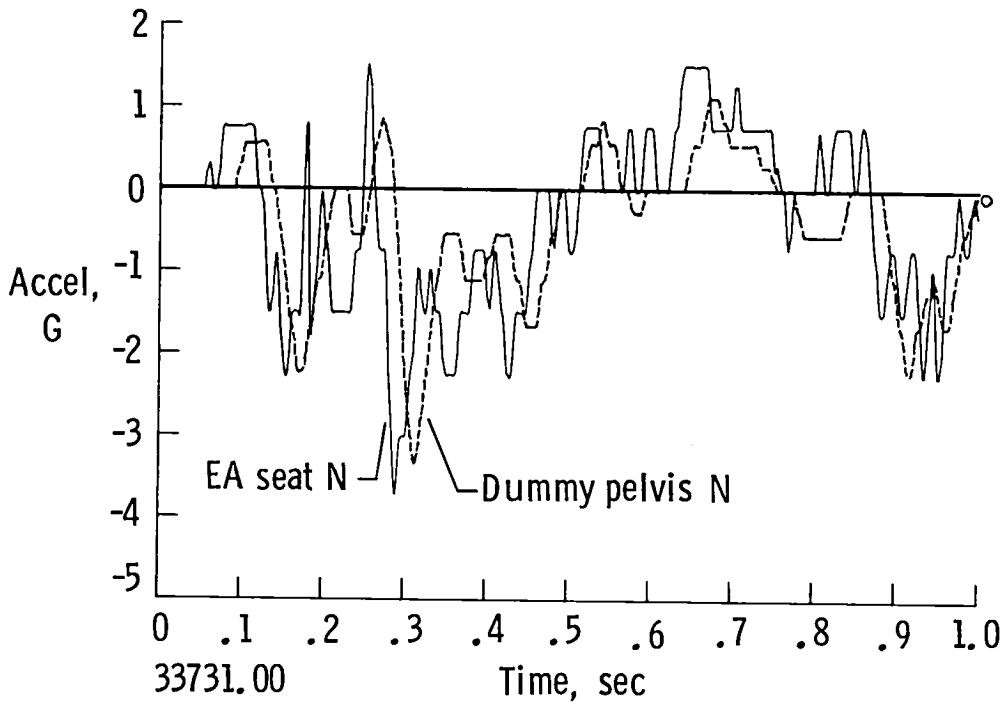


Figure 4

NASA STANDARD SEAT PERFORMANCE

Figure 5 uses the same format as figure 4 except that the NASA standard seat and dummy 14E pelvis accelerations are compared. Notice that the normal dummy pelvis acceleration in the standard seat also follows the seat normal acceleration quite closely except for some time lag. Since the input pulse was below the stroking level for the EA-seat, both seats and both instrumented dummies experienced comparable acceleration pulses.

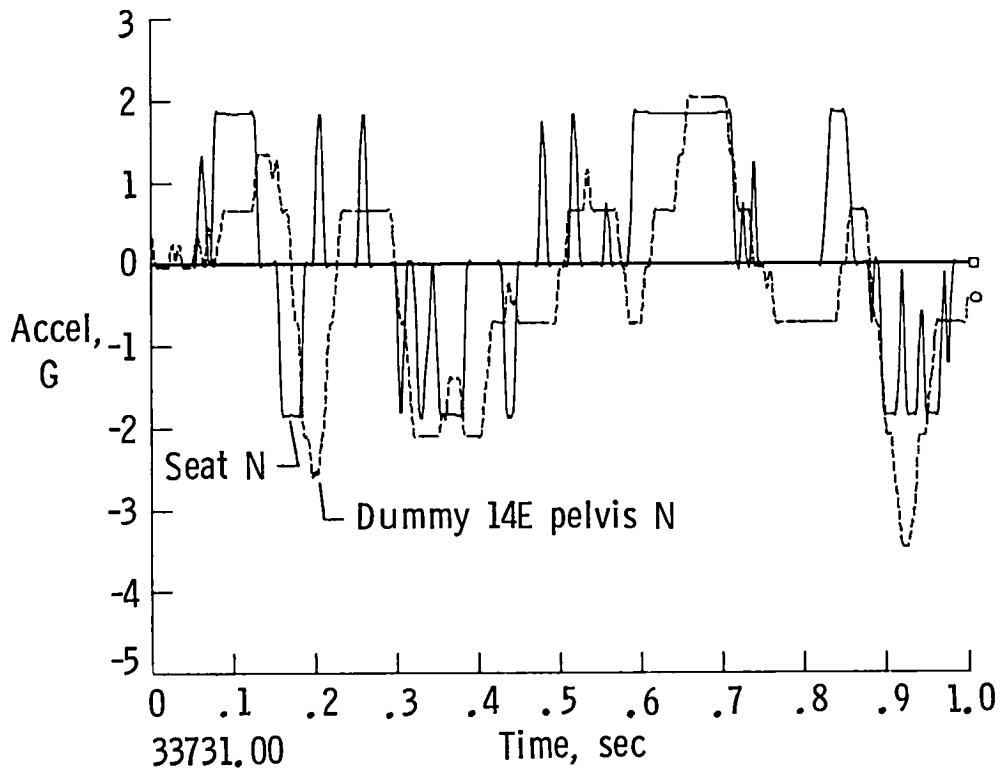


Figure 5

PILOT PELVIS ACCELERATION AND CONTINUOUS DRI

The dummy pilot received the highest normal (spineward) acceleration because the pitch rate imparted by the wing impact caused the aircraft nose to hit first with the highest vertical velocity. Figure 6 shows that the pilot normal pelvis acceleration peaked at 18.3 G's with base duration of about 0.07 seconds. The average acceleration over the 0.07 seconds is about 10 G's. In addition, the continuous DRI was plotted using the pelvis acceleration as the forcing acceleration. The peak DRI lags the input and slightly exceeds it at 19.8. By comparing the peak and average acceleration for 0.07 seconds with the curve in figure 2, one can see that the acceleration borders the moderate injury range. Referring to figure 3, a DRI value of 19.8, would indicate a 10-percent chance of spinal injury.

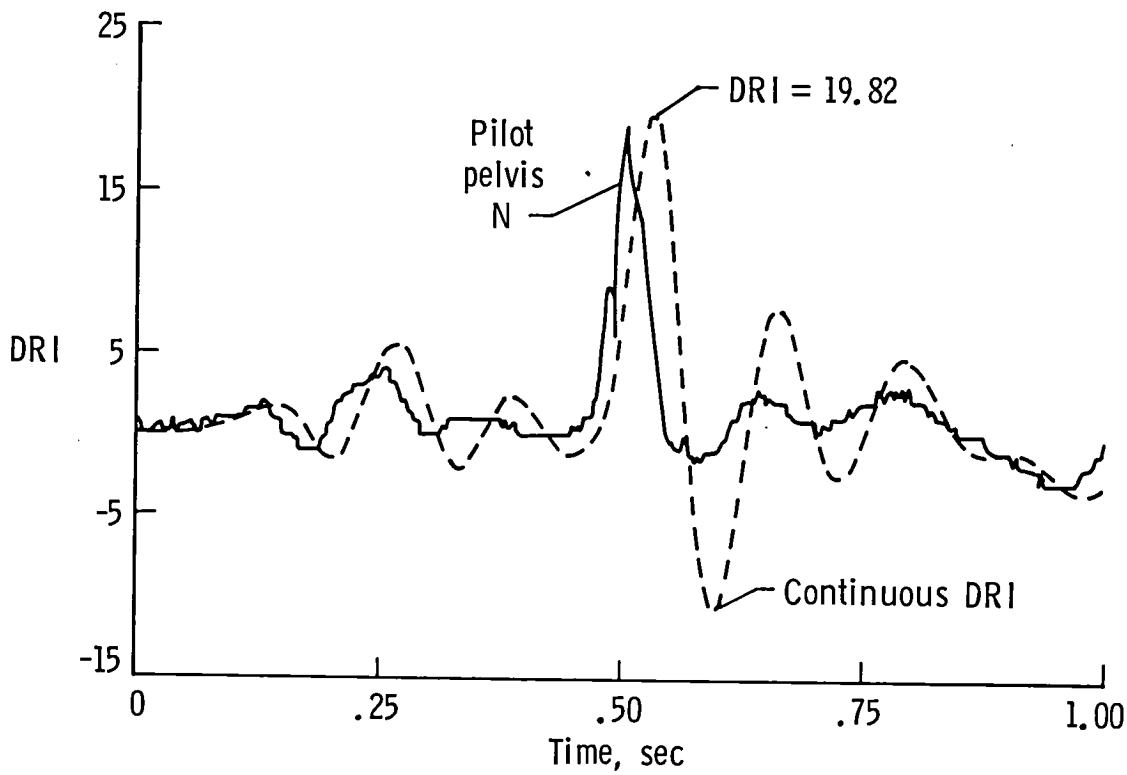


Figure 6

CID PLAN VIEW

Figure 7 is used to show the location of the various seats in the aircraft. The NASA EA- and standard seats were located at body station 1220 which is the 14 th row of seats. The pilot seat is considered row 1 and the attendant's seat near the main door is row 2. The seats at body station (BS) 540 are row 3 etc. The x-coordinate in inches measured from the nose is also given. (For example, the x-coordinate for body station 540 is 410 inches from origin at the nose.)

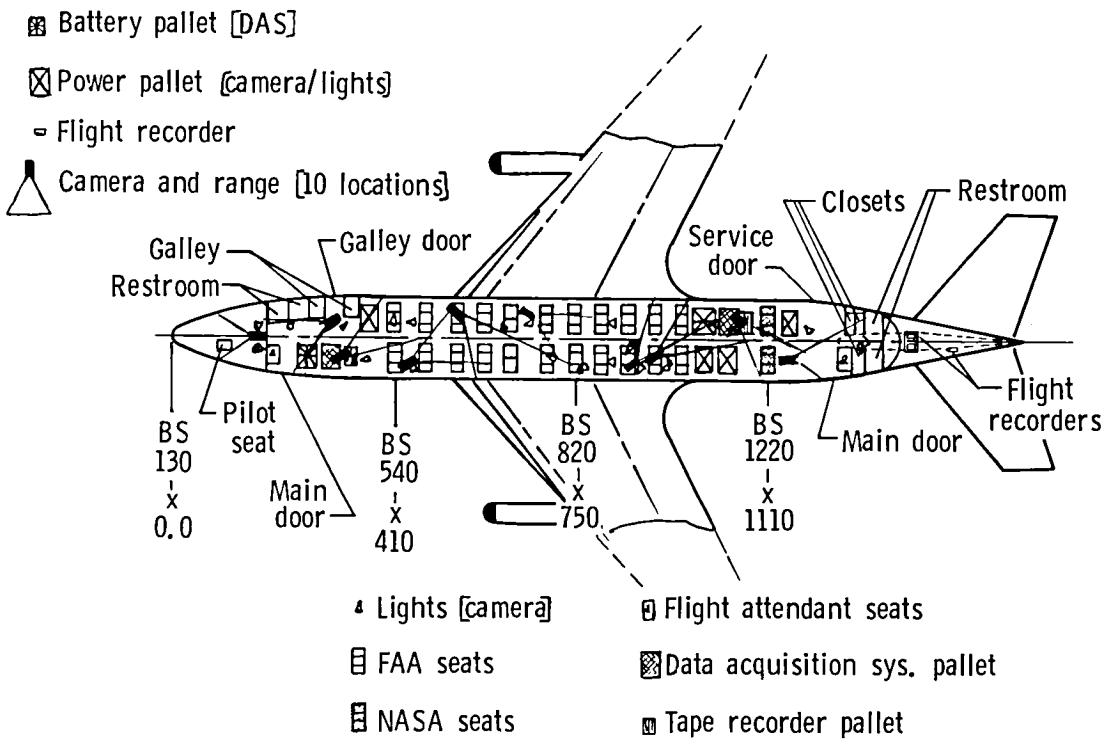


Figure 7

DUMMY OCCUPANT RESPONSE, DRI VERSUS DUMMY LOCATION

The dummy DRI was calculated for each instrumented dummy with good data traces and plotted versus the aircraft x-coordinate. The pilot was the only occupant that received a moderate acceleration. All of the other dummies received mild non-injurious accelerations. The number in front of each data point is the row number. The letter refers to the location from left to right with A being the far left seating position and F being the far right seating position. All instrumented dummies were located in the center position of each triple seat, thus they are in locations B and E (fig. 8).

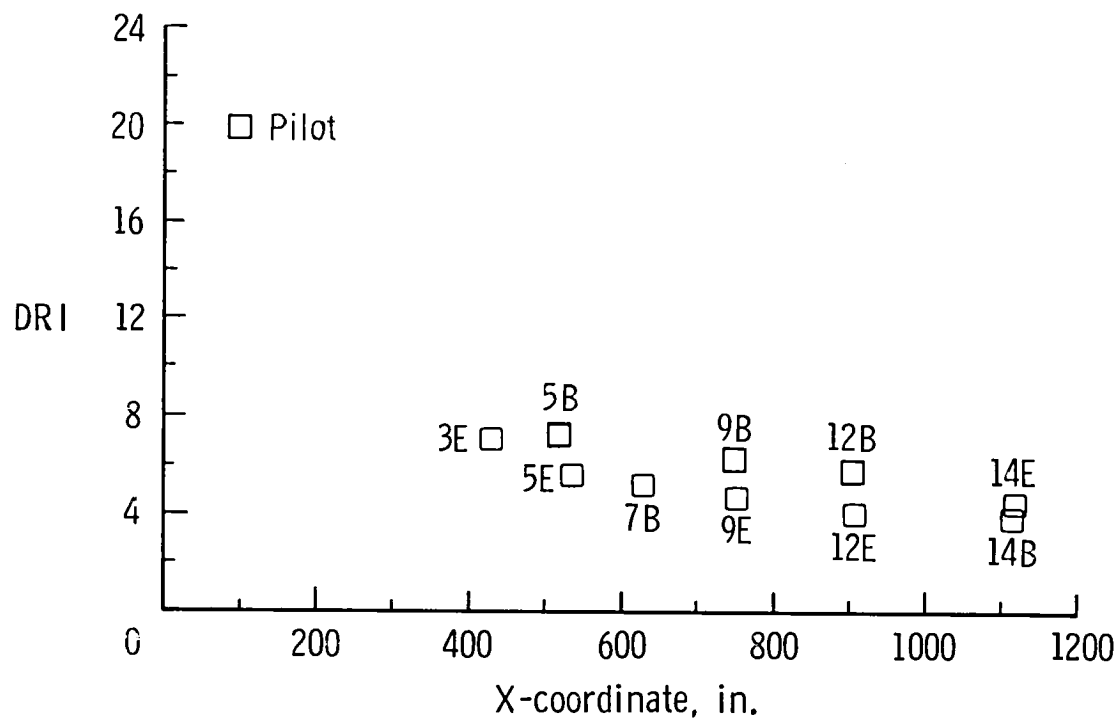


Figure 8

SUMMARY

In summary (fig. 9), the acceleration levels at the rear of the airplane were quite low and were below the stroking threshold of the NASA EA-seat. Therefore, dummies in the standard and EA-seat responded approximately the same.

All longitudinal accelerations were quite low for the primary impact with very low forces measured in the lap belts. The vertical (spineward) acceleration levels measured in the dummies were also relatively low and very survivable from an impact tolerance standpoint. The pilot with an 18 G peak acceleration received by far the highest vertical acceleration and could have possibly received slight spinal injury.

- Acceleration level below stroking threshold for NASA EA seat
- Acceleration levels measured in dummies were relatively low
    - Very survivable from human impact tolerances standpoint
    - Pilot received about 18 G's, the highest measured
- Injury criteria
    - Pilot had chance of receiving spinal injury

Figure 9

REFERENCES

1. Brinkley, James W.; and Shaffer, John T.: Dynamic Simulation Techniques for the Design of Escape Systems: Current Applications and Future Air Force Requirements. AMRL-TR-71-29, Paper No. 2, U.S. Air Force, Dec. 1971. (Available from DTIC as AD 740439.)

2. Military Specification, MIL-S-9479: Seat System, Upward Ejection, Aircraft, General Specification For. Department of Defense, Washington, D.C., March 1971.

STRUCTURAL LOADS PRELIMINARY RESULTS

Emilio Alfaro-Bou
NASA Langley Research Center
Hampton, Virginia

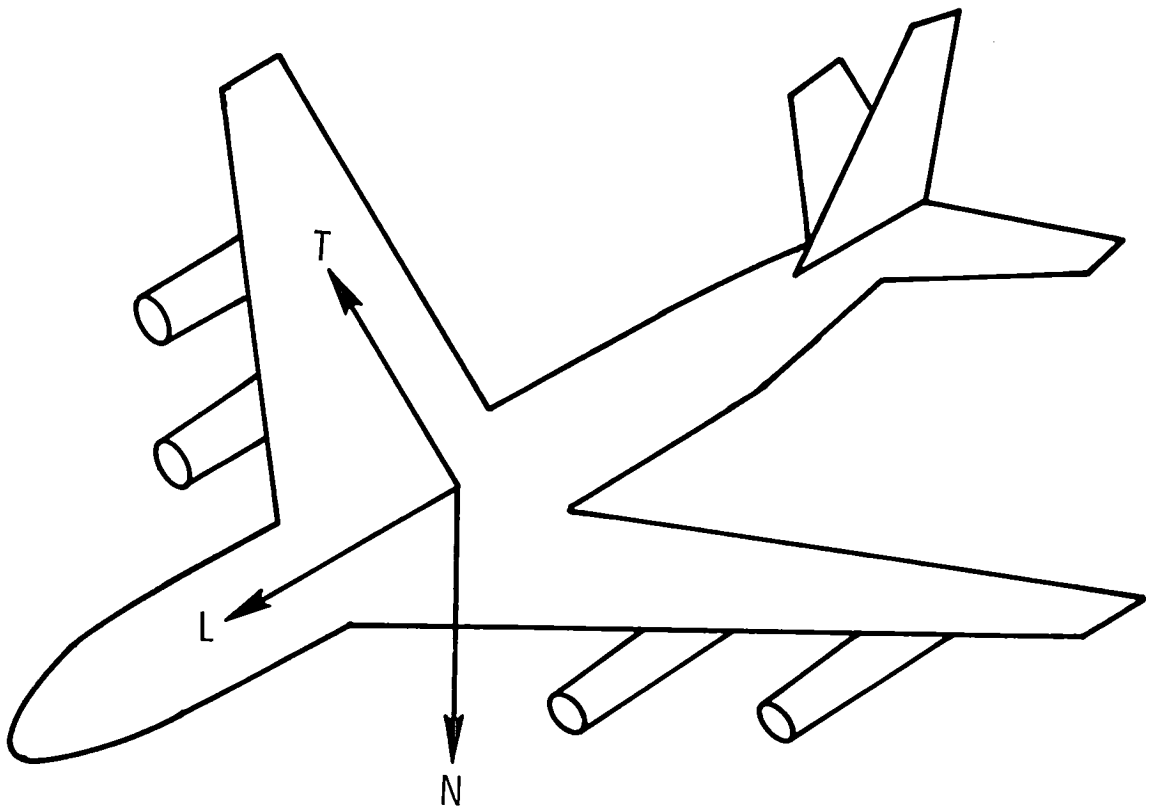
NASA/FAA Government/Industry CID Workshop
NASA Langley Research Center
April 10, 1985

STRUCTURAL LOADS PRELIMINARY RESULTS

Results from the initial impact in the Crash Impact Demonstration will be presented here. The results are preliminary as the data is still being analyzed and may change slightly after the analysis.

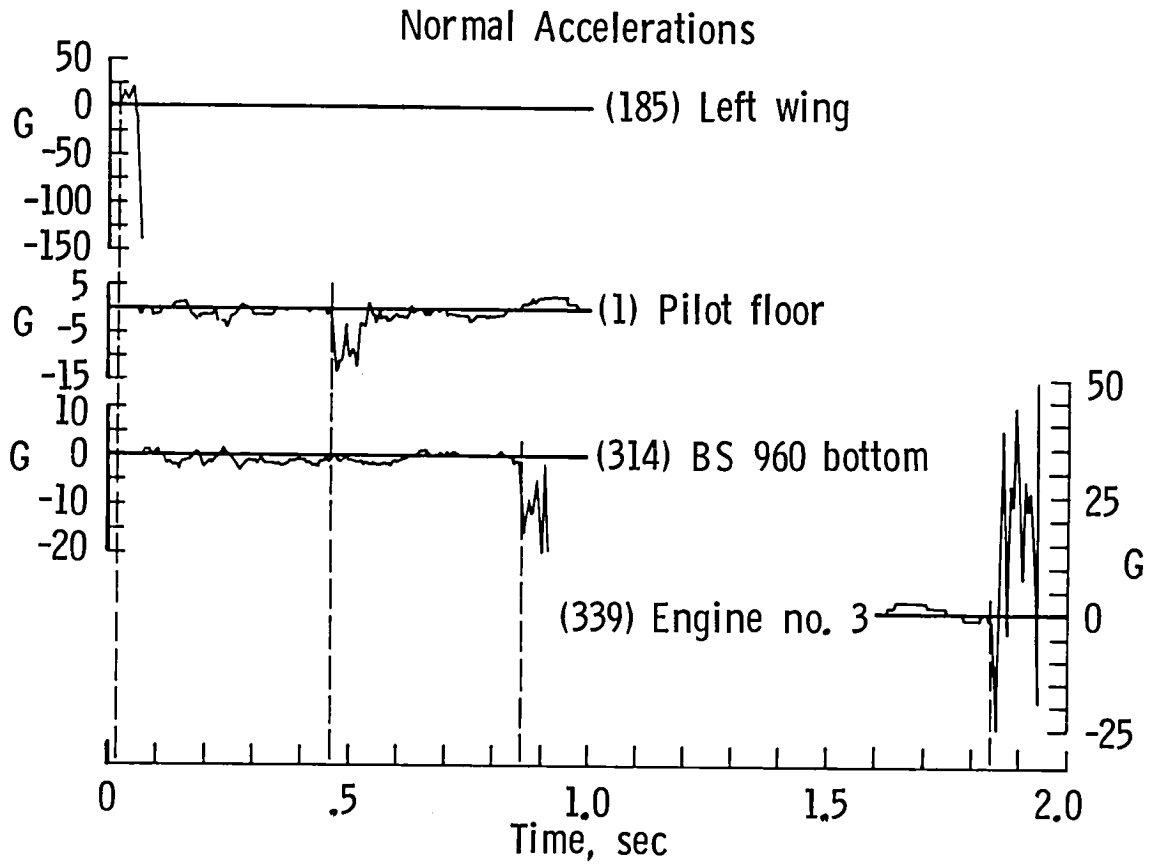
AIRCRAFT COORDINATE SYSTEM

The polarity of the accelerations is determined by the aircraft coordinate system. In the coordinate system selected, the normal acceleration is positive in the downward direction. The longitudinal acceleration is positive in the forward direction and the transverse acceleration is positive to the right.



C.I.D. SEQUENCE OF EVENTS

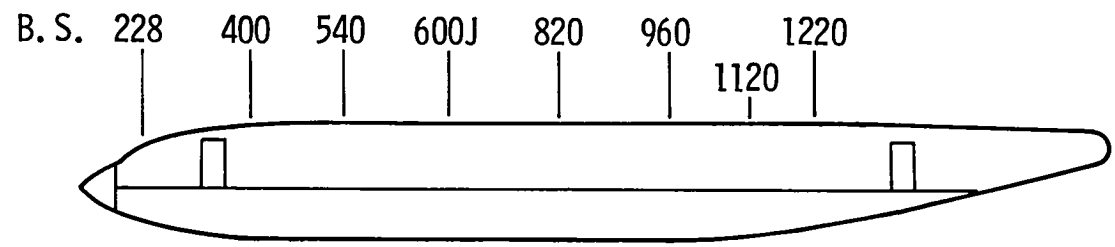
The sequence of events during the impact of the airplane to the ground started with the left wing touching the ground at 9 hr 22 min 11.02 sec in a -12 degree roll. As the airplane continued its descent it pitched down about 3 degrees and the forward cabin at Body Station 380 hit the ground at 11.46 sec. The airplane continued to slide and to rotate downward and the bottom of the fuselage at Body Station 960 hit the ground at 11.86 sec. Sliding continued and the airplane yawed to the left until engine #3 hit the wing cutters at 12.843 sec. The airplane stopped moving at 9 hr 22 min 21 sec.

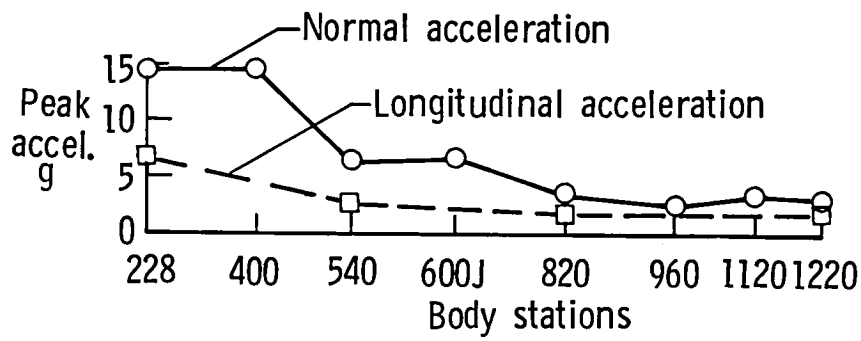


FLOOR ACCELERATION PEAKS DISTRIBUTION

The distribution of acceleration peaks in the normal direction from front to rear of the fuselage shows higher accelerations at the front of the airplane diminishing toward the rear. Under the pilot seat and at Body Station 400 acceleration peaks of 14 g were recorded. Body Station 380 was the area of the fuselage's initial contact with the ground due to the 3 degree pitch down of the airplane. The normal accelerations decrease to 6 and 7 g's in Body Stations 540 and 600J respectively and continue to decrease to less than 5 g toward the rear of the airplane.

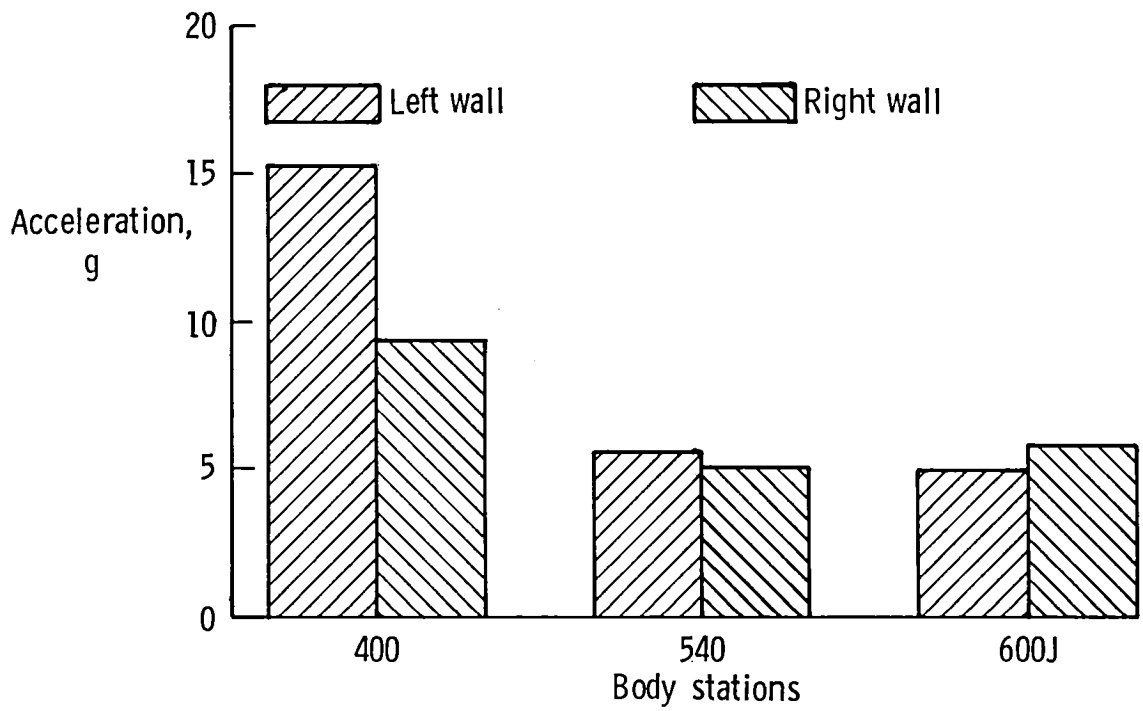
The longitudinal accelerations follow a similar pattern: higher at the front of the airplane (6 g) where the fuselage initial impact with the ground occurred and dimishing toward the rear (2 g).





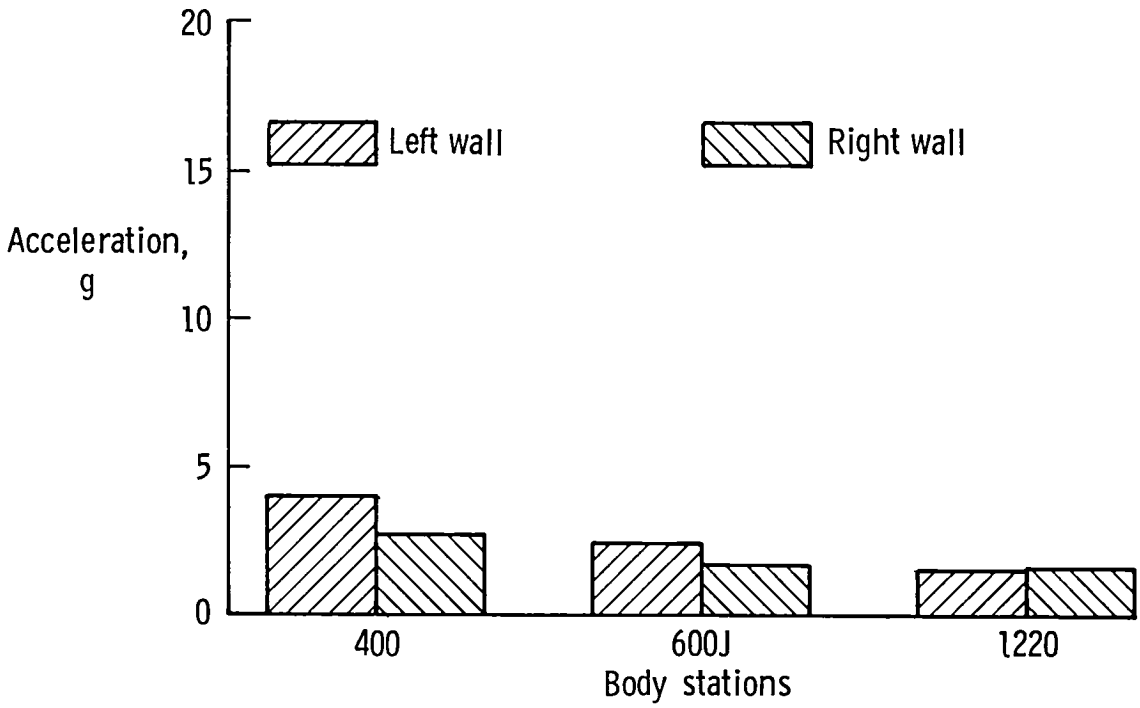
C.I.D. VERTICAL FLOOR ACCELERATION

The left side of the airplane forward of Body Station 540 experienced higher accelerations than the right side. At Body Station 540 and rearward the difference in acceleration between left and right sides is about +1 g. The magnitude of the accelerations seemed to vary with the contact position of the fuselage with the ground. The airplane had a negative roll (left) and the fuselage impacted pitched down. At this time the acceleration on the left side at the point of impact is higher. As the fuselage continues to pivot down and rotate to the right the difference in acceleration between right and left sides becomes smaller.



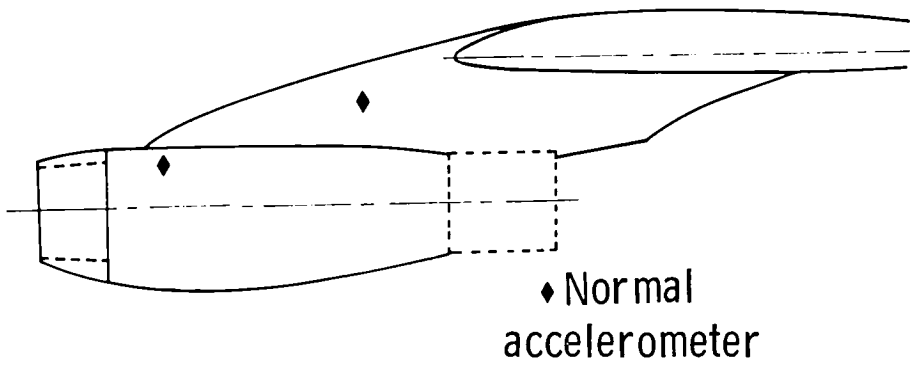
C.I.D. LONGITUDINAL FLOOR ACCELERATION

Similar to the pattern of the vertical accelerations, the longitudinal accelerations are also higher on the left side toward the front of the fuselage with the difference between left and right values diminishing toward the rear.



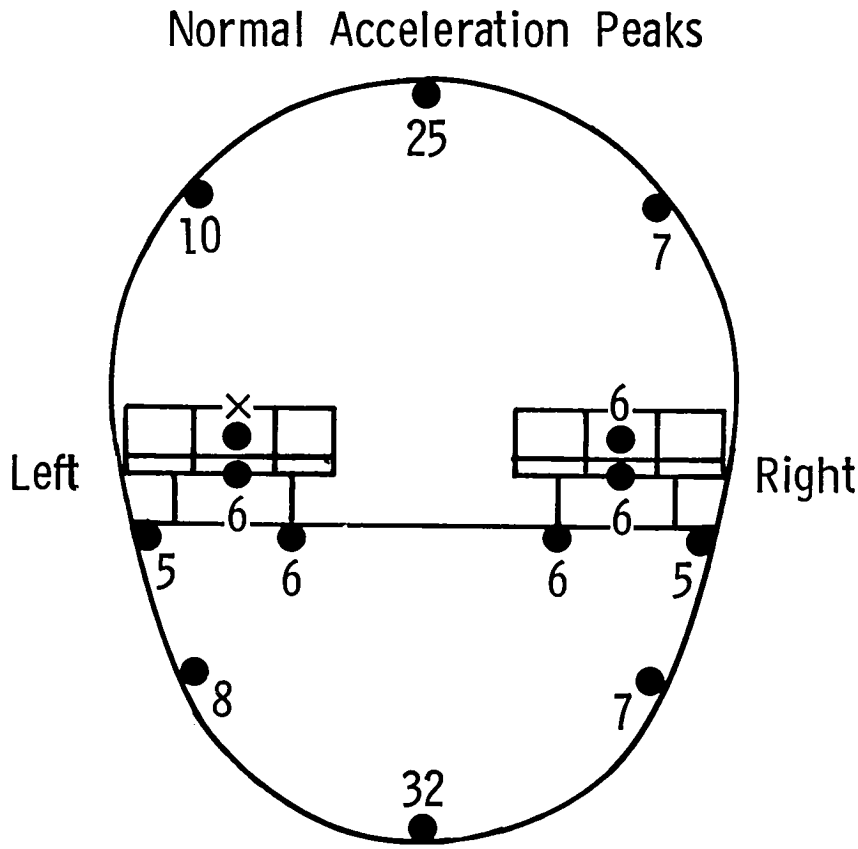
INBOARD NACELLE AND STRUT

On the left wing an acceleration peak of 36 g was obtained toward the front of the inboard pylon and 150 g in the rear of the pylon. On the right wing an acceleration peak of 5 g was obtained toward the front of the inboard pylon and 29 g in the rear of the pylon.



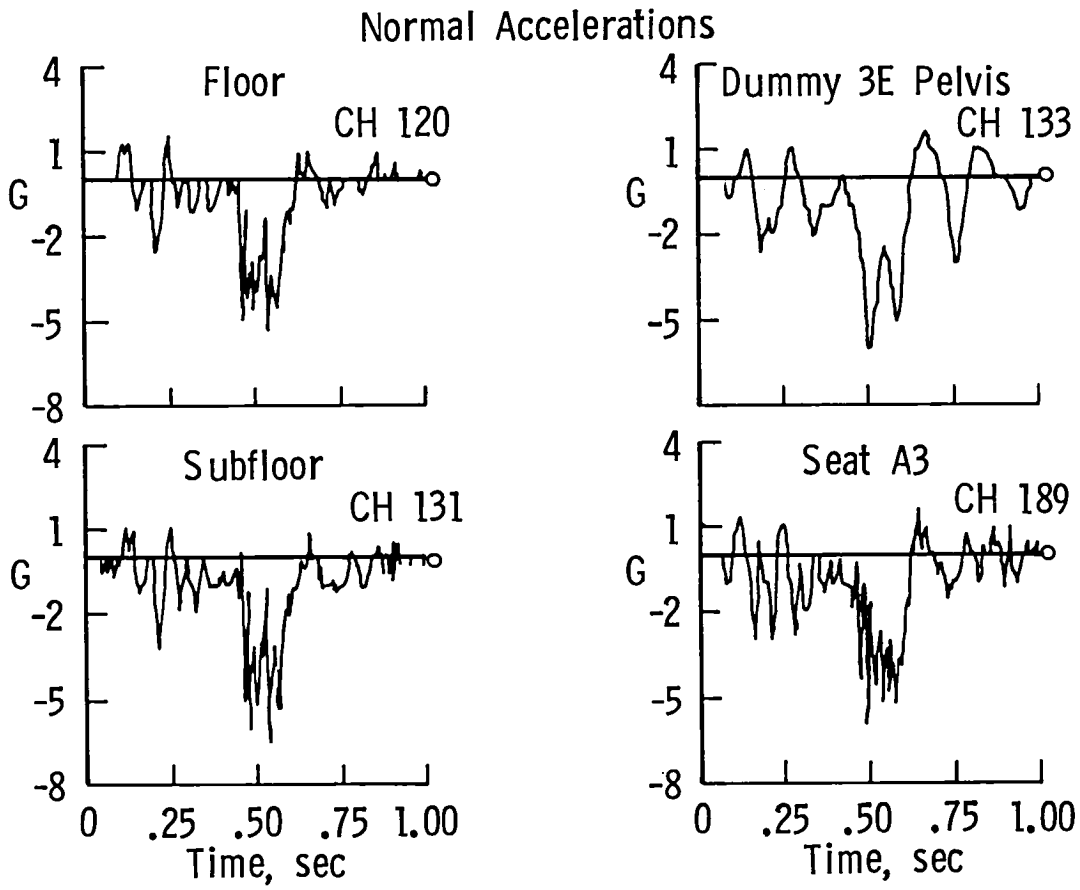
BODY STATION 540

This is a cross section of the instrumented frame at Body Station 540. The values shown are normal acceleration peaks recorded at those locations to determine the transmission of pulses from the ground up. Peak accelerations obtained were 32 g at the bottom, 7 - 10 g at the subfloor and upper wall, 6 g at the floor, and 25 g at the roof of the fuselage. On the seat frame and dummy pelvis, an acceleration of 6 g was obtained.



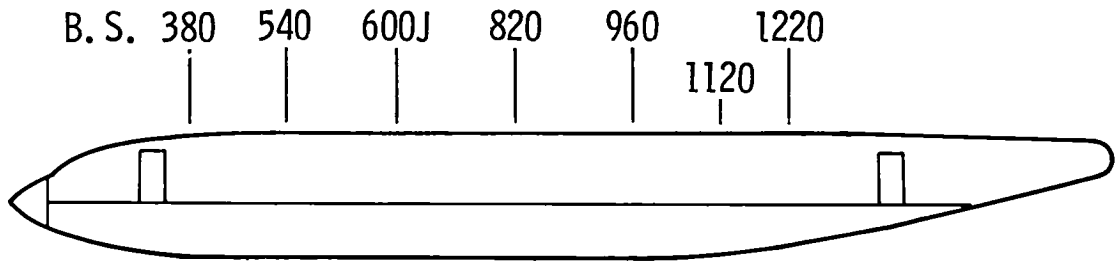
BODY STATION 540: NORMAL ACCELERATIONS

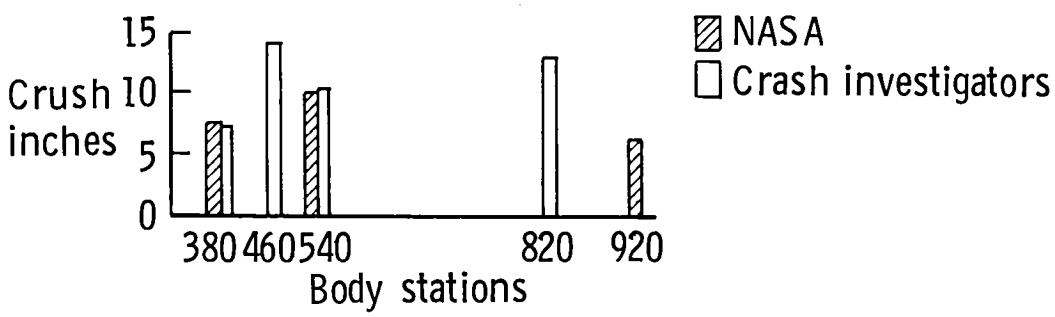
These acceleration time histories were measured on the right side of frame #2 at Body Station 540. The subfloor trace shows acceleration peaks of 7 g. At the floor-wall intersection the acceleration is 5 g. The acceleration on the seat frame is 6 g and at the dummy pelvis the acceleration is 6 g.



FUSELAGE CRUSH (PRELIMINARY)

A NASA team and a crash investigators team measured the crush of the fuselage bottom. The crush measured by the NASA team was 7" at Body Station 380, 10" at Body Station 540, and 7" at Body Station 920. The crush measured by the crash investigators team was 7" at Body Station 380, 14" at Body Station 460, 10" at Body Station 540, and 13" at Body Station 820. Both teams had good agreement in the crush measurements at Body Station 380 and Body Station 540. At the other body stations measurements were made by only one team.





SUMMARY

From a total of 351 instrumentation channels, 341 channels (97%) were in operation during the initial impact of the airplane. Both NASA seats, the energy absorbing seat and the standard seat, maintained their integrity during the impact. The floor accelerations at the seat locations were lower than the accelerations required for the energy absorbers to stroke; consequently, the energy absorbing seat did not stroke. The two seats remained firm in place during the crash and no seat attachment failures were observed. Due to the low accelerations experienced during the crash, both seats performed as standard seats. In the airplane structure, the accelerations were higher at both the point of impact as was shown in the left wing and at the forward end of the fuselage. The accelerations on the floor were higher toward the front than toward the rear and the floor accelerations on the left side were higher than on the right side at the front of the fuselage, but toward the rear they evened out.

- 341 channels in operation during initial impact
- Both NASA seats maintained their integrity
- No seat stroking was observed
- No seat attachment failures
- Accelerations higher at point of impact
- Front floor accelerations higher
- Left floor accelerations higher

DIGITAL FILTERING AND ACCELERATION PULSE INTERPRETATION

E. L. Fasanella
PRC Kentron, Inc.
Aerospace Technologies Division
Hampton, Virginia

NASA/FAA Government/Industry CID Workshop
NASA Langley Research Center
April 10, 1985

TOPICS

This presentation will address digital filtering of the CID data and a technique to analyze the acceleration data (fig. 1). Analog filtering was performed by electronic hardware (low pass analog filters) on board the aircraft to remove undesired high frequencies and to prevent errors due to sampling. Digital filtering is a computerized post-processing filtering technique that can be applied to the digitized time history data. Low pass, high pass, and notch filters can be mathematically simulated with this technique.

In order to validate acceleration traces, the integrated crash pulse velocity change was computed. Traces with velocity change outside the expected envelope were either rejected or set aside for additional study. Average accelerations were computed by dividing the primary impact velocity change by the pulse duration. An equivalent triangular pulse acceleration was computed by doubling the average acceleration and this value was compared to peak acceleration values. Selected traces were chosen that illustrate the effects of digital filtering for structure and dummy occupants. Other traces were chosen to illustrate the method used to obtain the average pulse acceleration and to triangularize the acceleration pulse.

- Digital filtering
  - Digital versus analog filtering
- Data interpretation
  - Peak and average accelerations
  - Velocity
  - Triangularizing the acceleration pulse
- Discussion of selected data traces

Figure 1

SAE CLASS 60 FILTER

A low pass filter with frequency response that lies within the inner and outer limits shown by the solid straight lines is defined by SAE J211a (ref. 1) to be a class 60 filter. The digital filter chosen to smooth CID accelerometer data is shown on figure 2 by a dashed line. The digital filter is flat with no attenuation (0 decibels) to the cutoff frequency f_c and then rolls off until it attenuates all frequencies above the terminal frequency f_t. This digital filter with f_c = 10 Hz and f_t = 188 Hz will be designated henceforth as the CID 100-Hz digital filter.

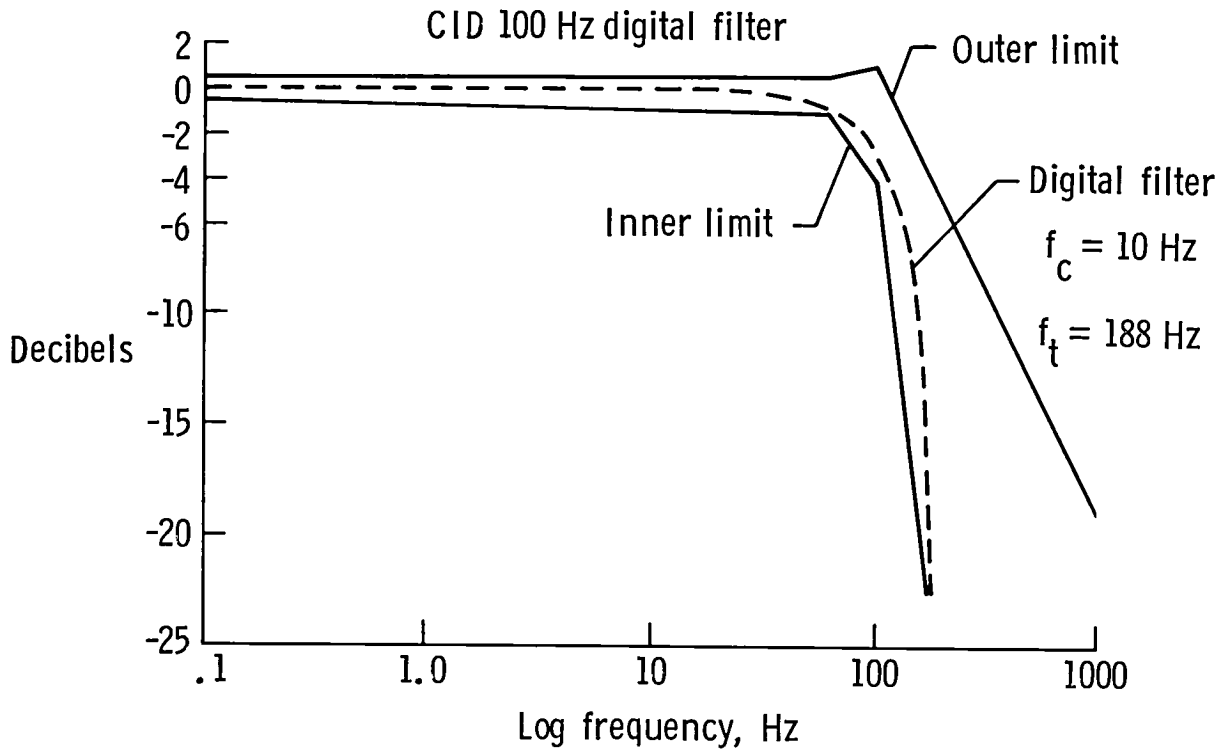


Figure 2

DIGITAL FILTERING EXAMPLE

The upper trace in figure 3 illustrates the "raw" acceleration time history for channel 276 without any digital filtering. At the bottom left corner of the lower plot, the number 33731.000 is the starting time of the plot in seconds and corresponds to 9 hours 22 minutes and 11 seconds. The lower plot is a magnification of the 0.02 second period from 33731.60 to 33731.62 seconds. The circles are the original raw data points that were sampled at every 1000th of a second, and these raw data points are connected by straight line segments. (In the top plot the circles are left out and only the line segments are present.) The data points represented by circles were input into the 100-Hz digital filter program. For each circle or raw data point, a corresponding square digitally filtered point is shown in the bottom plot. In actual practice, the filtering program uses N raw data points before time t_n and N data points after time t_n to calculate one filtered value at t_n.

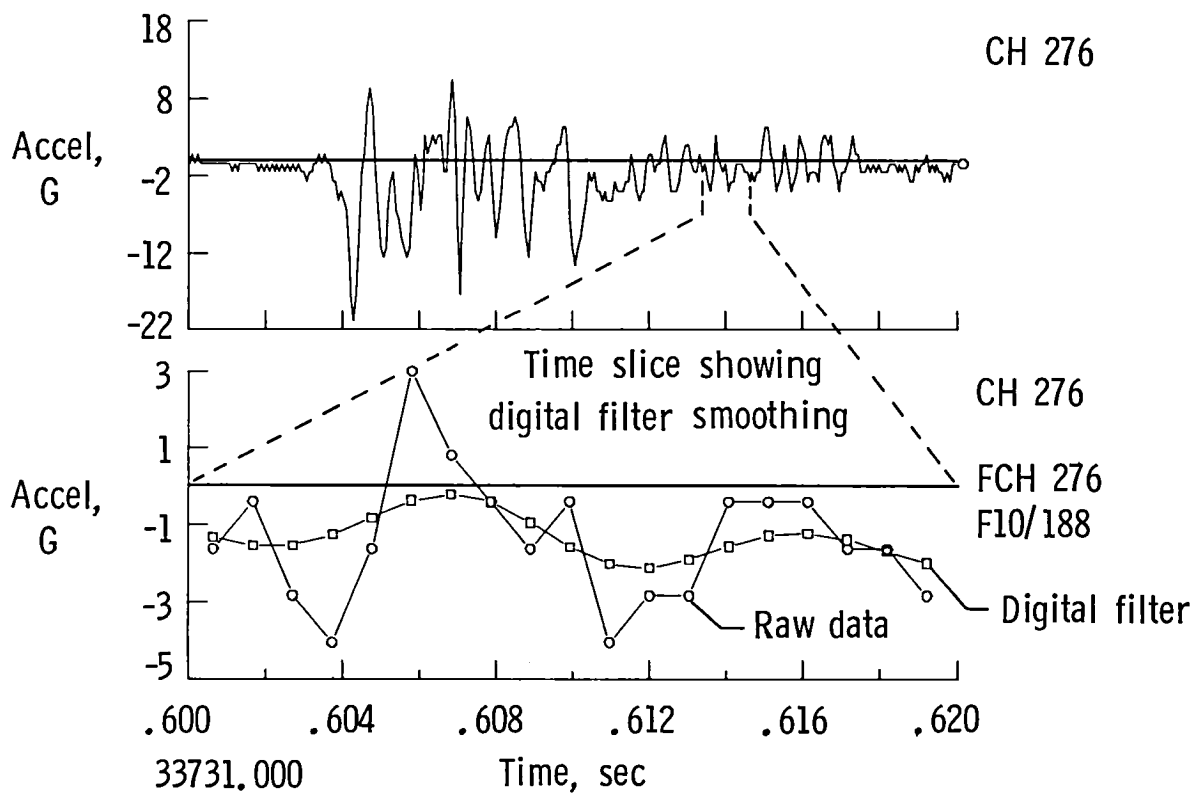
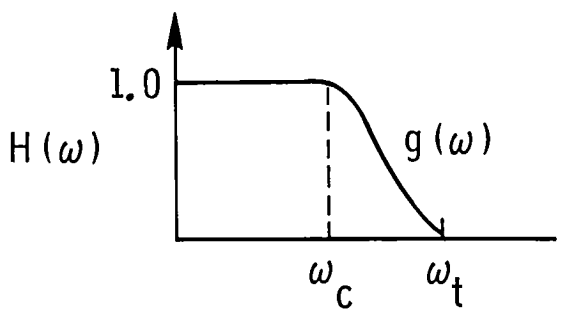


Figure 3

Figure 4 illustrates the low pass filter gain ratio H(w) in the frequency domain. The gain is one (no attenuation) for frequencies from 0 to the cutoff frequency w_c and then starts rolling off as defined by an arbitrary decreasing function g(w) with boundary conditions $g(w_c) = 1$ and $g(w_t) = 0$. To transform the gain function to the time domain, the inverse Fourier transform h(t) must be evaluated.

Low pass filter characteristics

- Frequency domain



$g(\omega)$ = arbitrary decreasing function with

Boundary conditions $\begin{cases} g(\omega_c) = 1 \\ g(\omega_t) = 0 \end{cases}$

where $\omega = 2\pi f$

- Time domain

$$h(t) = \frac{1}{2\pi} \int_{-\infty}^{\infty} e^{i\omega t} H(\omega)\, d\omega$$

Figure 4

DIGITAL FILTERING BACKGROUND MATHEMATICS

For simplicity, let us assume the function g(w), which defines the rolloff of the filter in the frequency domain, is a cosine function (ref. 2). Then the inverse Fourier transform h(t) can be evaluated in closed form as given in figure 5. Next assume the data points to be filtered are equally spaced with interval delta t. For this fixed delta t, let us evaluate an arbitrary 2N + 1 values of h(n delta t). The n th normalized value of h(n delta t) is denoted by h_n bar.

Evaluate Inverse Fourier Transform

$$h(t) = \frac{1}{2\pi} \int_{-\infty}^{\infty} e^{i\omega t} H(\omega)\, d\omega \quad \text{with rolloff } g(\omega) \text{ a } \underline{\text{cosine}} \text{ function}$$

$$\text{then } h(t) = \frac{\pi}{2t} \left[\frac{\sin \omega_t t + \sin \omega_c t}{\pi^2 - (\omega_t - \omega_c)^2 t^2} \right]$$

assume m equally spaced data points $(d_1, t_1), (d_2, t_2) \cdots (d_m, t_m)$

where $t_n = n\Delta t$

Evaluate h(t) to obtain 2N + 1 coefficients for a given fixed Δt

Denote $\bar{h}_n$ the n^{th} normalized coefficient

$$\bar{h}_n = \frac{h_n}{\sum_{-N}^{N} h_\ell}$$

Figure 5

DIGITAL FILTERING BACKGROUND MATHEMATICS

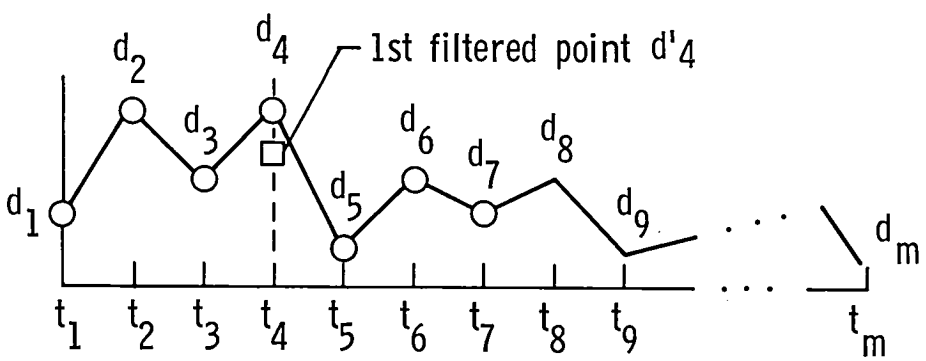
The N+1 filtered data point is denoted in figure 6 as d'_{N+1} and is given by a summation which is a Fourier convolution. Note from the formula (figure 6) that to calculate the first filtered data point N data points are used before the first filtered value and N data points are used after the first filtered value. In the simple example where N = 3, there are seven (2N+1) terms in the formula to calculate each filtered data value. The first filtered value d'_4 is generated by using points d_1 to d_7 in the formula. To calculate the second filtered value d'_5 the same process is used by taking the seven points d_2 through d_8 each multiplied by the proper h bar.

The integer N needed for 1 percent accuracy can be computed from the last formula where $f_t - f_c$ is the rolloff frequency region.

$$d'_{N+1} = \sum_{-N}^{N} \bar{h}_n d_{N+n+1} = \bar{h}_{-N} d_1 + \ldots + \bar{h}_0 d_{N+1} \ldots + \bar{h}_N d_{2N+1};$$

where $\bar{h}_{-i} = \bar{h}_i$

for example if N = 3 $\quad d'_4 = \bar{h}_{-3} d_1 + \ldots + \bar{h}_0 d_4 + \ldots + \bar{h}_3 d_7$

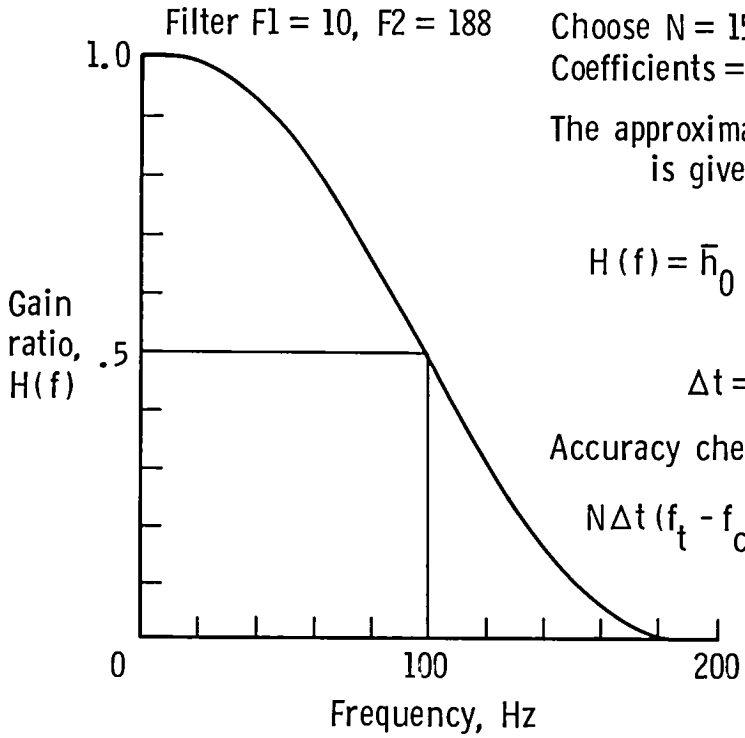


For 1% accuracy we require $N\Delta t\,(f_t - f_c) \geq 2$

Figure 6

ERROR ANALYSIS OF CID 100-Hz DIGITAL FILTER

To evaluate the accuracy of the 2N+1 terms used to represent the gain function, one can expand H(f) as a Fourier series using the formula given in figure 7. For the CID digital filter, F1, the cutoff frequency, was chosen to be 10 Hz, F2, the termination frequency, was chosen to be 188 Hz, and N was arbitrarily chosen to be 150. The gain function H(f) plotted on the left can be seen to accurately represent the intended filter. Using the accuracy check formula at the bottom of figure 7, N(delta t)*rolloff is equal to 53.7 for a sample rate of 500. Since this value is greater than two, the error of the filter is less than one percent. For a sample rate of 1000 a digital filter of 100-Hz can also be generated with error less than one percent. Since CID data were sampled at both 500 and 1000 samples per second, two 100-Hz digital filters had to be programmed, one for each sample rate.



Choose N = 150 (arbitrary)
Coefficients = 2N + 1 = 301

The approximation to the ideal H(f) is given by:

$$H(f) = \bar{h}_0 + 2 \sum_{1}^{150} \bar{h}_n \cos(2\pi n f \Delta t)$$

$$\Delta t = \frac{1}{\text{sample rate}} \simeq 0.002$$

Accuracy check

$$N\Delta t (f_t - f_c) = 151 \left(\frac{1}{500}\right)(178) = 53.7$$

Error < 1%

Figure 7

EXAMPLE OF DIGITAL FILTER WITH ERROR EXCEEDING 1 PERCENT

Figure 8 illustrates an example of a digital filter with N = 150 that demonstrates undesirable overshoot and undershoot from the ideal gain function. In this example if one calculates N(delta t)*(rolloff) using the accuracy check formula, a value of only 0.375 is obtained. Since this value is less than 2, the error would exceed 1 percent. To obtain the desired accuracy, either N or the rolloff region would need to be increased.

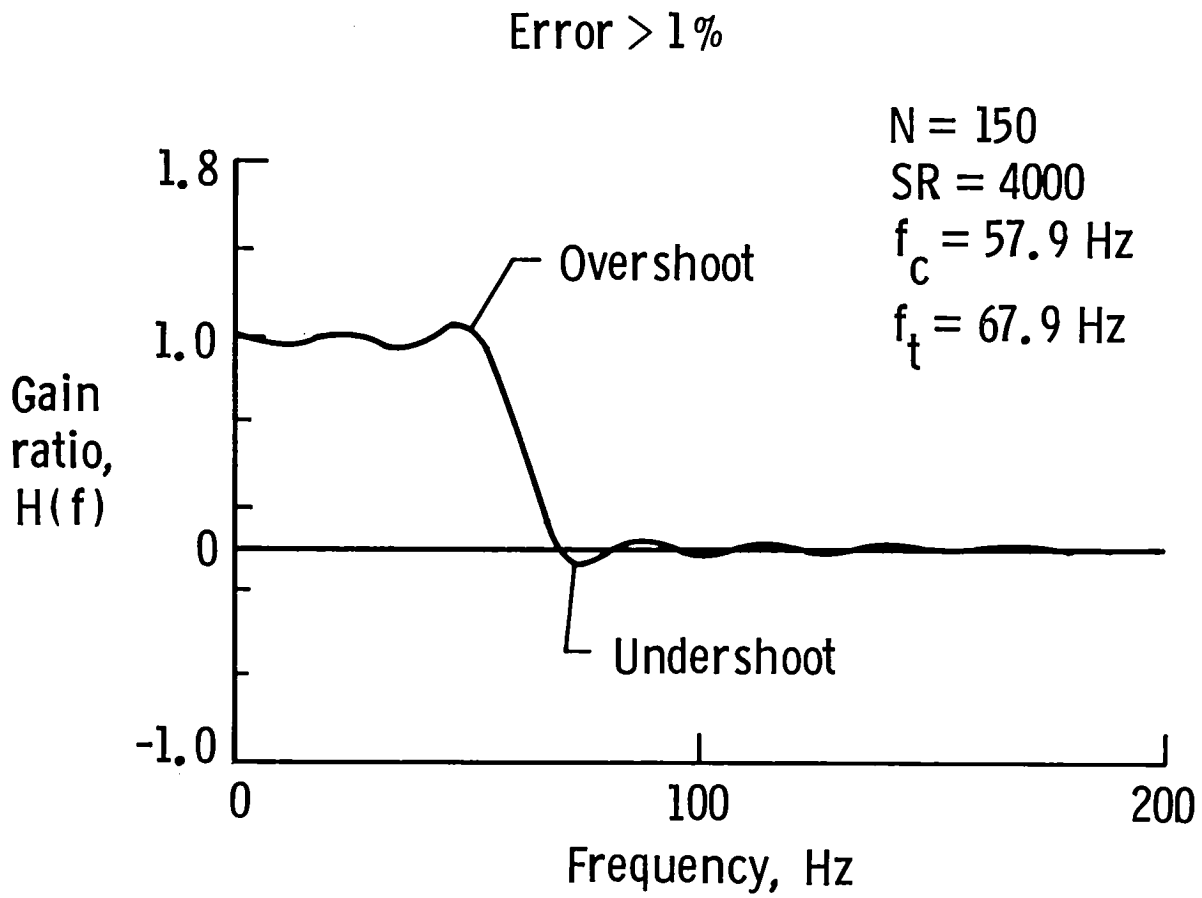


Figure 8

PILOT FLOOR ACCELERATION NORMAL DIRECTION

The pilot floor acceleration data (normal to the floor) were sampled at 500 samples per second and were taken from an accelerometer attached to the floor at body station 228. The two plots shown in figure 9 are from channel 1 for the first second after engine number one on the left wing contacted the ground. The top plot is the raw data as recorded with no post-crash digital filtering. The second plot shows the data after passing through the 100-Hz digital filter discussed previously. The filter attenuates the high frequencies and smoothes the digital data.

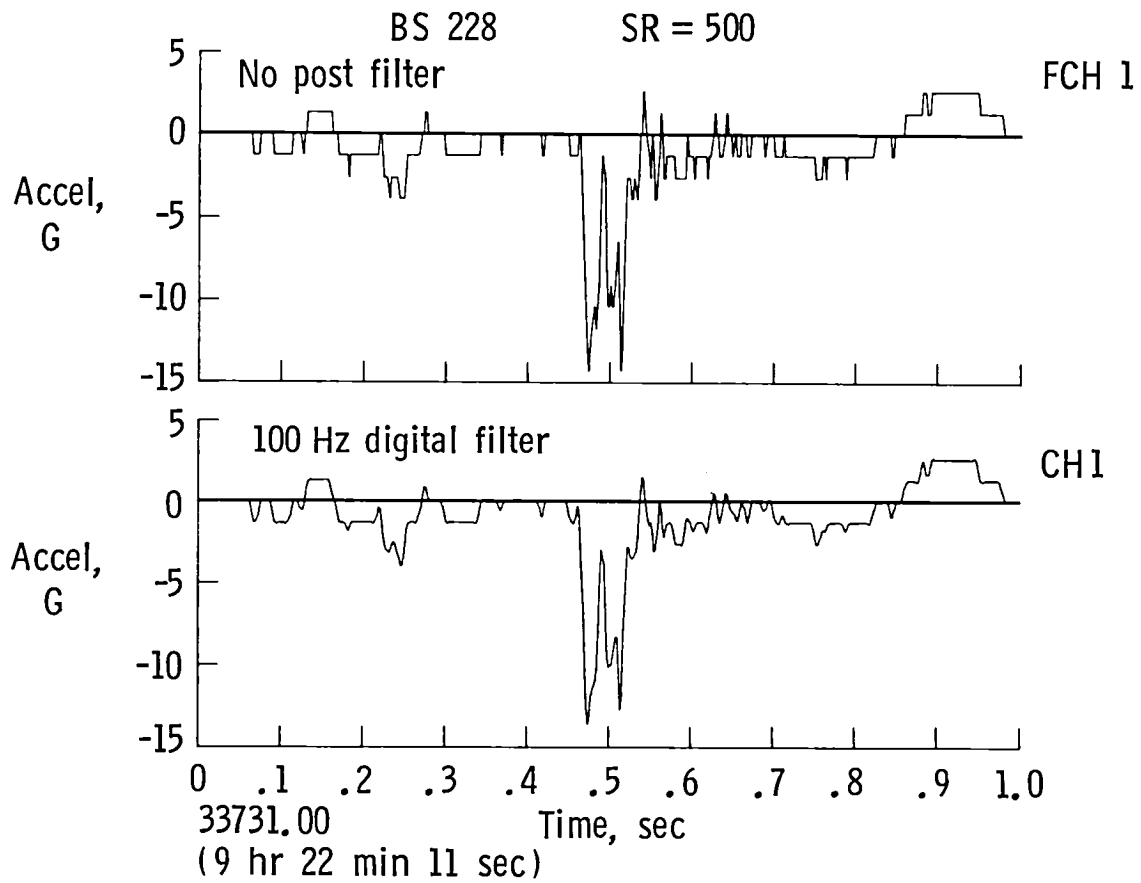


Figure 9

FLOOR TRACK ACCELERATION NORMAL DIRECTION

The two plots in figure 10 show the floor track acceleration for the first instrumented frame at body station 400. For this example, the sample rate is 1000. Again the top plot is the data with no post filter and the bottom plot is for the data passed post test through the 100-Hz digital filter with F1 = 10 Hz and F2 = 188 Hz. These data were taken from CID channel 276.

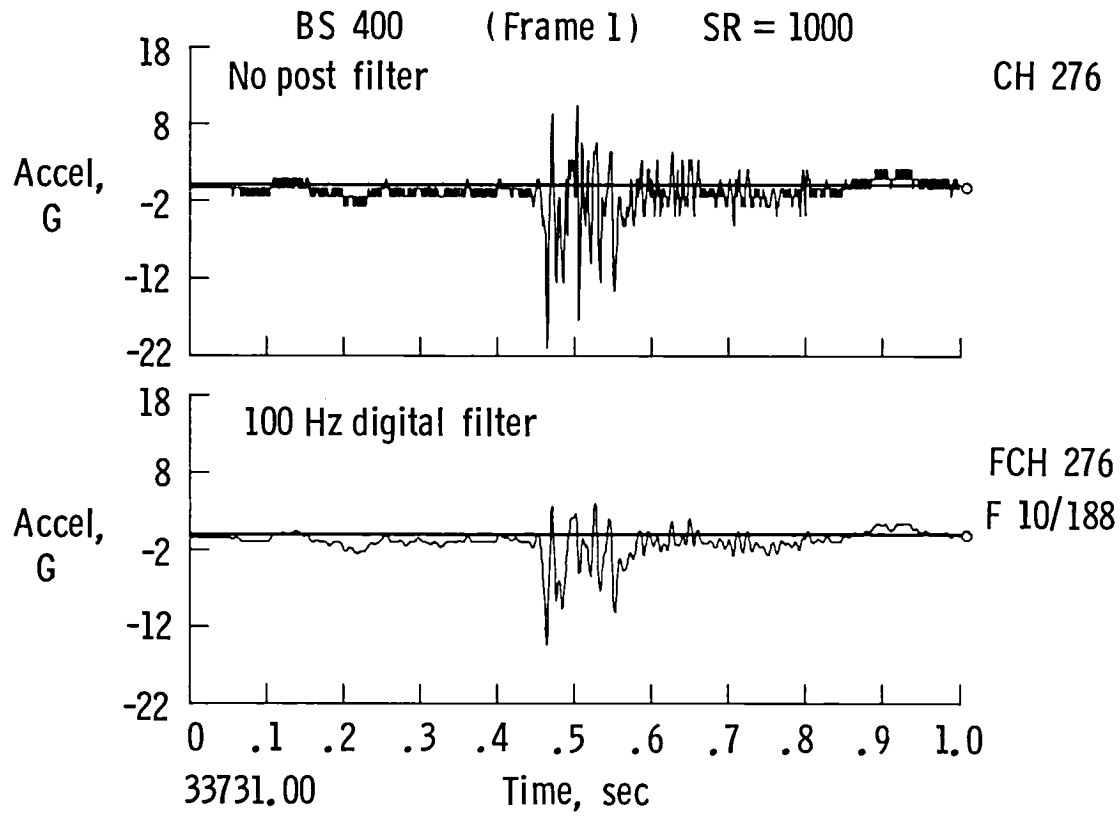


Figure 10

FLOOR ACCELERATION NORMAL FOR FRAME 2

These two acceleration traces (CID channel 120) were taken at body station 540. As we move back in the airplane, the acceleration levels become lower and lower and the digital nature of the data is more pronounced. In figure 11 the smoothing effect of the 100-Hz digital filter can clearly be seen. In the top plot, the acceleration data are quite "stairstep looking" due to the resolution of the 8-bit digital data over the +/- 150 G range required for the normal (vertical) direction. The lower plot, which is the same data filtered with the 100-Hz digital filter, has all the low-frequency characteristics of the raw data without the digital "stairsteps."

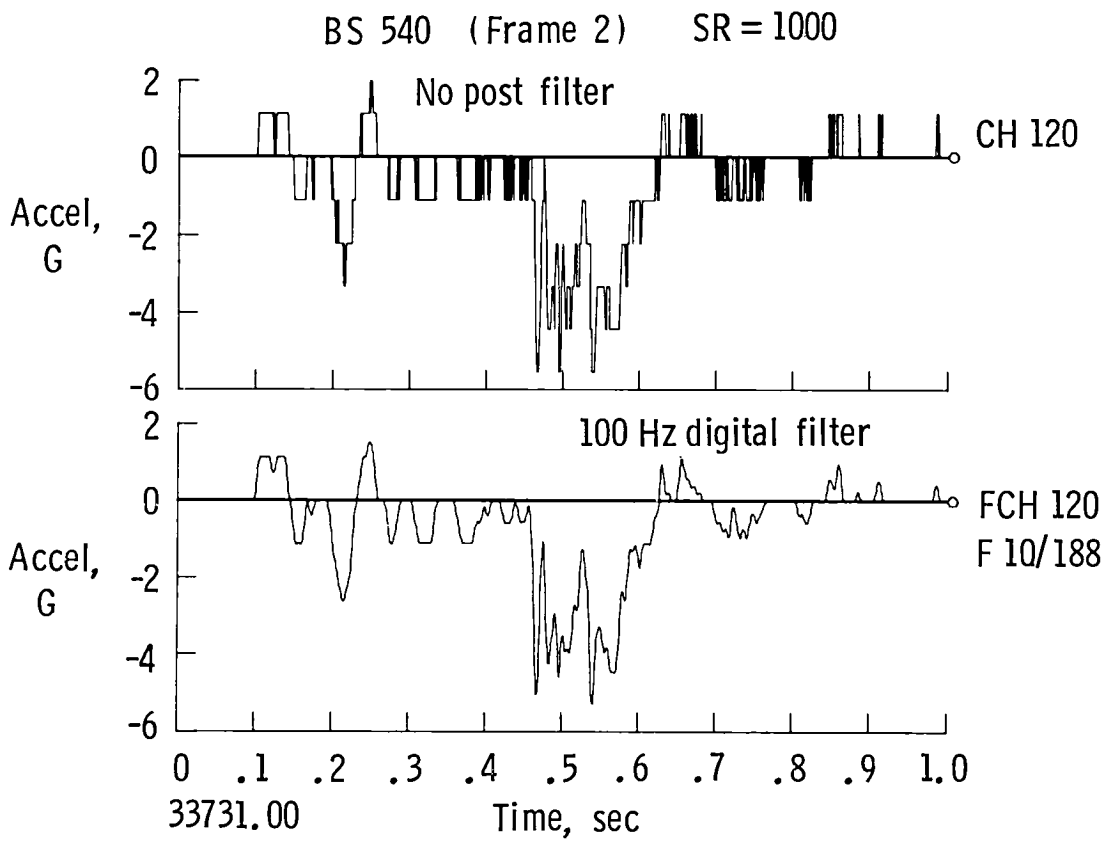


Figure 11

DUMMY 14B PELVIS ACCELERATION NORMAL

The pelvis acceleration along the spineward direction for the center dummy in the left seat in row 14 is shown in the two traces in figure 12. The sample rate is 1000 per second. Again the 100-Hz filter removes the high-frequency noise and cleans up the trace quite well.

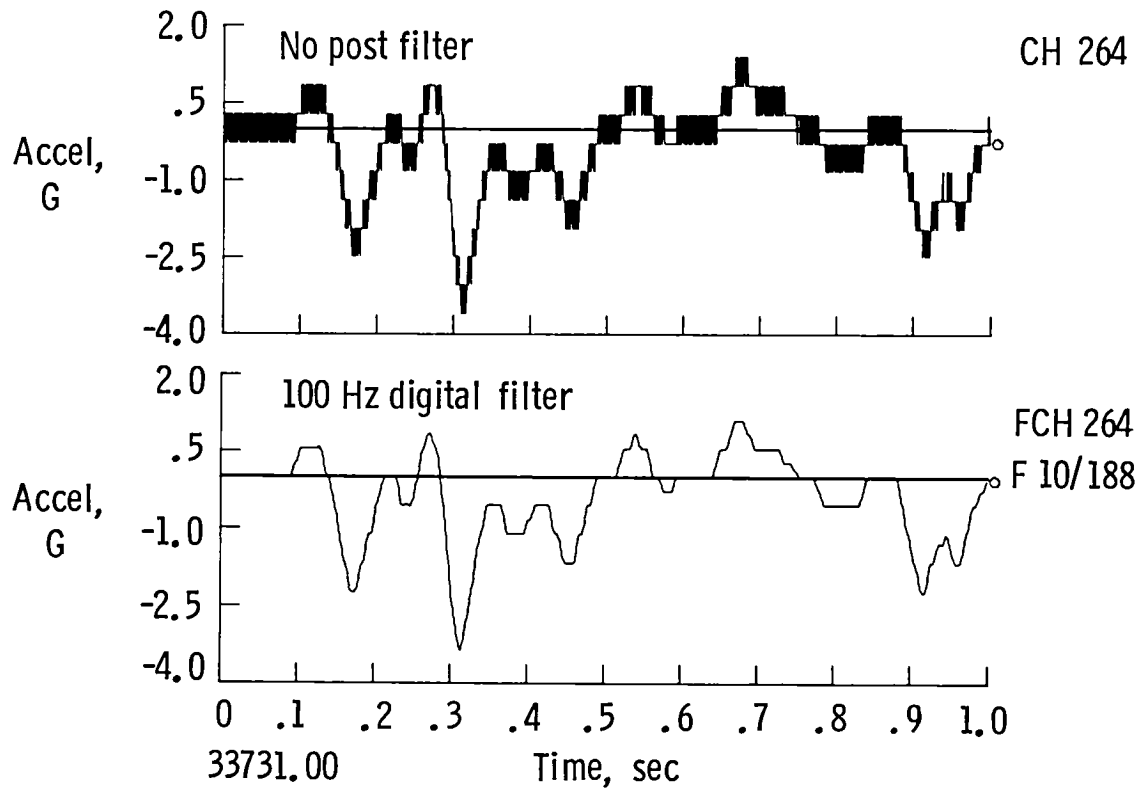


Figure 12

DUMMY 3E PELVIS ACCELERATION LONGITUDINAL DIRECTION

All longitudinal accelerations measured on the aircraft and dummies were relatively low. Since the resolution of the 8-bit system was approximately 1 G per count for this particular channel (an 8-bit system can have from 0 to 255 counts), the actual acceleration trace is only bounded by the data. The digital filter does a reasonable job; however, it cannot make up for the loss of resolution in this case (fig. 13).

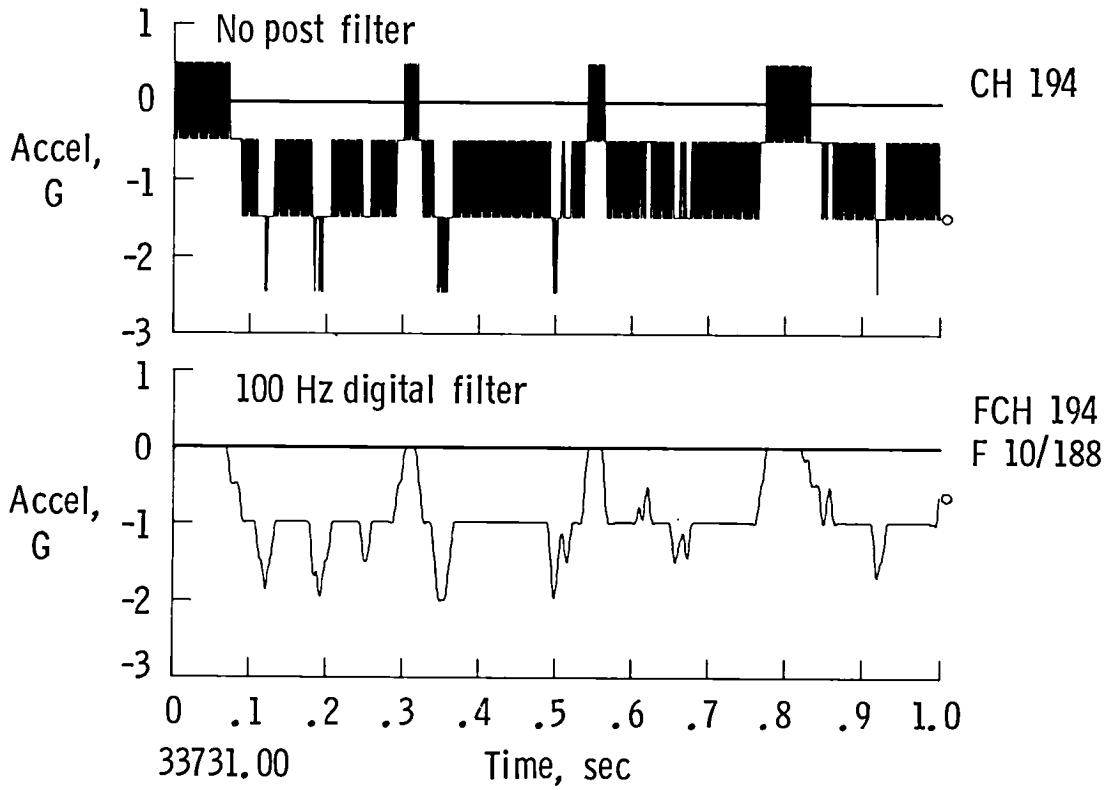


Figure 13

VERTICAL FLOOR ACCELERATION AND INTEGRATED VELOCITY

The top plot in figure 14 is of the normal acceleration of the floor at body station 540. The bottom plot shows the velocity curve obtained by integrating the top acceleration plot. The dominant acceleration pulse from 0.48 to 0.62 seconds in time occurs when the fuselage impacts the ground. The acceleration from 0 to 0.48 seconds is from the left wing impact. Notice that the total vertical velocity change is approximately 18 ft/s, but that the velocity change is composed of almost 4 ft/s taken out by the wing and about 14 ft/s taken out by the fuselage. The average acceleration for the fuselage impact can be computed from delta V of 14 ft/s divided by delta T of 0.14 seconds which when expressed in G-units is 3.1 G's. If the acceleration from 0.48 to 0.62 seconds were a triangular pulse, then the peak would be twice the average or 6.2 G's. For this example, twice the average acceleration and the peak acceleration directly from the plot are nearly the same. The average acceleration and twice the average acceleration are useful indicators in data interpretation of crash impact severity.

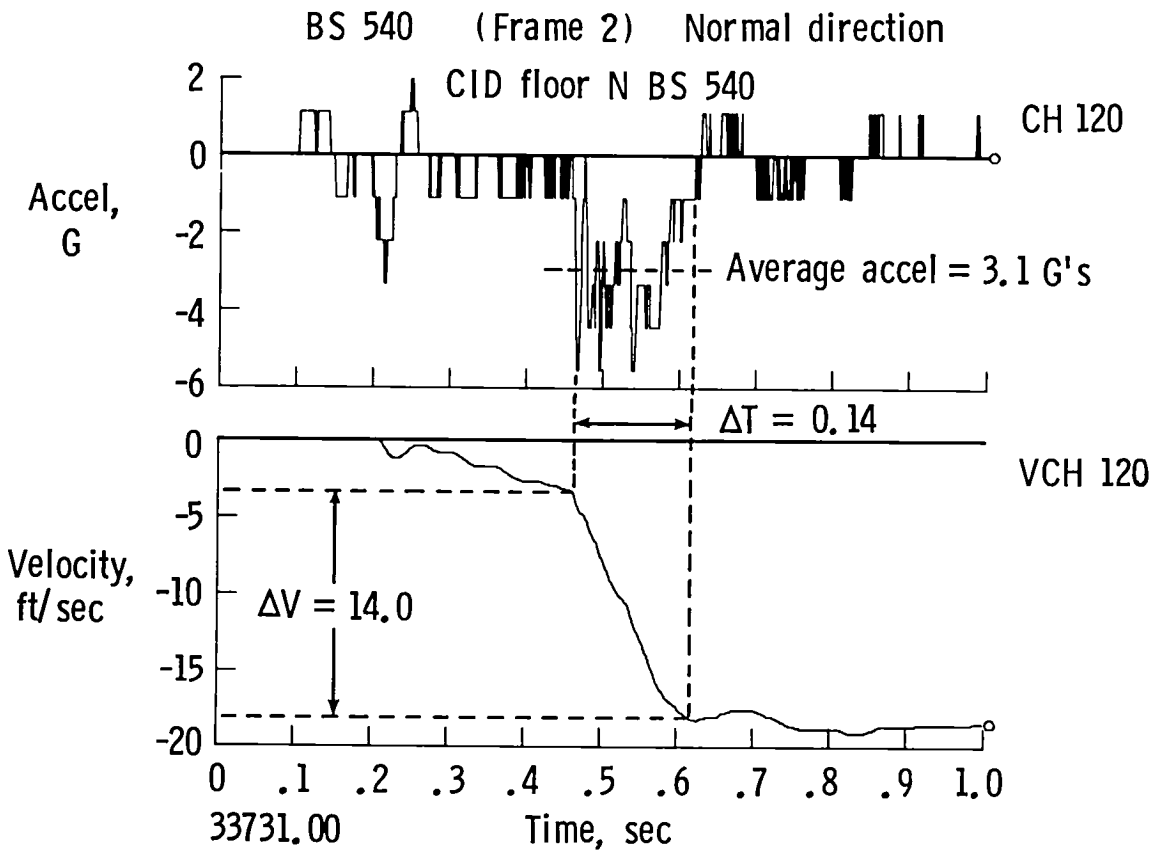


Figure 14

PILOT FLOOR ACCELERATION AND INTEGRATED VELOCITY (LONGITUDINAL)

Using the same technique as in figure 14, the longitudinal acceleration of the pilot floor is analyzed for the 0.13 second pulse shown in figure 15. Note that the average acceleration is only 0.84 G in this case. Twice the average acceleration, which would correspond to a 0.13 second triangular pulse, would only have a peak of 1.68 G's. The peak G taken from the top trace is about 6 G's, but it is of very short duration. The average acceleration or peak triangularized acceleration has more meaning in this case and can be compared with other locations in the aircraft with better results.

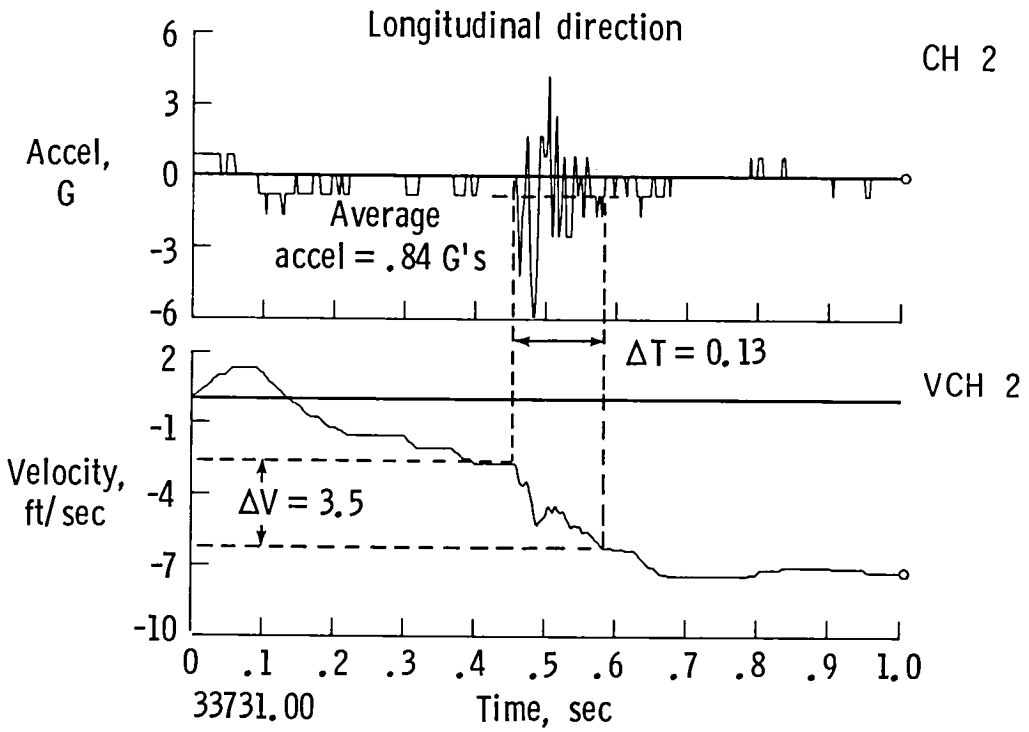


Figure 15

SELECTED CID CHANNELS - PRIMARY IMPACT

The primary impact is defined to be the impact from the time the left wing contacted the ground (9 hrs 22 min 11 sec or 33731.0 sec) until the rear of the fuselage made contact (about one second). The wing cutter impact which occurred later will not be analyzed in this discussion. A cross section of data from 51 representative CID channels was analyzed and distributed at this conference. Figure 16 shows the format of the 34 fuselage accelerometer channels that were analyzed. For each channel the location of the accelerometer, the direction, the body station, the peak acceleration value, time the peak occurred, the velocity change of the main pulse, the average acceleration of the main pulse, twice the average acceleration, the sample rate, and the analog filter on board the aircraft are all given. In addition, one-second traces from the time of left wing contact are shown.

Fuselage accelerometer data:

Cha	Location	DIR	BSTA	Peak val G	Peak time S	ΔV ft/s	ΔT S
2	Pilot floor	L	228	6.10	0.48	3.51	0.13
1	Pilot floor	N	228	14.30	0.48	17.60	0.08
3	Pilot floor	T	228	4.00	0.14	10.00	0.12
276	FR #1 floor rt track	N	400	14.50	0.47	14.00	0.12
286	Frame 1 top	N	400	16.20	0.48	15.20	0.12

Cha	Location	AVEACC G	2 × AVE G	Sample rate Hz	Analog filter Hz
2	Pilot floor	0.84	1.68	500	100
1	Pilot floor	7.29	14.58	500	100
3	Pilot floor	2.59	5.18	1000	100
276	Fr # 1 floor ft track	3.62	7.25	1000	100
286	Frame 1 top	3.93	7.87	1000	180

Figure 16

SELECTED CID CHANNELS - PRIMARY IMPACT

Figure 17 illustrates the format of the 14 selected channels of wing and pylon accelerometer data. Some of the velocity changes and other analysis are not given because of accelerometer overranging that occurred for some channels. All of the 14 selected channels were sampled at 500 samples per second and were filtered on board with 100-Hz analog filters.

Wing and pylon accelerometer data:

Sample rate: 500 per second
Analog filter: 100 Hz

Cha	Location	DIR	BSTA	Peak val G	Peak time S	ΔV ft/sec	ΔT S	AVEACC G	2 × AVE G
332	L Engine front pylon	N	XXXX	80.00	0.15	- - - - - - - - - - - - -			
339	R Engine front pylon	N	XXXX	5.10	0.62	14.40	0.19	2.35	4.71
336	L Engine rear pylon	N	XXXX	162.70	0.12	- - - - - - - - - - - - -			
342	R Engine rear pylon	N	XXXX	28.70	0.62	- - - - - - - - - - - - -			
184	L Wing F spar in	L	806	19.10	0.11	- - - - - - - - - - - - -			

Figure 17

LAP BELT LOAD CELL DATA

Figure 18 presents the lap belt load cell data for three selected channels. Since load cells have lower frequency response than accelerometers, a 50-Hz digital filter was chosen to filter the lap belt load cell data. The digital filter for load cell data attenuates more of the high frequencies with Fl = 6 Hz, F2 = 94 Hz, and - 3 dB attenuation for 50 Hz. The loads measured in the lap belts were very low because of the low longitudinal accelerations in the crash.

Load cells digitally filtered post crash (fl = 6 Hz, f2 = 94 Hz, -3db at 50 Hz)

Cha	Location	BSTA	Peak val LB	Peak time S	Sample Rate 1/S	analog Filter Hz
267	Dummy 14B left belt	1220	80.00	0.98	500	60
103	Dummy 14E left belt	1220	43.00	0.54	500	100
104	Dummy 14E rt belt	1220	60.00	0.54	500	100

Figure 18

SUMMARY

In summary, the post processing digital filter is quite effective for removing unwanted high frequency and noise without distorting the signal. In addition, digital filtering is effective for smoothing low-level low resolution digital data where the digital "stairstep" phenomena are pronounced.

Integrating the acceleration data to obtain velocity traces is quite useful. The velocity change provides a check on the validity of the acceleration trace. (Zero offsets in acceleration must be removed before integrating.) Average accelerations can be obtained from the velocity trace by dividing the change in velocity for an acceleration pulse by the pulse duration. One can obtain the peak of an equivalent triangular pulse by doubling the average acceleration (fig. 19).

- Digital filter effective for
    1. Removing unwanted high-frequency vibrations and noise
    2. Smoothing digital data
- Integrated acceleration (velocity) useful for
    1. Obtaining velocity changes
    2. Establishing validity of acceleration traces
    3. Obtaining average accelerations
    4. Triangularizing the acceleration pulse

Figure 19

REFERENCES

1. Society of Automotive Engineers: Instrumentation for Impact Tests. SAE J211a, revised 1971.

2. Graham, Ronald J.: Determination and Analysis of Numerical Smoothing Weights. NASA TR R-179, 1963.

PRELIMINARY FLOOR, SEAT, AND DUMMY DATA

Mark R. Cannon
Richard E. Zimmerman
Simula Inc.
Phoenix, Arizona

NASA/FAA Government/Industry CID Workshop
NASA Langley Research Center
April 10, 1985

SUMMARY OF SEAT EXPERIMENTS

The seats installed by Simula numbered 23 total, and figure 1 shows that 10 seats were installed in the "as is" condition and 13 were modified. Both groups included a variety of seat experiments. The table also shows a brief summary of the types of seats and modifications that were performed. The presentation given by Dick Johnson (ref. 1) outlined what some of these typical modifications were.

STANDARD SEATS		
PILOT SEAT		1
TRIPLE PAX, FORWARD-FACING		6
DUAL PAX, AFT-FACING		2
WALL-MOUNTED, FOLD DOWN, FLIGHT ATTENDANT		1
		10
MODIFIED SEATS		
TRIPLE PAX FWD FACING	LAP BELT E/A	2
	REAR LEG E/A	4
	PROTOTYPE TRACK FITTINGS	1
	COMPRESSION E/A	2
	REAR LEG AND BRACE E/A	2
AFT-FACING WITH COMPRESSION E/A		1
WALL-MOUNTED, FOLD DOWN, FLIGHT ATTENDANT		1
		13

Figure 1.

SEAT MODIFICATIONS

In general, the modifications were concerned with improving the retention of the occupant and seat structure to the existing aircraft structure. The designs were matched to the strength that the floor structure was believed to have. There were no energy absorbers introduced for the purpose of reducing the loads on the occupant such as is done in some crashworthy seat systems for small aircraft. This was assumed to be inappropriate for a transport seat. The energy absorbers were simply to limit the loads applied to the floor of the aircraft. Other things done to improve seat retention included releases built into the structure to allow it to deform rather than break and separate. Legs and seat pans were reinforced, with emphasis placed on lateral bracing. The track fittings were changed. A report on the design of these experiments is in preparation.

POSITION OF SEAT EXPERIMENTS ABOARD AIRCRAFT

Figure 2 shows where various seating experiments were in the aircraft; they were arranged in two sets. There was a set of eight seats up front, a couple of seats in between, and then another set of eight in the aft part of the aircraft. The experiment was reproduced in this way because the G loading might have been quite different in the aft portion of the cabin from that in the forward part of the cabin. It was thought that data for two different crash environments might be obtained. The pitch (seat spacing) on these seat experiments was very large compared to a commercial transport. It was felt that if seats with the dummies in them were put as close together as they would be in a commercial transport, the different seat designs would interact with one another in an unpredictable and uncontrolled manner. It was believed that if the seats interacted with the dummies striking seats ahead of them it would not be possible to interpret the data. For example, it might be impossible to differentiate between acceleration due to floor input and dummy impact. Also, stroking seats mounted behind nonstroking seats could be a problem with a small pitch. Therefore, the seats were isolated as much as possible in the available cabin space. The placing of the seats also considered the proximity of modified and unmodified seats of the same type and the probability of failure.

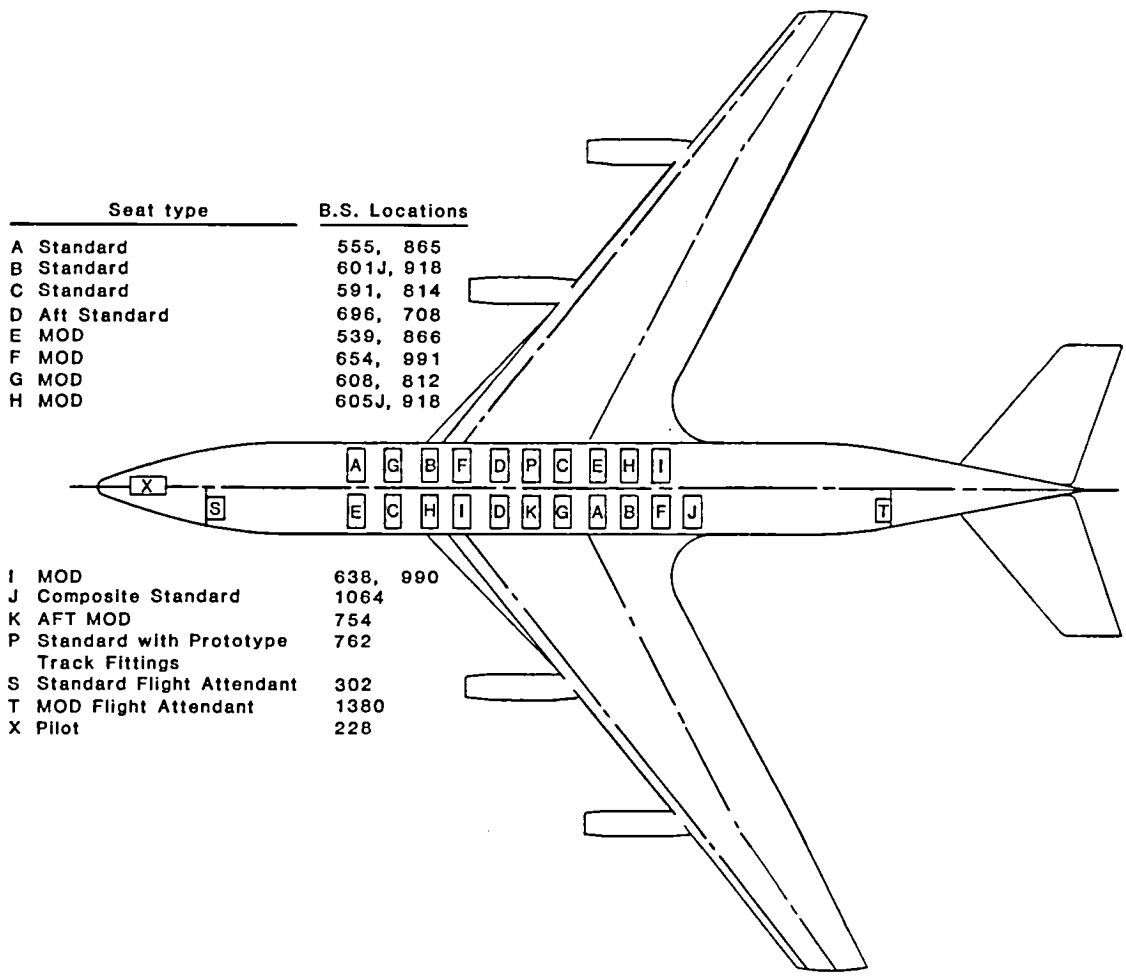


Figure 2.

LOCATION OF FLOOR ACCELEROMETERS

Figure 3 shows where the accelerometers were placed on the floor plan. There were vertical accelerometers at all locations because the floor was not anticipated to have much rigidity in that direction and the acceleration could easily vary with location. Because of the limitations of data channels, the decision was made to infer that the lateral acceleration on one side of the aircraft would be similar to data obtainable on the other side. It was reasoned that acceleration could not vary much in the lateral direction because the structure had much greater rigidity in that direction. The same reasoning was applied to the longitudinal direction. The lateral and longitudinal accelerations were measured only at selected locations. Accelerometers were also placed on the seat pan and in the dummy. There were also tensiometers on the lap belts of the instrumented dummies and on the pilot and flight attendant restraint harnesses.

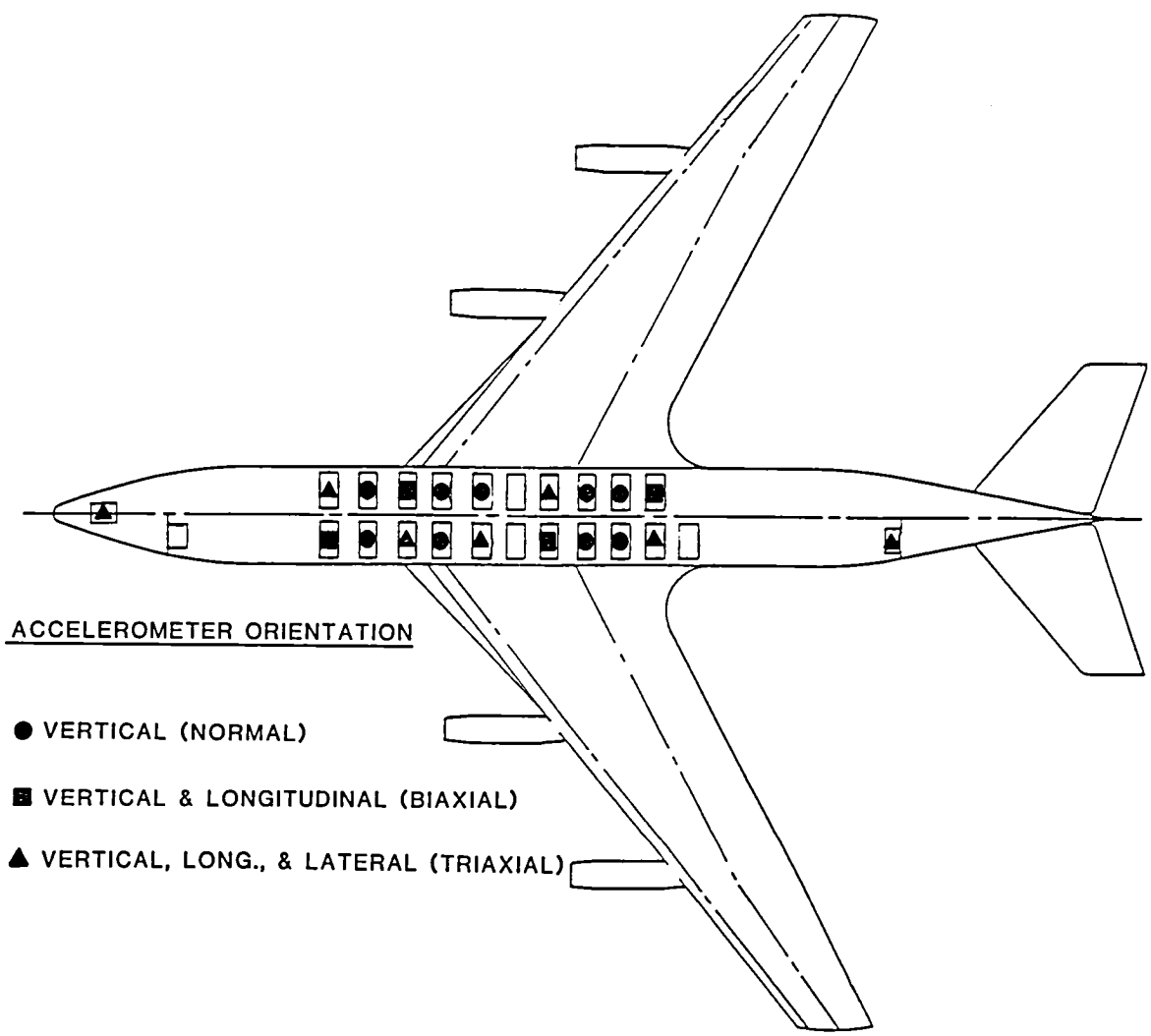


Figure 3.

TYPICAL MOUNTING LOCATION OF BIAXIAL
AND TRIAXIAL ACCELEROMETERS IN THE FLOOR

The floor accelerometers were mounted on the floor beams under the aisle end legs of the seat structure, as shown in figure 4.

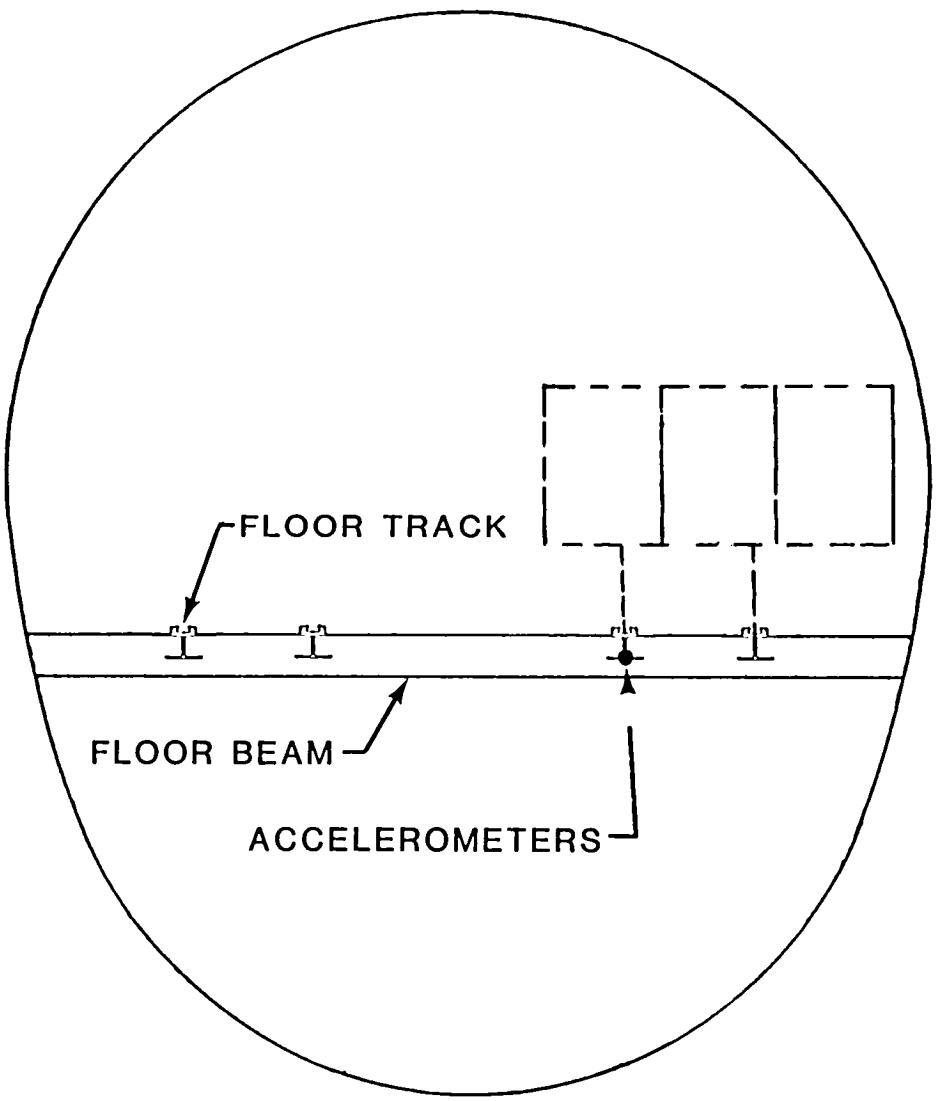


Figure 4.

POSITION OF ACCELEROMETERS ON THE SEAT

All of the seats had an accelerometer mounted at the hardest point on the seat structure, on the seat pan near the rear leg (fig. 5). The leg that was closest to the aisle was selected because it was likely to experience the highest deceleration due to the assymmetry of the seat structure. This was based on the assumption that the more heavily loaded window-end of the seat would yield first. On some of the seats there was a second accelerometer near the window end (a uniaxial longitudinal accelerometer only). It was placed there because the two ends of an assymmetric stroking seat would probably experience quite different longitudinal accelerations.

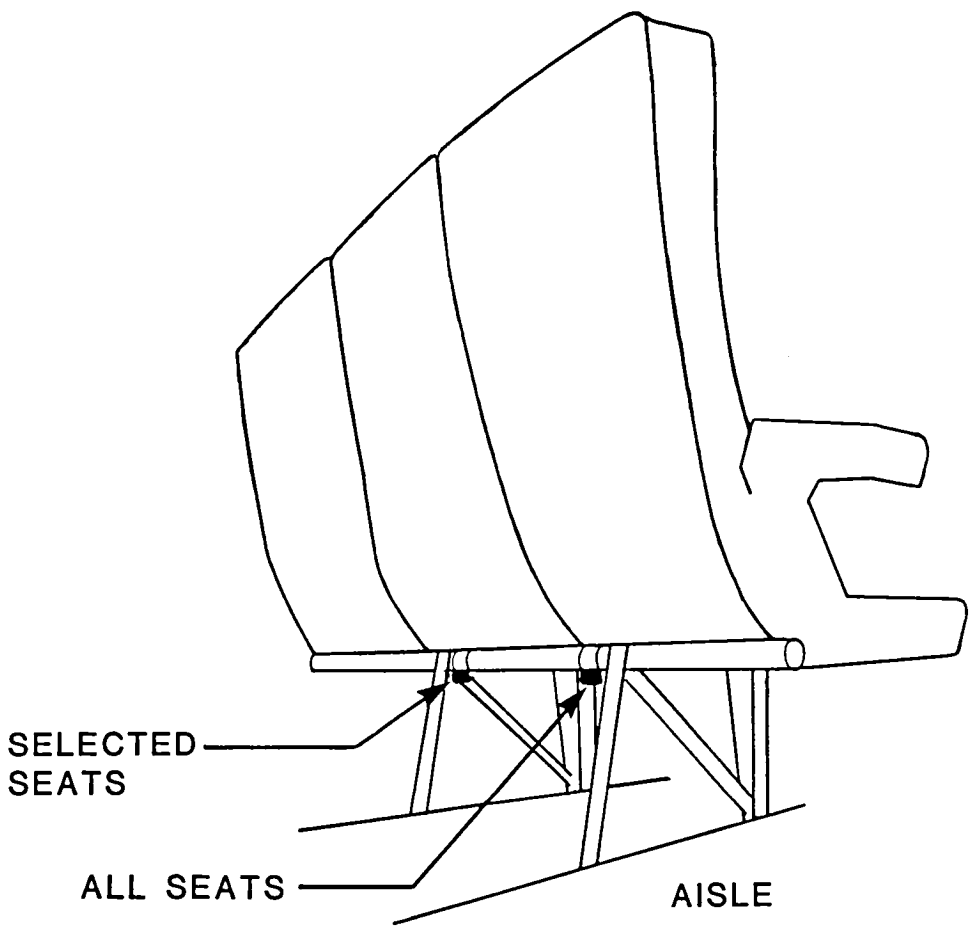


Figure 5.

SEAT LOCATIONS WITH ACCELEROMETERS

Figure 6 shows which seats were equipped with the two different arrangements of seat pan accelerometers.

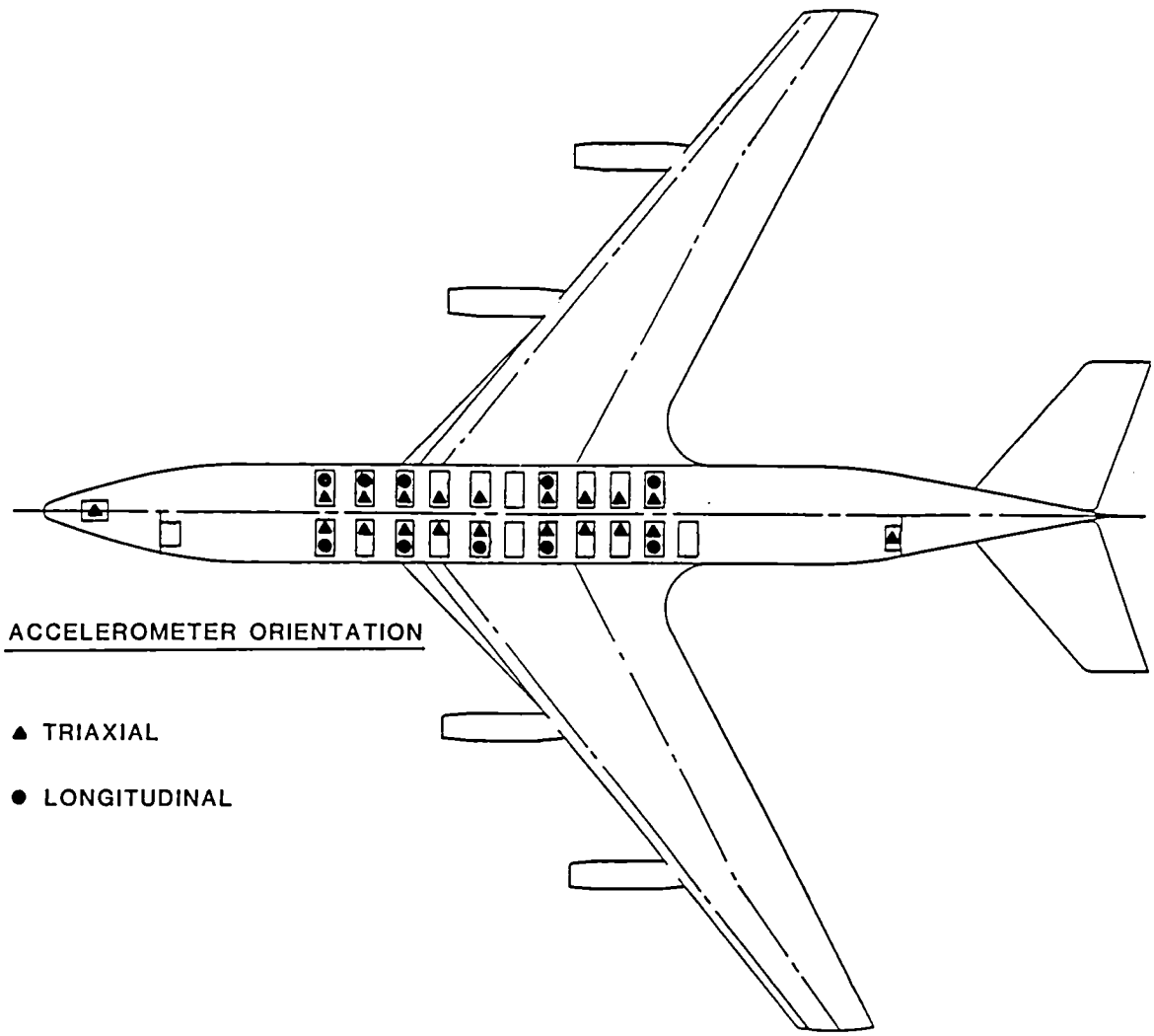


Figure 6.

LOCATION OF DUMMY INSTRUMENTATION

The pelvis, thorax, and head of selected dummies were instrumented. All had at least a triaxial pelvis accelerometer and lap belt tensiometers. Tensiometers were also placed on the pilot and flight attendant restraint harnesses. Three dummies had biaxial head accelerometers and either biaxial or triaxial thorax accelerometers. (See fig. 7.)

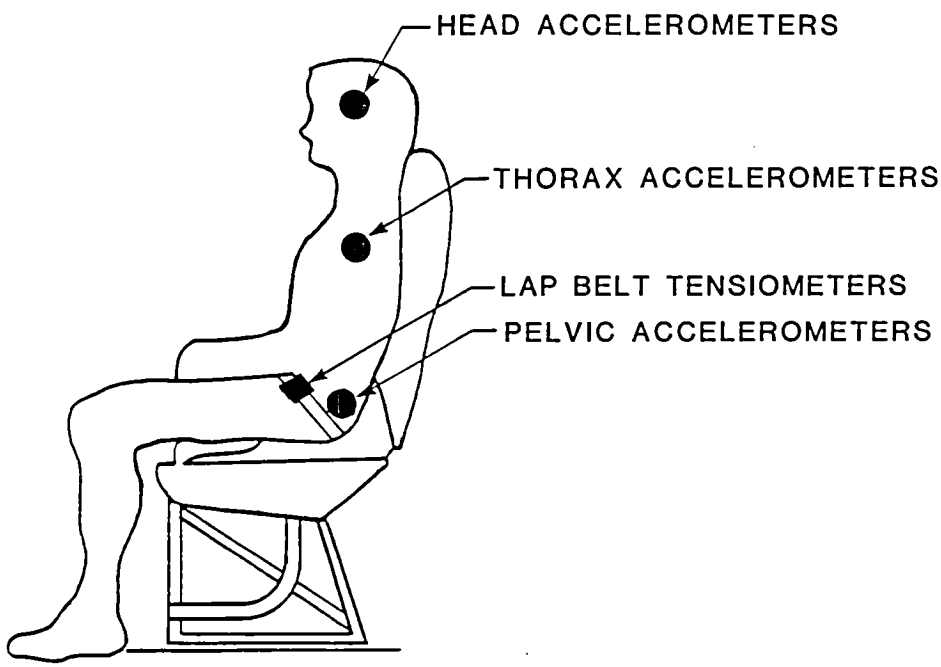


Figure 7.

DUMMY LOCATIONS WITH ACCELEROMETERS

Figure 8 shows where the various dummy instrumentation configurations were placed in the aircraft.

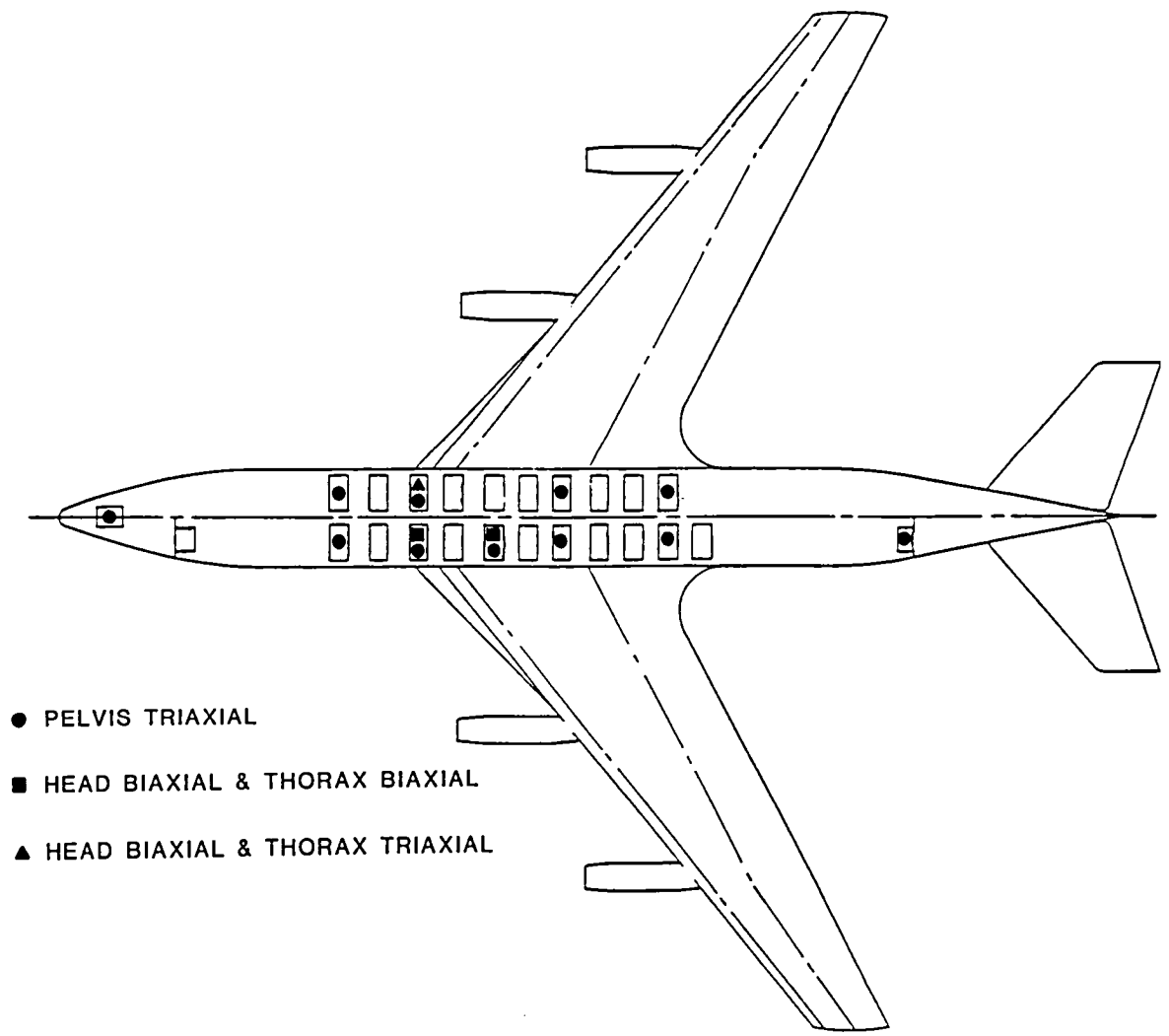


Figure 8.

POSTTEST OBSERVATIONS

Posttest observations revealed several occurences. None of the energy absorbers was stroked in any way, due to the fact that there was not enough loading on the modified seats. It was also observed that none of the dummies jackknifed over the lap belts, indicating there was not a very high forward G loading. In a laboratory test with a 9-G forward impact with appreciable velocity, the dummies will fold over; they did not in this test. The only impact damage that we observed on the seat structures occurred where the landing gear destroyed the floor structure. There was some very slight seat pan deformation on some seats. There was a little lateral deformation on seats near the area of floor damage. There was no damage to any track fittings, but one seat, just behind where the floor was ripped, did have one front leg fitting come out of the track.

FLOOR ACCELERATIONS

The floor acceleration data of interest occurred when the aircraft struck the ground, and also when the aircraft struck the obstacles that were to cut the wings. Obstacle impact is of some interest for the crashworthiness experiments because somewhat larger accelerations occurred at this time. This is true in all axes. The times associated with these events were as follows:

- Wing/ground impact at approximately 33731.06 sec (2200 msec)*
- Fuselage/ground impact at approximately 33731.46 sec (2600 msec)
- Fuselage/obstacle impact at approximately 33732.91 sec (4050 msec)

The obstacle impact appears most severe in all axes.

*Data received begins at 33728.86 sec (used as starting time of 0 msec).

VERTICAL FLOOR ACCELERATIONS (G) - GROUND IMPACT

Figure 9 shows vertical acceleration during ground impact. This includes the engine, and then the fuselage, striking the ground. Accelerations are shown for four different points in the aircraft, at the aft flight attendant seat and at three other points along the length of the cabin. There are accelerations similar to those shown in reference 2: 2-4 G accelerations at most locations and somewhat higher at the flight attendant seat. The data is consistent with the physical observations made after the test. Figures 10 and 11 show the longitudinal and lateral components of accelerations at the same locations.

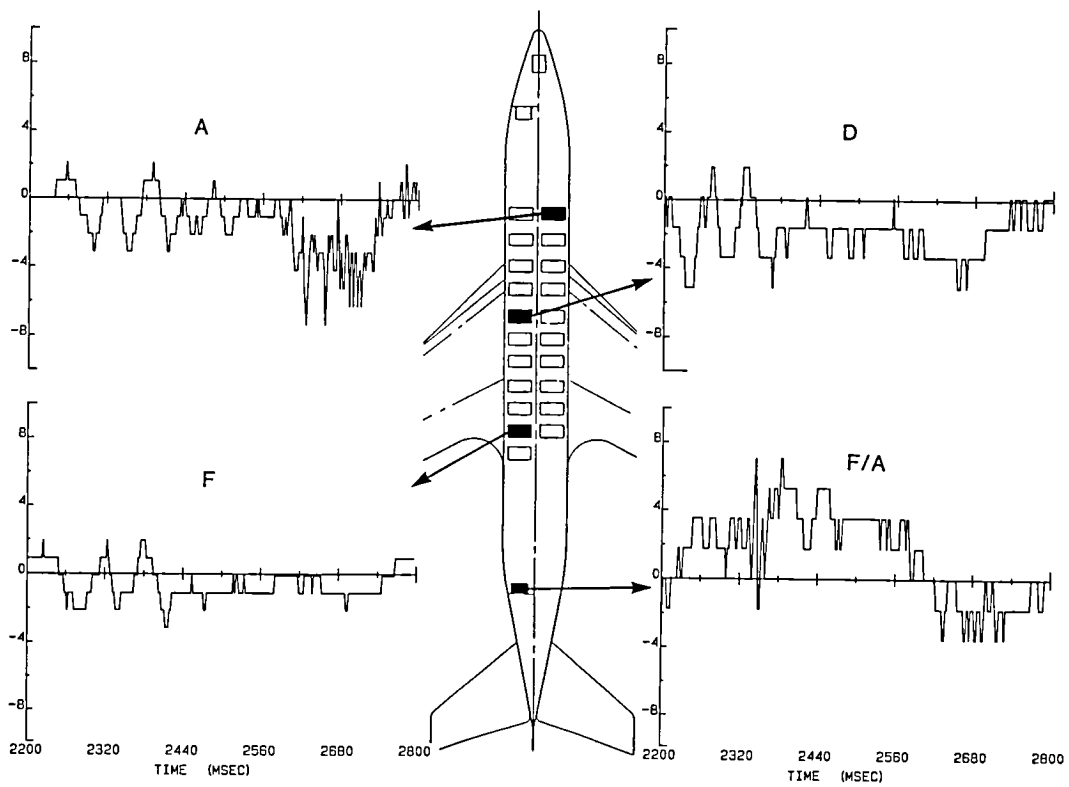


Figure 9.

LONGITUDINAL FLOOR ACCELERATIONS (G) - GROUND IMPACT

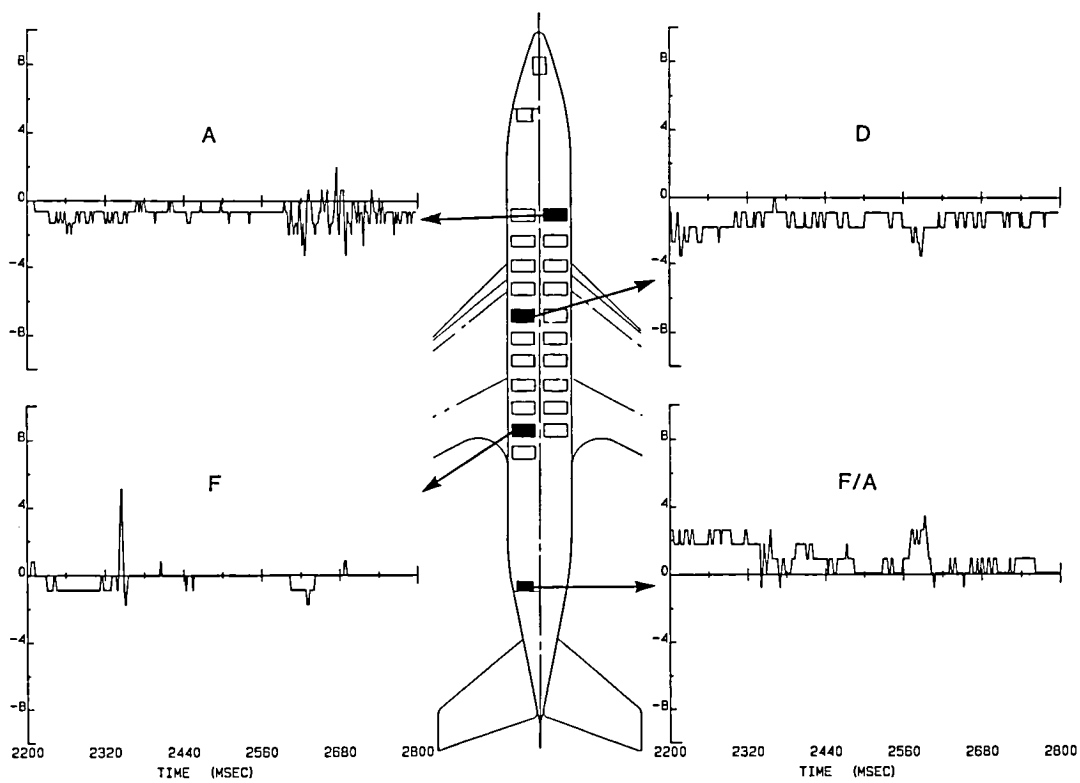


Figure 10.

LATERAL FLOOR ACCELERATIONS (G) - GROUND IMPACT

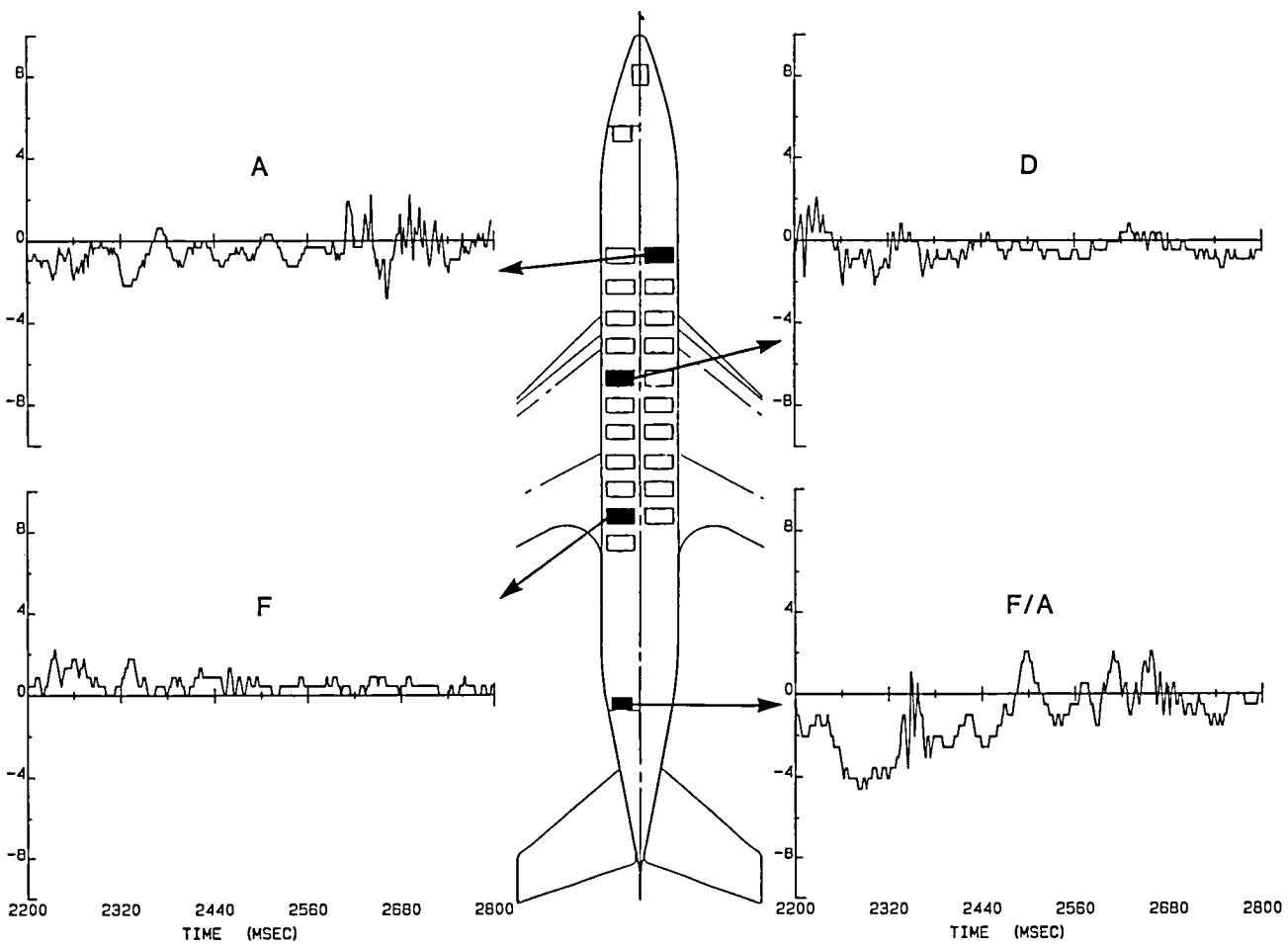


Figure 11.

VERTICAL FLOOR ACCELERATIONS (G) - OBSTACLE IMPACT

When the aircraft hit the obstacles there were some 15- to 20-G vertical acceleration peaks. (See fig. 12.) They were very sharp peaks, with little energy. That is typical of data for all three coordinate axes. The channel for seat F shows a higher acceleration, but it is not really consistent with the other channels. (Apparently an instrumentation problem existed.) This channel behaved well during ground impact, but not after the aircraft hit the obstacle. Serious doubt exists that there were accelerations of such magnitude. Figures 13 and 14 show the longitudinal and lateral acceleration components at the same locations.

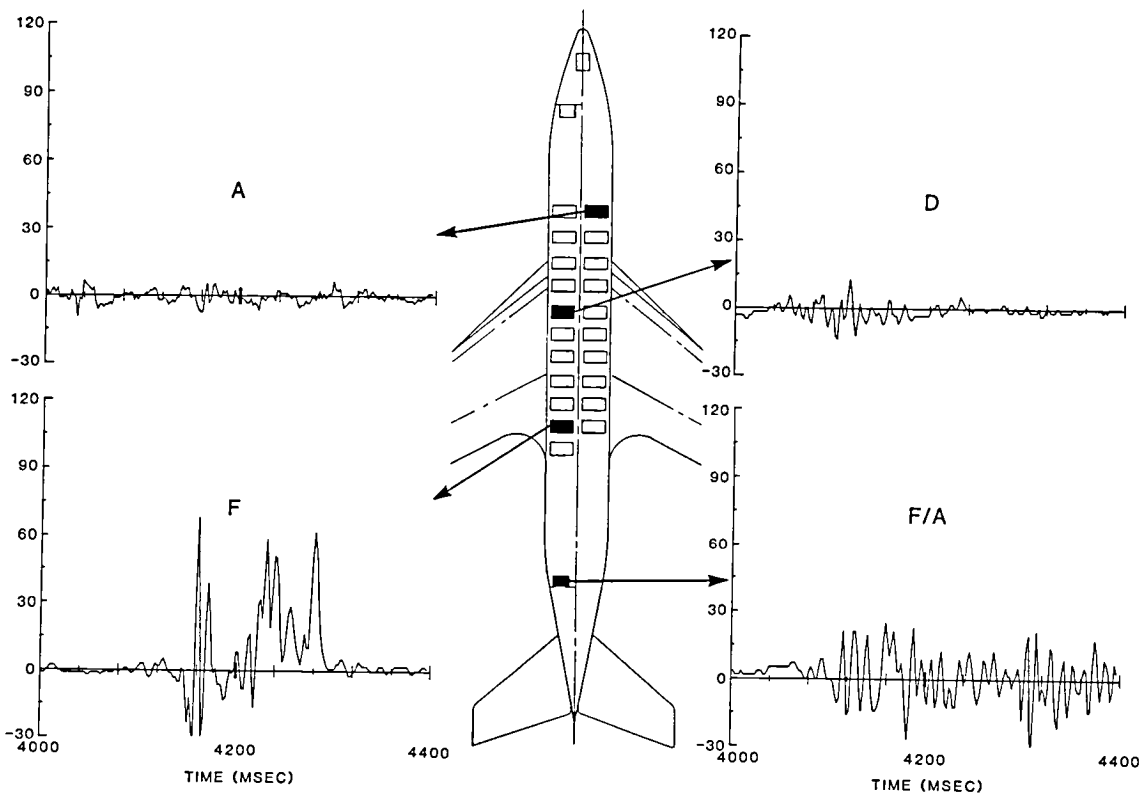


Figure 12.

LONGITUDINAL FLOOR ACCELERATIONS (G) - OBSTACLE IMPACT

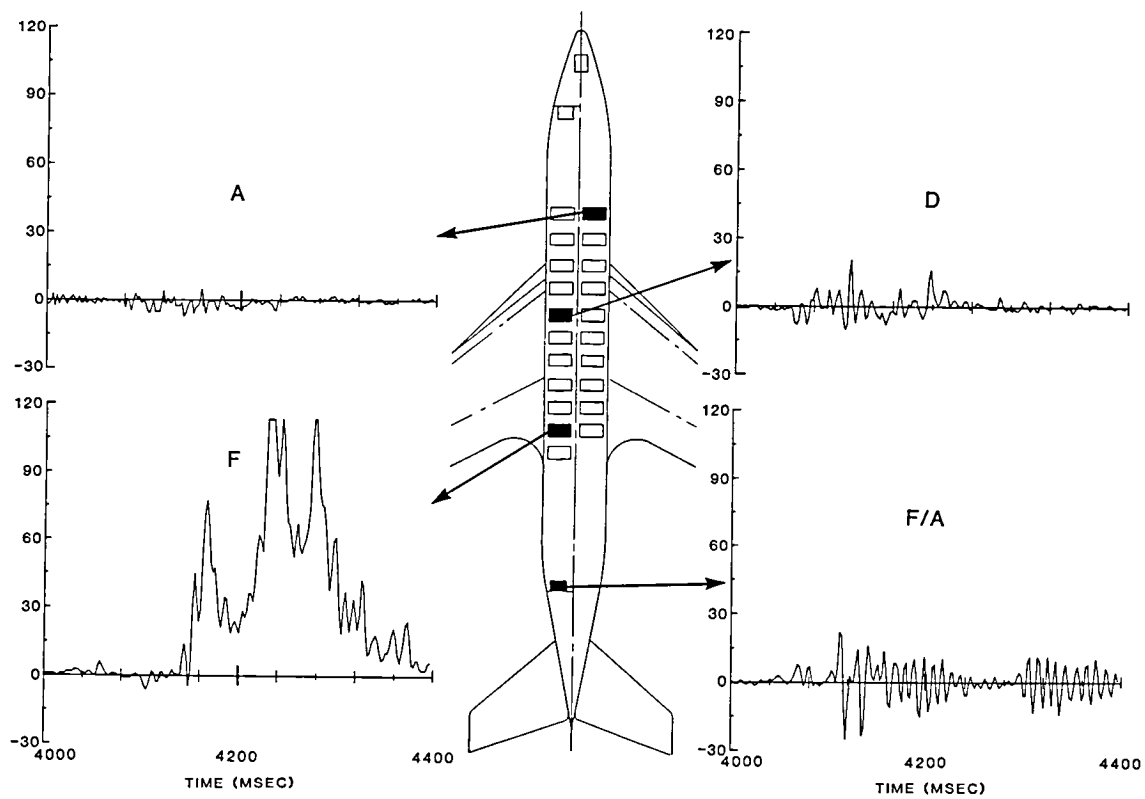


Figure 13.

LATERAL FLOOR ACCELERATIONS (G) - OBSTACLE IMPACT

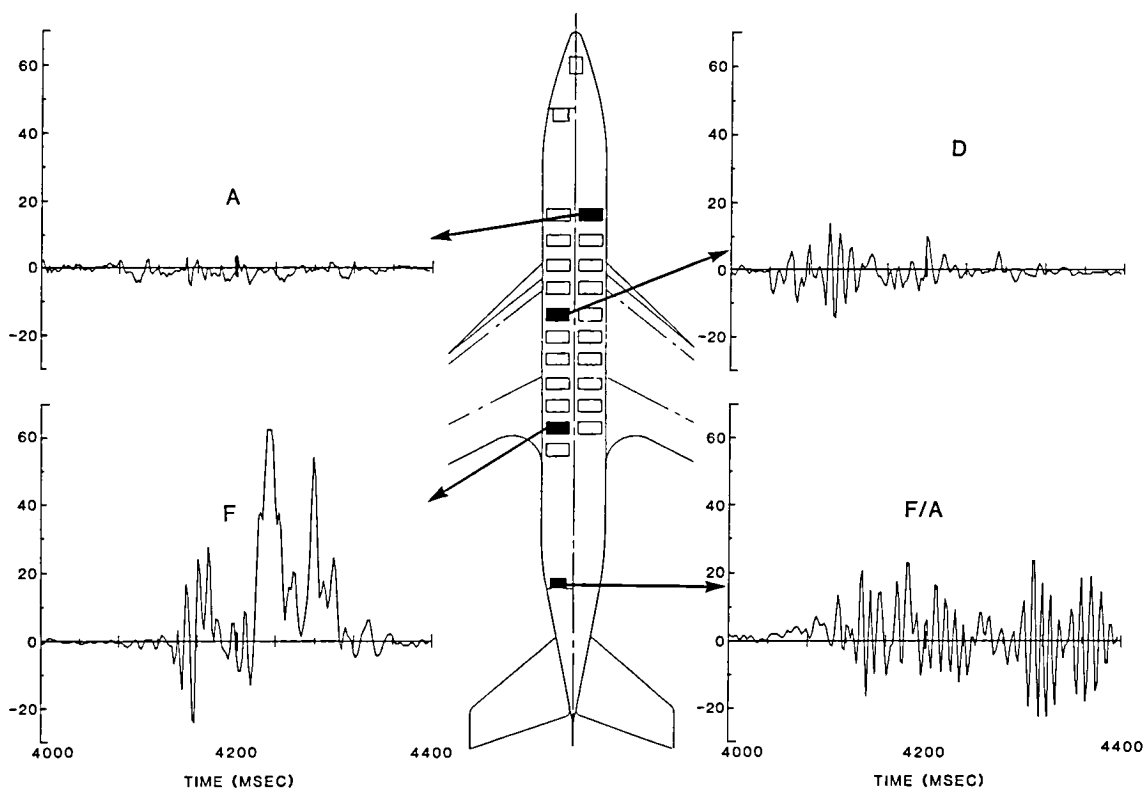


Figure 14.

FLOOR, SEAT, AND PELVIS ACCELERATIONS - GROUND IMPACT

The next three figures (Figures 15-17) show vertical, longitudinal, and lateral accelerations for the floor, seat, and dummy pelvis at Seat A. They are arranged so that the floor accelerations near the bottom end of the seat leg, the seat pan acceleration near the top end of the leg, and the dummy pelvis accelerations above this leg can be viewed simultaneously. The figures therefore display how the floor accelerations were transmitted through the seat/occupant system. The seat pan acceleration is reasonably similar to the floor acceleration. This would be expected in view of the relatively rigid seat leg structure and the fact that nothing deformed. Therefore, this is a good indication that the data is probably valid. The pelvis of the dummy responded somewhat differently, as expected. Approximate velocity changes are shown for the three accelerations; they are not identical. But when the resolution of the data as indicated by the steps in the pelvis data is considered along with other potential instrumentation errors, the correlation between the velocity changes shown here is reasonably good. Also, note that these velocity changes are reasonably consistent with the velocity changes that were demonstrated in references 2 and 3. For the longitudinal acceleration components (fig. 16), the seat pan response again reflects the floor response fairly closely. For the lateral accelerations (fig. 17), the seat pan acceleration is not nearly as similar to the floor acceleration. This is as expected, because the seat is much less rigid in the lateral direction.

VERTICAL ACCELERATIONS - SEAT A (R.H.) GROUND IMPACT

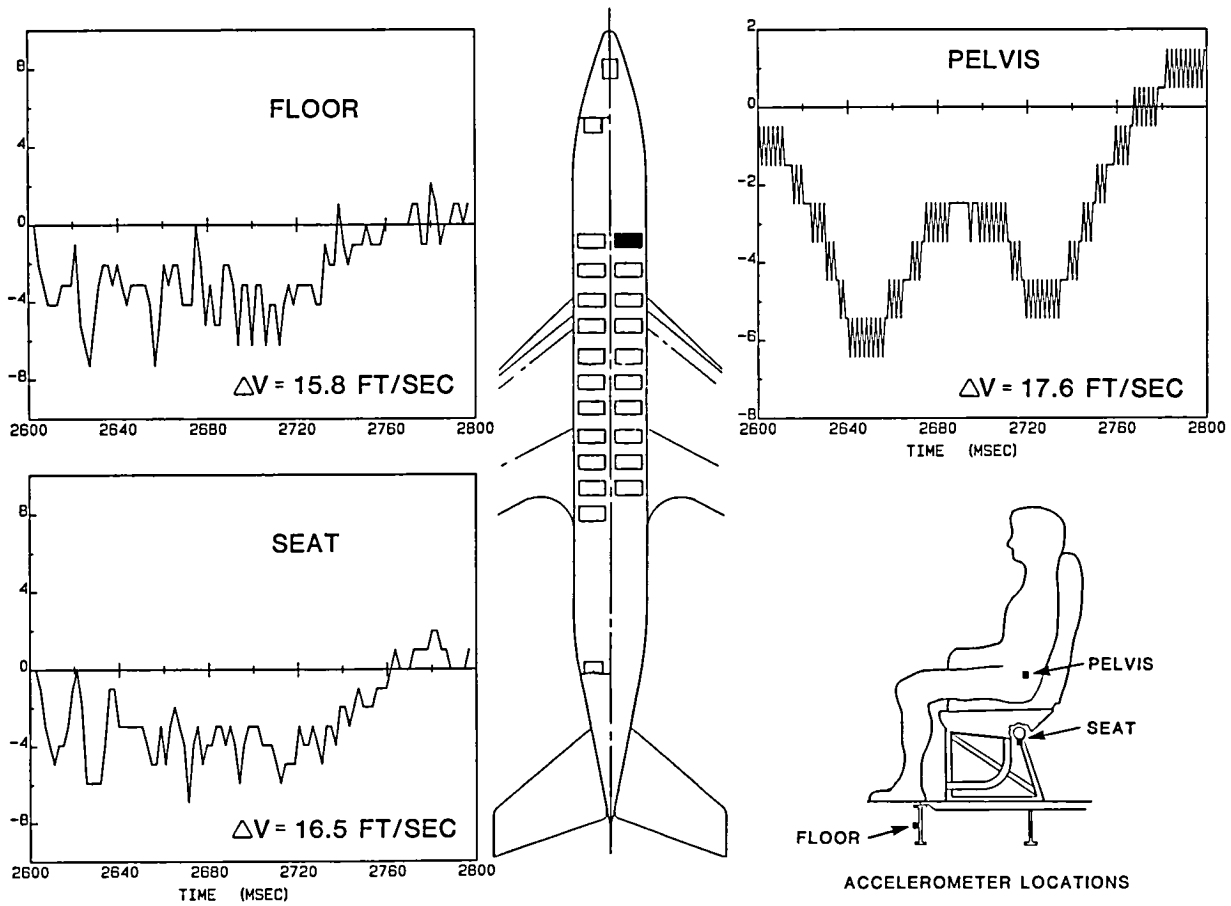


Figure 15.

LONGITUDINAL ACCELERATIONS - SEAT A (R.H.), GROUND IMPACT

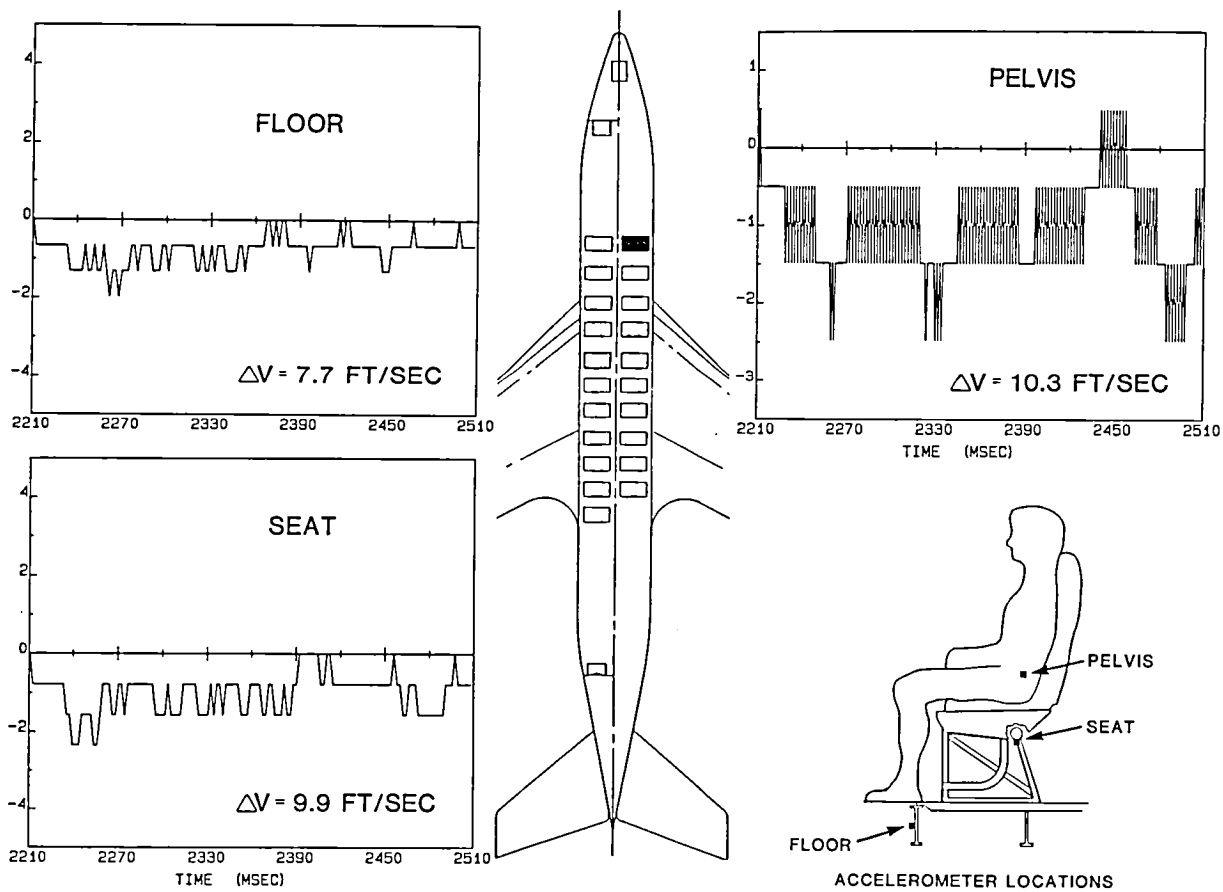


Figure 16.

LATERAL ACCELERATIONS - SEAT A (R.H.), GROUND IMPACT

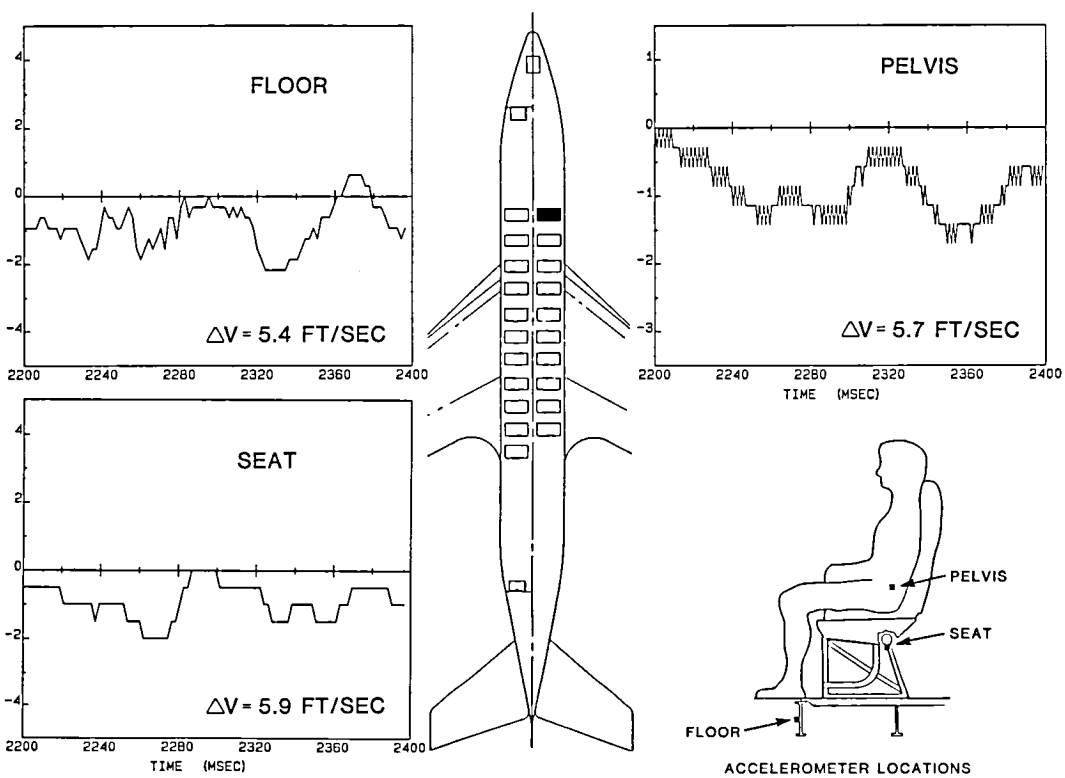


Figure 17.

FLOOR, SEAT, AND PELVIS ACCELERATIONS - OBSTACLE IMPACT

The following three figures (figures 18-20) show floor, seat, and pelvis data for obstacle impact. This includes four seat accelerations along the length of the cabin, and seat and pelvis accelerations for Seat A.

The vertical seat accelerations for four seats along the length of the aircraft are shown in figure 18, which shows that the accelerations on those seat pans during obstacle impact are a function of position along the aircraft. There are some higher values than were seen on ground impact. There are very brief and occasional accelerations of over 20 G; sometimes there is a sharp spike up to 40 G. However, they are extremely steep and narrow and represent very little energy. It therefore does not appear unusual for unmodified seats to have survived this impact.

Figure 19 shows the longitudinal data during obstacle impact for the same four seats. Again, the response is shown to be most severe in the aft portion of the aircraft.

Figure 20 shows the lateral acceleration component. Note that the main pulses are wider. This is probably consistent with the cutter tearing through the aircraft as it slid sideways.

VERTICAL SEAT ACCELERATIONS – OBSTACLE IMPACT

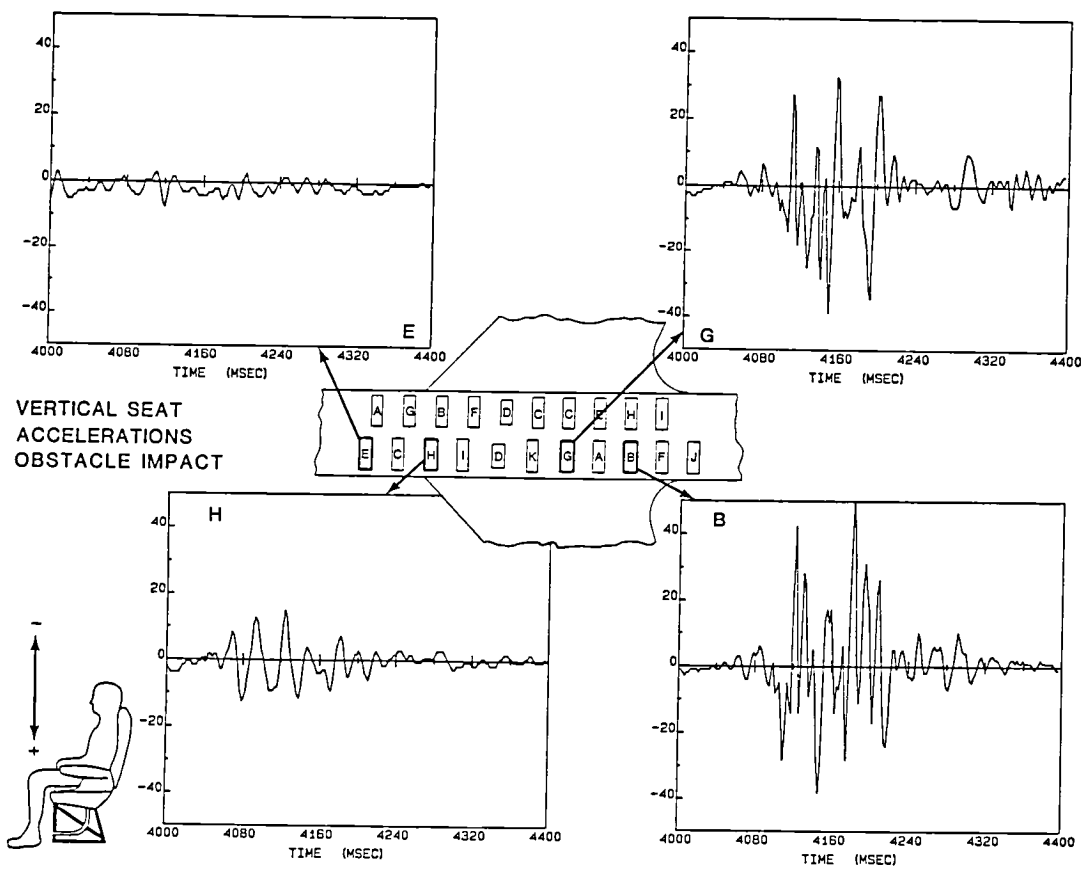


Figure 18.

LONGITUDINAL SEAT ACCELERATIONS - OBSTACLE IMPACT

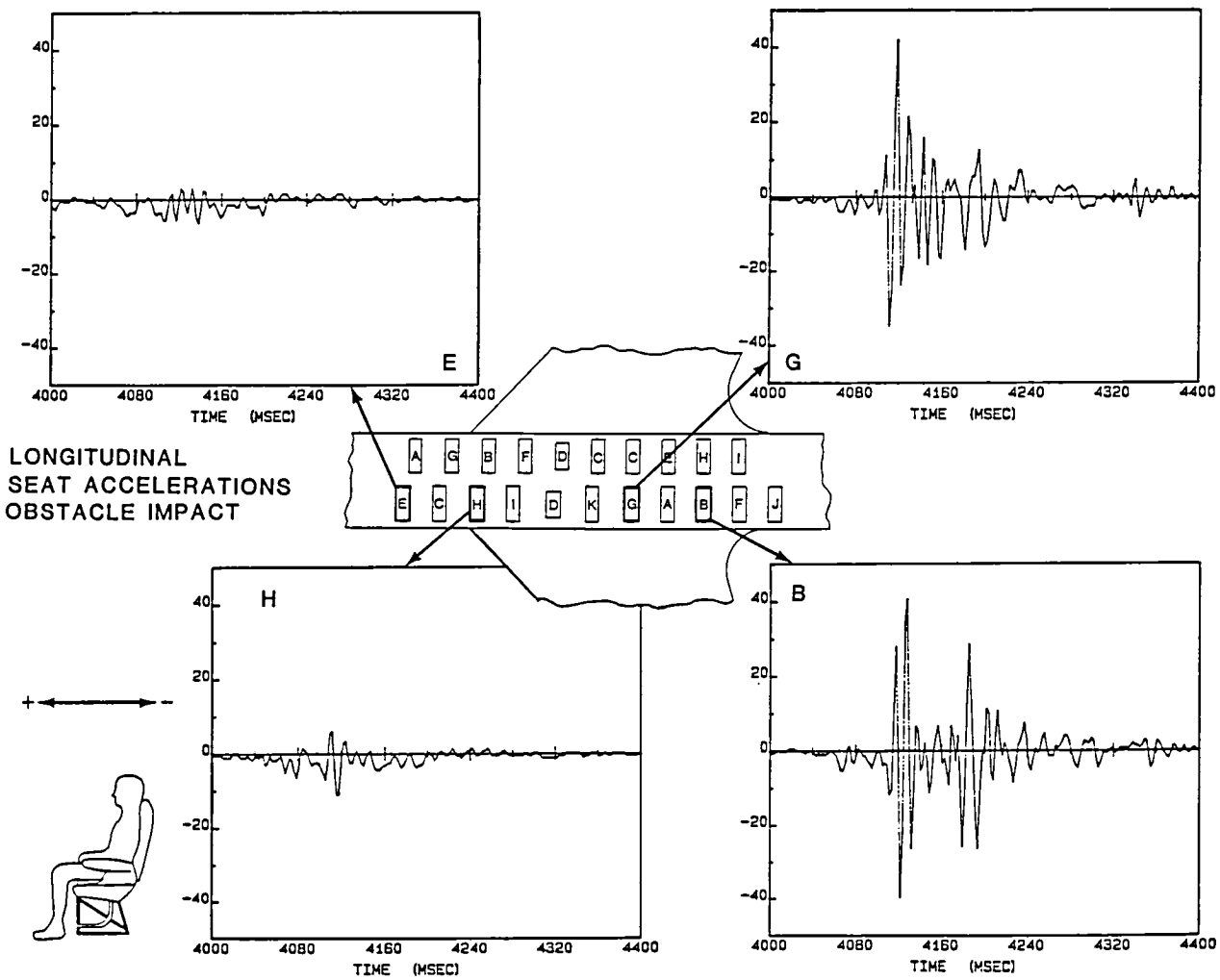


Figure 19.

LATERAL SEAT ACCELERATIONS - OBSTACLE IMPACT

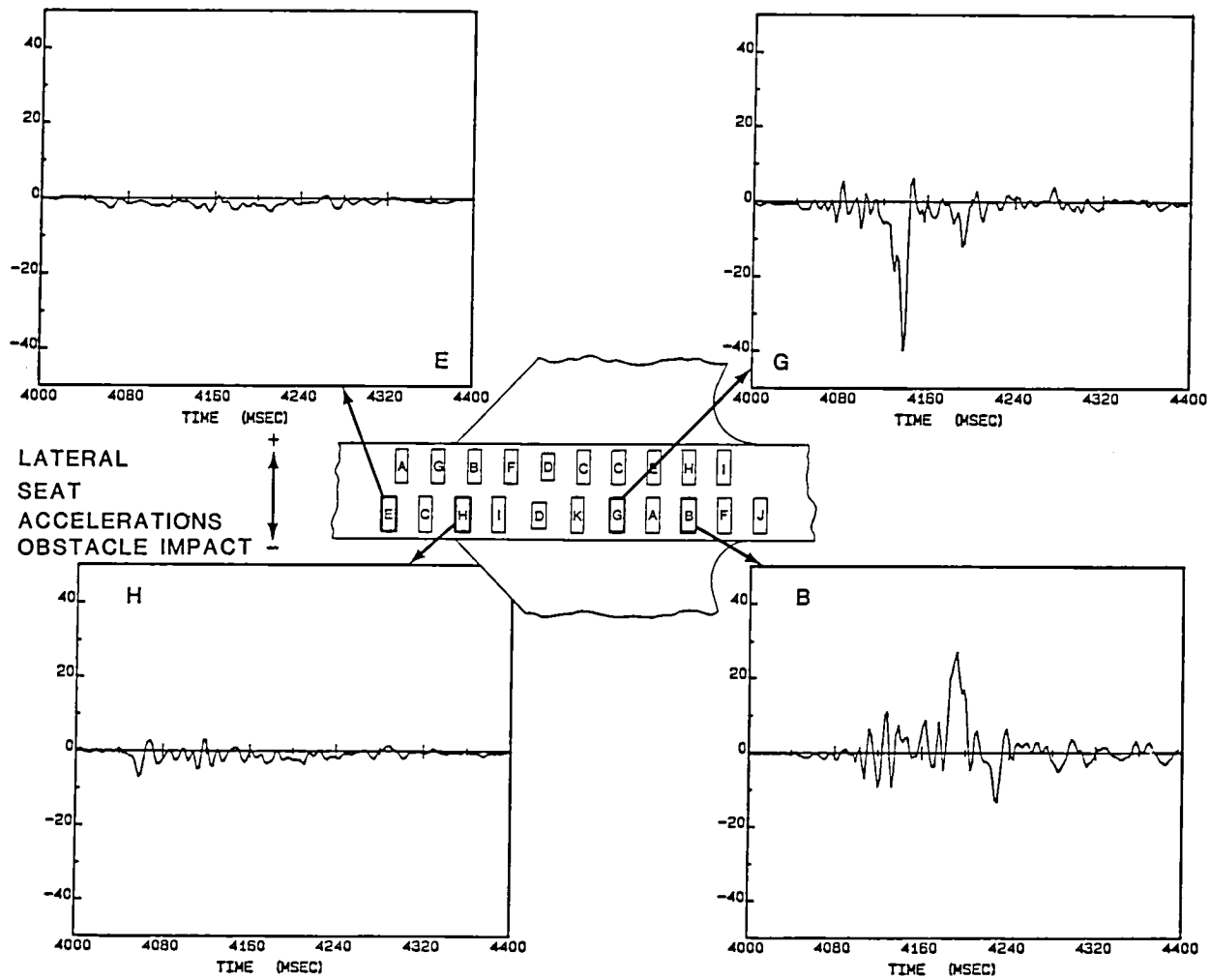


Figure 20.

VERTICAL ACCELERATIONS - SEAT A (R.H.), OBSTACLE IMPACT

The next three figures (figures 21-23) show seat and dummy response during obstacle impact. Figure 21 shows comparisons of the floor, seat, and pelvis response for Seat A. This was the most forward seat in the cabin, and similar data for this seat during ground impact has already been shown. Again, the data is consistent. The fact that the floor and seat pan accelerations matched fairly well gives confidence that the transducers were performing properly. This is particularly true of the vertical acceleration. The dummy response is quite different, as would be expected. However, the velocity change for the dummy is also quite different, and this is not so encouraging.

The longitudinal data seen in figure 22 also shows reasonable correlation between floor and seat pan. Here, the dummy velocity change is more nearly matched to that of the seat pan.

Figure 23 shows the lateral component of acceleration during ground impact. The lesser stiffness of the seat in this direction causes more of a disparity between floor and seat pan accelerations.

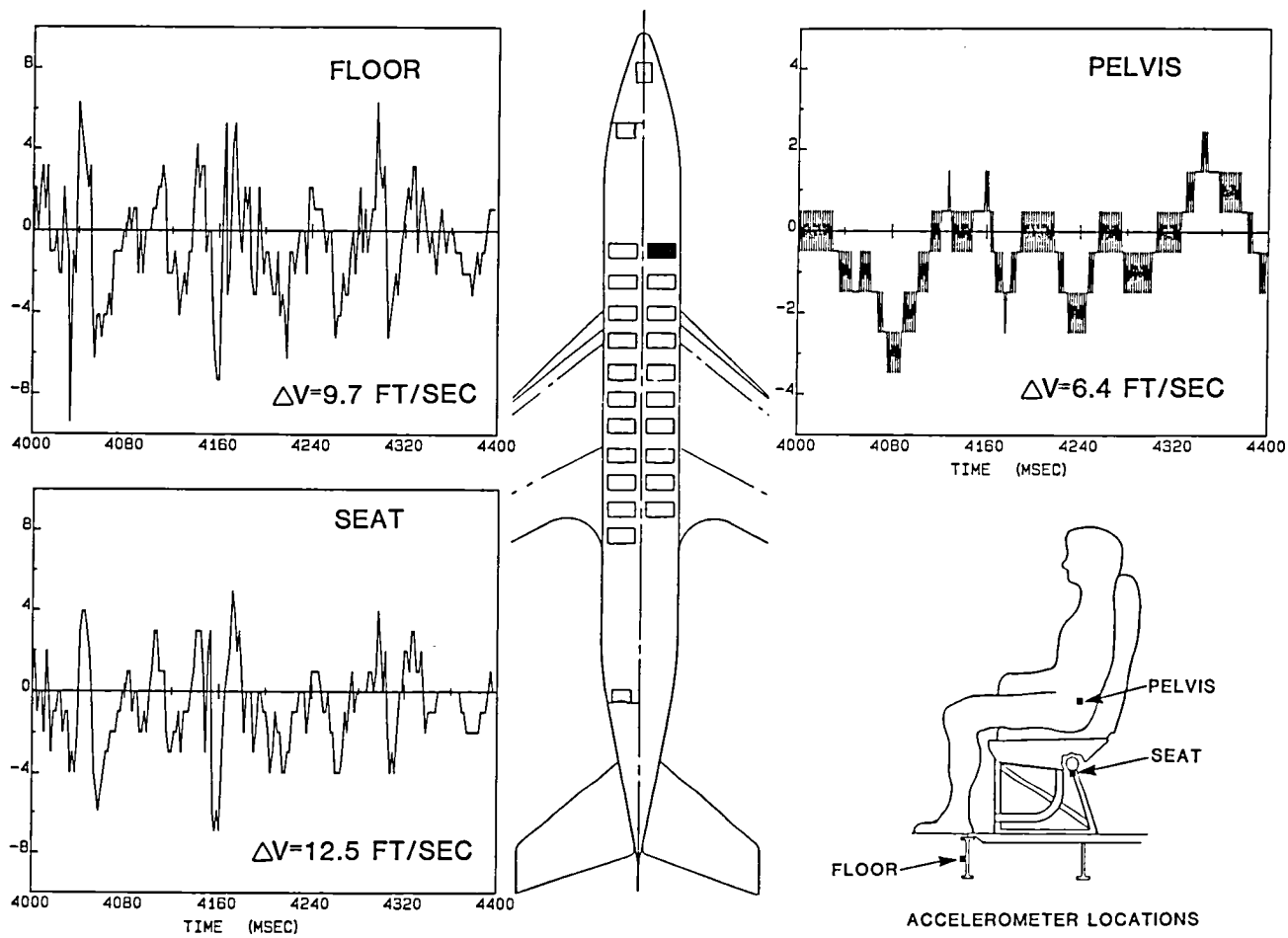


Figure 21.

LONGITUDINAL ACCELERATIONS - SEAT A (R.H.), OBSTACLE IMPACT

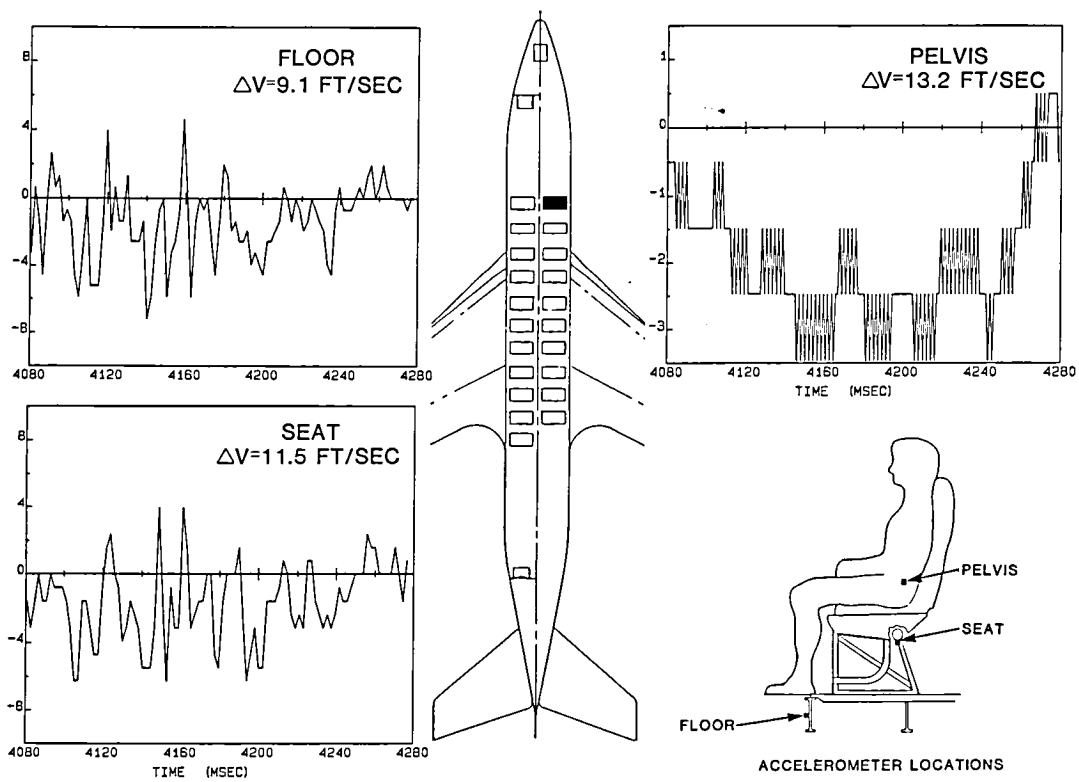


Figure 22.

LATERAL ACCELERATIONS - SEAT A (R.H.), OBSTACLE IMPACT

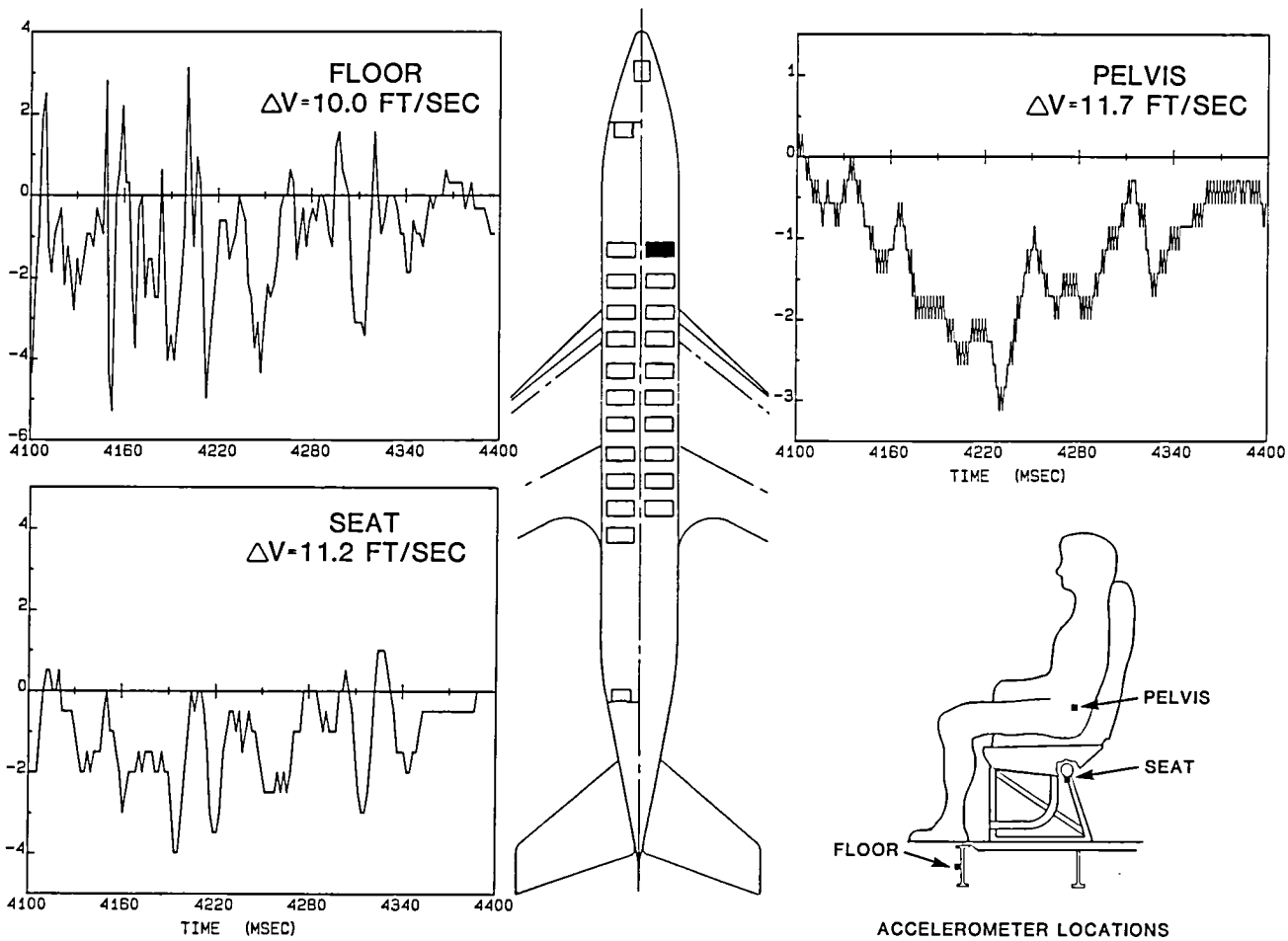
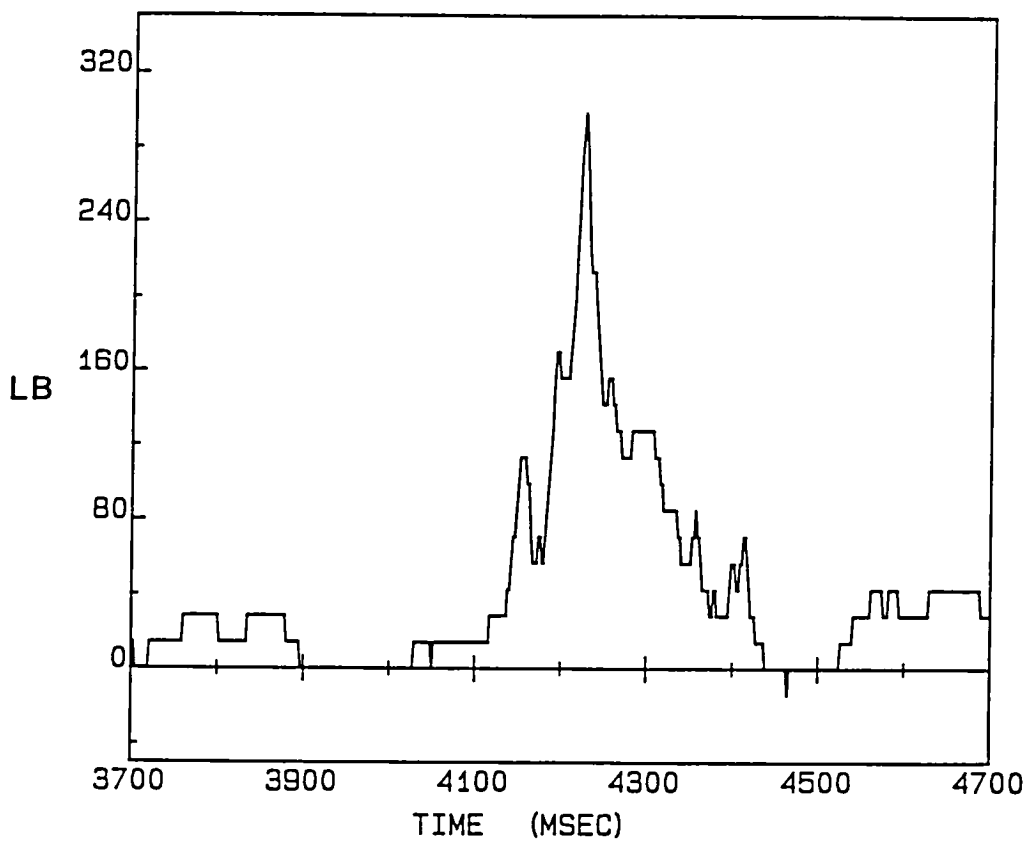


Figure 23.

TYPICAL LAP BELT LOAD

Figure 24 shows a typical lap belt tensile load, with about a 300-lb peak. This is a low load for a lap belt, and most of the lap belt data reviewed is similar. It is relatively consistent with the measured G loads and the film data which shows that the dummies did not jackknife.



OBSTACLE IMPACT

Figure 24.

OVERHEAD BIN ACCELERATIONS (G) - OBSTACLE IMPACT

Figure 25 shows overhead bin data. The FAA had a few accelerometers on an overhead bin that was placed in the aircraft. There was a mass attached to the door of the bin and the accelerometer was mounted to its back. There are peaks of 6 G or more in the vertical and longitudinal directions. Higher values are seen in the lateral direction. This data is from the time of obstacle impact.

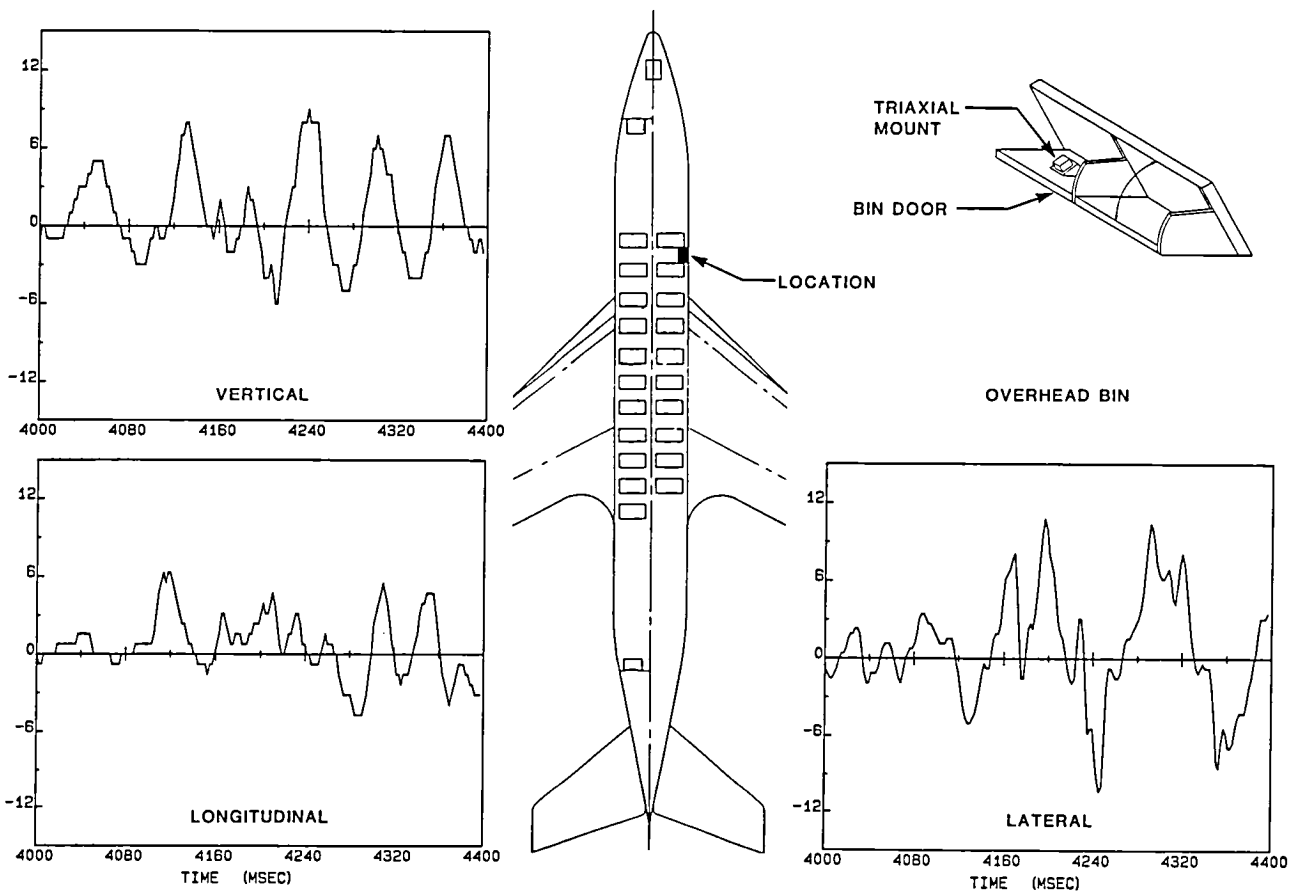


Figure 25.

CONCLUSIONS

According to preliminary examination of the data, out of 179 data channels that were onboard the aircraft in support of the seat experiments, there is data from 168. There was a somewhat more severe environment imposed in the structure by the obstacles than by the ground impact. Therefore, both ground impact and obstacle impact are of interest for crashworthiness experiments. Most of the data channels that were studied are fairly consistent with the physical evidence: they show acceleration levels that are reasonable, and in many cases these integrate out to a reasonable velocity change.

Finally, from observation thus far, the ground impact did not fail or significantly damage any seat. Nor did any of the energy absorbers in the modified seats extend. The accelerations do not appear high enough and/or energetic enough to cause this to happen. Of course, at this time, the onboard films have not been studied; only some videotapes have been viewed. Some of the seats were so badly damaged by the fire that any failures which might have occurred were obscured. A close examination of the onboard films using a stop-action projector will allow a more thorough evaluation.

REFERENCES

1. Johnson, Richard A.: Controlled Impact Demonstration Seat/Cabin Restraint Systems - FAA. Full-Scale Transport Controlled Impact Demonstration, NASA CP-2395, 1986, pp. 49-60.

2. Fasanella, E. L.: Digital Filtering and Acceleration Pulse Interpretation. Full-Scale Transport Controlled Impact Demonstration, NASA CP-2395, 1986, pp. 103-123.

3. Alfaro-Bou, Emilio: Structural Loads Preliminary Results. Full-Scale Transport Controlled Impact Demonstration, NASA CP-2395, 1986, pp. 91-102.

CONTROLLED IMPACT DEMONSTRATION
AIRFRAME BENDING BRIDGES

Stephen J. Soltis
Federal Aviation Administration
Los Angeles Area Office
Long Beach, California

NASA/FAA Government/Industry CID Workshop
NASA Langley Research Center
April 10, 1985

There are two issues at stake here. One issue concerns occupant load protection (what type of loads did the occupant see), and most of the CID workshop discussions dealt with the loads that the seat or occupant would see. Another issue is whether the airframe provides a protective shell for the occupant. The bending moment bridges that will be discussed address that issue.

We have seen several goals and objectives in most of the CID presentations. These are much the same as those that you've seen previously. These goals and objectives come from the CID program plan itself and relate to the moment bridges themselves.

One goal is the calibration of the "KRASH" and "DYCAST" models for transport aircraft. The FAA uses computer analysis techniques to predict the response of CID during impact. The moment bridges can provide a direct correlation between the predictive loads or moments that the models will predict and what was experienced during the actual impact.

Another goal is to examine structural failure mechanisms and correlate with analytical predictions. Regarding failure mechanisms, do or do we not break the fuselage shell? There has been quite a bit of discussion, with respect to the analytical models, concerning the potential occurrence of a break in the fuselage shell.

As the third goal we would like to provide baseline metal crash data to support the NASA composite crash dynamics research; of course, any structural data would provide that.

Primary CID Goals/Objectives

- **Calibration of "Krash" and "Dycast" Models to Transport Aircraft**
- **Examine Structural Failure Mechanisms and Correlate with Analytical Predictions**
- **Provide Baseline Metal Crash Data to Support NASA Composite Crash Dynamics Research**

Now, what do the moment bridges provide? Well, they in fact do address those objectives directly. You can say they may be directly related to and correlated with the analyses, both KRASH and DYCAST. We have a direct correlation between predicted and measured moments. The moment bridges provide an understanding of fuselage loading and breakup. Should the fuselage break, the moment bridges were located so that they could detect the time and location of the break. The moment bridges also can provide an assessment of the dynamic and static fuselage strength capability. They can actually measure the strength capability during the impact for comparison with analytical techniques. Bending moment bridges are the highest and best use of available instrumentation--any structural instrumentation falls into that category.

BENEFITS OF FUSELAGE INSTRUMENTATION

- MAY BE DIRECTLY RELATED TO AND CORRELATED WITH ANALYSIS (DYCAST/KRASH)
- PROVIDES AN UNDERSTANDING OF FUSELAGE LOADING AND BREAK-UP
- ASSESS DYNAMIC/STATIC FUSELAGE STRENGTH CAPABILITY
- HIGHEST AND BEST USE OF AVAILABLE INSTRUMENTATION

The overall scheme that was used for the moment bridge instrumentation makes use of a total of 12 fuselage bending bridges distributed along the length of the fuselage. Eight were distributed to measure vertical bending, and there were four bridges that would measure lateral bending. A typical distribution is shown on this diagram. The lateral bridges were installed, but they were not calibrated due to some schedule and also cost problems. The lateral bridges were essentially installed to detect unsymmetrical loads in an impact that is or appears to be symmetrical, and should there be some unsymmetrical loading, to detect and measure that loading. CID did have an unsymmetrical impact and maybe a little bit of data was lost due to a lack of lateral bending bridge calibration.

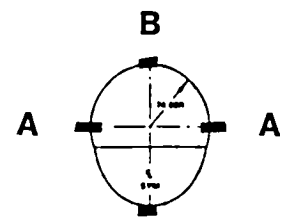
Overall Fuselage Instrumentation

Total of 12 Fuselage Bending Bridges Distributed Along Fuselage Length

8 Vertical Bending B-B

4 Lateral Bending A-A

Bending Bridges



Fuselage Crossection

This represents just a brief depiction of where the bridges are located on the airframe. These stations are roughly the same locations where the accelerometers were located along the circumference of the fuselage.

Moment bridges were located at Station 410. These were installed to assess the nose loads. There is a production break located in this area. There is some discussion whether or not airframes break at production breaks. Should a fuselage break occur in the area of the production break during the test, the moment in that vicinity would be measured.

Station 510 was located essentially to assess the forward fuselage load just aft of the actual nose load itself.

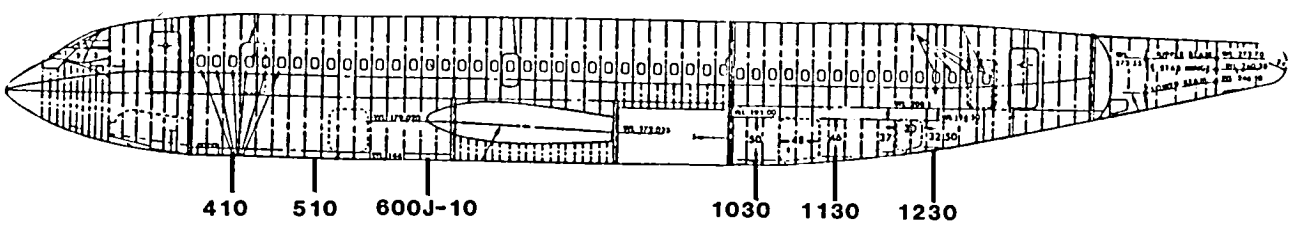
Station 600J-10 was located to assess fuselage loads at the forward edge of the wing box. There is also a manufacturing break in the same vicinity.

Station 1030 was located to assess fuselage loads aft of the wing box and at the aft edge of the main gear cavity.

Station 1130 was located to assess aft fuselage load. It is in the area of a manufacturing break and in the transition area where the fuselage cross section starts necking down.

Station 1250 was located to assess aft fuselage loads outside of the lower fuselage ground contact area to see what type of loads one might get there from the cantilevered overhang of the fuselage itself.

Rationale For Locations of Fuselage instrumentation



STA. 410 - ASSESS NOSE LOAD
- PRODUCTION BREAK

STA. 510 - ASSESS FWD FUSELAGE LOAD

STA. 600J-10 - ASSESS FWD FUSELAGE LOAD
- FWD EDGE OF WING BOX
- MANUFACTURING BREAK

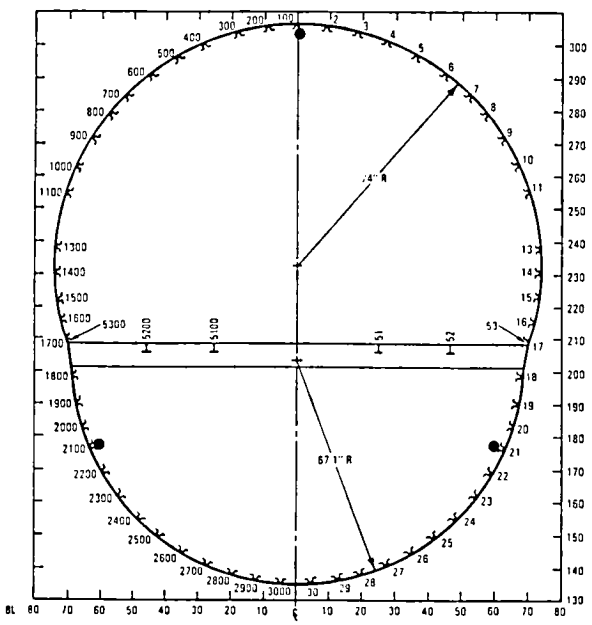
STA. 1030 - ASSESS AFT FUSELAGE LOAD
- AFT OF WING BOX
- AFT EDGE OF MAIN GEAR CAVITY

STA. 1130 - ASSESS AFT FUSELAGE LOAD
- MANUFACTURING BREAK
- TRANSITION AREA

STA. 1250 - ASSESS AFT FUSELAGE LOAD
- OUTSIDE OF LOWER FUSELAGE GROUND CONTACT AREA

This depicts the strain gage locations at Station 510. Station 510 only had a vertical bending bridge installed. The two strain gages located on the upper crown of the figure and the two located on stringers 2900 and 29 on either side of the fuselage are wired to form a four arm bending bridge. They were calibrated, and the procedure will be discussed later. The actual location and stringer placement of the strain gages were based on a review of the stress analysis of the airframe. Primary structural members that would give a high stress reading per the airframe structural analysis were selected. All of the strain gages were located on fuselage cross-sections in the same manner.

Body Station 510 Bending Bridges



- Vertical Bending

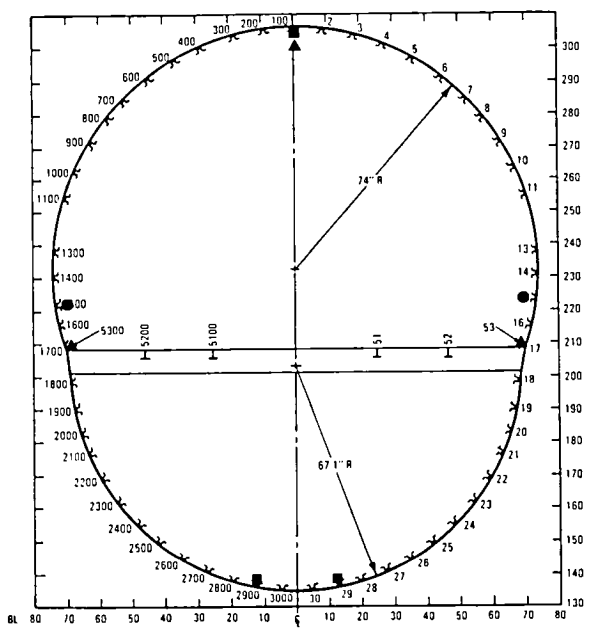
Typical Cross Section With Stiffner Locations - Rear View

At Station 600J-10, the same strain gage installation philosophy was used. A vertical bending bridge is installed with strain gages located at the upper crown and floor line locations. A double bending bridge is installed at this station and also at Station 1030. Fuselage bending is measured both between the upper crown and the floor line and at the lower part of the fuselage itself.

The lateral bending bridges are located on stringers 1500 and 15 which are somewhat the outermost members on the fuselage cross section.

Some of the rationale for a double vertical bridge was on Stations 600J and 1030. These locations should experience the highest bending moments. It was desired to have redundant bridges, first of all, so that we could actually measure the highest bending moment should any single bridge lose signal. Secondly, it was also desired to assess how the bridges may differ between strain gages located on the lower crown of the fuselage and strain gages located near the floor line, should there be a difference in readings during the actual impact due to the fuselage crush. The two bending moment time history traces should record identically. If one finds a significant departure in the two traces, the credibility of the lower bending bridge may be lost.

Body Station 600J-10 Bending Bridges



- ▲ Vertical Bending Floor
- ■ Vertical Bending Lower
- • Lateral Bending

Typical Cross Section With Stiffener Locations - Rear View

The bending bridges were calibrated by applying known loads at known distances to the bridges themselves. There were a couple of calibration schemes proposed and this depicts the calibration procedure that was selected. First, all the onboard equipment was documented to identify the weight distribution of the aircraft for the 1 g static condition in order to correct the measured moments to zero moment reference.

Down loads were applied to the horizontal stabilizer in 21% load increments by placing load shot bags on the horizontal stabilizer up to a 12,800 lb total load. This load equals approximately 15% of the airplane's design limit load at Station 1030. The moment resulting from the 1 g cantilever overload of the aft fuselage also equals about 15% of the airplane's design limit load at Station 1030. Thus, the aft fuselage calibration load ranged from 15-30% of the airplane's design limit load.

The nose gear reaction was also recorded for each load level by a load cell installed directly in line with the nose gear strut. This provided for a simultaneous calibration of both the forward and aft fuselage bending bridges.

The aft bridge calibration used the distributed weight on the horizontal stabilizer as the known load; the forward bridge used the change in the nose gear strut load as the known load.

Fuselage Calibration Procedure

On Board Equipment Documented

Down Load Applied to Horizontal Stabilizers

- Distributed Lead Shot Bags
- 16-21% Load Increments
- 12800# Total Load

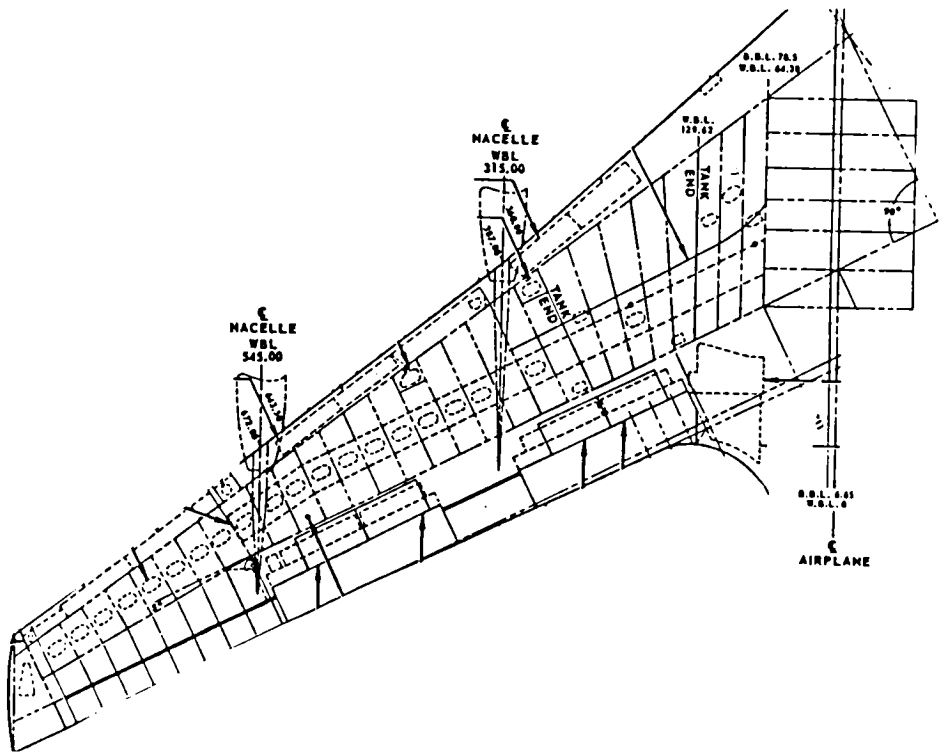
Nose Gear Reaction Recorded for Each Load Increment VIA Load Cell

Simultaneous Calibration of Both Fwd/Aft Fuselage Bending Bridges

Wing bending bridges were also installed on CID. Depicted here are the approximate locations of the wing bending bridges. One bridge is located just outward of the closing member of the wing and the landing gear cavity. This location is also the end of the inboard fuel tank. Another bending bridge is located just outboard of the inner nacelle. These bridges only measure vertical loading.

The wing bending bridges are used to measure the magnitude of the wing loads during impact to assess the proximity of those moments to design loads. These moment bridges would also measure the wing loading should a wing be fractured.

Locations of Wing Bending Bridges



The wing calibration procedure was very similar to that used for the fuselage. First, the fuel load was documented so one would again know what the initial conditions were prior to start of calibration. Downloads were applied inboard of the wing tip, again by means of distributed lead shot bags in 25 percent load increments up to a total load of 5,000 lb on each wing tip. Both wings and the inboard and outboard wing bridges were calibrated simultaneously.

Wing Calibration Procedure

Fuel Load Documented

Down Load Applied Inboard of Wing Tip

Distributed Lead Shot Bags

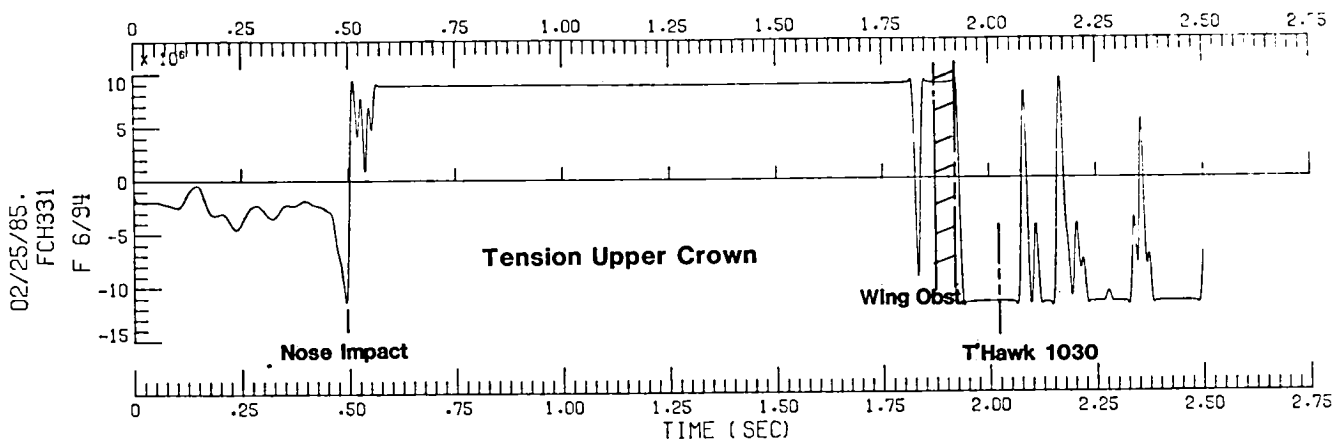
25% Load Increments

5000# Total Load (Each Wing)

Simultaneous Calibration of Both Wings and InBd/OutBd Wing Bending Bridges

The analysis of the moment bridge is incomplete at this time and all these comments represent nothing more than a cursory analysis. B.S. 410 is the forward fuselage bridge and it was located close to the point of impact. The range on the moment bridges was initially proposed to be somewhere between 2 times to about 2-1/4 times limit load. It was felt that the bridges would behave linearly beyond limit load based on some static testing of fuselage shells. Those tests show compressive instability failures of the fuselage shell and linear behavior up to ultimate load levels. Based on the instrumentation listing, the bending bridge ranges were limited to a little less than limit load. That restricted range didn't make too much of a difference, except in a few isolated cases.

Fuselage B.S. 410 Vertical Bending



This trace illustrates the aircraft impact, obstruction encounter, and the aircraft's response to those events. Analysis of this time history can find:

Wing Impact
Nose Impact
Wing Obstruction Encounter
Fuselage Impact with the Tomahawk

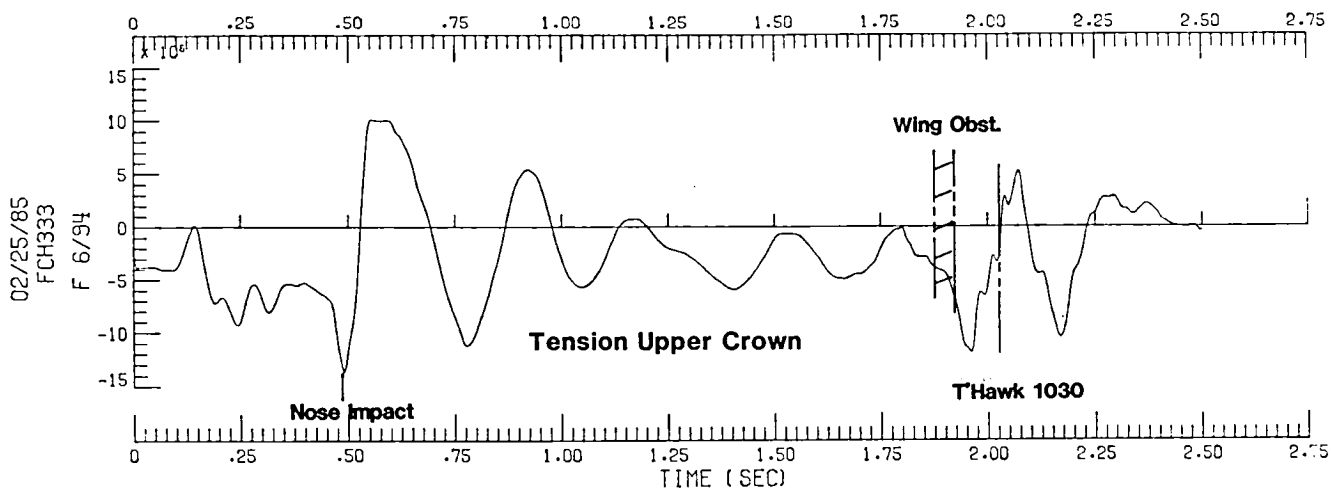
The time intervals identified on the moment bridge trace for those events correlate well with both photographic data and the accelerometer time histories.

The B.S. 510 moment time history appears to be a single one-degree-of-freedom damped response. Analysis of that trace can also determine the frequency of response and the structural damping.

The zero moment reference line has yet to be determined; however, it appears as if the airframe is oscillating about the 1 g static load condition.

A little flat spot was noted on one of the peaks where the moment bridge range was slightly exceeded.

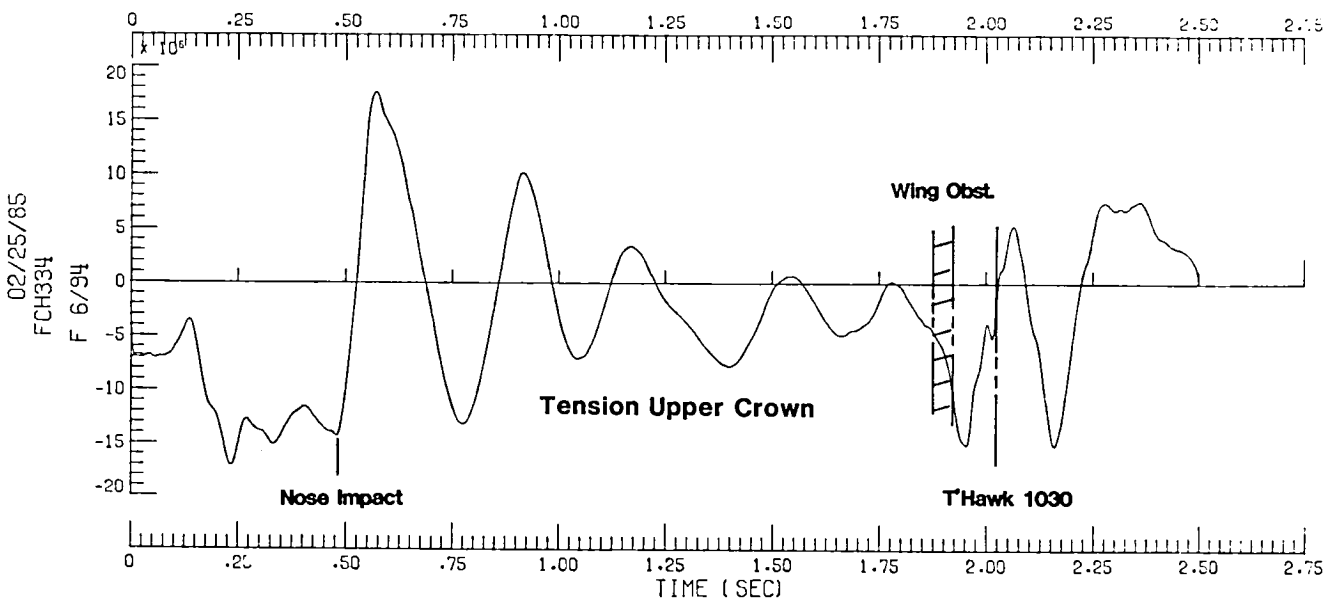
Fuselage B.S. 510 Vertical Bending



The 600J-10 time history looks essentially identical to the B.S. 510 time history. One can see the same type of response and the same time reference for the events which took place. Looking at some of the peak moment values, estimating a zero moment reference and using some ratios, one can determine airframe accelerations that seem to match measured accelerometer data. Integrating the acceleration estimates in a simplistic way results in finding velocity change estimates at B.S. 600J-10 and at Station 510 that seem to match the measured data. It appears as if the moment bridges could be used to estimate the initial impact conditions. One can see a consistency here between B.S. 510 and B.S. 600J-10. A consistency of the wave shape, frequency damping and response is noted. It appears as if the bending moment bridges performed well.

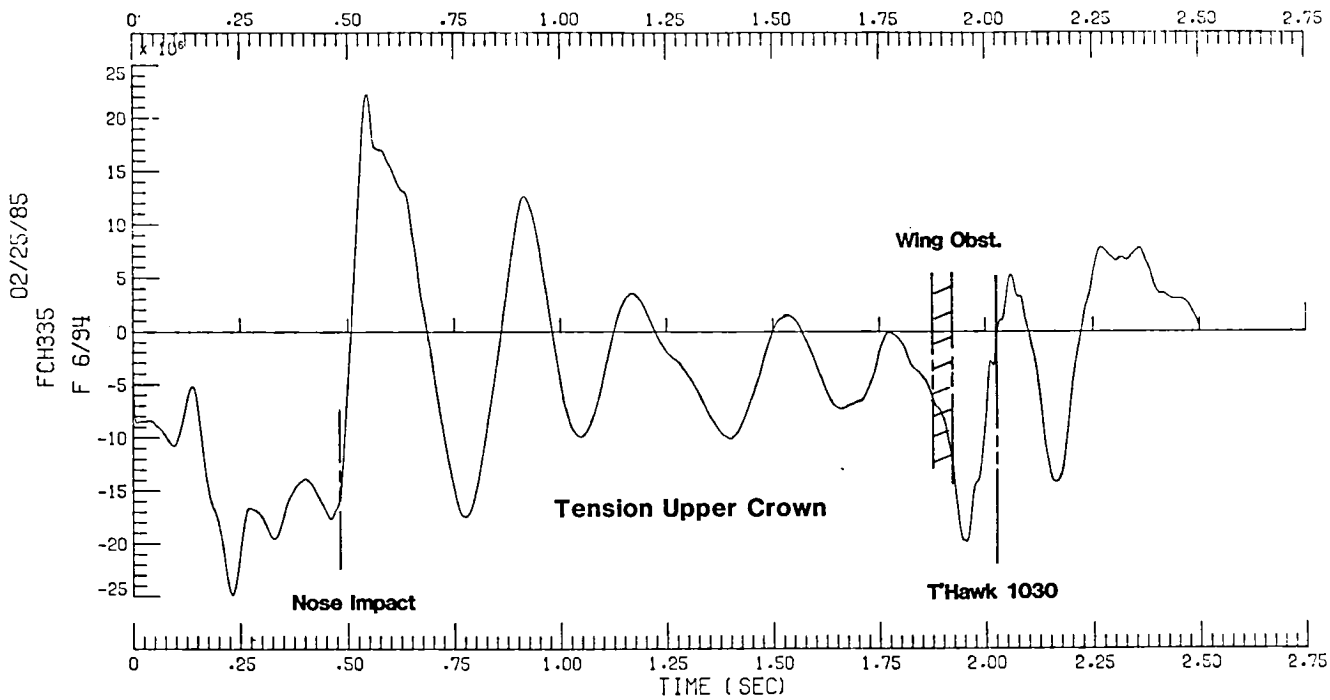
The B.S. 600J-10 peak moments exceeded those at B.S. 510 as expected.

Fuselage B.S. 600J-10 Vertical Bending (Floor)



The 600J-10 lower bridge response looks just like the responses of the other bridges located in the forward fuselage. The 600J-10 (Floor) and 600J-10 (Lower) moment bridges possess the same response, shapes and magnitudes. There is consistency of readings between the bridges. This consistency of response also reflects on the technicians that installed these bridges. They did an excellent job and deserve a lot of credit for the placement and wiring of these bridges.

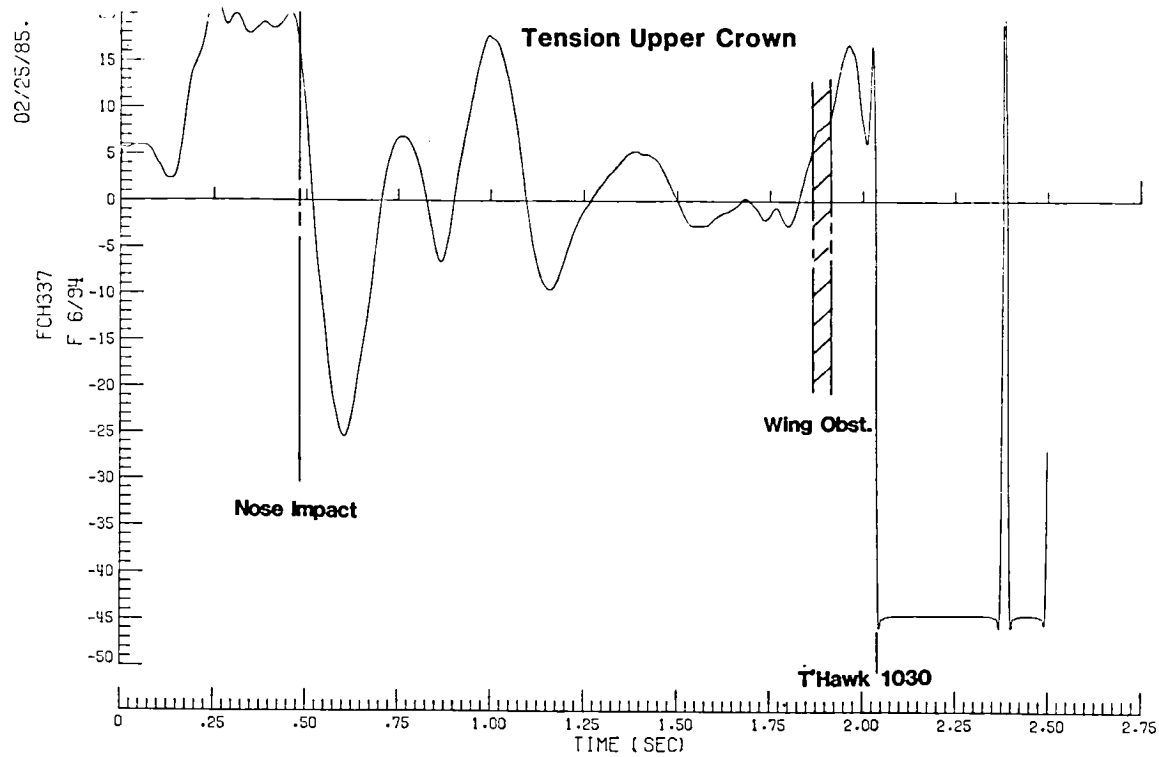
Fuselage B.S. 600J-10 Vertical Bending (Lower)



The shape of the aft fuselage moment time histories differs from those in the forward fuselage. The aircraft did experience both a vertical and lateral impact and that is reflected in the response of the aft fuselage moment bridges. These bridges appear to contain a vertical mode coupled with an airframe torsional mode induced by the lateral motion of the empennage.

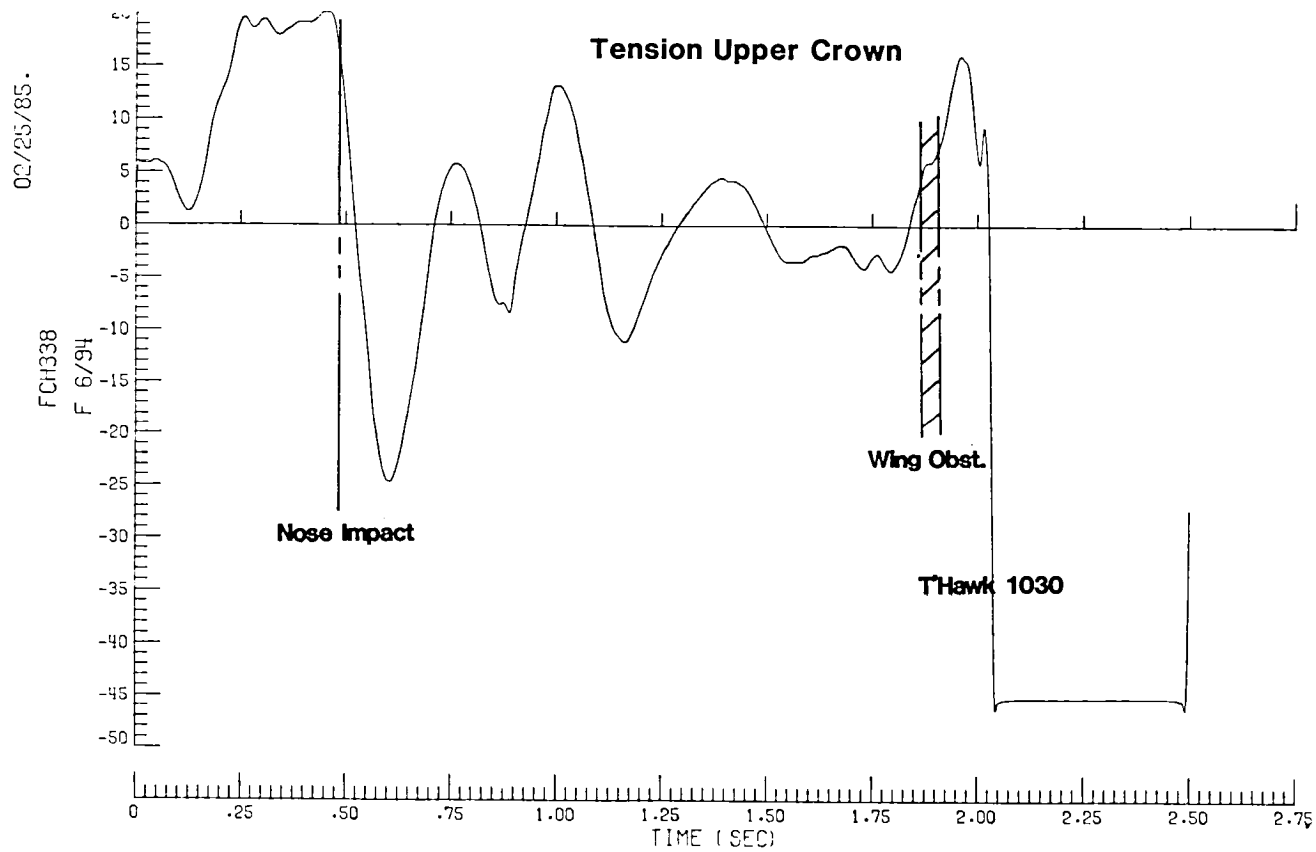
The significant events can again by observed on the moment bridge time history. It can readily be seen where the tomahawk destroyed the B.S. 1030 moment bridge with the corresponding loss of signal.

Fuselage B.S. 1030 Vertical Bending (Floor)



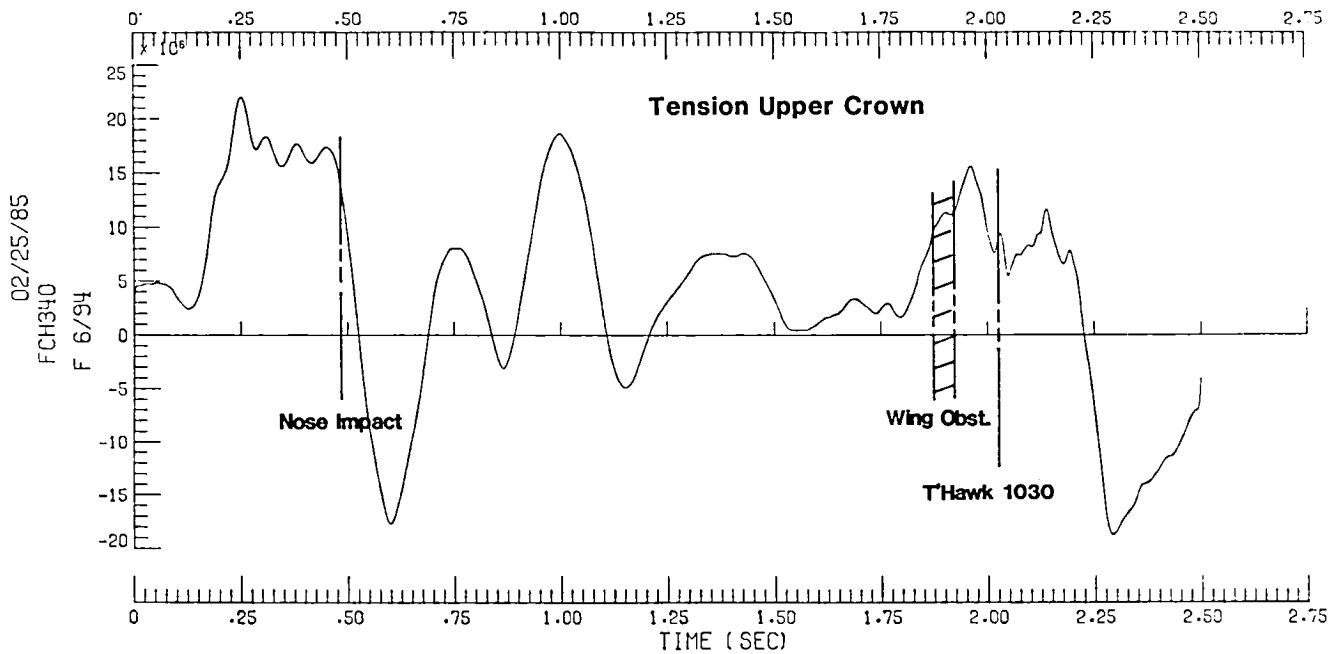
The B.S. 1030 (Lower) bridge response is essentially identical to that at B.S. 1030 (Floor). There again exists a consistency of data.

Fuselage B.S. 1030 Vertical Bending (Lower)



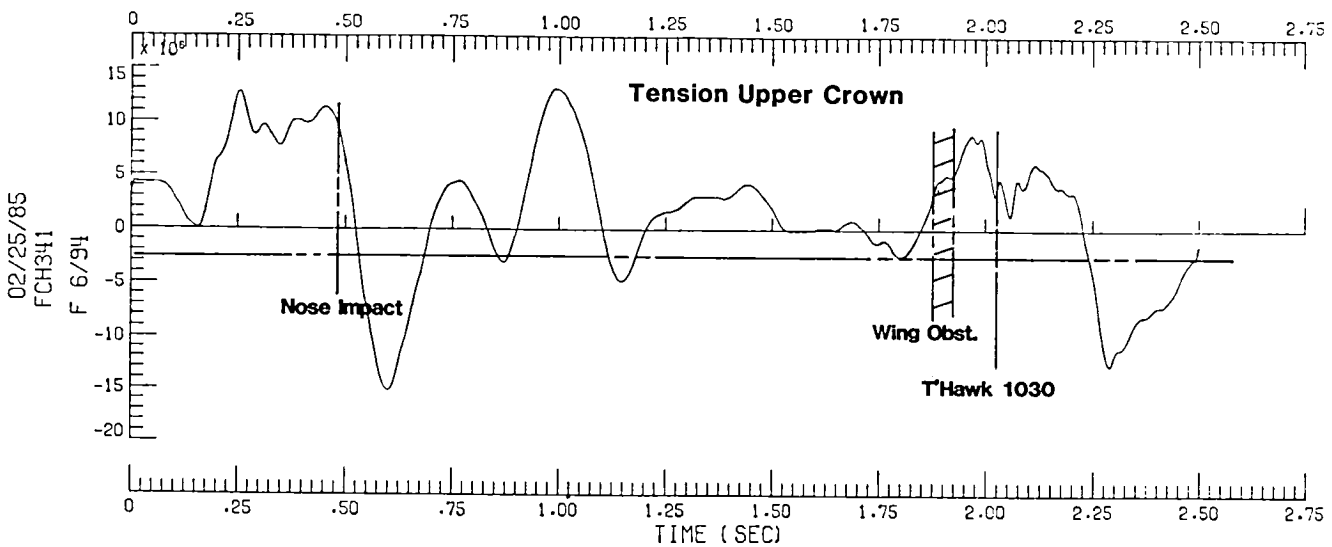
The B.S. 1030 moment bridge again demonstrates consistency of data. The magnitudes of the moments at B.S. 1130 are less than those at B.S. 1030 as expected.

Fuselage B.S. 1130 Vertical Bending



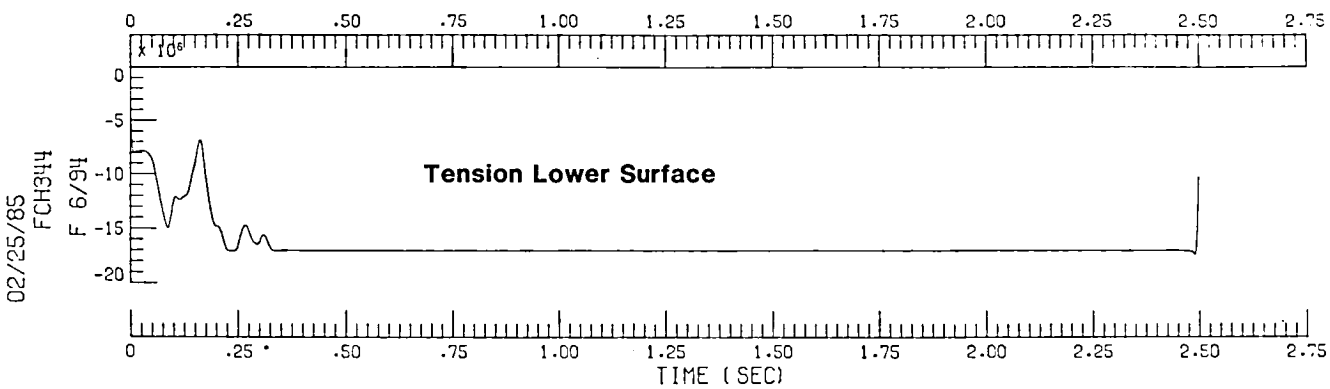
The basic response is again consistent with the other aft fuselage bridges. The magnitudes of the moments does again decrease as one goes aft along the fuselage.

Fuselage B.S. 1250 Vertical Bending



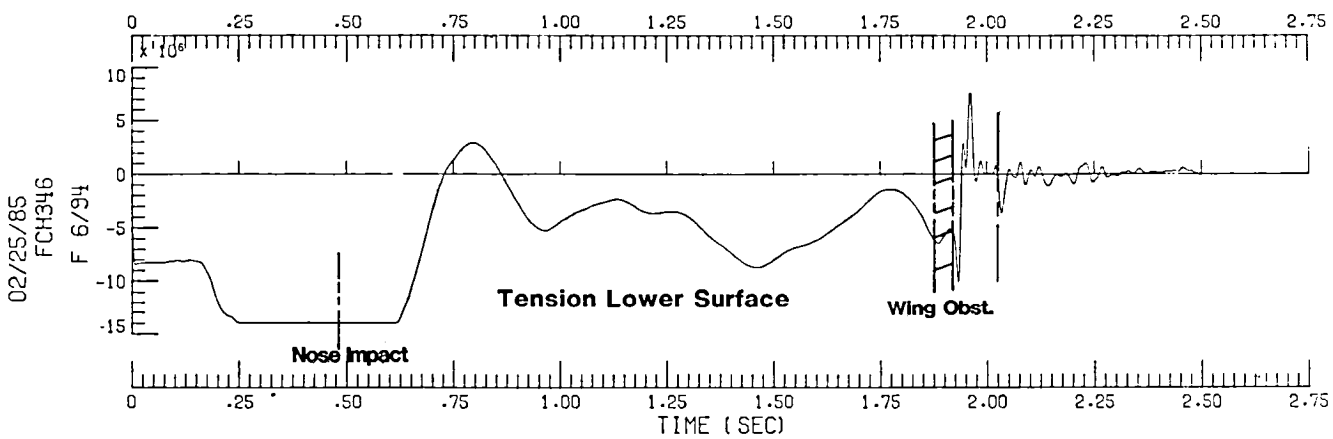
The signal from this bridge was lost soon after impact. The strain gages on the lower arm of this bridge were exposed and were not protected from ground impact and were most likely scrubbed off the surface of the wing by the ground impact.

L/H Wing (OutBd) Vertical Bending

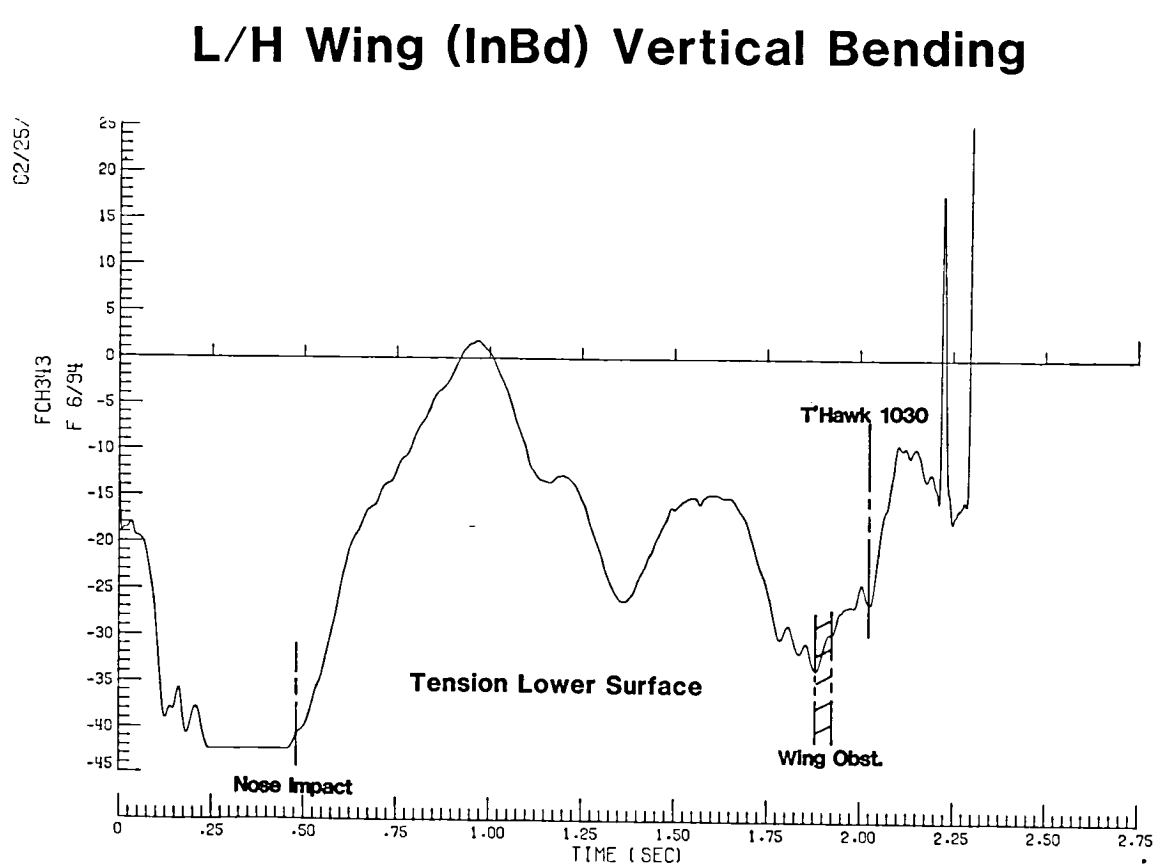


This data has yet to be analyzed; however, the encounter with the ground obstacles and subsequent loss of signal are evident. The range of the bridge was exceeded during the nose impact.

R/H Wing (OutBd) Vertical Bending

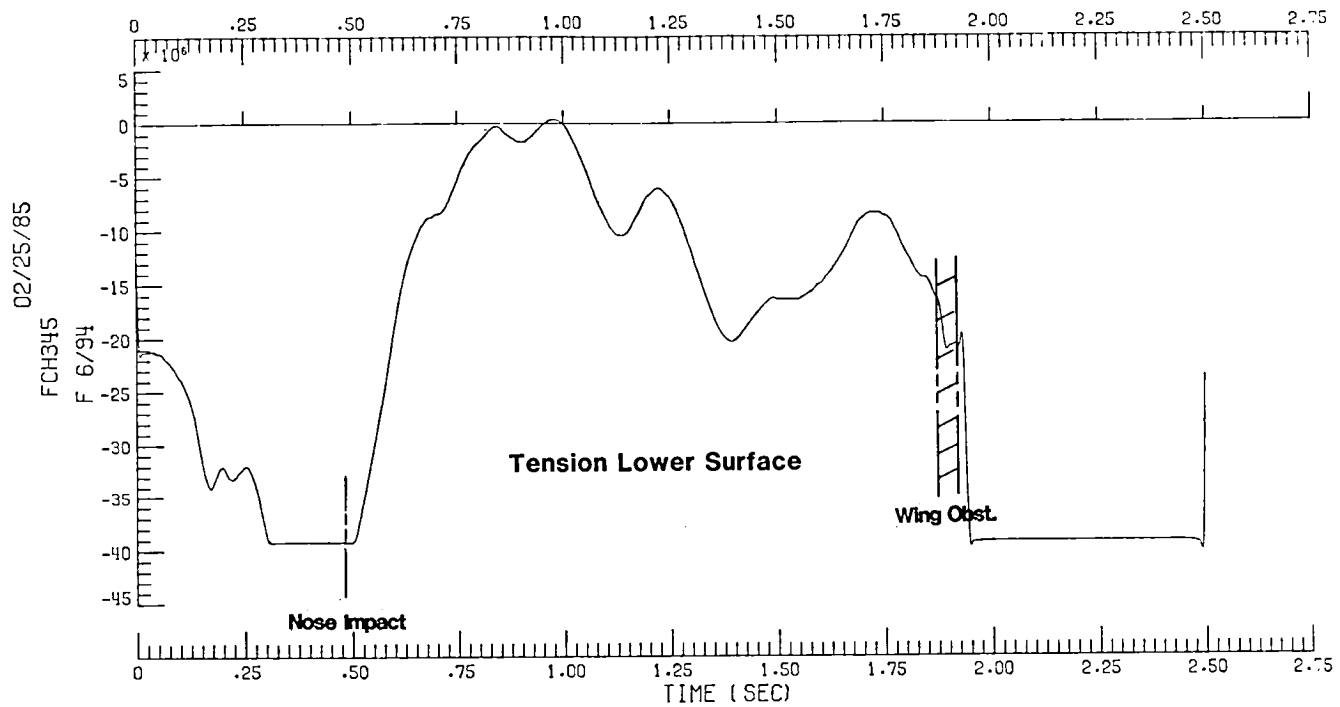


Data was recorded by the L/H wing inboard bridge. The L/H wing made ground contact. The significant events are again depicted. The range of this bridge was exceeded during nose impact. This bridge lost signal subsequent to impact with the ground obstructions.



The R/H wing and L/H inboard bridges surprisingly contain almost identical responses (including magnitudes). That wouldn't be expected since the left wing made ground contact, whereas the right wing never did strike the ground. The nearly identical response between these wing bridges is not widely understood at this time.

R/H Wing (InBd) Vertical Bending



The bending bridges did achieve their goals and objectives. The data traces do provide some insight with respect to airframe loads and structural response. They demonstrate quite clearly what's happening to the airframe.

A direct quantification of metal airframe loads was measured by the moment bridges.

The measured moments can be correlated with the KRASH and DYCAST computer models.

The bending bridge data support airframe failure mechanisms analysis and provide residual airframe strength estimation. It did not appear as if any of the bending bridges on the airframe exceeded limit loads. (The observed airframe fracture was due to the fuselage encounter with the tomahawk which tore out the keel beam.)

The airframe bridges can be used to estimate the impact conditions and those estimates are correlating with some of the other data measurements.

Structural response, frequency and structural damping are readily measured by the moment bridges.

Bending Bridge Instrumentation Achieved Goals/Objectives

Data Traces Provide Insight with Respect to Airframe Loads and Structural Response

Airframe Loads

- Direct Quantification of Baseline Metal Airframe Loads
- Measured Moments can be Correlated with Krash/Dycast Models
- Supports Analysis of Failure Mechanisms and Estimation of Residual Airframe Strength
- May be Used to Estimate Impact Conditions

Structural Response

- Frequency
- Structural Damping

CONTROLLED IMPACT DEMONSTRATION
FLIGHT DATA RECORDERS/COCKPIT VOICE RECORDERS

Leo J. Garodz
Federal Aviation Administration
Technical Center
Atlantic City Airport, New Jersey

NASA/FAA Government/Industry CID Workshop
NASA Langley Research Center
April 10, 1985

We know what the probable cause of the accident was in the CID program, obviously, and that was not why we had flight data recorders on the airplane. We decided, about 3 years ago, to see how well we could get suitable instrumentation and flight data recorders on a Boeing 720 aircraft to correlate the performance data on the aircraft itself with data from the various experiments we had on the aircraft in the crashworthiness area. Also, in trying to come up with the scenario alluded to earlier (ref. 1), where we had a certain sink speed, glidepath angle, and so forth, we went through 20 years of air carrier accident data to try to arrive at an impact scenario. The required data are not, in all cases, in NTSB accident reports. So, we're hoping that we can provide enough information from this experiment to be able to develop a survivable crash scenario should the need arise. (See fig. 1.)

Basically, on the airplane we had three DFDRs (digital flight data recorders), one each from Sundstrand, Fairchild, and Lockheed. We borrowed them with the promise that we would not hurt them, and they were subsequently practically destroyed by fire, but they all operated properly. We also had a Teledyne Flight Data Acquisition Unit (FDAU), which is nothing more than a signal conditioner. We had 11 sensors, which I will describe in more detail shortly. In addition, we had a new Fairchild Cockpit Voice Recorder (CVR) installed. We wanted to make sure that we would get data during the slideout of the aircraft, or if there had been a second impact we wanted to be able to get additional data assuming the original power supply of the aircraft failed. So we had a 28-V battery and a 115-V/400-Hz inverter also installed on the airplane. We left the existing foil flight data recorder on the airplane, and we had a Navy Deployable Flight Incident Recorder (DFIR). We also had a special Lear Siegler Solid-State Memory Unit on the airplane. Neither of these two devices was attached to sensors or recording; they both had prerecorded data sets in them. Figure 2 shows the various groups that participated.

Figure 3 shows the parameters to be recorded. We wanted aircraft performance data during impact and slideout, so we put in a new transducer for pressure altitude. We could not tie into any of the aircraft systems that dealt with the RPV system because there is a potential for signal contamination there, so we wanted a completely independent sensor system with the exception of two signals. We had new transducers for altitude and airspeed. For magnetic heading, we were allowed to tie into the existing sensor system on the airplane. We procured a special triaxial accelerometer for this experiment with a vertical acceleration range of 50 g's, a longitudinal range of 50 g's, and a lateral range of 10 g's. This assumed that we could have a fairly high kinetic energy impact condition. We found out later that the range was too high. We lost some resolution as a result. We had a vertical gyro installed in the aft end of the aircraft to give us our pitch and roll information. Because of the ground effect on the airplane, the airspeed and pressure altitude signals started to get a little unreliable as the plane got closer to the ground. Accordingly, we also wanted to record radar altitude. We procured a special vertical speed indicator, which was a pressure transducer with vertical accelerometer complimentation, from Teledyne to see if it could record vertical velocity independently.

Figure 4 is a schematic of the overall installation of the three recorders. Everthing was to be mounted on a common pallet the flight data acquisition unit; pressure altitude, indicated airspeed, pitch, roll, and

vertical speed sensors; and the static inverter/battery power supply. For the final flight we did not use aircraft electrical power; we used the battery pack and static inverter unit. Figure 5 shows the installation, which was in the aft end of the passenger area of the aircraft. Here we had the three data recorders, flight data acquisition unit, static inverter, and battery pack. Of course, we also had the existing flight data recorder and the CVR units in the aft closet area. The FAA had put them there some time ago, probably for easier maintenance.

Figure 6 shows the installation of the existing cockpit voice recorder and foil flight data recorder in the most aft bulkhead in the aircraft. The vertical speed sensor (fig. 7) was located on top of that pallet for ease of maintenance.

On December 2, one day after the crash, we were the first group, as in any accident, to go in and retrieve the flight data recorders (fig. 8). We took the flight data recorder pallet out and placed the units, the three flight data recorders, the flight data acquisition unit, and the battery pack on the lakebed (fig. 9). We then had the units shipped down to Lockheed for preliminary checkover (fig. 10). They were pretty well scorched on the outside, but later on we found that overall they were in pretty good shape inside. Figure 11 shows the Lockheed digital flight data recorder. It has a protection environment for impact and fire. What we were concerned about was saving the data tape.

Figure 12 shows the tape deck removed from the unit as well as the drive mechanism. Figure 13, which is a back view, shows some scorching inside in the tape drive section, but again, this was of no concern to us. Figure 14 shows a closeup of the tape drive system recording heads and the interconnect module.

Lockheed took this data tape and put it on a regular recorder at their plant (fig. 15), plugged it into their data reduction or data retrieval and plotting system, and came up with good data.

What we learned from this was survivability in the impact and fire environments; all the flight data recorders survived (fig. 16). In fact, the flight data recorders with the battery pack ran for 8 minutes after the initial impact. The impact environment was, as far as g loads go, not a problem from a high-g viewpoint in survivability of the data tape. However, as far as operations went, regular operation of the recording mechanism was a problem. Data from the foil recorder were processed by Douglas (fig. 17). The cockpit voice recorder data were handled by the National Transportation Safety Board, and the tapes from the DFDRs were handled by their respective vendors.

Recording operations were our major problem. Right at impact, certain things can happen. The tape can stretch and the electrical-mechanical drive system can malfunction momentarily. (I'm speaking now of the three flight data recorders.) We had a momentary recording malfunction to the three flight data recorders, on the order of 5 to 7 seconds. The three contractors or vendors from whom we procured the flight data recorders feel that they can still come up with useful data right at the point of impact and for about 3 or 4 seconds after impact. However, this is a deficiency in the recording

system. Because we wanted to compare the data that we acquired on the tapes with those from the experiments on the airplane, this may pose a problem for the time interval right at and immediately after impact.

We found that the sampling rates were too low although they were higher than those required now by regulations. For example, the sampling rate for roll angle is one per second, but you saw what the aircraft was doing as it was coming in for impact. One moment we got a sample of zero degrees; the next thing you have is the aircraft in a 6-degree bank angle, then a 12-degree bank angle. The sampling rate for normal acceleration is also fairly low. Existing regulaitons require only 4 samples per second; we had 16 samples per second, and we're starting to lose some data just during the initial impact. We're not getting the frequency response we would like to have.

As far as correlation with the crashworthiness experiments onboard - structural loads, seat loads, and anthropormorphic dummy loads - that remains to be seen.

REFERENCE

1. Barber, Russ: CID Flight/Impact. Full-Scale Transport Controlled Impact Demonstration, NASA CP-2395, 1986, pp. 17-28.

REQUIREMENTS

- PROCURE/INSTALL STATE-OF-THE-ART DFDRS/CVRS AND APPROPRIATE SENSORS TO ACQUIRE AIRCRAFT PERFORMANCE DATA DURING IMPACT AND "ROLLOUT"

OBJECTIVES

- DEMONSTRATE ADEQUACY/USEFULNESS OF ADDITIONAL DATA IN POST-IMPACT ACCIDENT INVESTIGATION/ANALYSIS IN HUMAN FACTORS AND CRASHWORTHINESS AREAS AND CRASH SCENARIO DEVELOPMENT

COMPONENTS AND LOCATION

- FAA
  - BASIC INSTALLATION
    - THREE DFDRS
    - ONE FLIGHT DATA ACQUISITION UNIT (FDAU)
    - 11 SENSORS
    - ONE COCKPIT VOICE RECORDER (CVR)
    - BATTERY/INVERTER POWER SUPPLY
  - CURRENT B-720 INSTALLATION
    - ONE FDR
    - ONE CVR
- NAVY
  - DEPLOYABLE FLIGHT INCIDENT RECORDER (FIR)
  - ELECTRONIC LOCATOR TRANSMITTER (ELT)
  - (NON-OPERATIONAL RECORDING SYSTEM)
  - (PRE-RECORDED DATA SET)
- OTHER:
  - LSI AVIONICS SOLID-STATE MEMORY UNIT
  - (NON-OPERATIONAL RECORDING SYSTEM)

Figure 1

ORGANIZATION	KEY PERSONNEL	POSITION
FAA (TECHNICAL CENTER) (ATLANTIC CITY, NJ)	LEO GARODZ	DFDR/CVR PROG MGR
LOCKHEED AIRCRAFT SERVICES (ONTARIO, CALIF)	DICK NANCE GRAHAM LEROY DAVID GONZALEZ	PROGRAM MANAGER, SR SR. SYSTEMS ENGINEER SYSTEMS ENGINEER
TELEDYNE CONTROLS (W. L.A., CALIF)	LARRY FOX GEORGE ORENDY	PRINCIPAL DESIGN ENGR TECHNICAL ADMINISTRATOR
FAIRCHILD AVIATION RECORDERS FAIRCHILD WESTON SYSTEMS, INC.	HANS F. NAPEL BARRY HAWKINS	DIRECTOR OF ENGINEERING (MARKETING MANAGER)
SUNDSTRAND DATA CONTROL (REDMOND, WASHINGTON)	RAY E. JOHNSON MICHAEL RHODE	DFDR DATA REDUCTION SPEC. (MARKETING MANAGER)
NAVY (NATC) (PATUXENT RIVER, MD)	DAN WATTERS	PROGRAM MANAGER
LEIGH INSTRUMENTS LTD. (CANADA)	JAMES W. WELLS	PROGRAM MANAGER
LEAR SIEGLER, INC.	ISADORE LURMAN	PROGRAM MANAGER

Figure 2

PARAMETER	RANGE	SOURCE
1. TIME (ELAPSED)		INTERNAL TO FDAU
2. ALTITUDE	-1000 to 40,000 ft	NEW TRANSDUCER
3. AIRSPEED	75 to 350 knots	NEW TRANSDUCER
4. MAG HEADING	0 to 360^{o}	EXISTING AIRCRAFT SIGNAL
5. VERTICAL ACC: N	+50 g	
6. LATERAL ACC: N	+10 g	NEW TRANSDUCER
7. LONGITUDINAL ACC: N	+50 g	
8. PITCH ALTITUDE	+82^{o}	NEW VERTICAL GYRO
9. ROLL ANGLE	+180^{o}	
10. RADAR ALTITUDE	0 to 2500 ft	EXISTING AIRCRAFT SIGNAL
11. VERTICAL SPEED	0 to 600 ft/min	NEW TRANSDUCER

Figure 3

720B — FLIGHT DATA RECORDING SYSTEM

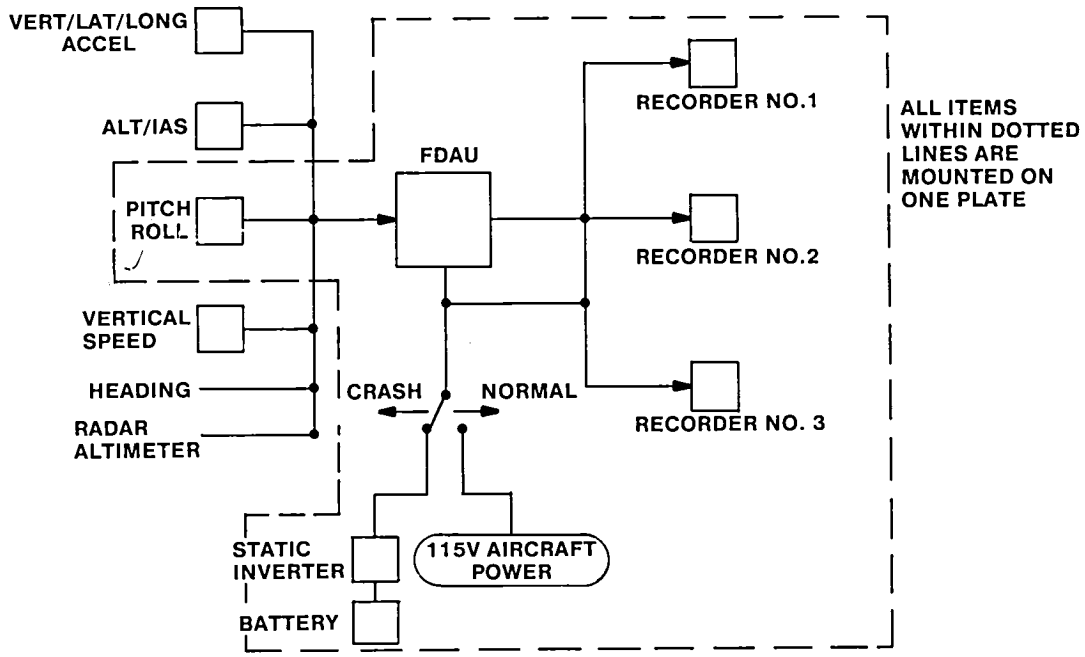


Figure 4

INSTALLATION DETAILS

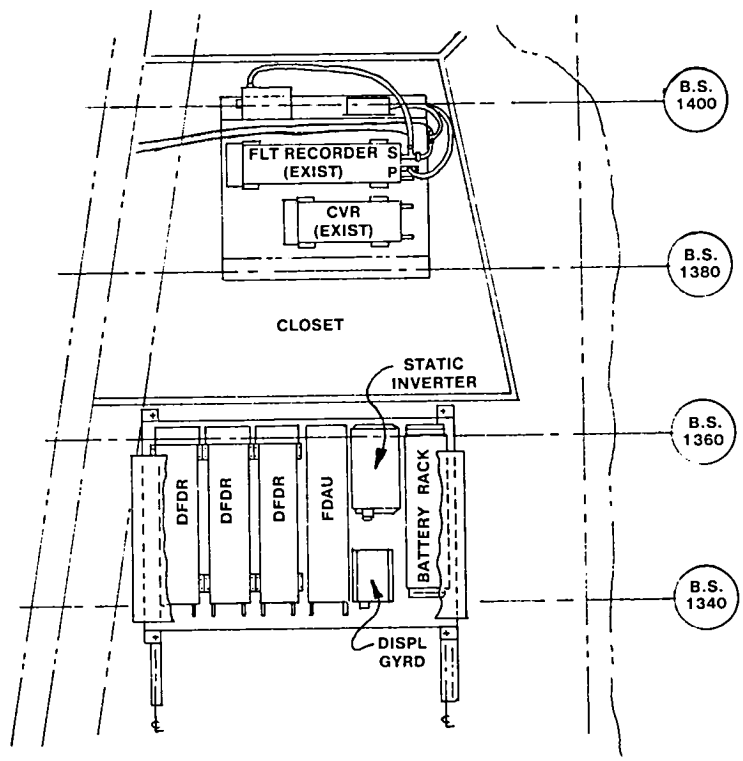


Figure 5

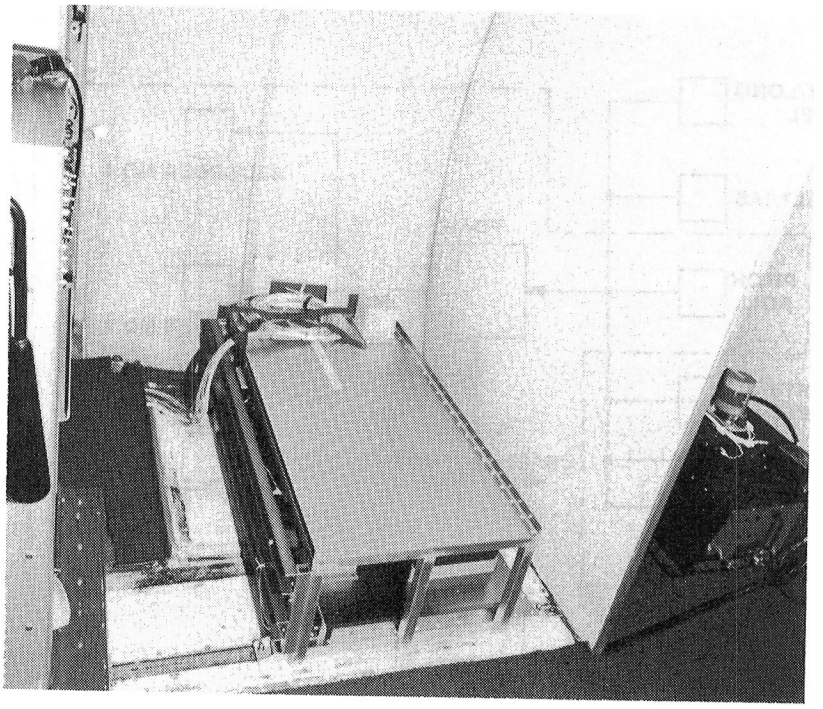


Figure 6

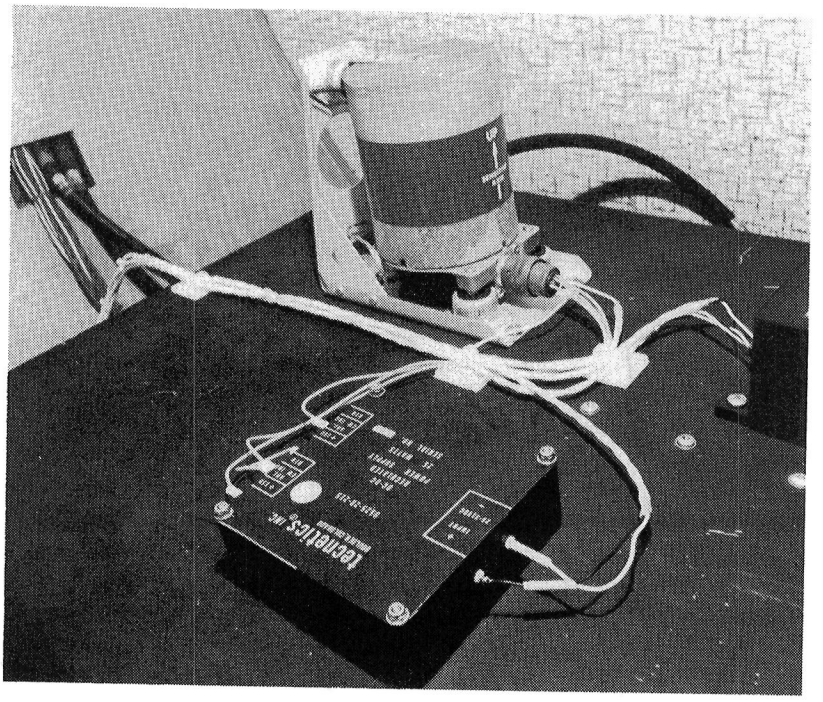


Figure 7

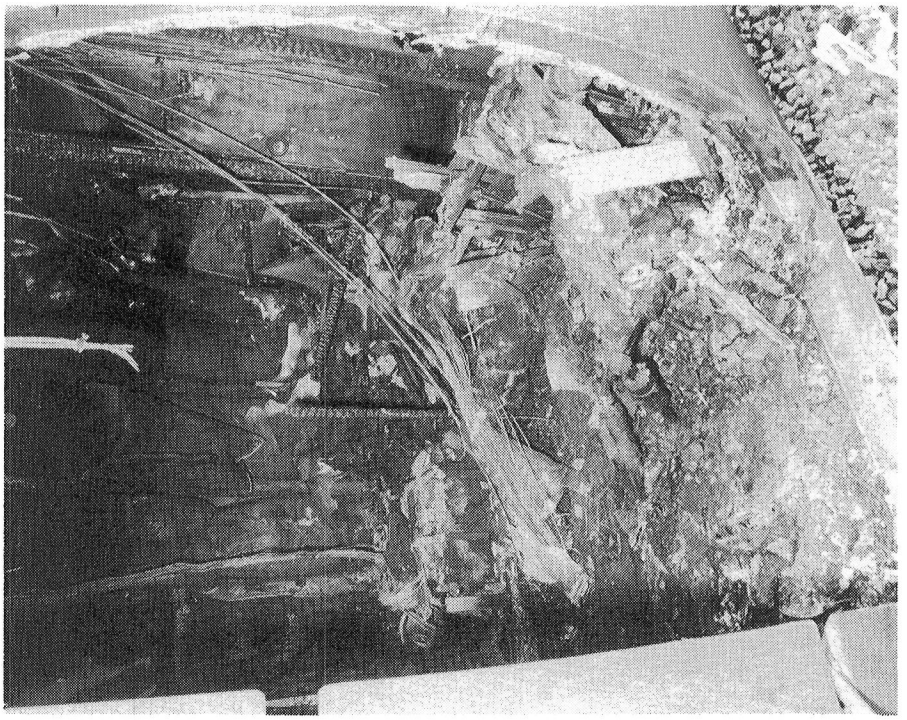


Figure 8

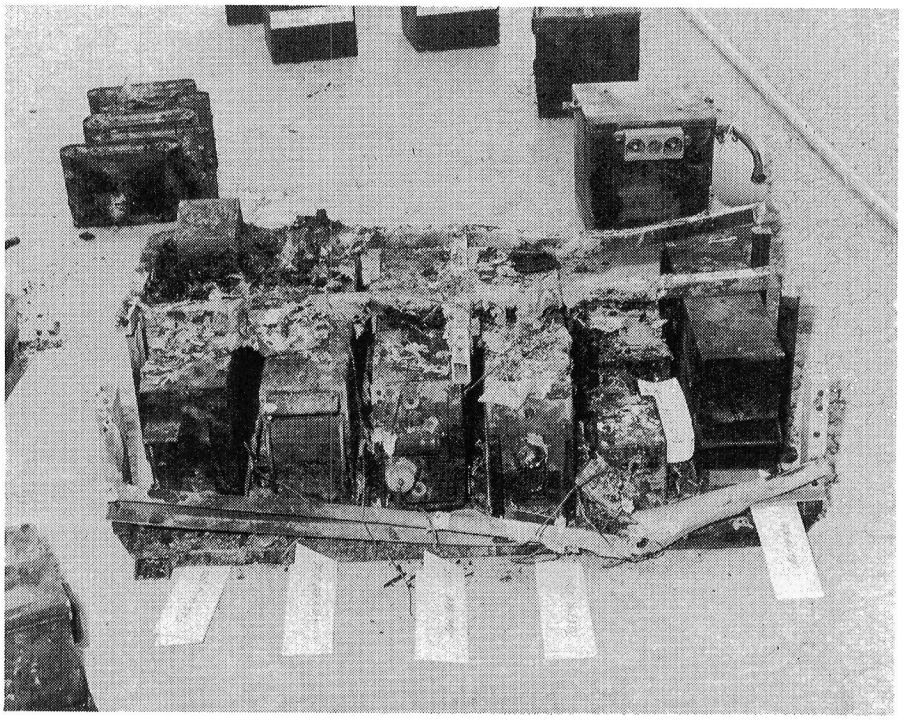


Figure 9

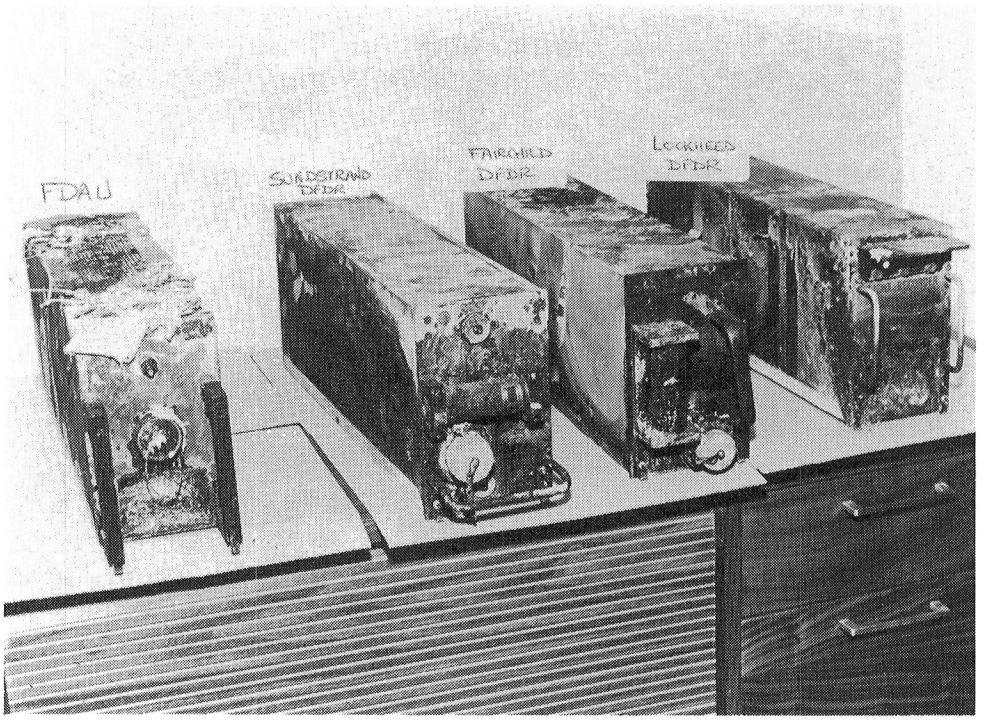


Figure 10

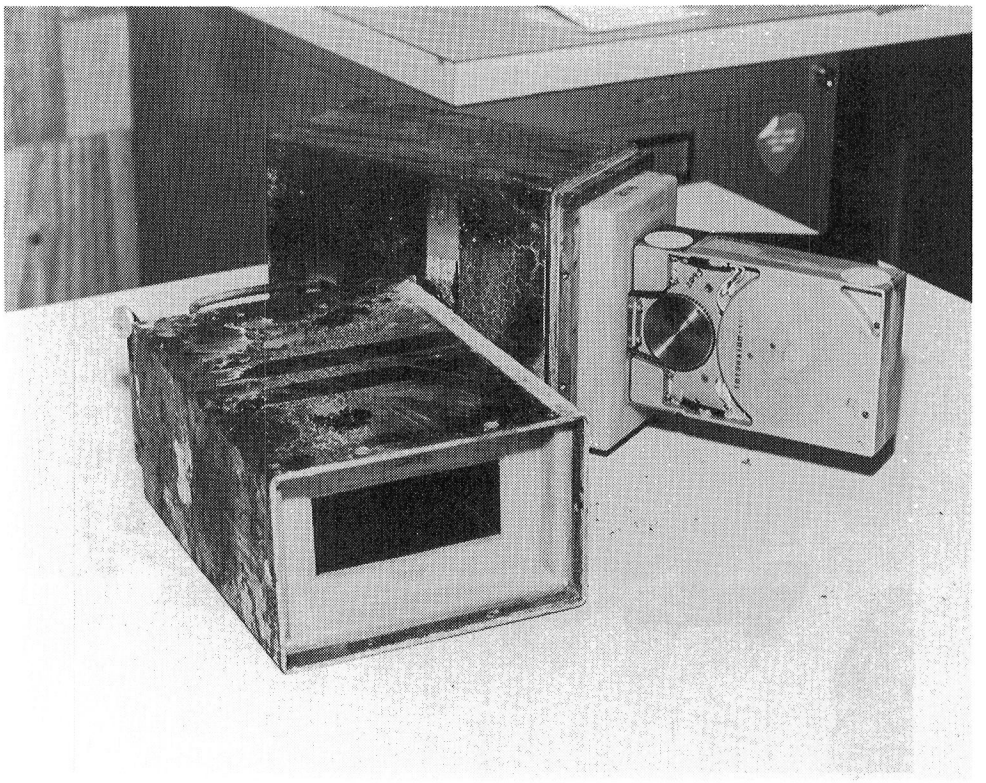


Figure 11

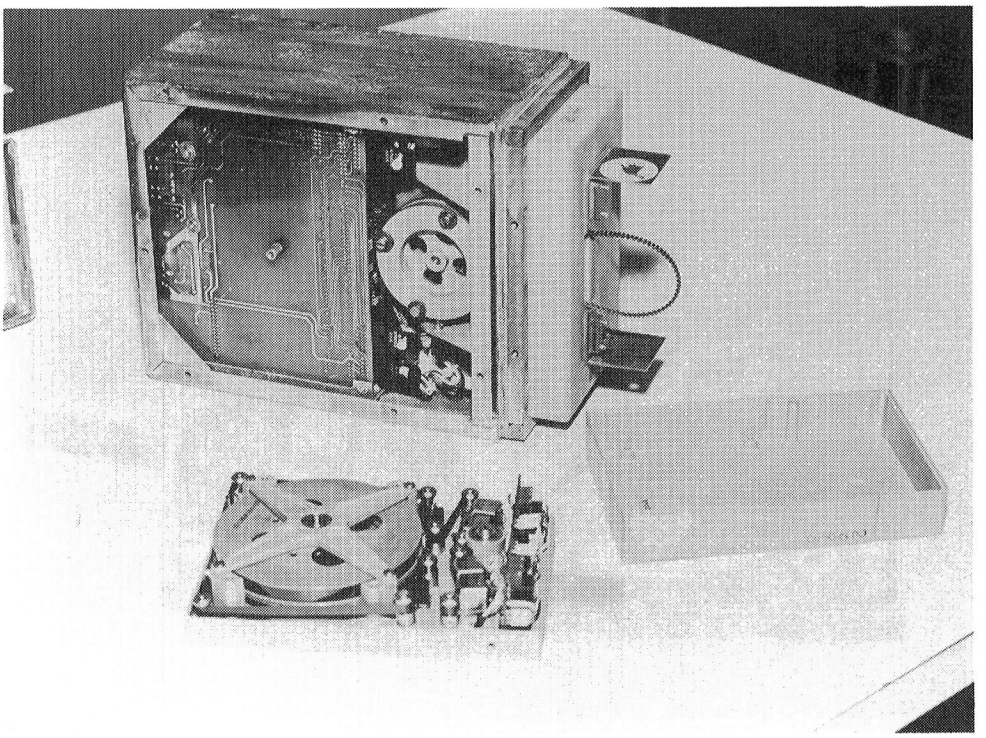


Figure 12

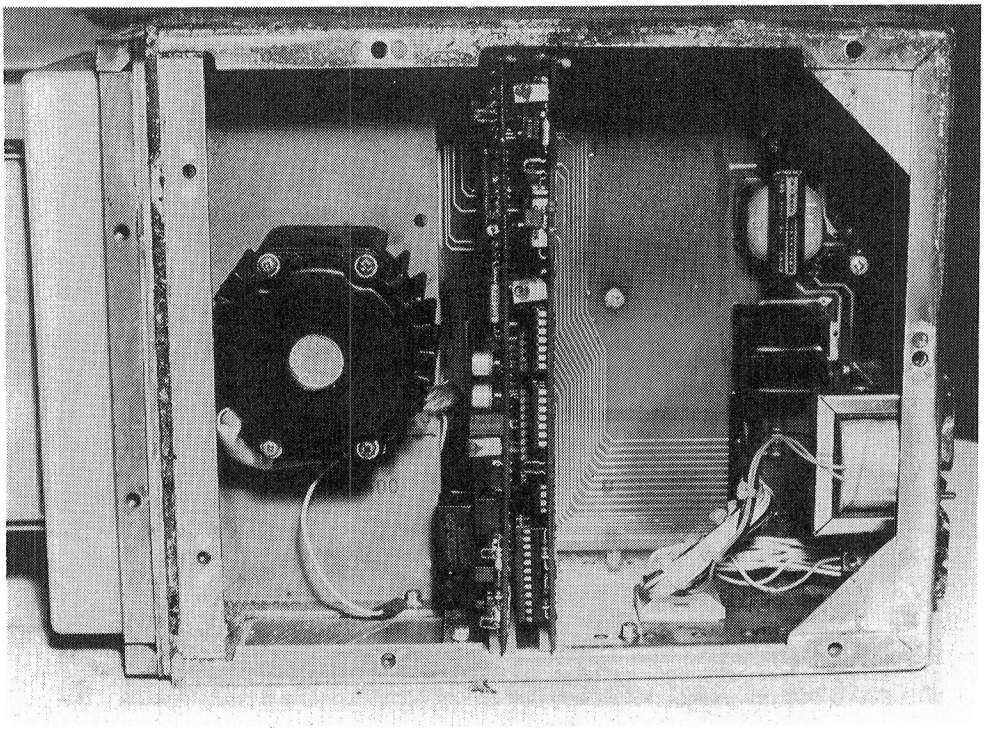


Figure 13

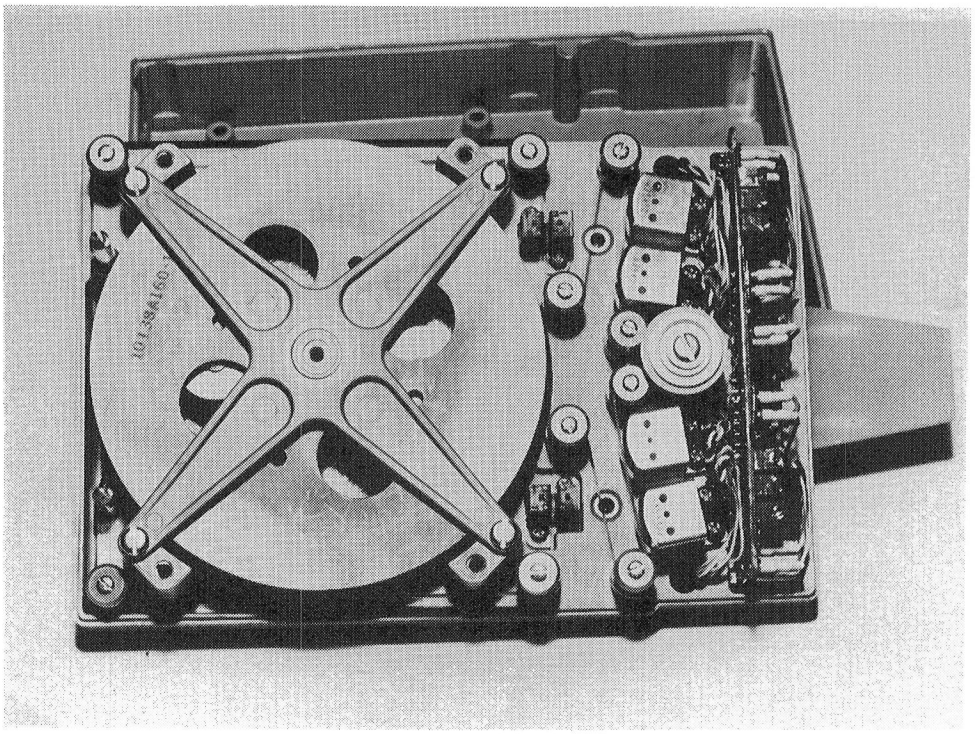


Figure 14

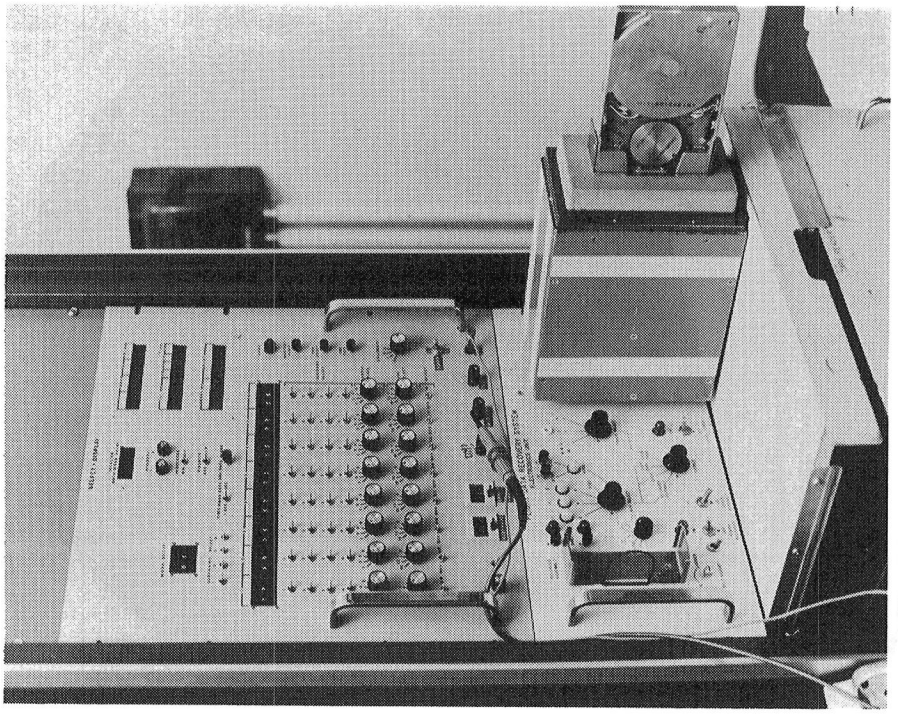


Figure 15

- FDR/CVR
  1. SURVIVABILITY
     - A. FIRE ENVIRONMENT
     - B. IMPACT ENVIRONMENT
     - C. BATTERY/INVERTER POWER SUPPLY
  2. RECORDED DATA PROCESSING/ANALYSIS
     - A. FDR (ANALOG-FOIL)
     - B. CVR
     - C. DFDR (MAGNETIC TAPE)
  3. PRELIMINARY RESULTS
     - A. RECORDER OPERATIONS
     - B. IMPACT EFFECT ON RECORDERS
     - C. SAMPLING RATES
     - D. CORRELATION
- LSI SOLID-STATE MEMORY UNIT
- NAVY FIR
  1. DEPLOYABILITY
  2. SURVIVABILITY
  3. ELT/STROBE OPERATION

Figure 16

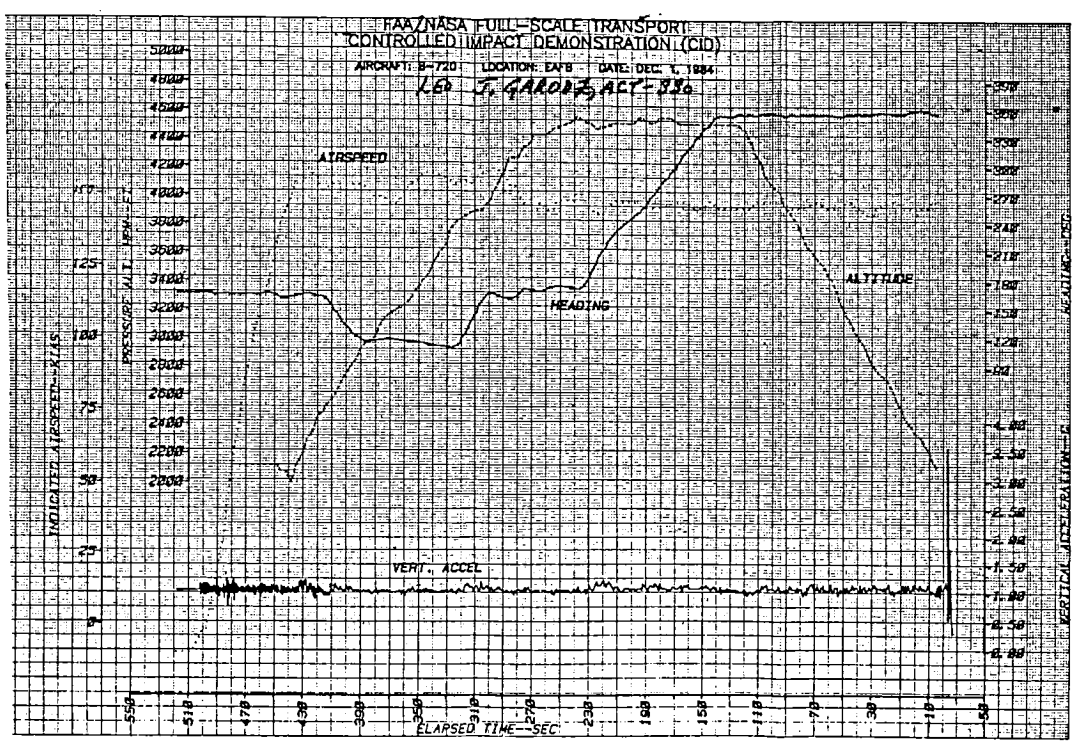


Figure 17

UNITED STATES NAVY - CANADIAN FORCES SOLID STATE FLIGHT DATA RECORDER/CRASH POSITION LOCATOR EXPERIMENT ON THE B-720 CONTROLLED IMPACT DEMONSTRATION

D. M. WATTERS
Naval Air Test Center
Patuxent River, Maryland 20670-5304

NASA/FAA Government/Industry CID Workshop
NASA Langley Research Center
April 10, 1985

INTRODUCTION

The Solid State Flight Data Recorder/Crash Position Locator (SSFDR/CPL) project was established in January 1983 as a joint United States Navy/Canadian Forces (USN/CF) project under the auspices of the international Air Standardization Coordinating Committee (ASCC) Working Party 19 Airborne Electronic Equipment and Test Project Agreement (TPA 805-19). The prototype SSFDR and CPL Radio Beacon Airfoil (RBA-46) was developed by Leigh Instruments, Ltd., Carleton Place, Ontario, Canada configured for Boeing B-707 or B-720 type aircraft. Standard United States Air Force E-3A (B-707) AN/URT-26(V)19 Radio Beacon Set Base (MRU-27), Battery Assembly (ARU-21) and ejection frangible switches were installed in the National Aeronautics and Space Administration (NASA)/Federal Aviation Administration (FAA) B-720 aircraft by the Naval Air Test Center (NAVAIRTESTCEN), Patuxent River, Maryland, and the Naval Air Rework Facility, North Island, San Diego, California. Later the prototype RBA-46 and Dispenser (ARU-21) were installed and ground tested in the B-720 aircraft. This SSFDR/CPL system (figures 1 and 2) was aboard the NASA/FAA B-720 aircraft (figure 3) during the Controlled Impact Demonstration (CID) conducted on 1 December 1984 at NASA Dryden Flight Research Facility, Edwards Air Force Base, California.

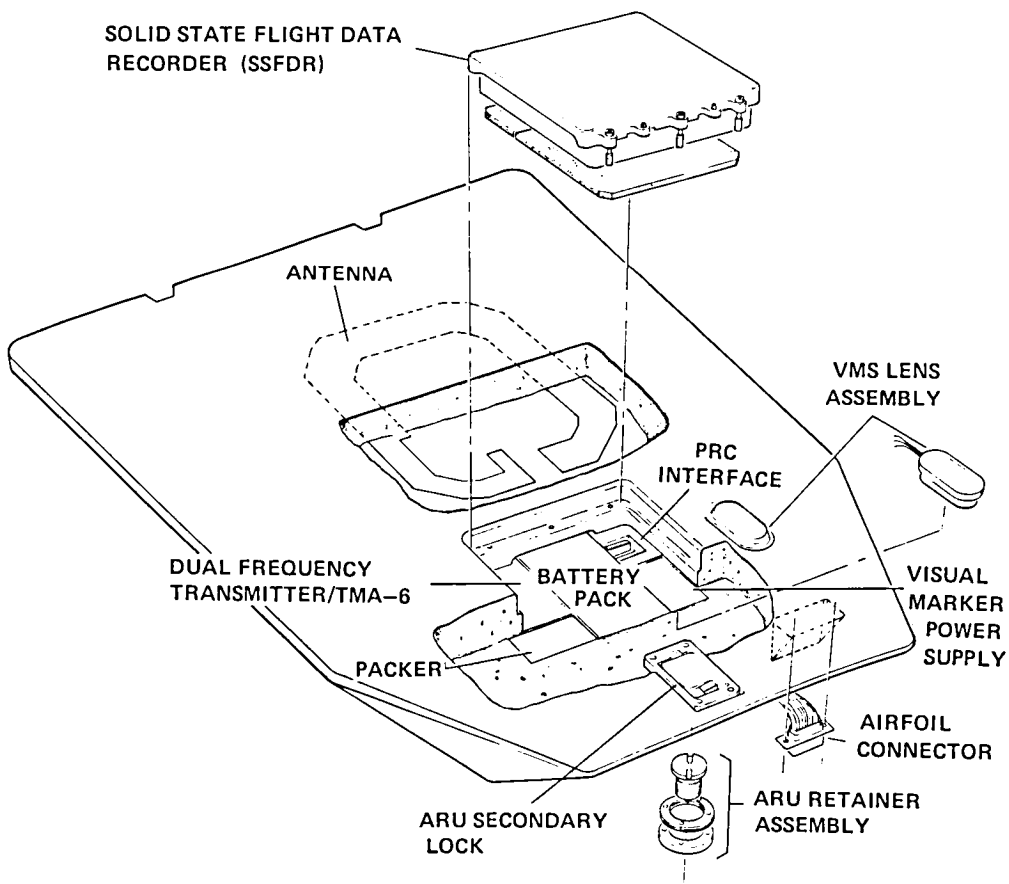


Figure 1
B-720 AIRFOIL (RBA-46) PAYLOAD CONFIGURATION

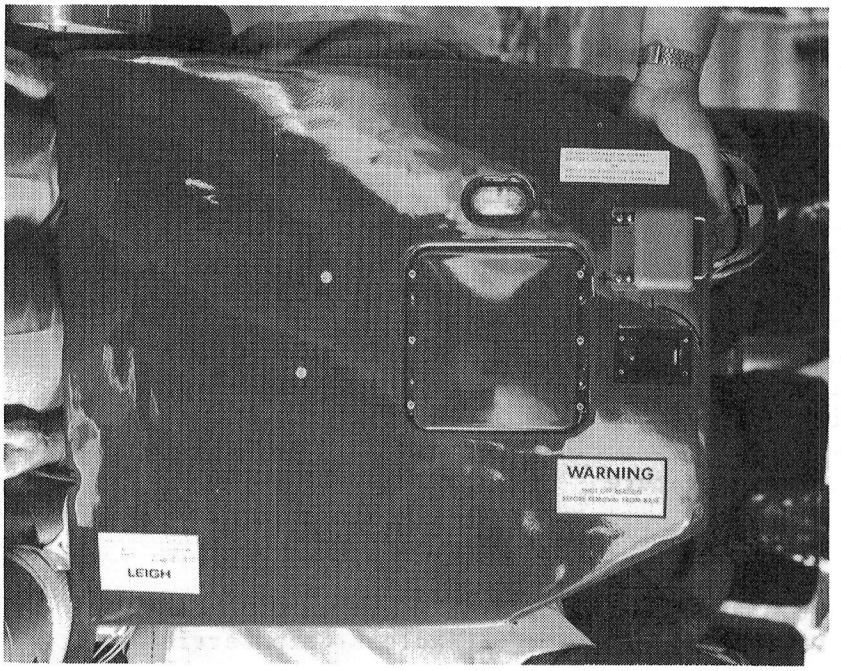


Figure 2
B-720 AIRFOIL (RBA-46) PRE-CID HARDWARE



Figure 3
B-720 AIRCRAFT/RBA-46 AIRFOIL INSTALLATION

SOLID STATE FLIGHT DATA RECORDER DEVELOPMENT

The Solid State Flight Data Recorder (SSFDR) shown in figure 4 was designed using Electronically Erasable Programmable Read Only Memory (EEPROM) Silicon Nitride Oxide Semiconductor (SNOS) chip technology as specified below:

DEVICE SPECIFICATION

Type	- EEPROM, NCR 52832, SNOS
Capacity	- 32 Kbits (4k x 8)*
Write Rate	- 12.8 Kbits/sec
Read Rate	- 500 Kbits/sec
Erase Rate	- 300 Kbits/sec
Endurance	- 10^5 Cycles/Memory Cell
Retention	- 30 Days at Stated Endurance
Operating Voltage	- 5 VDC ±10%
Packaging	- Encapsulated Surface Mount Technology
Operating Temperature	- (-55°C to +125°C)

INTERNAL MODULE SPECIFICATION

Form Factor	- 2.6" x 1.8" x 0.3" (1.4 in^3)
No. of Devices	- 8 Leadless Chip Carrier
Packaging	- Encapsulated Polyurethane Foam

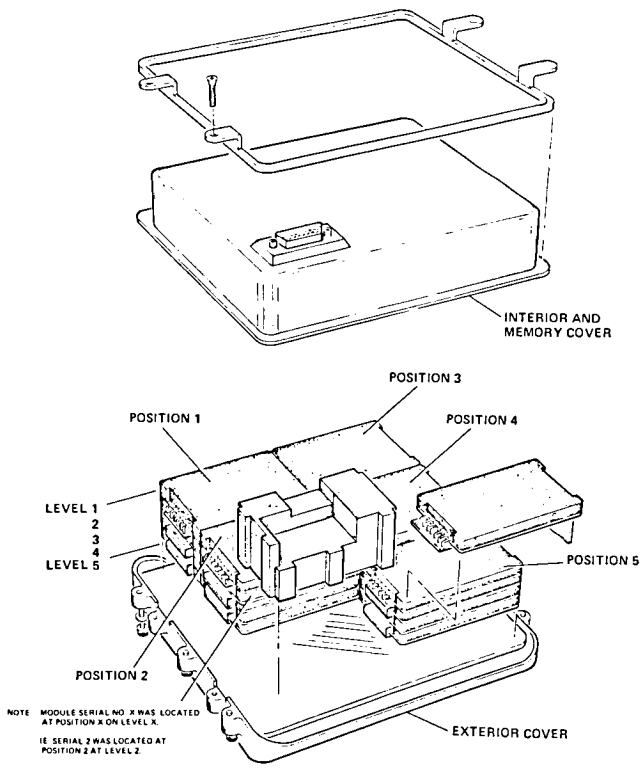


Figure 4
SSFDR MEMORY MODULE ARRANGEMENT

SSFDR SPECIFICATIONS

Form Factor	- 7.12" x 7.0" x 1.55" (77.25 in^3)
Weight	- 3 lbs
Power	- 1.1 Watts (max)
No. of Modules	- 25 (max)
No. of Modules (B-720)	- 5 with devices & 20 dummy
Memory Capacity	
	- 6 Mbits* (32 Kbit chips)
Packaging	- Aluminum, Fiberglass, Intumescent coating

* Only 32 Kbit EEPROM devices were available for this development. Currently, 64 Kbit devices are available that would effectively increase the maximum SSFDR capacity to 12 Mbit.

The B-720 SSFDR contained five memory modules and twenty dummy modules. Each of the five memory modules contained two 32 Kbit memory chips (64 Kbits total). The five memory modules were spaced to measure thermal gradients within the SSFDR. The memory modules/chips (320 Kbits total) were pre-programmed with alternating ones and zeros (checkerboard pattern) prior to CPL/B-720 installation. Also, temperature stick-on indicators were attached to each memory module and interior and exterior SSFDR covers prior to CPL/B-720 installation.

CRASH POSITION LOCATOR DEVELOPMENT

The design concept for the RBA-46 CPL was formulated by Mr. D. M. Watters, NAVAIRTESTCEN, in early 1983. The design concept included the following new features currently not included in production CPLs:

1. Overt radio beacon transmission at 121.5 MHz (civilian), 243 MHz (military) and 406 MHz (SARSAT) emergency frequencies.

2. Covert radio beacon transmission (spread frequency 2.55 MHz to 300 MHz transceiver-transponder).

3. Remote transceiver frequency selection switch.

4. Remote overt/covert frequency selection switch.

5. Automatic antenna tuning.

6. Visual Marker Strobe (VMS).

7. Pyrotechnic operated CPL release unit.

Given these technical development requirements and contractual funding and schedule constraints, a detailed feasibility study was conducted and reported (reference (1)). It was concluded in this study that the following, although technically feasible, could not be implemented in the B-720 RBA-46 CPL:

1. 406 MHz SARSAT transmitter (hardware unavailable).

2. Covert radio beacon transceiver/transponder (AN/PRC-112(V) not available).

3. Remote frequency selection switches.

4. Automatic antenna tuning.

Thus the B-720 RBA-46 CPL design configuration was established as shown in figure 5 with electronic circuitry and space provisions to implement the figure 6 design configuration after the B-270 CID. The B-720 RBA-46 CPL overall specifications are as follows:

Form Factor	- 23" x 26" x 4.5" (1200 in^3)
Weight (with SSFDR)	- 11 lbs
Power Supply	- $LiSO_2$ Battery Pack
Power Draw	- 6.6A
Visual Marker Strobe	- Modified ACR/SDU-5
Overt Operating Frequencies	- 121.5 MHz and 243 MHz
Covert Operating Frequencies (AN/PRC-112(V) provisions)	- 255 to 300 MHz
Antenna	- "G" Shaped Broadband
Release Unit	- Pyrotechnic Squib Actuated

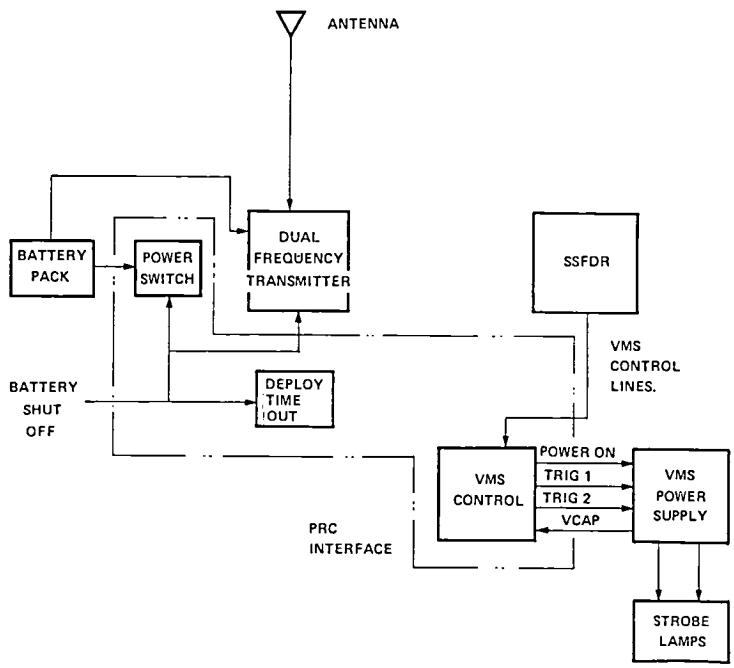


Figure 5
B-720/RBA-46 PAYLOAD BLOCK DIAGRAM

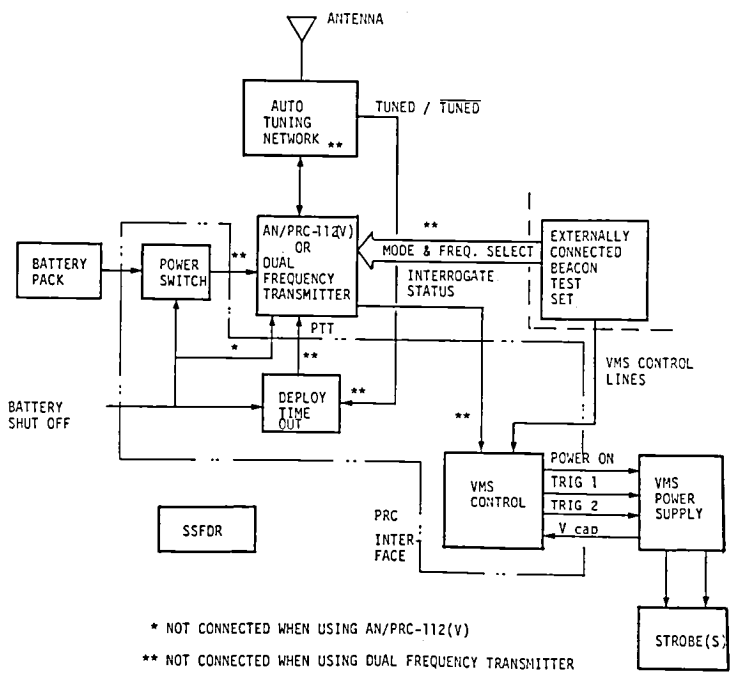


Figure 6
RBA-46 LOCATION RELATIVE TO B-720 AFTER CID

B-720 SSFDR/CPL CID

The NASA/FAA B-720 impacted onto the dry lake bed at Edwards AFB at 9:22 am, December 1, 1984. The engines on the left wing struck the ground first and yawed the aircraft to the left. The aircraft continued into the crash site grid striking the rhinos and strikers, which ripped open the right inboard engine and wing tanks. A fire ball then erupted from the right inboard engine engulfing the aircraft and the RBA-46 SSFDR/CPL. At the time of initiation of the fire, the RBA-46 airfoil had not ejected. The aircraft continued down the crash site grid, sliding and yawing to the left. The right wing separated from the fuselage, violently tumbling and spilling fuel, eventually coming to rest on the left side of the aircraft. The aircraft continued to slide finally coming to rest on the left edge of the gravel crash site grid. The CPL RBA-46 did not separate from the aircraft until the aircraft came to rest. It is clearly visible from video and camera coverage that when the airfoil did release, the aircraft was at a yaw angle of about 30^{o} to 45^{o}.

The radio beacon transmission was actuated and was picked up by the Navy P-3A chase aircraft for a short time, after which reception was lost. The pilot reported that he received a signal on both 121.5 MHz and 243 MHz for a period of approximately 5 seconds. Five minutes after the crash a portable direction finding unit located on the roof of the NASA Dryden Flight Research Facility, 4 miles distant from the crash, was unable to pick up the beacon transmission.

The fire crews started fighting the fires approximately 90 seconds after the time of impact. The crews continued to spray the fire with foam for over an hour and a half. The foam used by the fire crews is a 3% to 6% solution of AFFF (FC-203 Light Water Brand Aqueous Film Forming Foam) in water.

Approximately four hours after the crash the NASA/FAA safing team located the CPL and installed the Battery Shut-off (BSO) on the RBA-46.

Navy personnel access to the crash site was allowed on the morning of December 2, 1984. The CPL RBA-46 was found resting top side up, 15 feet forward and 13 feet perpendicular from the tray location on the starboard side of the aircraft. Figure 7 shows the final location of the CPL RBA-46. An immediate inspection indicated the airfoil suffered moderate fire damage with paint peeling but not intumescing. The visual marker strobe lamp housings were intact but extensively burned such that it was impossible to see if the lamps had survived. The airfoil suffered minor structural damage, with assorted dents, etc. The SSFDR cavity was intact with the top surface of the recorder being blackened by fire. Figures 8 and 9 show the CPL RBA-46 as found at the B-720 crash site.

The extended plunger on the ARU-21 release unit indicated that the pyrotechnic deployment system operated. The radio beacon base (tray) suffered some heat and fire damage, and was charred and blackened by smoke.

The frangible switch in the nose survived and the switch in the belly was recovered and found to have actuated. It is assumed that this switch fired the ARU-21 squib. There were no other release switches installed in the normally open system in the aircraft.

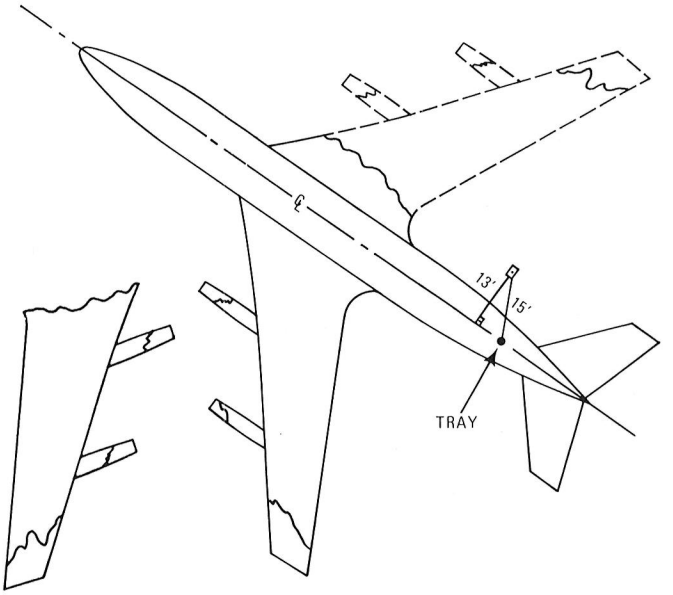


Figure 7
RBA-46 LOCATION RELATIVE TO B-720 AFTER CID

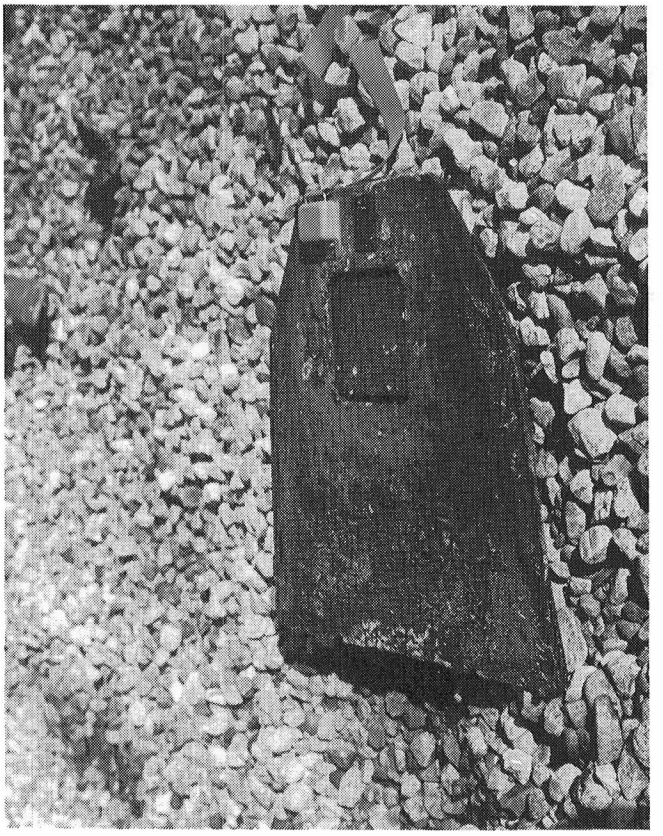


Figure 8
RBA-46 EXTERNAL SURFACE AFTER B-720 CID



Figure 9
RBA-46 INTERNAL SURFACE AFTER B-720 CID

POST B-720 CID ANALYSIS OF THE RBA-46 SSFDR/CPL

INITIAL INSPECTION

On December 10, 1984, the RBA-46 SN001 arrived at Leigh Instruments Ltd, Carleton Place, Ontario, Canada, for an engineering investigation of condition and performance. No modifications or work had been done to the airfoil since it was removed from the crash site at Edwards AFB, California.

Initial inspection showed charring on both sides of the airfoil. Structurally the airfoil was intact with various dents, etc. on its surface. The airfoil was soaked in fluids which were a combination of antimisting kerosene (AMK) jet fuel and fire fighting foam. Henceforth this fluid will be referred to as "crash fluid".

Upon removal of the BSO, the CPL did not transmit and the strobes did not flash. The airfoil was then subjected to a detailed analysis.

The MRU-57 Radio Beacon Base (tray) arrived at Leigh Instruments Ltd. on January 18, 1985. Initial inspection shows the tray to have suffered mild fire damage, slight charring, and paint peeling, and it was covered with smoke deposits.

All safety lock wire was intact and the plunger in the ARU-21 Release Unit was in the extended position. Removal and inspection of the squib showed it to have fired. None of the plastic or rubber components showed any sign of melting, indicating that the tray had not been subjected to prolonged fire. The rear mounting hooks showed no sign of damage. The break away connector showed minor signs of corrosion caused by the crash fluids.

The tray suffered minimal heat damage; as a consequence it is assumed that the cartridge was fired by the electrical input to the release circuitry and not by overheating.

PAYLOAD CAVITY ANALYSIS

The SSFDR was removed from the RBA-46 airfoil to provide access to the CPL payload cavity. Each assembly was then tested to determine its state. Figure 10 shows the payload cavity before disassembly.

The SSFDR case was wet with crash fluids. All the assemblies in the cavity had their encapsulating foam soaked with crash fluids. The fluids had seeped in around the SSFDR because there was no seal installed. Sediment due to corrosion was found on the SSFDR connector as well as on the surface of the foam and on the wiring harness. These consisted primarily of green copper deposits. Figures 11 and 12 show the SSFDR before disassembly.

The payload assemblies did not shift nor show any signs of sustaining physical damage due to heat (fire) or impact. The wiring harness was intact.

The crash fluids consisted of AMK jet fuel and fire fighting foam. The fire fighting foam is electrically conductive, very corrosive and has a very low surface tension. Low surface tension allows it to flow rapidly into cracks, etc. This fluid extensively damaged various components of the airfoil payload as shown in figure 13.

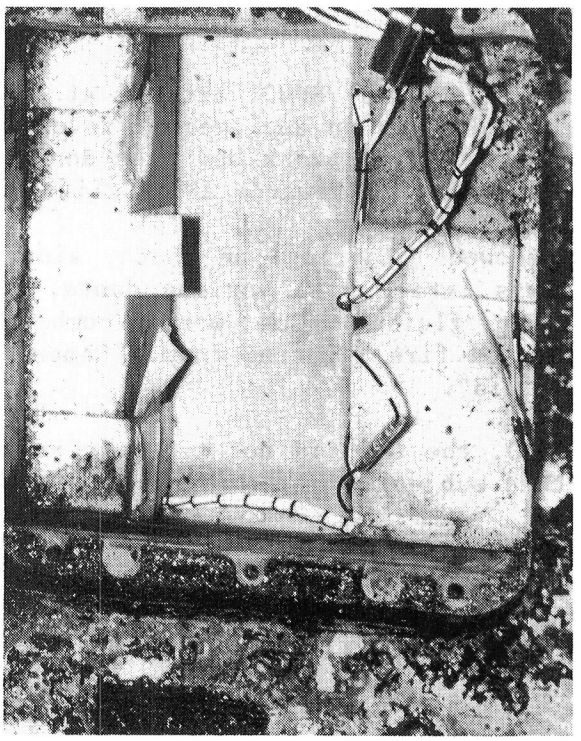


Figure 10
RBA-46 PAYLOAD CAVITY WITH SSFDR REMOVED

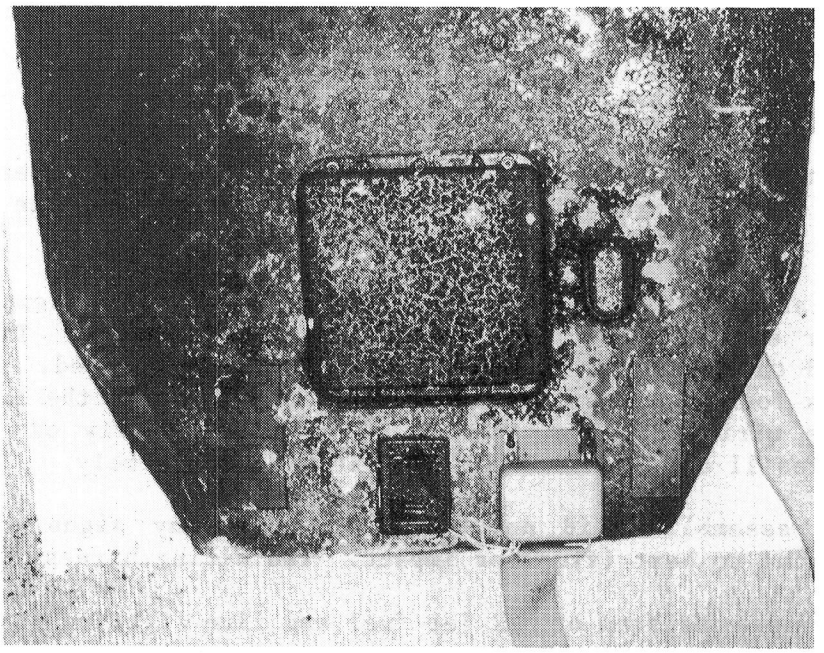


Figure 11
RBA-46 SSFDR EXTERNAL SURFACE PRIOR TO DISASSEMBLY

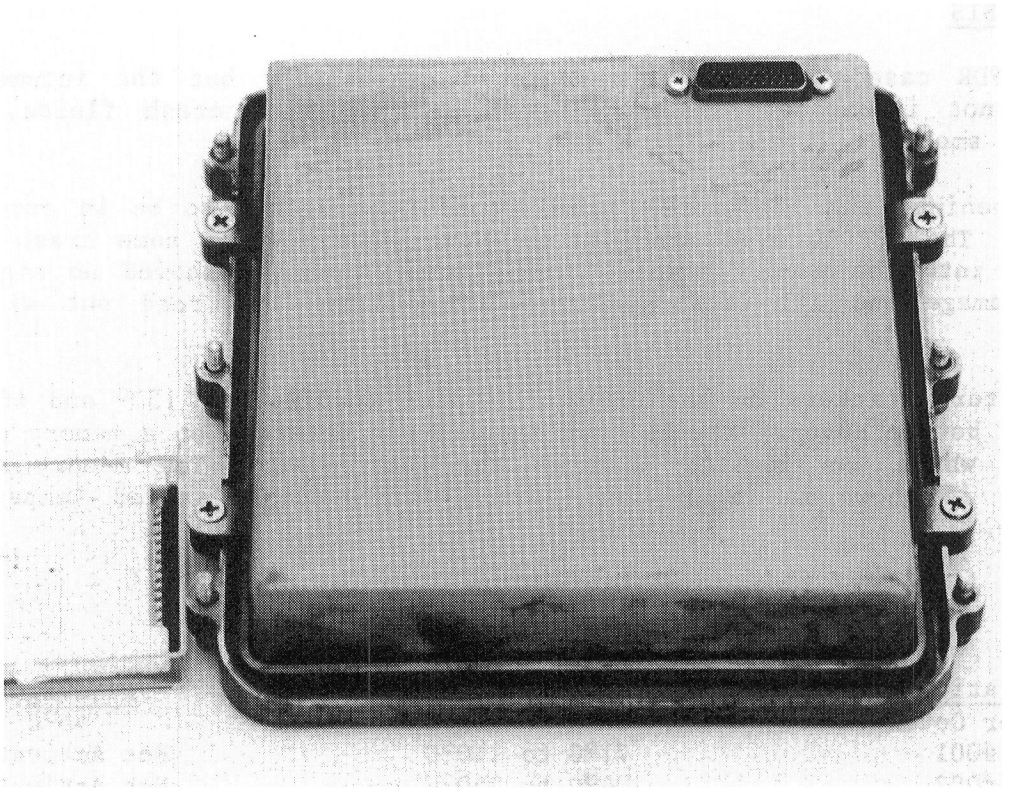


Figure 12
SSFDR INTERNAL SURFACE AFTER B-720 CID

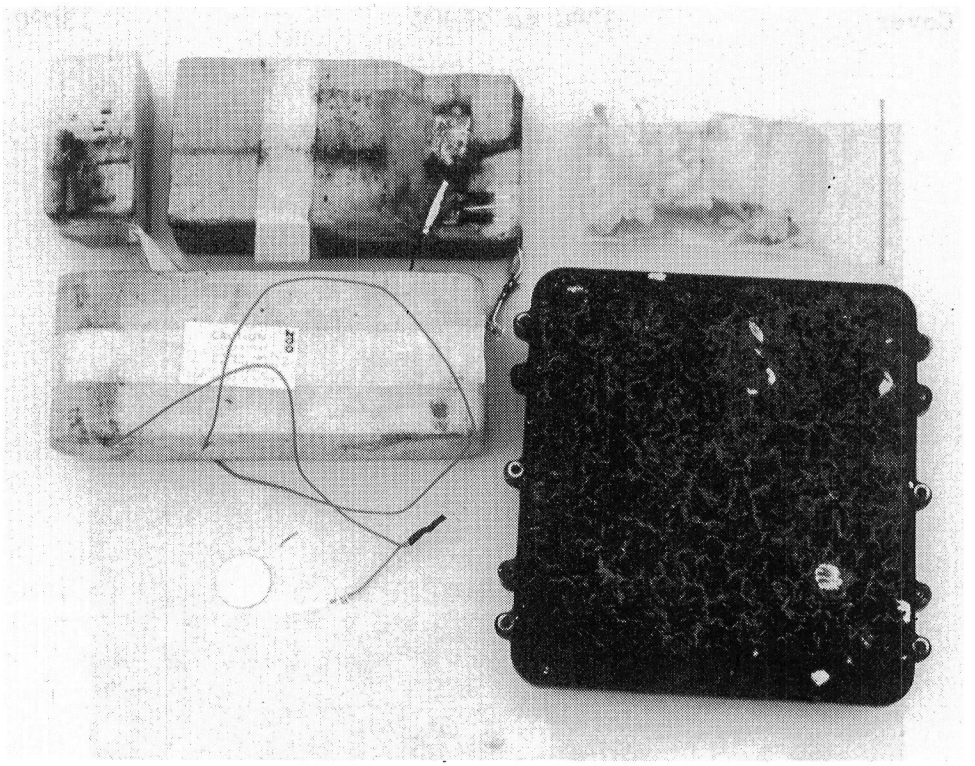


Figure 13
RBA-46 PAYLOAD COMPONENTS REMOVED FROM CAVITY

SSFDR ANALYSIS

The SSFDR case cover top was scorched extensively but the intumescent paint did not intumesce. The underside was wet with crash fluids, with evidence of smoke.

Upon opening, the interior of the recorder was found to be in excellent condition. The SSFDR cover seal was in good shape however some crash fluid had seeped into the memory modules. The memory modules showed no signs of physical damage and all data (checkerboard pattern) was read out with no errors.

Temperature stickers on the SSFDR indicated readings of 130° and 46° for the top and bottom cover. The highest temperature obtained on a memory module was 121°C, which was located next to the top cover. The memory module arrangement is shown in figure 14. Table 1 provides detailed temperature information.

Table 1
SSFDR Temperature Measurements

Location	Range	Readings
Interior Cover	37°C to 260°C	46°C
Module #001	71°C to 110°C	Not Activated
Module #002	204°C to 260°C	Not Activated
Module #003	37°C to 65°C	49°C
Module #004	160°C to 199°C	Not Activated
Module #005	116°C to 154°C	121°C
Exterior Cover	37°C to 260°C	130°C

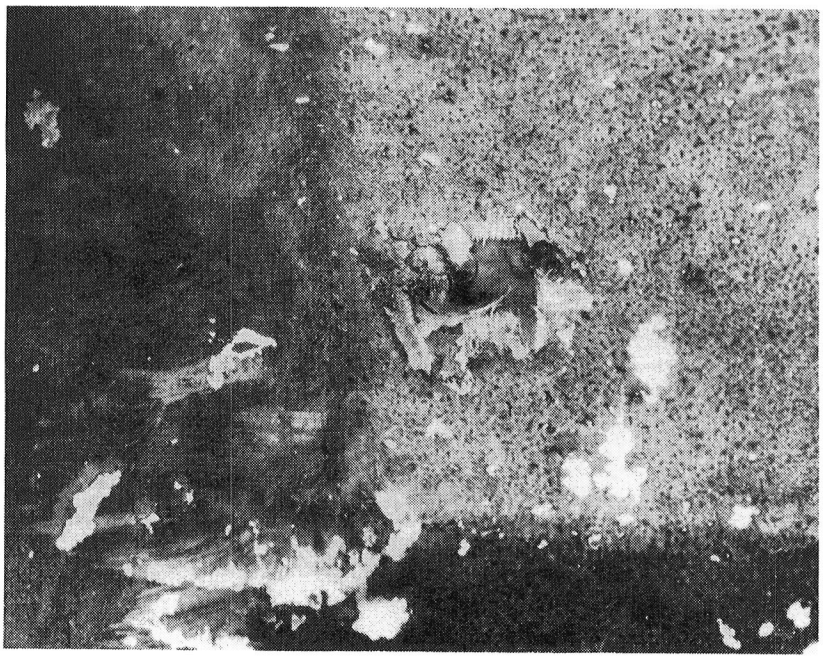


Figure 14
PUNCTURE IN RBA-46 AIRFOIL EXTERNAL SURFACE

CONTROLLED IMPACT DEMONSTRATION
ON-BOARD (INTERIOR) PHOTOGRAPHIC SYSTEM

Clyde J. May
NASA Langley Research Center
Hampton, Virginia

NASA/FAA Government/Industry CID Workshop
NASA Langley Research Center
April 10, 1985

INTRODUCTION

Langley Research Center (LaRC) was responsible for the design, manufacture, and integration of all hardware required for the photographic system used to film the interior of the CID B-720 aircraft during actual crash conditions. The photographic system devised to accomplish this task was comprised of four main elements (Fig. 1). Four independent power supplies were constructed to operate the ten high-speed 16 mm cameras and twenty-four floodlights. An up-link command system, furnished by Ames Dryden Flight Research Facility (ADFRF), was necessary to activate the power supplies and start the cameras. These events were accomplished by initiation of relays located on each of the photo power pallets.

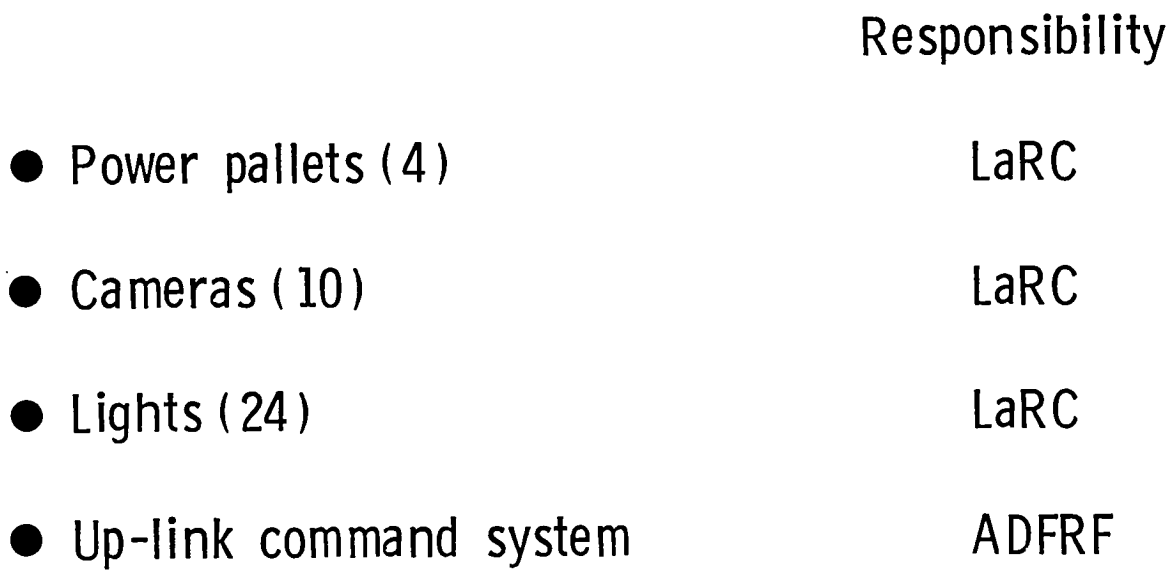


Figure 1

CID AIRCRAFT PLAN VIEW

A plan view of the B-720 aircraft (Fig. 2) shows the distribution of the interior photographic equipment throughout the cabin area. Power pallet no. 1 was located on the right side of the forward cabin aft of the galley. Power pallets nos. 2 & 3 were located just aft of the left wing, and pallet no. 4 was on the right side forward of rear service door. The forwardmost camera and two lights were located in the cockpit.

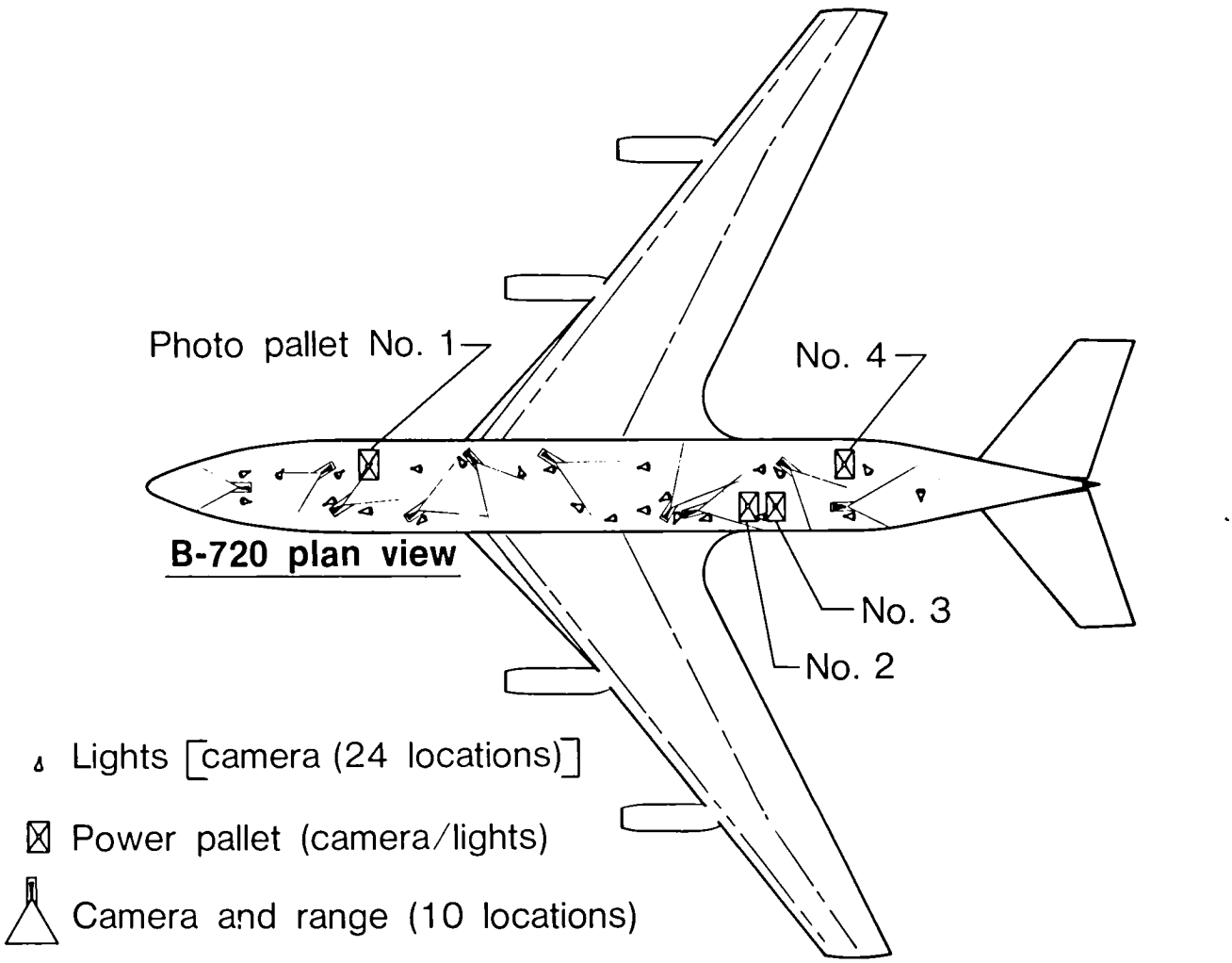


Figure 2

CID AIRCRAFT INTERIOR VIEW

This interior photograph (Fig. 3) was taken looking aft from the galley and shows how the cameras and lights were attached to the upper fuselage.



Figure 3

PHOTOGRAPHIC POWER SYSTEM

It was desirable to design and construct a power system to drive the cameras and lights completely independent of the aircraft power systems. As stated previously, four power supplies were installed. A list of the components used in this power system is given in Fig. 4. All of these components were qualified for use on aircraft or missiles except the alkaline lantern batteries. These alkaline batteries did not have to survive any stringent environment as they were used only to activate the primary silver-zinc batteries prior to impact.

1. Battery (28VDC) silver-zink	Delco-Remy	PP-3250/DJW-15
2. Battery (12VDC alkaline	Duracell	ID9260
3. Relay, camera power 50-amp, 28VDC, 3 pst, 50 G's		6042H202
	Cutler-Hammer	MS27222-2
4. Relay, control (200 G's) 4PDT, magnetic latching	P and B	TL17DG
5. Relay, external power 200A, 28VDC, 25 G's		6041H202
	Cutler-Hammer	AN3370-1
6. Diode, 157 AMP. DC	Motorola	MR1215SL
7. Fuses	Bussman	ANL type
8. Connectors, power	Amphenol (MS)	MIL-C-5015
9. Connectors, control	Bendix	MIL-C-23216
10. Terminal strip	Fed. stock	MS27212-3-8

Figure 4

CID PHOTO POWER PALLETS

The physical layout and construction of the power pallets are depicted in the photograph of power pallets nos. 2 and 3 (Fig. 5). Each pallet was covered by a fire resistant heatshield and bolted to the aircraft seat rails. The pallets were constructed to withstand the most severe expected impact (15 g) but in one vertical impact test a pallet survived 60 g's. The heatshield was designed to survive a major cabin conflagration, and performed as expected.

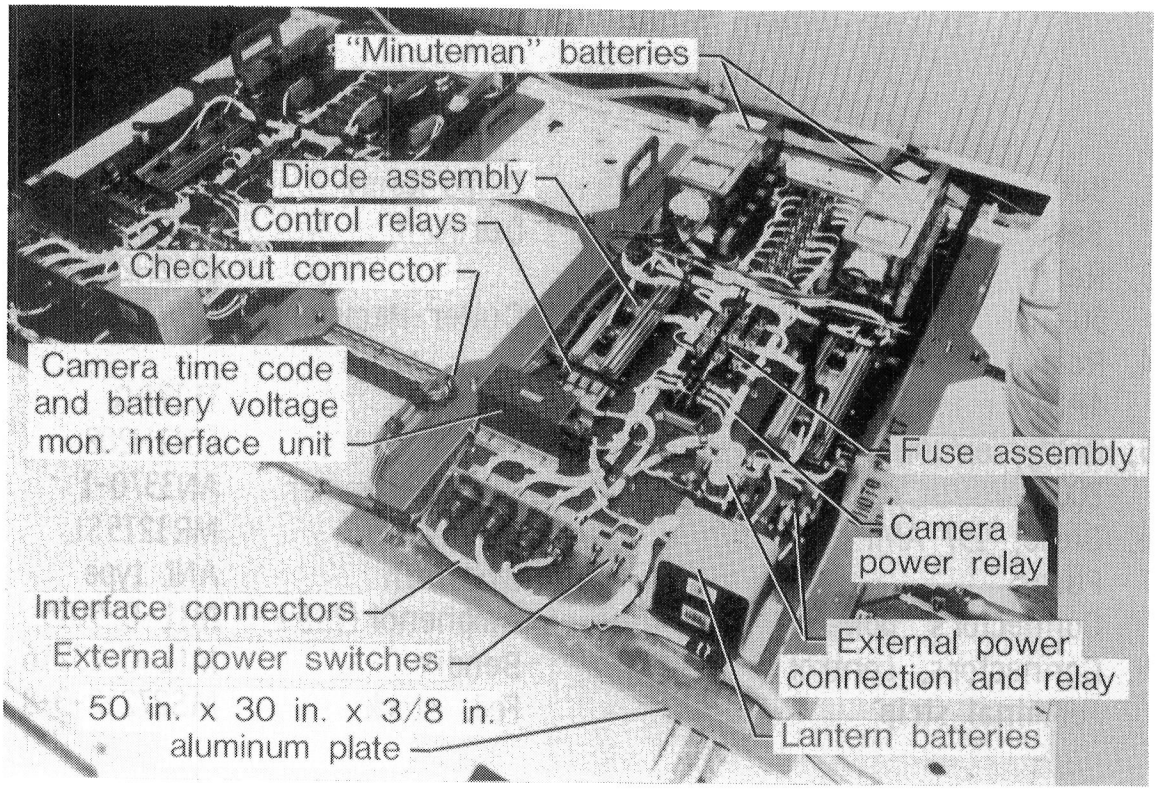


Figure 5

PHOTOGRAPHIC POWER SYSTEM BATTERY

The most unique feature of the power system design was the power source (Fig. 6); a remotely activated, hermetically sealed unit with dual 28-volt sections was selected. We obtained these batteries, which were manufactured in 1964, from outdated surplus of the minuteman program at Hill Air Force Base, Utah. The LaRC Impact Facility had been using these batteries to operate cameras and photolights on several crash tests without experiencing a single failure. These SE12G batteries were selected for this application because they had no maintenance requirements, low cost and presented an acceptable risk.

- Battery, 28 volt, remotely activated, hermetically sealed, dual section (PP-3250/DUW-15)
- Built by Delco-Remy for Autonetics, A Division of North American Aviation (1964)
- Obtained by NASA Langley from outdated surplus of Minuteman Project, Hill AFB, Utah
- Silver-zink dry charged cells
- Electrolyte: Potassium Hydroxide solution
- Weight: < 17.5 lbs.

Figure 6

SE 12G BATTERY POWER SPECIFICATIONS

The SE 12G batteries were rated to deliver greater than 44 watt-hours from the "A" section and 84 watt-hours from the "B" section. The CID required 46 watt-hours and 92 watt-hours, respectively. During testing here at Langley, 90 and 103 watt-hours were obtained. They were more than adequate to meet our requirements. To provide some redundancy in the unlikely event one battery should fail, two batteries were connected in parallel on each pallet. Forty-six (46) SE 12G batteries were expended on the CID program without a failure. (See Fig. 7.)

	Battery "A"	Battery "B"	
	28 ± 0.7 volts	28 (+2, -4) volts	
Spec.	> 44 watt-hours	>84 watt-hours	218 seconds
Req'd	46 watt-hours	92 watt-hours	210 seconds
Test	90 watt-hours	103+ watt-hours	

Figure 7

SE12G BATTERY ASSEMBLY

An exploded view of this remotely activated battery is shown in Figure 8. The potassium hydroxide electrolyte, stored in the reservoir, is forced into the cells when the pyrotechnic gas generators are initiated. Within one second after activation, the batteries reach full voltage. The batteries are externally vented to prevent pressure buildup within the case after activation. To prevent contamination of the power pallets by the caustic gas and/or liquid expelled, the vents were piped overboard the aircraft.

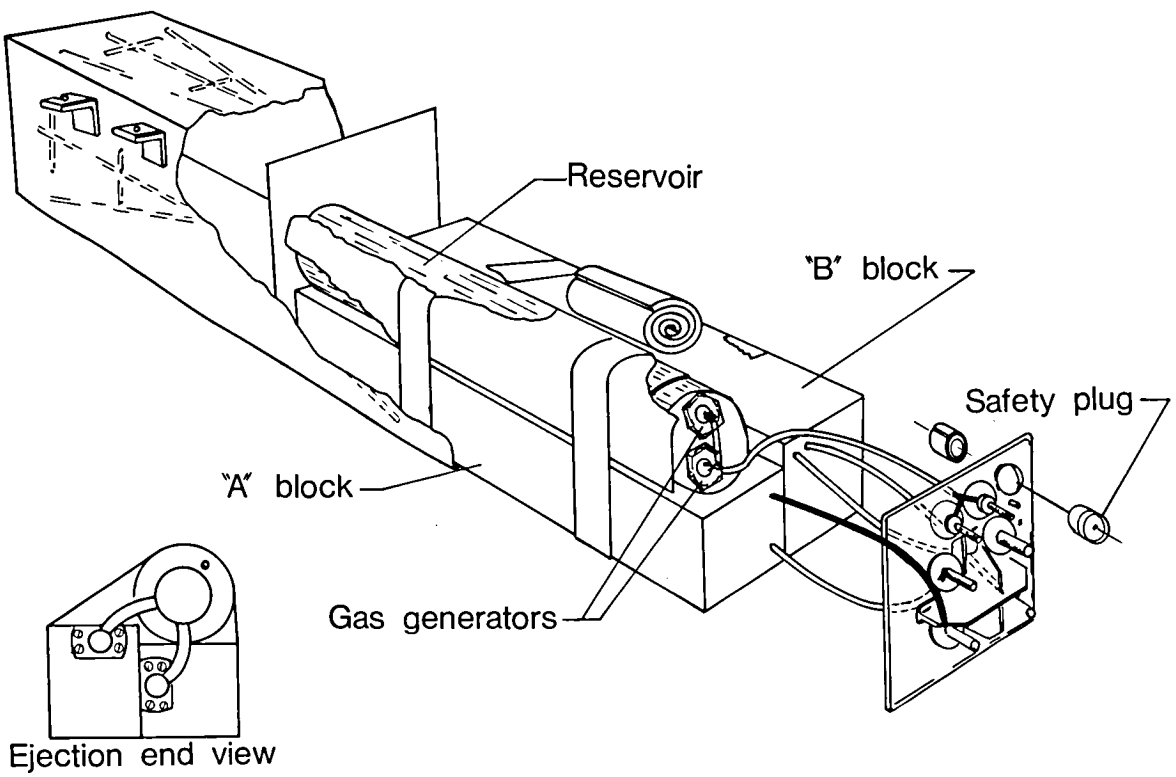


Figure 8

SE 12G BATTERY

Cell blocks and reservoir from a disassembled SE 12G battery are shown in Figure 9.

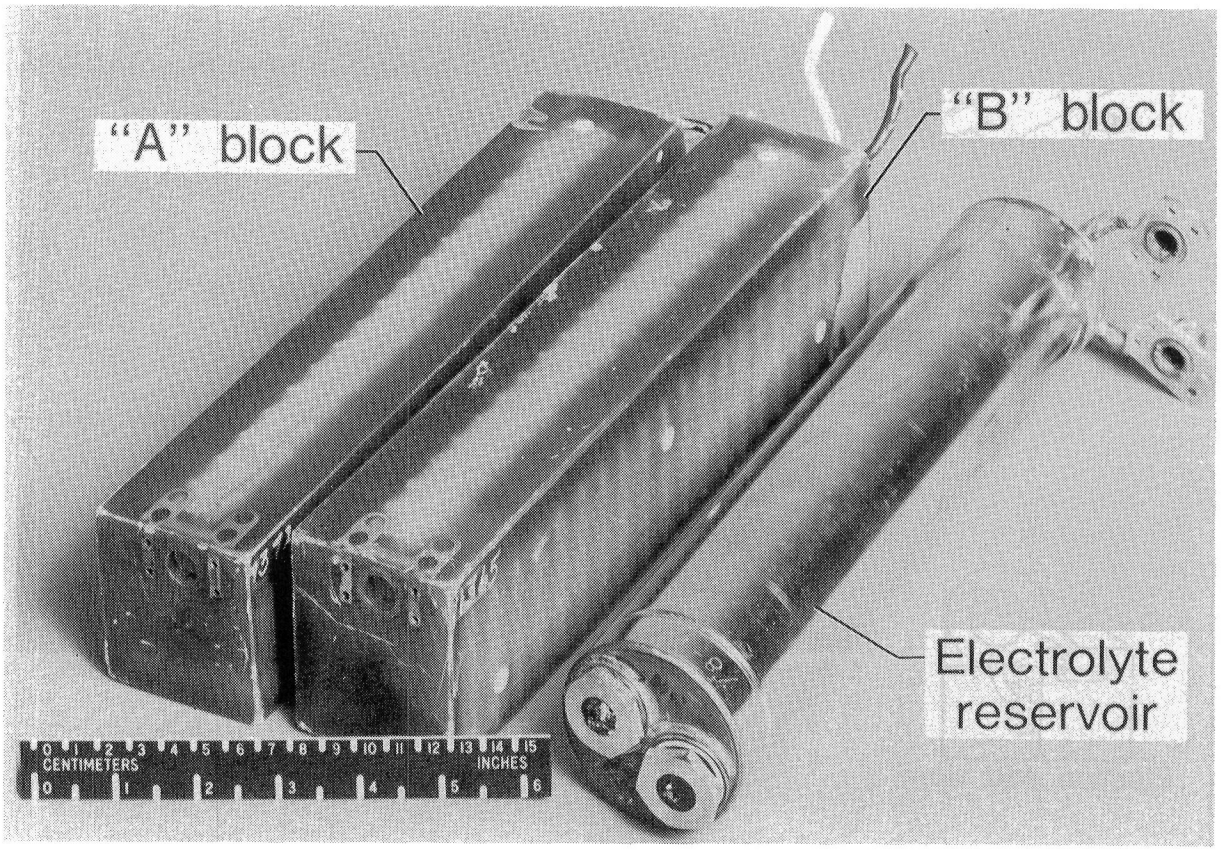


Figure 9

PHOTO POWER DISTRIBUTION

The 13KW of power required by the photographic system was distributed as shown in Figure 10. Pallets 1 and 2 supplied power to six (6) lights and three (3) cameras each. The multiple power source design concept was chosen to guarantee some film data would be obtained if one or more pallets were lost upon aircraft impact.

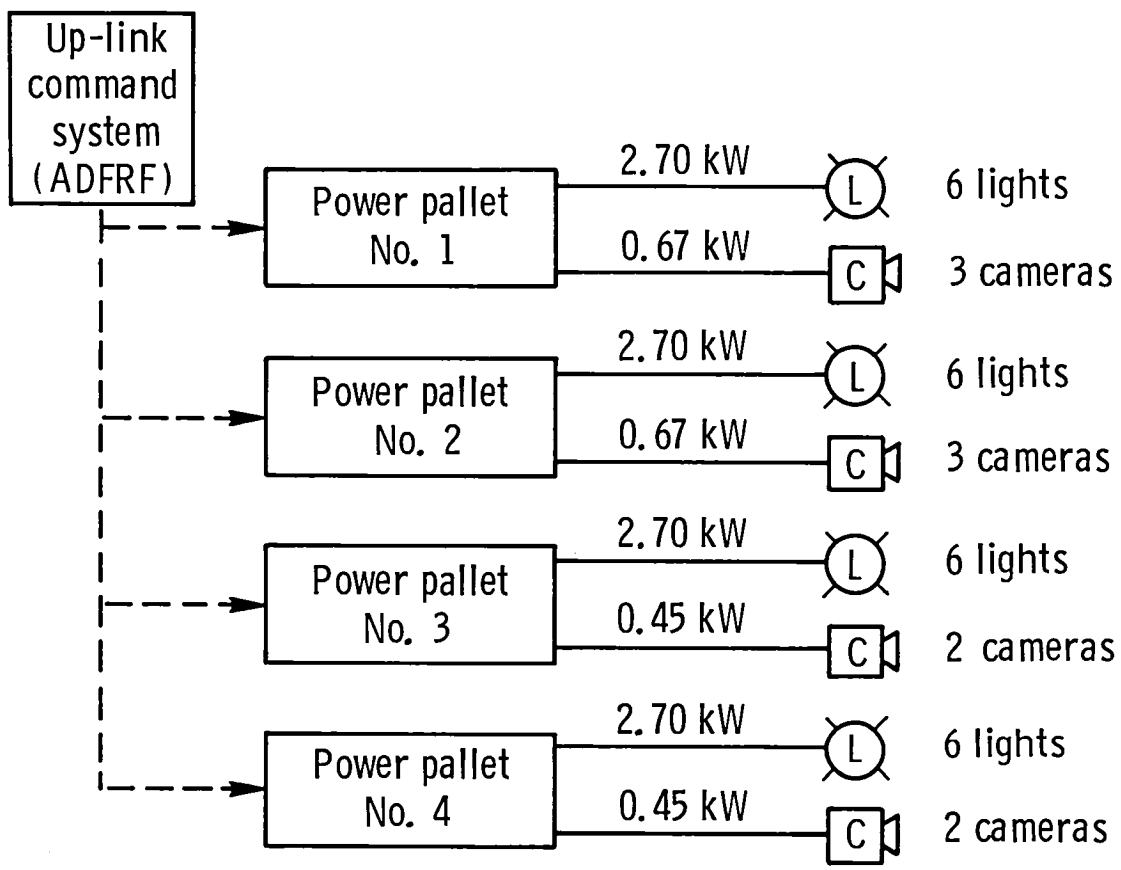


Figure 10

PHOTOGRAPHIC POWER SYSTEM ONE-LINE DIAGRAM

Each power supply was a relatively simple yet functional design as shown in this one-line diagram (Fig. 11). The up-link command energized relay K2 which completed the main battery activate circuits. The squibs were initiated by the two 12-volt alkaline lantern batteries and electrolyte was forced into the cells by the resultant gas generated. In less than one second the batteries were at full voltage and the photo lights illuminated. These batteries perform better when activated under load. For this reason, the lights were tied directly to the batteries. The second command was given to energize relay K1 to start the cameras. Diodes were employed to isolate each battery and the external power, which was supplied by a power cart for ground operational tests on the aircraft. Each circuit was fused to prevent a short circuit on the battery if the external conductors were severed during the crash. Each of the two remotely activated batteries supplied two 28-volt sources, designated "A" and "B." For clarity, only the "A" battery is shown in the diagram. The loads were divided between the two batteries with "B" carrying twice the load as "A."

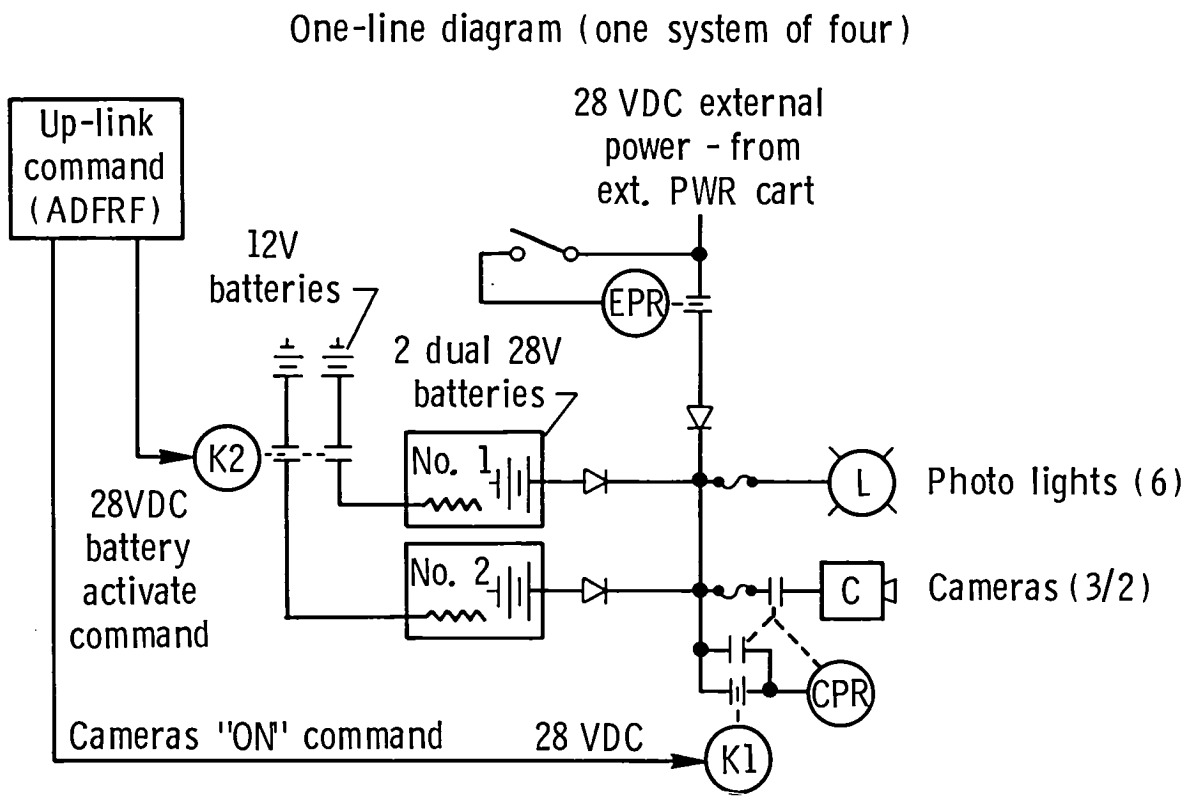
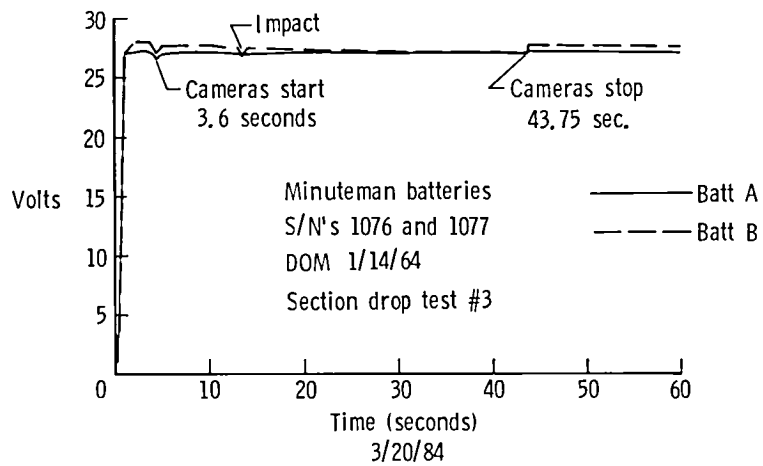


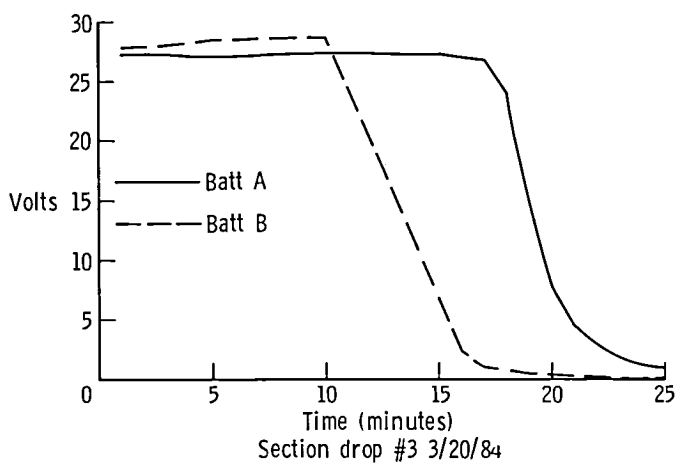
Figure 11

TIME-VOLTAGE DISCHARGE CURVES

Three fuselage section drop tests were performed at Langley (ref. 1). Fuselage section drop test #3 was used as a qualification test for the photographic system with one power pallet with two (2) paralleled batteries, and a full complement of six (6) lights and three (3) cameras. The battery voltages were recorded during this test and the results are shown in Figure 12. The data is typical of other recorded tests. Figure 12a displays the events which occurred in the first 60 seconds. The batteries reached full voltage within one second after activation, cameras were started at 3.6 seconds, fueslage impact on a concrete surface occurred at 15 seconds and the cameras were fully stopped by their end-of-film cutoff switches in about 44 seconds. The lights continued burning until battery depletion (Fig. 12b). Battery A began decaying in about 10 minutes and Battery B in about 17 minutes.



(a)



(b)

Figure 12

PHOTO SYSTEM TELEMETRY REQUIREMENTS

The telemetry requirement of the photo system was for eight (8) "real time" downlink channels to monitor battery voltages. These voltages were recorded by the on-board tape recorders, ground tape recorders, and on strip chart recorders in the control rooms. Two uplink commands were required to activate the batteries and start the cameras. (See Fig. 13.)

- Photo power system "Real time" data
  - Battery voltages

    8 channels required
- "Up-link" command signals required
  - Battery activate

    28 VDC to relay on four pallets
  - Cameras "start"

    28 VDC to a relay on four pallets

Figure 13

CAMERAS

The D.B. Milliken cameras (Fig. 14), now manufactured by Teledyne Camera Systems, Arcadia, CA, were chosen for use on the CID because of their ruggedness, reliability and experience.

- Selected for ruggedness and reliability
- First used by LaRC on Mercury Program (1958)
- Used last 10 years on numerous crash tests at LaRC Crash Facility
- Survived up to 100 g's during those tests
- Now manufactured by Teledyne Camera Systems

Figure 14

TYPICAL CID CAMERA AND LIGHT INSTALLATION

A typical camera and light installation is shown in Figure 15. This particular installation was in the galley. A sheet of heat retardant material was mounted under each camera and a heat shield (not shown in photograph) was placed over the camera which left only the lens and electrical connector exposed.

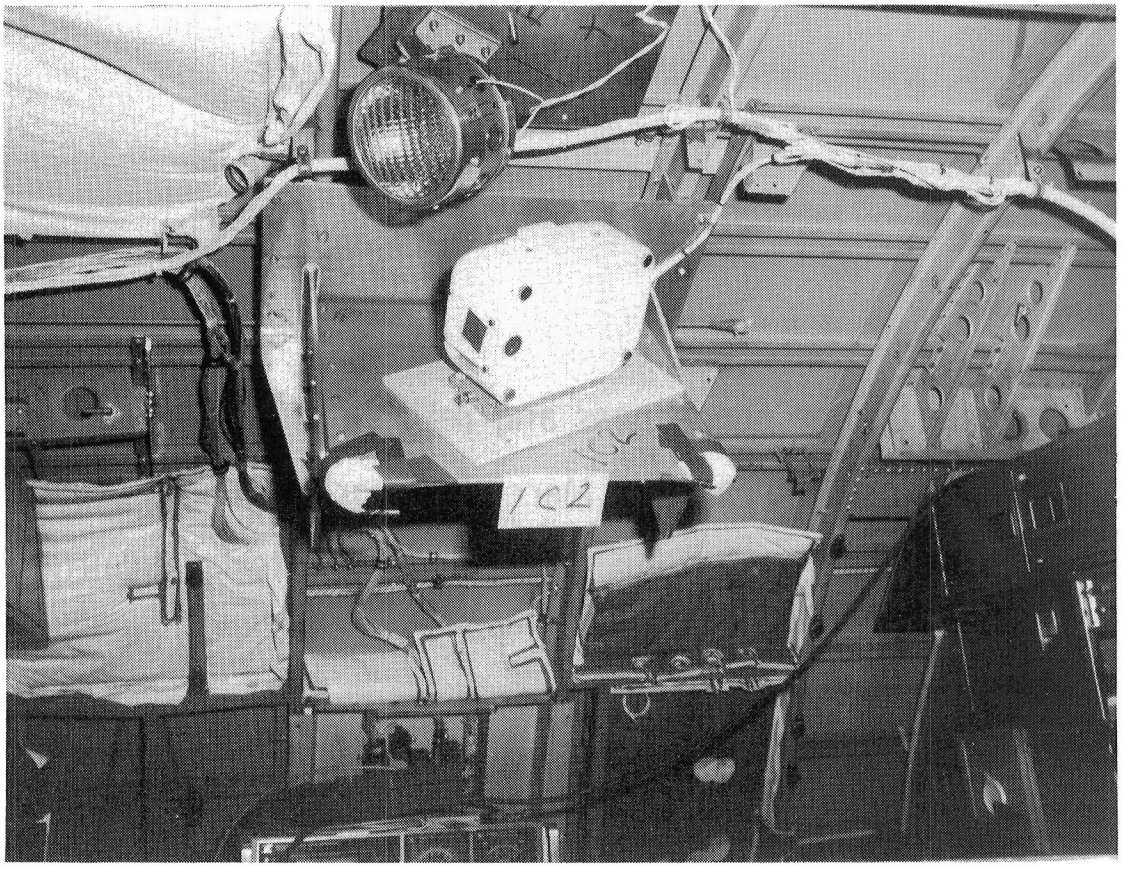


Figure 15

CAMERA SPECIFICATIONS

A brief summary of the camera specifications are listed in Figure 16. The time code was impressed on both the left and right sides of the film by light emitting diodes (LED). The end-of-film cutoff switch removes power from the camera when film has been expended.

- Description: 16 mm high speed (400 fps) motion picture camera, Teledyne Camera Systems Model DBM-55
- Speed stability: ± 1% or 1 fps
- Power requirements: 28 ± 4 volts DC; 7.5 amps at 400 fps
- End of film cut-off switch
- Timing lights: Light emitting diodes (LED)
- Operational environment:
  - Acceleration: 25 G's
  - Temperature: - 65°F to 150°F
  - Vibration: 5 to 5000 Hz with 10 G peak loading
- Film used: Eastman Ektachrome Video News Film - 7239 - Daylight

Figure 16

TIME CODE AND VOLTAGE MONITOR

The Inter-Range Instrument Group (I.R.I.G.) "B" time code impressed on the film was supplied from two independent time code generators, one on each Data Acquisition System (DAS) pallet. These timing signals were transmitted to an LED drive unit located on each photo power pallet and then distributed to each camera. The photo power system battery voltages were conditioned within the same unit containing the LED drive circuitry and sent to the DAS for recording and telemetering to the ground stations. Figure 17 shows a block diagram of the time code distribution.

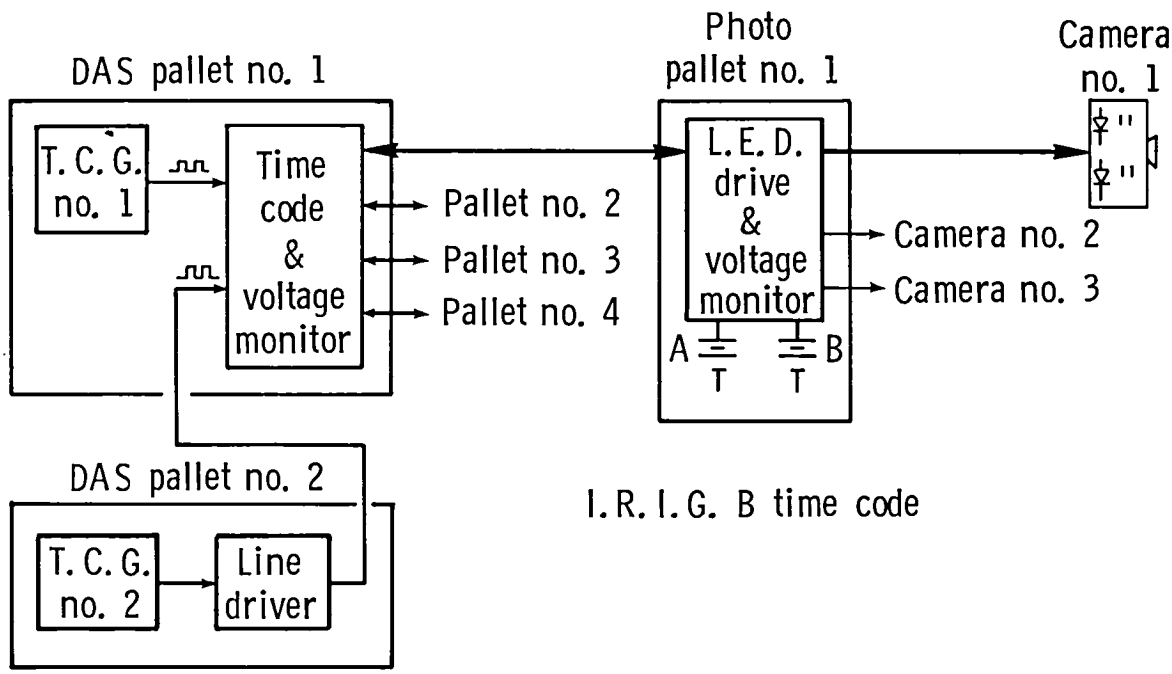


Figure 17

CAMERA ANOMALY

Only one camera anomaly occurred on the CID (Fig. 18). The take-up reel jammed on one camera, for some unexplained reason, shortly after it started, causing the film to "bunch-up" within the camera housing. The film was removed in a darkroom, as was all the other film, and successfully processed.

- Take-up reel jammed on one camera on CID
- Film recovered and processed

Figure 18

POST CRASH PHOTO OF CAMERA, HEATSHIELD AND MOUNTING PLATE (FRONT VIEW)

The post crash condition (front view) of a typical camera, heatshield and mounting bracket is shown in Figure 19. The heat resistant material under the camera and the heatshield provided excellent protection for the camera despite the fact that the aluminum mounting bracket practically melted away. The smoke deposits on the camera housing was cleaned off revealing the original paint hardly scorched.



Figure 19

POST CRASH PHOTO OF CAMERA, HEATSHIELD AND MOUNTING PLATE (REAR VIEW)

Figure 20 is the rear view of the same camera and other hardware shown in Figure 19.

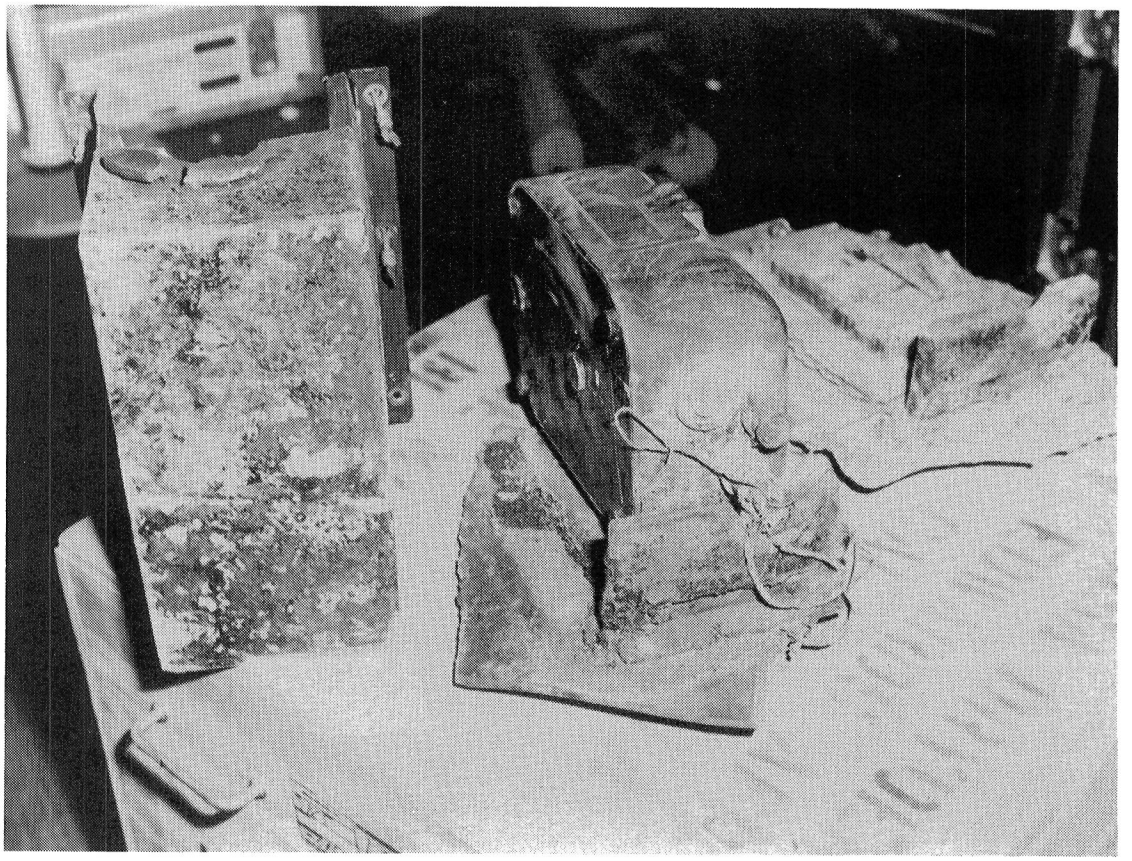


Figure 20

POST CRASH PHOTO OF CAMERA (INTERIOR VIEW)

The interior of the cameras were surprisingly clean when opened after the crash (Fig. 21). The lenses were destroyed, however, and the portion of the electrical connectors protruding from the heatshield was melted.

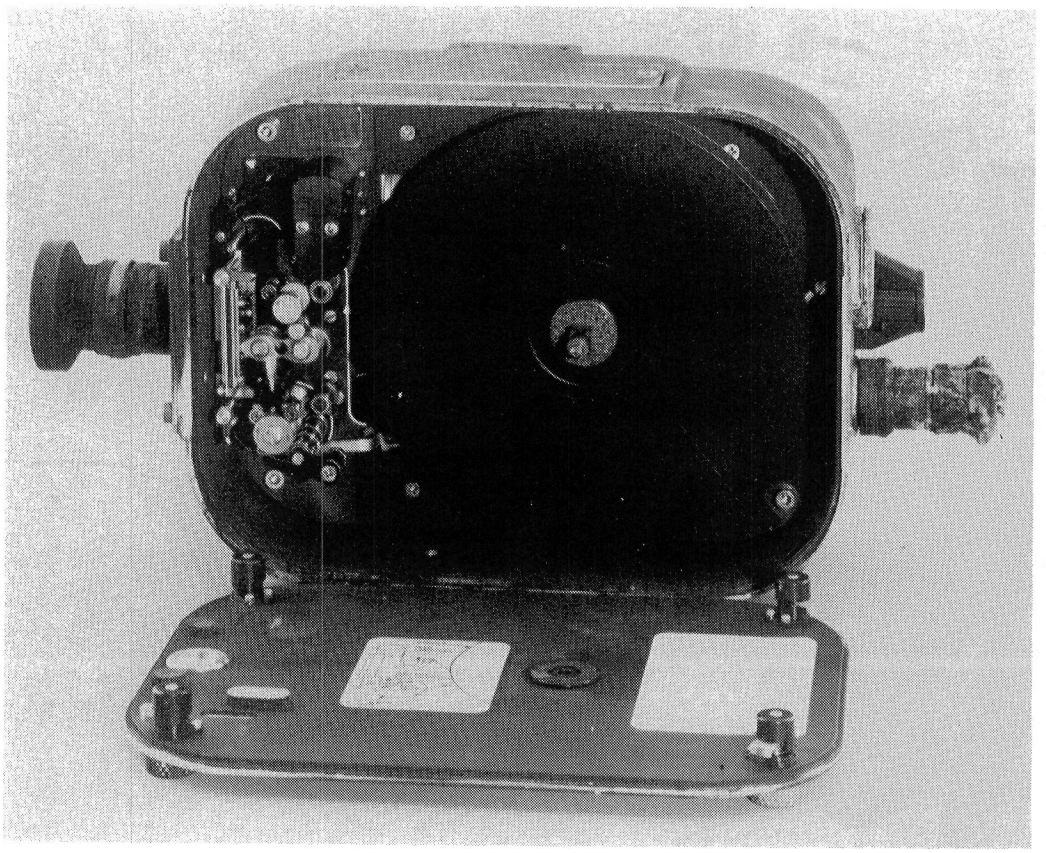


Figure 21

POST CRASH CAMERA CONDITION

Actual physical damage to the cameras was very slight, except for the lenses which could not be reused (Fig. 22). Total repair costs for all cameras was less than the original cost of one camera. Three of the CID cameras are currently being used on the LaRC Landing Loads Facility carriage testing program.

- All 10 lens were surveyed
- Seven (7) cameras are serviceable with only a clean-up
- Three (3) cameras require replacement of parts
    - Two requires relatively minor rework
    - One requires major replacement of gears, etc. mounting bracket melted, camera fell through floor, sustained water damage, gears rusted
- Total repair cost: Approximately $3,000
- Original cost: $7,200 each

Figure 22

CID PHOTO LIGHT FIXTURES

The photo lamp holders and mounting brackets, as well as the camera mounting hardware and heatshields, were designed, manufactured and tested at the LaRC. A shock-absorbing polyurethane, trade name "Sorbothane", was used to isolate the lamp holder from the mounting bracket and the mounting bracket from the aircraft structure to prevent breakage of the lamp filament (Fig. 23). After other shock-absorbing designs failed, this method proved highly successful in shock tests, as well as on the CID. Sorbothane is manufactured by Hamilton Kent, a division of BTR, Inc.

- Lamp holders and mounting brackets were designed, manufactured and tested at LaRC
- "Sorbothane", shock-absorbing material, was installed between lamp holder, mounting bracket and aircraft structure

Figure 23

TYPICAL LIGHT AND CAMERA INSTALLATION

The lamp holders and cameras were attached to the aircraft structure as shown in Figure 24. A swival section of micarta was used between the lamp holder and its mounting bracket so the lamp could be rotated for optimum illumination of the camera field-of-view, then drilled and locked into position with aircraft bolts.

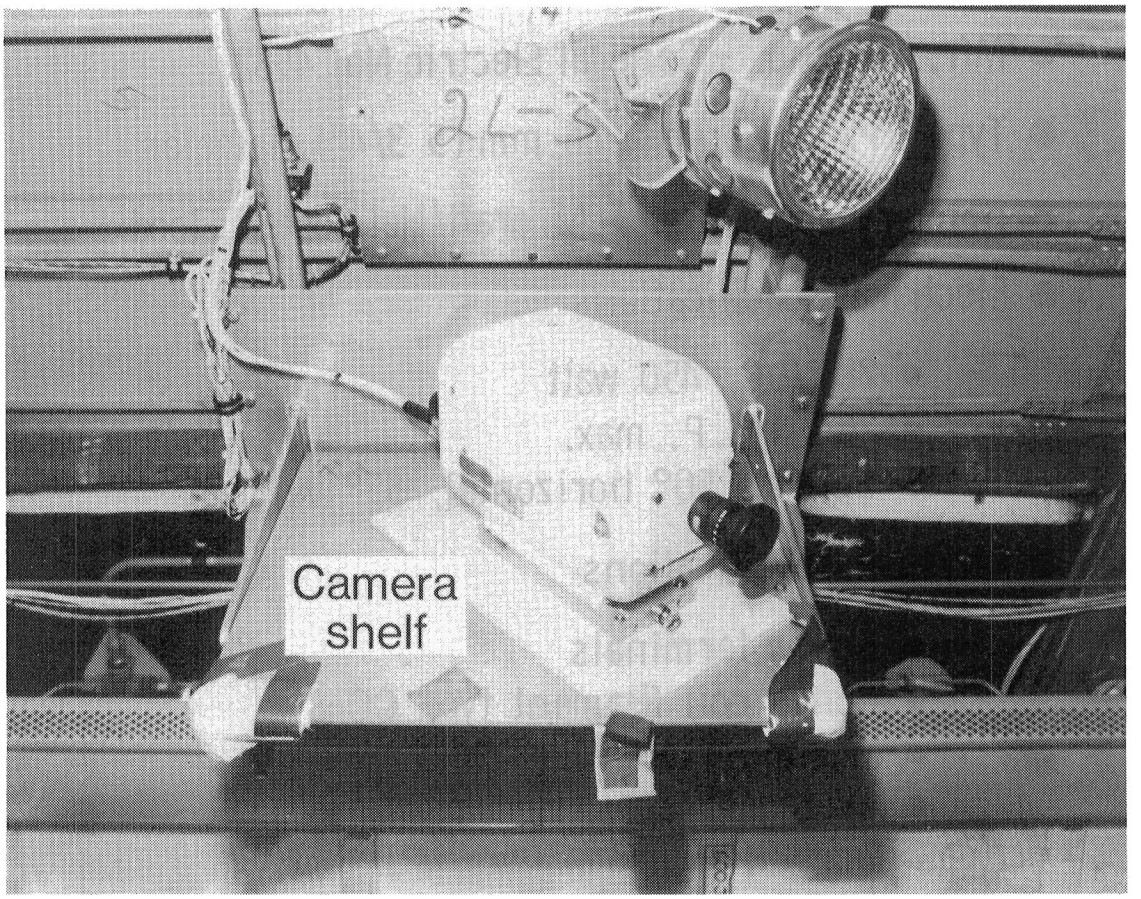


Figure 24

PHOTO LAMP SPECIFICATIONS

The specifications for the photo lamps used on the CID are given in Figure 25.

- Mfr./part no. - General Electric No. 4582
- Type - PAR46 bulb, 146 mm (5 3/4") diameter
- Primary application - Aircraft/Helicopter Flood
- Electrical specifications
  - 28 VDC, 450 watt
  - 20000 C.P. max.
  - Spread, 50° horizontal, 55° vertical
- Physical specifications
  - Screw terminals
  - Coiled coil filament type CC-8
  - Maximum length, 3 3/4"
  - Average life, 10 hours

Figure 25

POST CRASH PHOTO OF LIGHT FIXTURE

This photograph of one light fixture (Fig. 26) was taken shortly after the crash. It is obvious that the assembly, as did all 24, survived the crash with no physical damage. However, the extreme heat did melt the wires and polyurethane material.

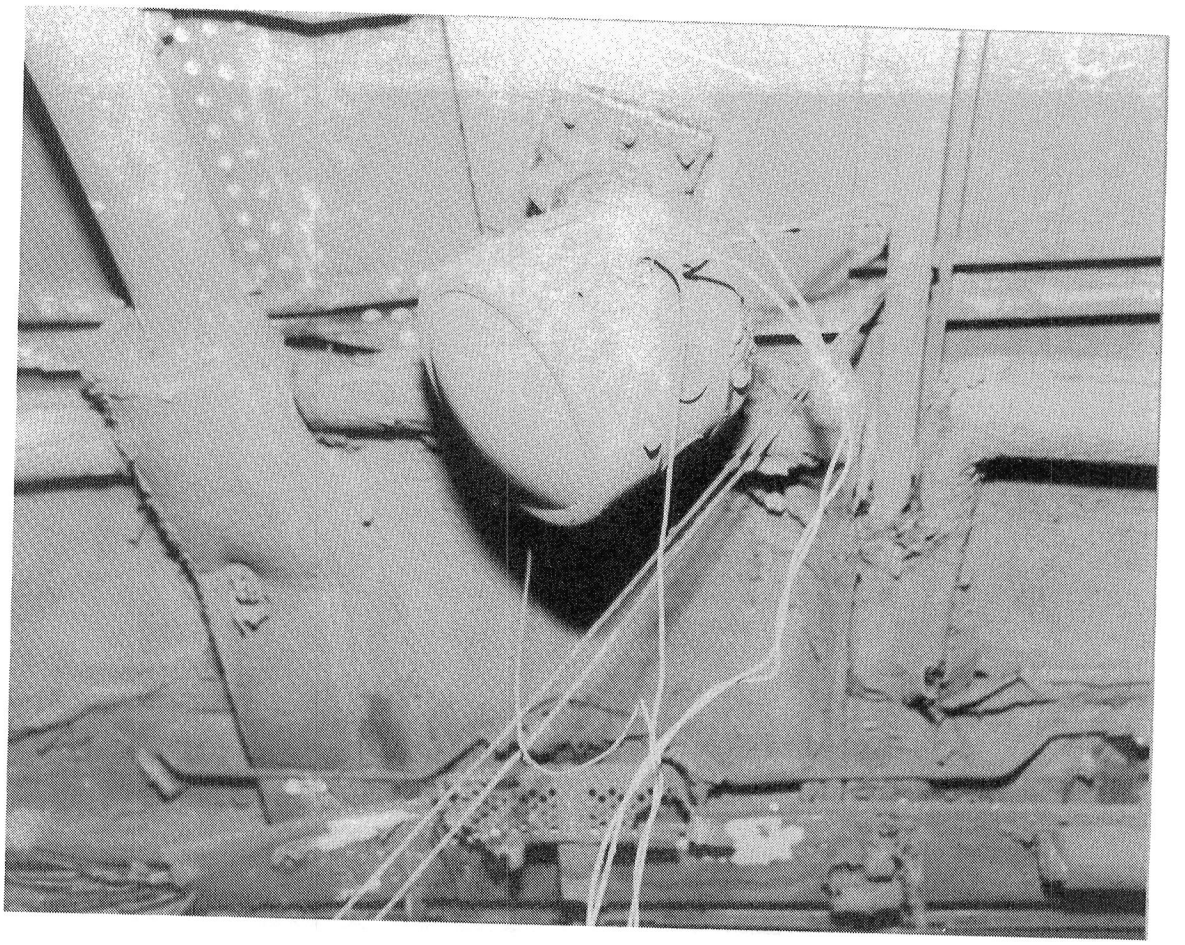


Figure 26

POST CRASH POSITION OF PHOTO PALLETS 2 & 3

Photo power pallets 2 and 3, which were located just aft of the left wing, are hardly discernible among the debris (Fig. 27). They fell through the floor, as did the other pallets, when the floor melted away. Red tags were placed on each unit by the safing crew, to indicate a possible personnel hazard because they still contained batteries.

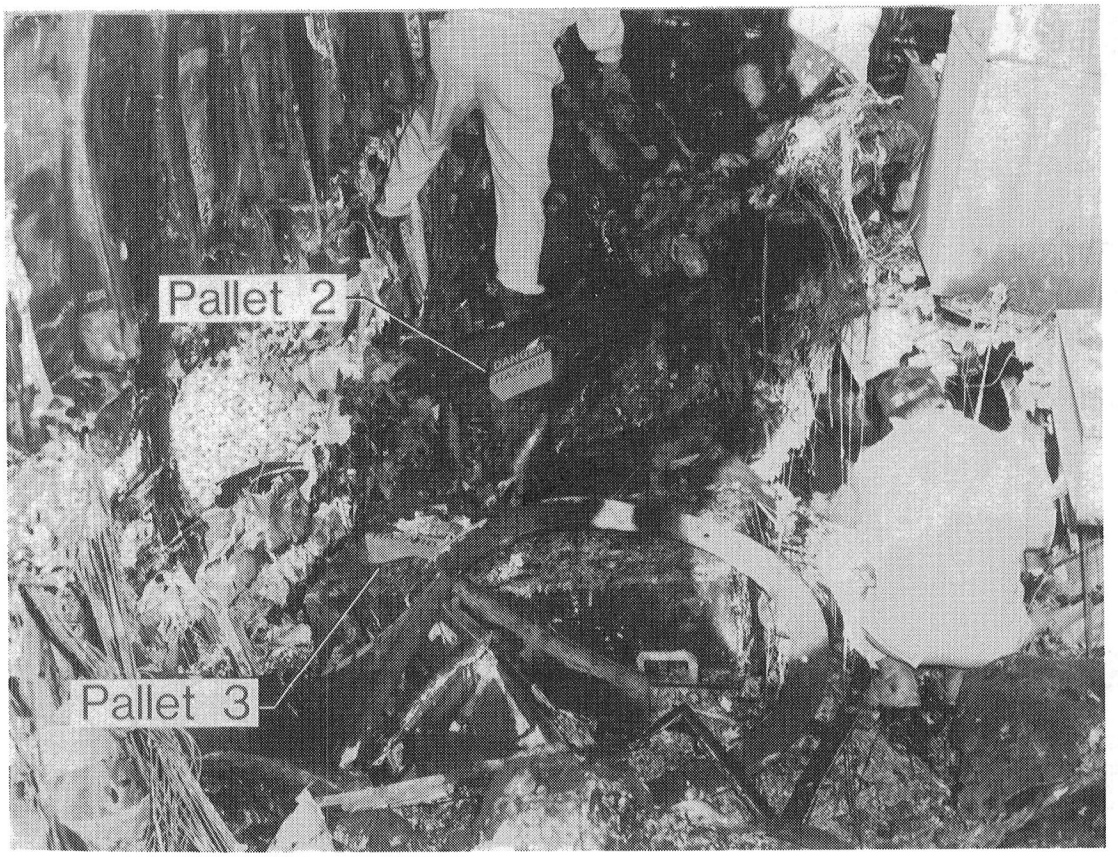


Figure 27

PHOTO PALLET NO. 3 - POST CRASH CONDITION (WITH HEATSHIELD)

Photo pallet No. 3 after removal from the aircraft (Fig. 28). The heatshield damage looks worse than it really was. Only the outer coating was partially burned away.

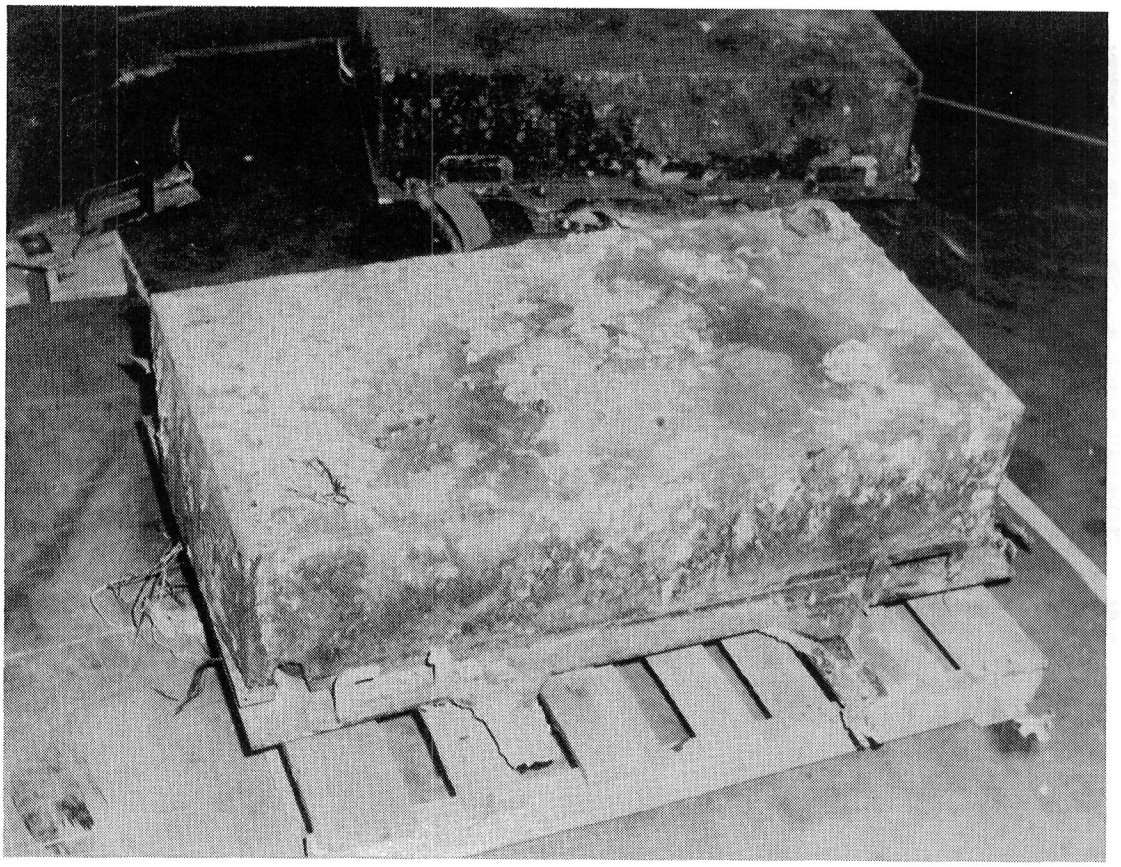


Figure 28

PHOTO PALLET NO. 3 - POST CRASH CONDITION (HEATSHIELD REMOVED)

Except for smoke deposits, there was surprisingly little damage to the pallet components when the heatshields were removed. Pallet number 3 (Fig. 29) was one of the worst and except for the batteries (not shown), fuses and wiring, most of the other hardware could have been salvaged.

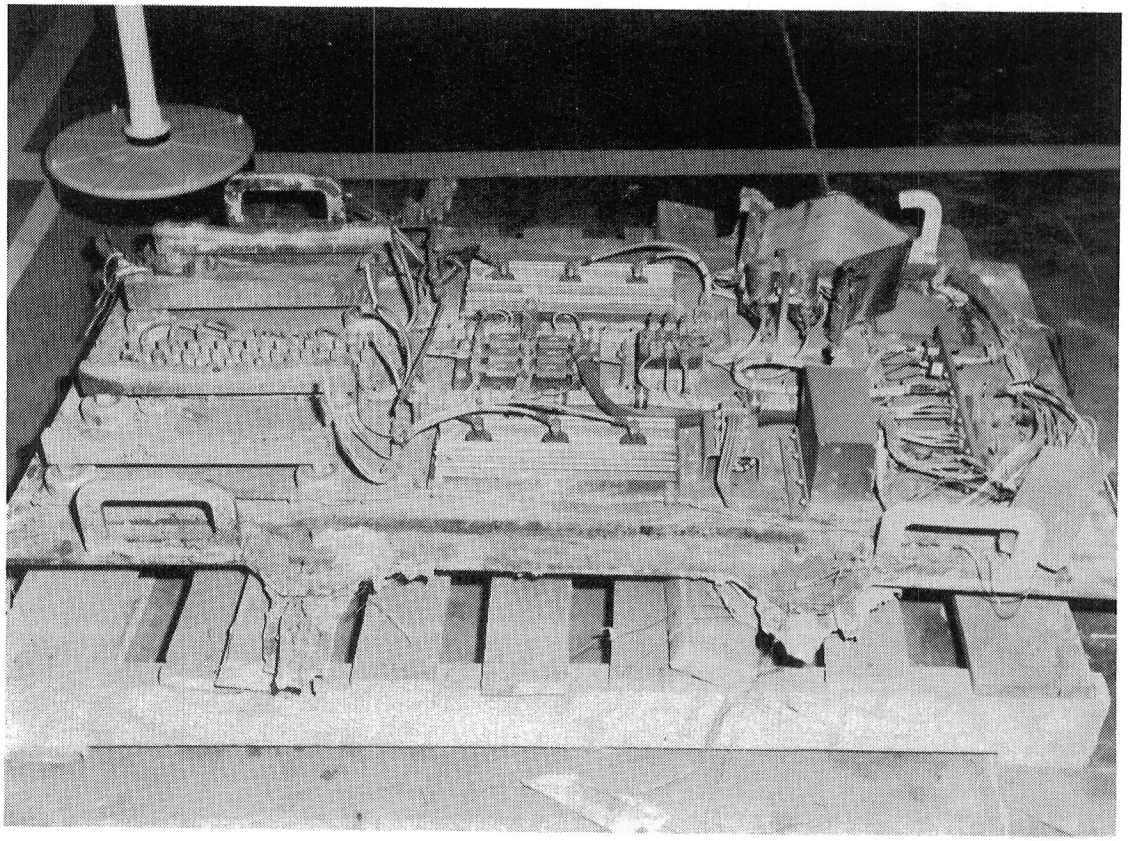


Figure 29

SUMMARY

- Photo system performed beyond expectations
  - All four (4) power distribution pallets with their 20 year old Minuteman batteries performed flawlessly
  - All 24 lamps worked
  - Recovered all ten (10) on-board high speed (400 fps) 16 mm cameras with good resolution film data

REFERENCE

1. Pride, J. D.: CID-720 Aircraft LaRC Preflight Hardware Tests: Development, Flight Acceptance and Qualification. Full-Scale Transport Controlled Impact Demonstration, NASA CP-2395, 1986, pp. 303-328.

CID-720 AIRCRAFT

HIGH-ENVIRONMENT

FLIGHT INSTRUMENTATION SYSTEM

R. S. Calloway
NASA Langley Research Center
Hampton, Virginia

NASA/FAA Government/Industry CID Workshop
NASA Langley Research Center
April 10, 1985

This paper summarizes the presentation at the Government/Industry CID Workshop on April 10, 1985, at Langley Research Center. The paper is organized into three major sections:

I. Design and Development
II. Installation and Combined System Tests
III. Performance on CID

The HIGH-ENVIRONMENT FLIGHT INSTRUMENTATION SYSTEM was designed to acquire Langley's structural response data during the Full Scale Transport-Controlled Impact Demonstration Test.

There was only one opportunity for data acquisition. Thus a high reliability and crashworthy design approach was implemented. The approach featured multi-level redundancy and a vigorous quality assurance testing program. Complying with an accelerated schedule, the instrumentation system was developed, tested and shipped within 18 months to Dryden Flight Research Facility. The flight instrumentation system consists of two autonomous data systems, DAS #1 and #2, and an excellent checkout subsystem. Each data system is partitioned into four pallets. The system was designed to operate on manned and unmanned flights. There are 176 data channels per data system. These channels are sequentially sampled and encoded into 1 megabit/sec pulse code modulation (PCM) data signal. To increase the probability of success, a special PCM distribution subsystem was developed. This subsystem distributes the PCM signal to two transmitters, one delay memory, and eight recorder tracks. The data on four of these tracks was digitally delayed approximately 300 msec to maximize data acquisition during impact. Therefore each data system's data is redundantly recorded onboard and on the ground. There are two time code generators. Parallel time from each is encoded into both data systems. Serial time from each is redundantly recorded on both onboard recorders. Instrumentation power is independent of aircraft power and self-contained. Each data system's power subsystem consists of an external power supply for system checkout and dual flight batteries for the actual flights. The flight instrumentation described also includes many special interface subsystems, high reliability power control and distribution subsystems, accurate real-time monitoring capability and thermal protection covers. The high environment flight instrumentation system successfully acquired 343 out of 352 channels of structural response data during the controlled impact. The electronic subsystems survived a post-crash fire and are operational.

DESIGN APPROACH

Approximately four years ago, the Aircraft Instrumentation System Section was asked to make a cost estimate for a 1100 channel data system. After many discussions on the number of channels versus cost and delivery schedule, a compromise was established. This compromise was to design and deliver a 352 channel data system to Dryden in 18 months. Since there was only one opportunity to acquire data, a High Reliability and Crashworthy Design Approach was implemented. The approach includes the following features; multi-level redundancy, fault tolerant techniques, and environmental protection techniques.

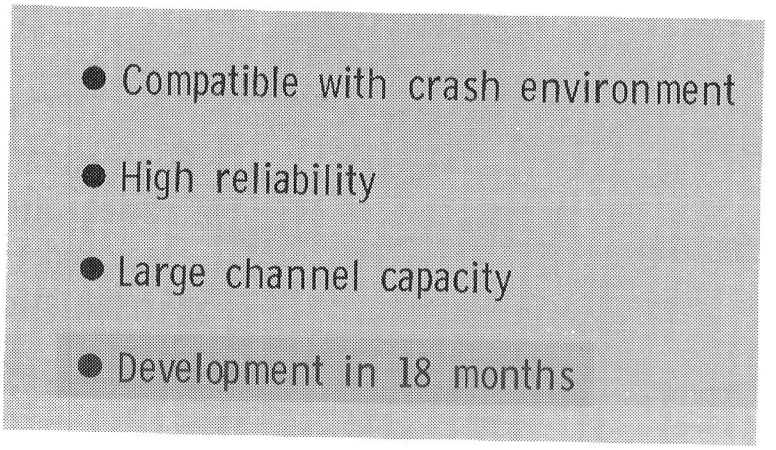


FIGURE 1

ACCELERATED SCHEDULE

Complying with an accelerated schedule, two data systems were developed, tested, and shipped to Dryden Flight Research Facility within 18 months. There was a vigorous quality assurance test program on the component and the system level. The quality assurance program included shock, vibration, and temperature testing. In addition, a third data system was built and tested to qualification levels in an actual airplane section.

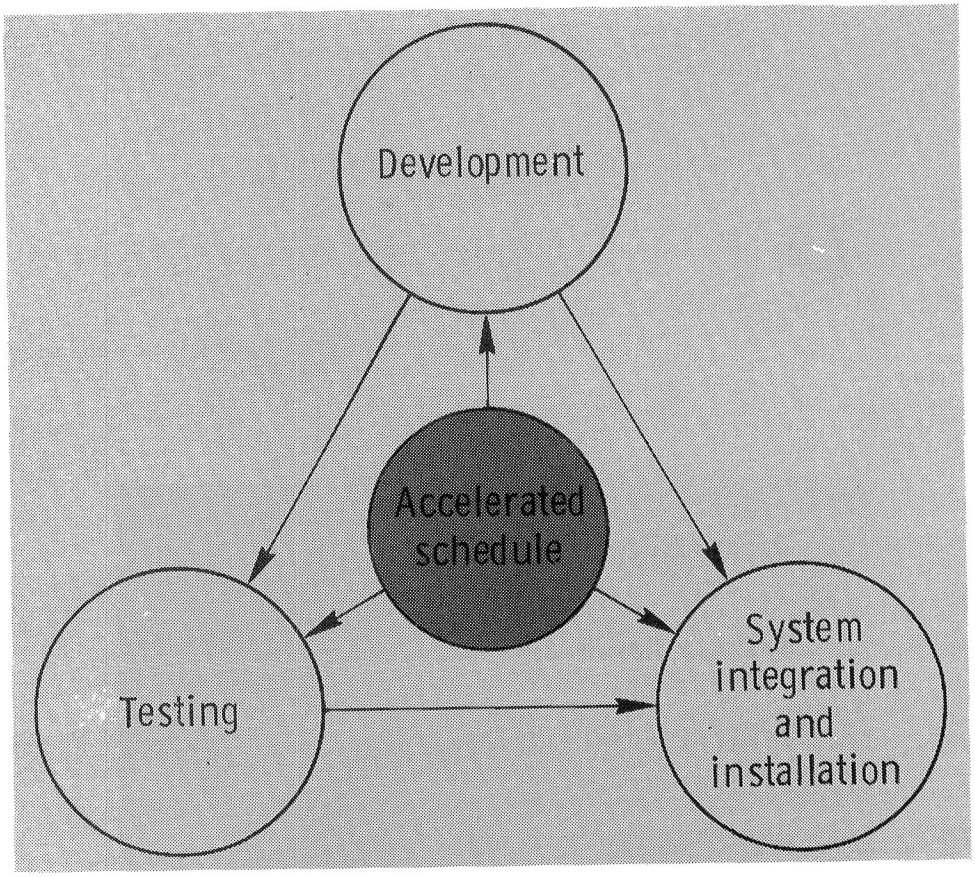


FIGURE 2

MEASUREMENT REQUIREMENTS

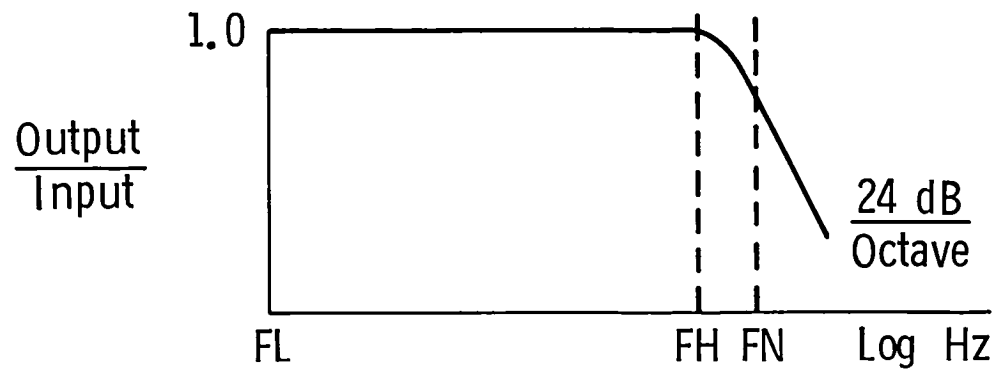
There were 352 data channels. In addition, there were 36 channels used to monitor the data system performance parameters.

- Data channels 352
  - Acceleration/shock . . 298
  - Tension (seat belt) . . 32
  - Structural strain . . . 22
- Monitor channels 36
- Total channels 388

FIGURE 3

FILTER FREQUENCY RESPONSE

There were three filter classes used: 36, 60, and 108. Each four-pole butterworth filter had the following amplitude tolerances: ±1/2 dB at .1 Hz, -1 to 1/2 dB at .6 cutoff frequency, and -4 to 1/2 dB at cutoff frequency.



Filter class	FL	FH	FN
36	0.1	36	60
60	0.1	60	100
108	0.1	108	180
Tolerance, dB			
High	1/2	1/2	1/2
Low	-1/2	-1	-4

FIGURE 4

MEASUREMENT FREQUENCY DISTRIBUTION

There were 243 100-Hz filters, 101 180-Hz filters, and 8 60-Hz filters.

Total filter channels: 352

Frequency	Quantity
• 180 Hz	101
• 100 Hz	243
• 60 Hz	8

FIGURE 5

INSTRUMENTATION BLOCK DIAGRAM

Due to the large channel requirement, the design was partitioned into two autonomous data systems. Each system records and transmits redundantly a PCM signal containing 176 unique data measurements. In addition, each system redundantly records the PCM and time code signals from the other system's outputs. Subsystems were selected on the basis of superior performance history at Langley and crashworthiness. Many subsystems were developed at Langley. Procured subsystems were modified to improve reliability as required.

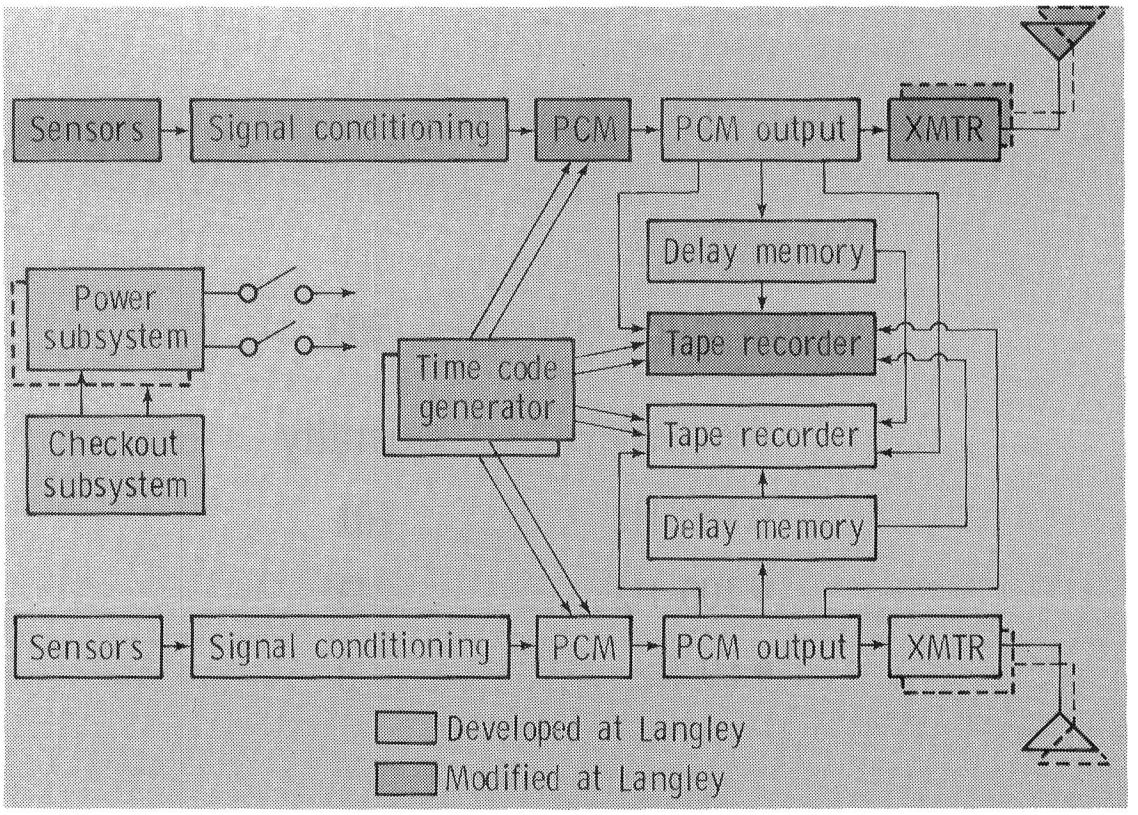


FIGURE 6

SIGNAL CONDITIONING

The Metraplex signal conditioning was selected for the following reasons:

- Successful acquisition of data in crash environments.
- Modular design featuring maximum in-the-field flexibility.
- Individual excitation regulation per channel.
- Solid state calibration technique eliminating relay switching problems during the impact sequence.

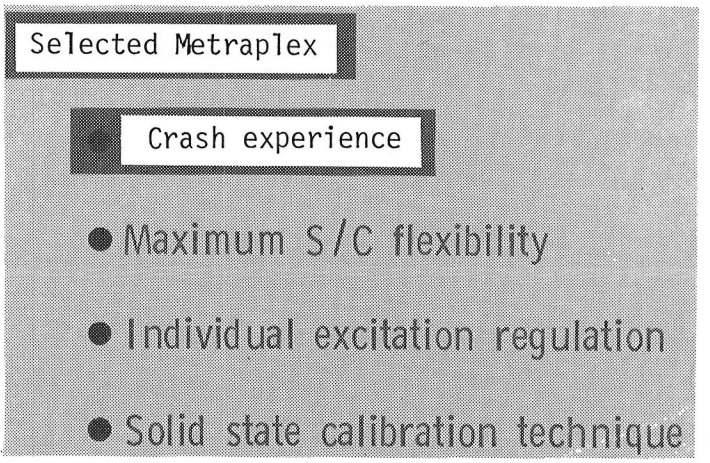


FIGURE 7

SIGNAL INTERFACE

An example of a typical sensor interface to the data system is shown. The 7264 accelerometer uses a half bridge design. To increase accuracy the completion resistors were installed at the sensor location. With a 10V excitation voltage supplied to the bridge a sensitivity of 2 mV/G is obtained.

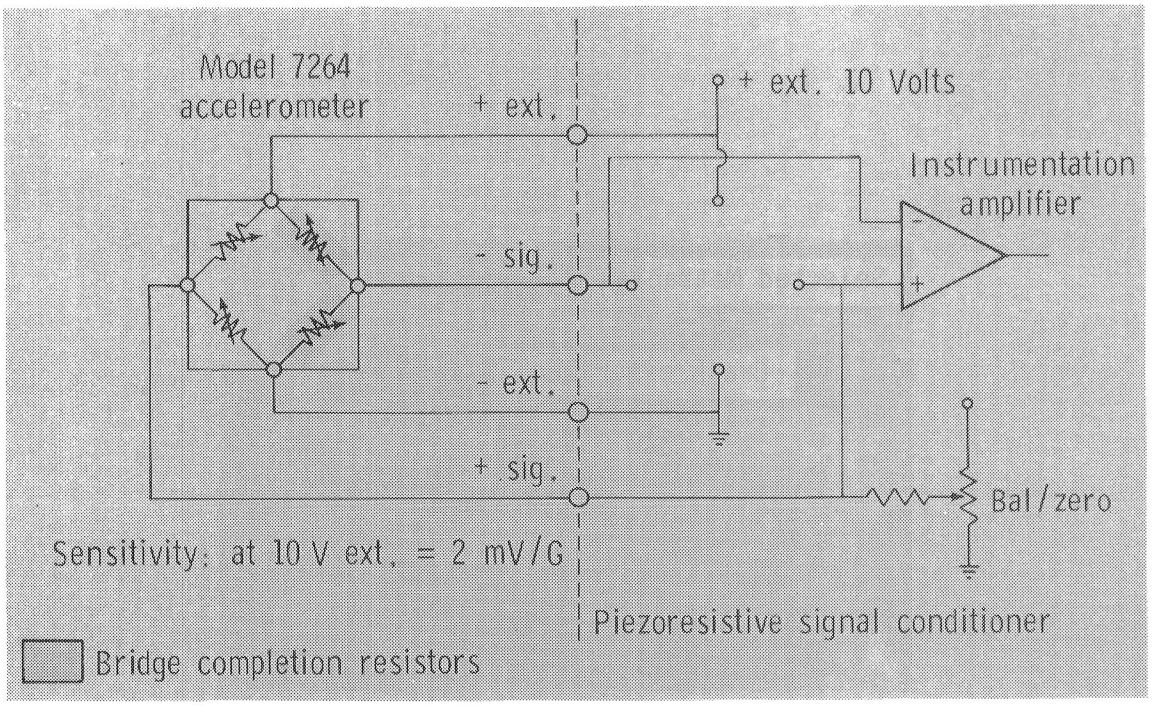


FIGURE 8

SIGNAL CONDITIONER

There are two signal conditioners shown in this figure. All components used on the project were inspected by Fred Austin, Quality Assurance Officer. His inspections included the following areas; parts and material, crashworthiness, and workmanship. To improve reliability the signal conditioners were modified at the vendor's facility and at Langley upon delivery. A combined list of improvements follows:

- Higher Quality Integrated Circuits
- Improved Filter Specifications with Test Documents
- Mil Spec Connectors
- Self-locking Helicoils
- Extended Base Plate for Mounting Purposes
- Heavy Gage Front Plate for Improved Crashworthiness

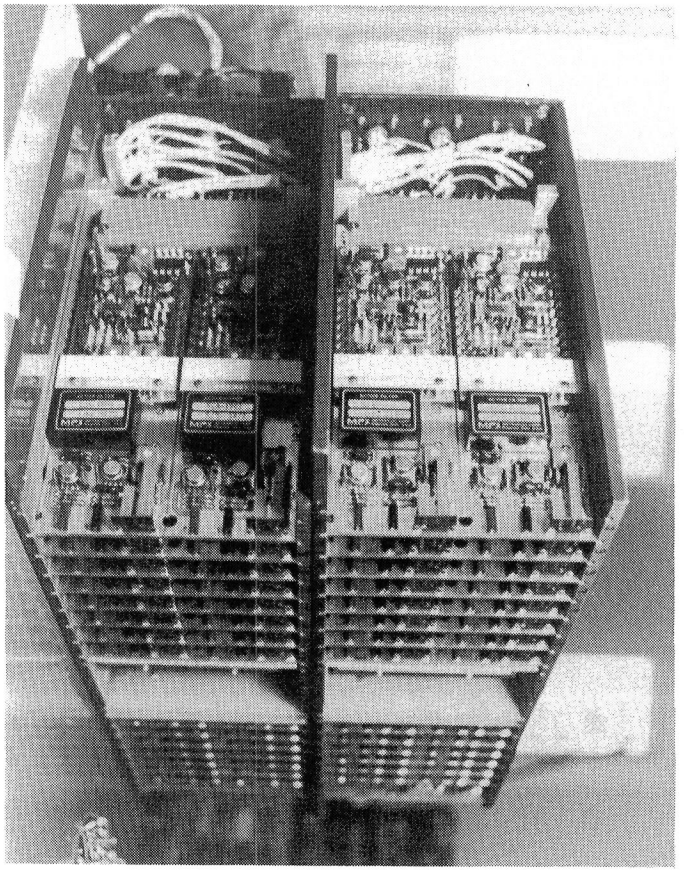


FIGURE 9

DIGITAL SUBSYSTEM

The teledyne PCM multiplexer was selected. This PCM's maximum operating rate was 1.5 megabit. Therefore the unit could easily operate at the desired 1 megabit rate. The unit met crashworthy criteria and has a excellent performance history at Langley Research Center and Dryden Flight Research Facility. The teledyne PCM multiplexor excelled in an independent survey by JSC/Lockheed and was the clear choice for this program.

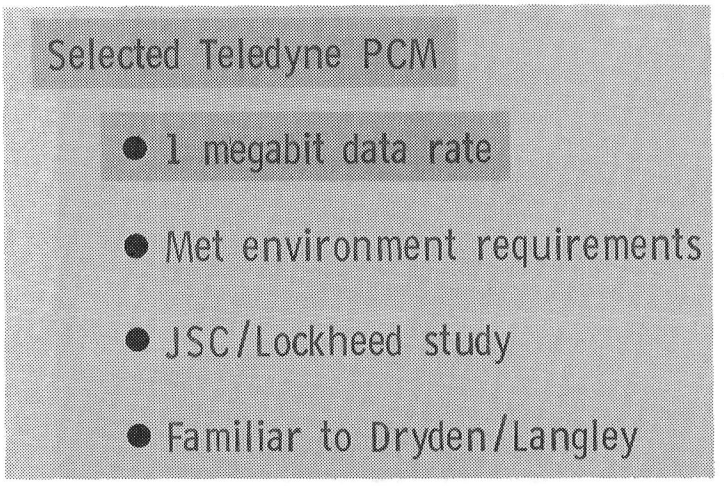
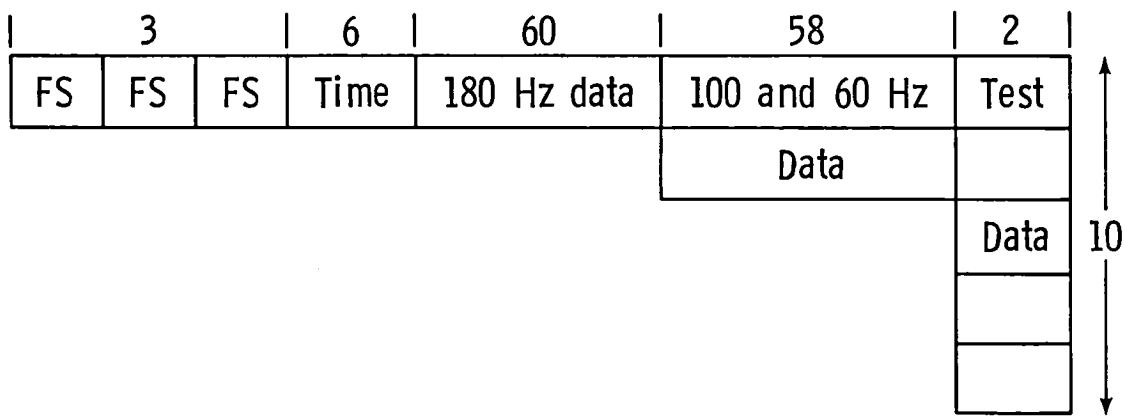


FIGURE 10

PCM FORMAT

Each PCM subsystem had a 129 word mainframe. Each word contained 8 bits. The subsystem sampled at 125K words/sec or 1 megabit/sec and had an equivalent sampling index of approximately 5 or greater for all channels. With the 4 pole butterworth filters, the maximum possible aliasing error was 2% RMS.



PCM setup

Bit rate	1 megabit	Sampling index
Bits/word	8	180 Hz data 5.38
Words/frame	129	100 Hz data 4.85
Words/sec	125 K	60 Hz data 8.08

2% RMS alias error (max) with 4 pole Butterworth filters

FIGURE 11

PCM DISTRIBUTION

The PCM distribution electronics were developed to increase the probability of successful data acquisition in a crash environment. Some of the main features are listed:

- Multi-level redundancy: There were 4 outputs per data system, each containing digital data representing the 176 data channels.
- Capability to drive long cable lines: The outputs of each data system are redundantly recorded on the other data system's on-board recorder.
- There are 2 on-board transmitters/data system.
- Fault tolerant techniques were used to prevent catastrophic failure.

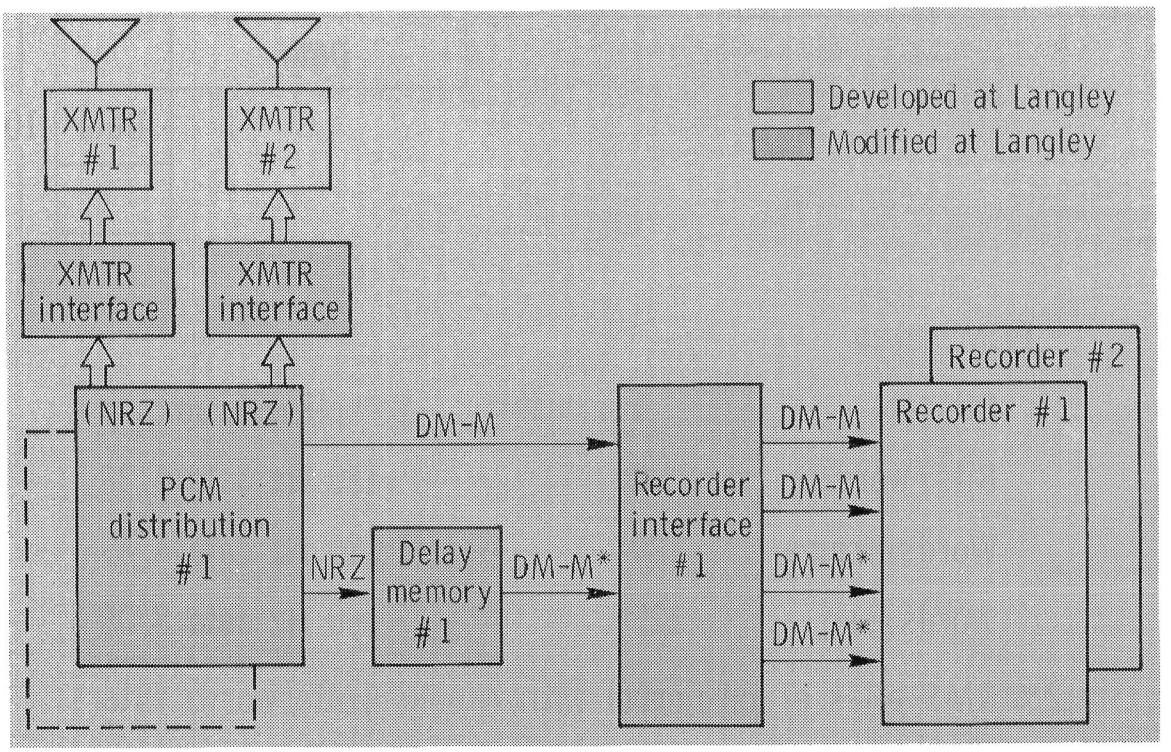


FIGURE 12

TIME CODE SUBSYSTEM

To ensure time correlation, there were two time code generators, one per data system. The outputs per time code generator were recorded on both on-board tape recorders and encoded, in the parallel format, into both PCM data signals. To correlate time on the on-board film, each time code generator modulated one of two LEDS located in each on-board camera.

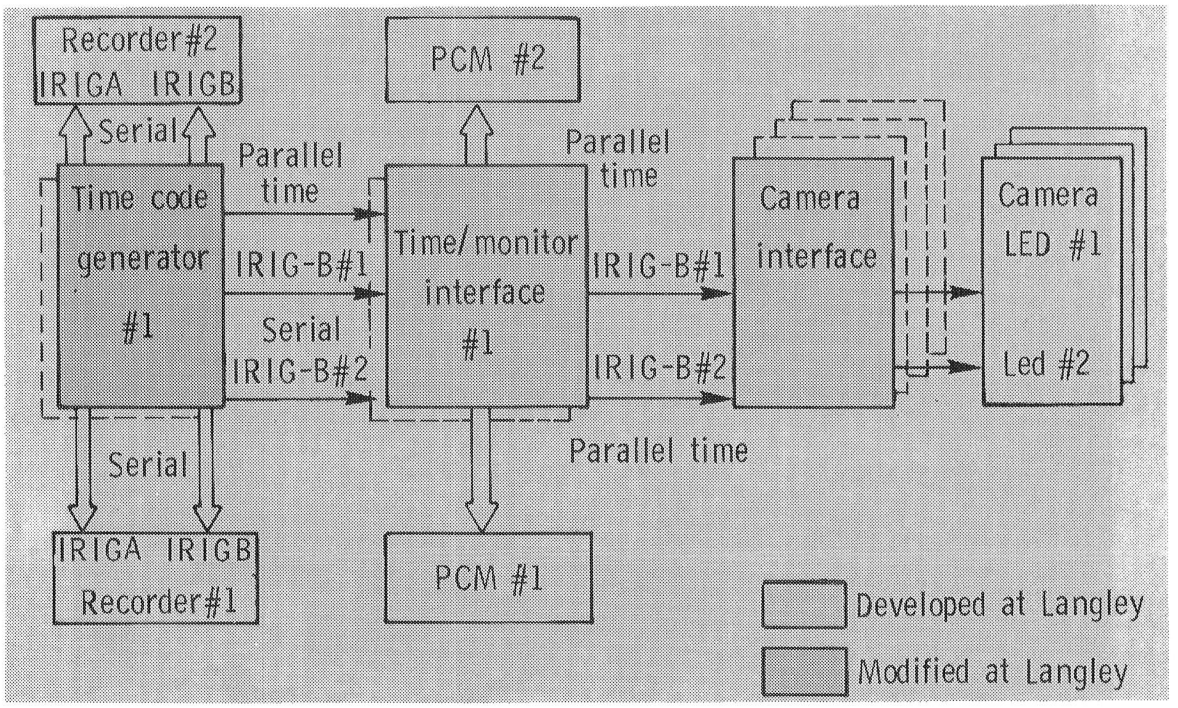


FIGURE 13

DAS MAIN PALLET

Each data system is partitioned into four pallets. The main pallet is shown below. Located on the top shelf are the digital subsystem with special shock isolation, the delay memory subsystem, the time code subsystem and the power control and distribution subsystem. There are six signal conditioning units located on the other three shelves. The layout features maximum accessibility for in-the-field operation and maintenance. The external power supply is shown in the right lower corner.

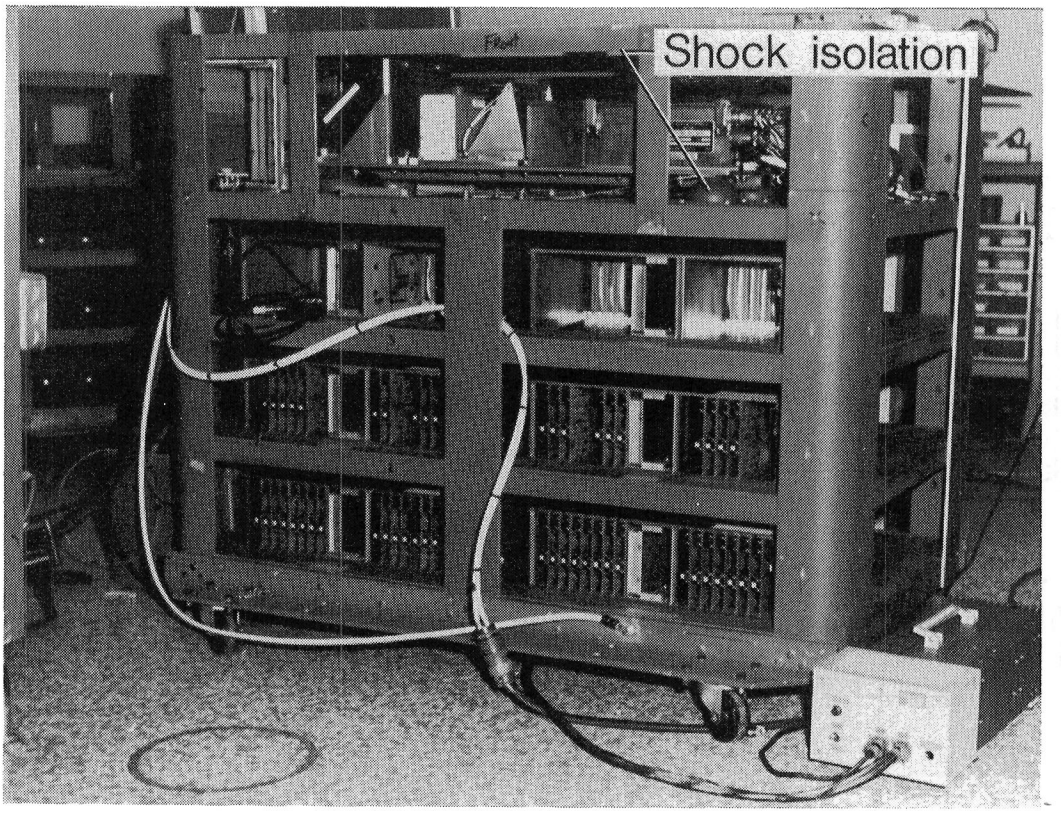


FIGURE 14

ON-BOARD RECORDING SUBSYSTEM

The Bell and Howell Mars 1000 recorder was selected for the following reasons:

- Met 1 megabit data rate requirement.
- Extensive experience with unit on aircraft programs at Langley.
- Successful data acquisition in crash environments.

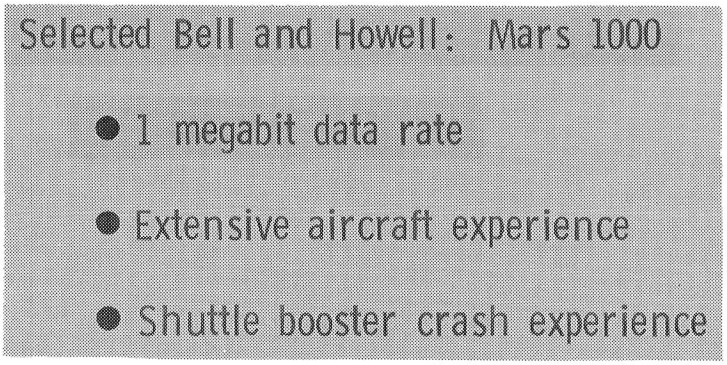


FIGURE 15

ON-BOARD RECORDING SUBSYSTEM

The recording subsystem electronics were developed to increase the probability of successful data acquisition in a crash environment. In conjunction with the PCM distribution electronics, this special circuitry provided the following features:

- Multi-level redundancy; there were 4 recorder tracks per data system dedicated to each data system's PCM signal.
- There were 2 recorder tracks per data system dedicated to each data system's serial IRIG time output.
- There was an on-board delay memory per data system. The data on four tracks per recorder was digitially delayed approximately 300 msec to maximize data acquistion during impact.
- Accurate real-time monitoring capability was developed to ensure on-board data acquisition.

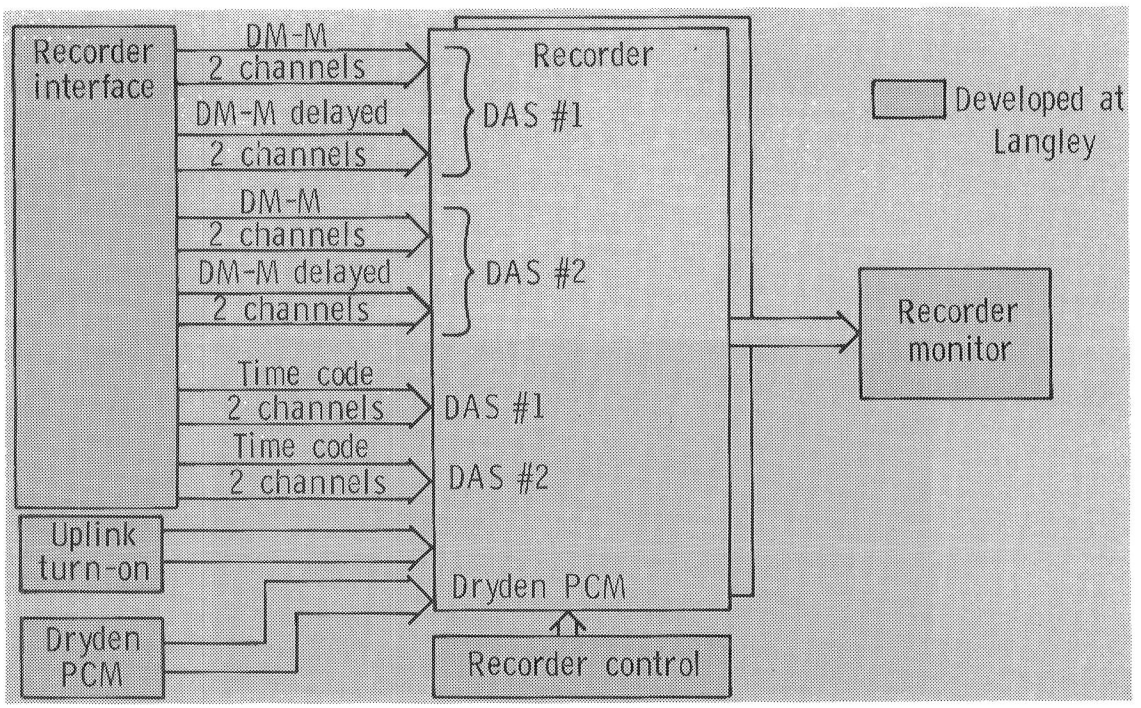


FIGURE 16

RECORDER SUBSYSTEM

Some additional features of the interface electronics were:

- Recorder interface expands 2 PCM signals into 8 signals for redundant recording.
- Recorder monitor; a 10 KHz signal is recorded and monitored via the playback head real-time using phase-lock loop techniques.
- Special shock and vibration isolation techniques were developed to increase probability of successful data acquisition.

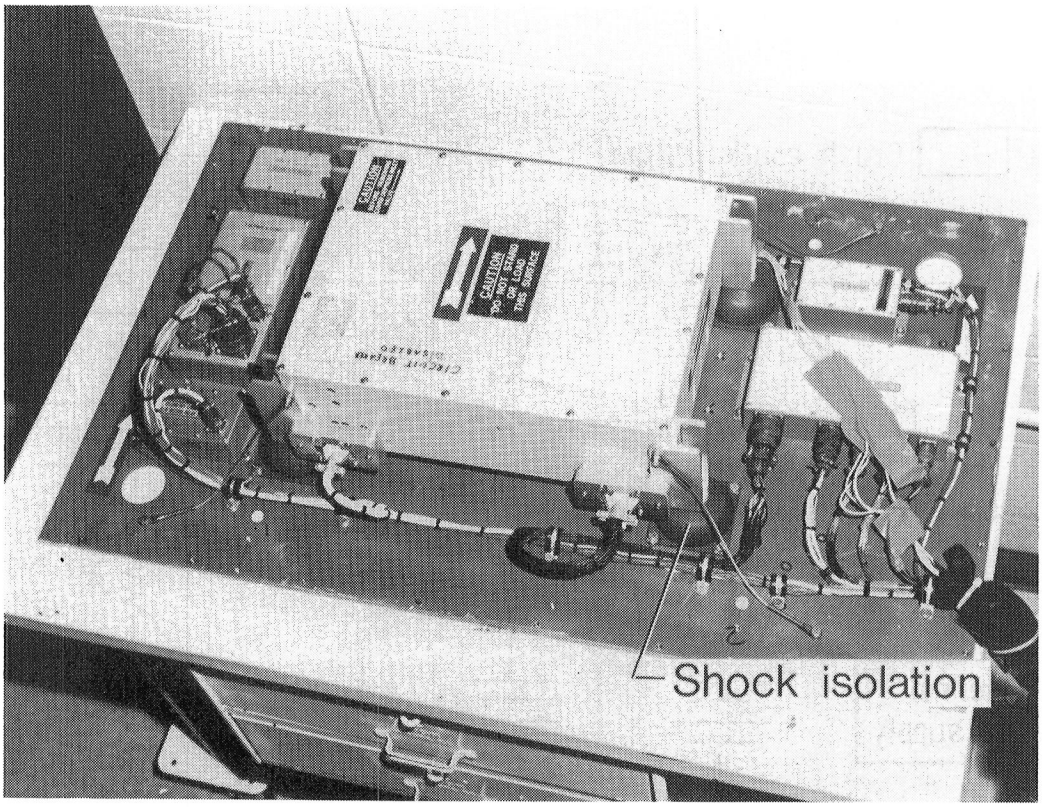


FIGURE 17

POWER SUBSYSTEM

Instrumentation power was independent of aircraft power and self-contained. Each data system's power subsystem consists of an external power supply for system checkout and dual flight batteries for the actual flights. A relay control subsystem was developed to transfer power from the external power supply or the internal batteries to the data system.

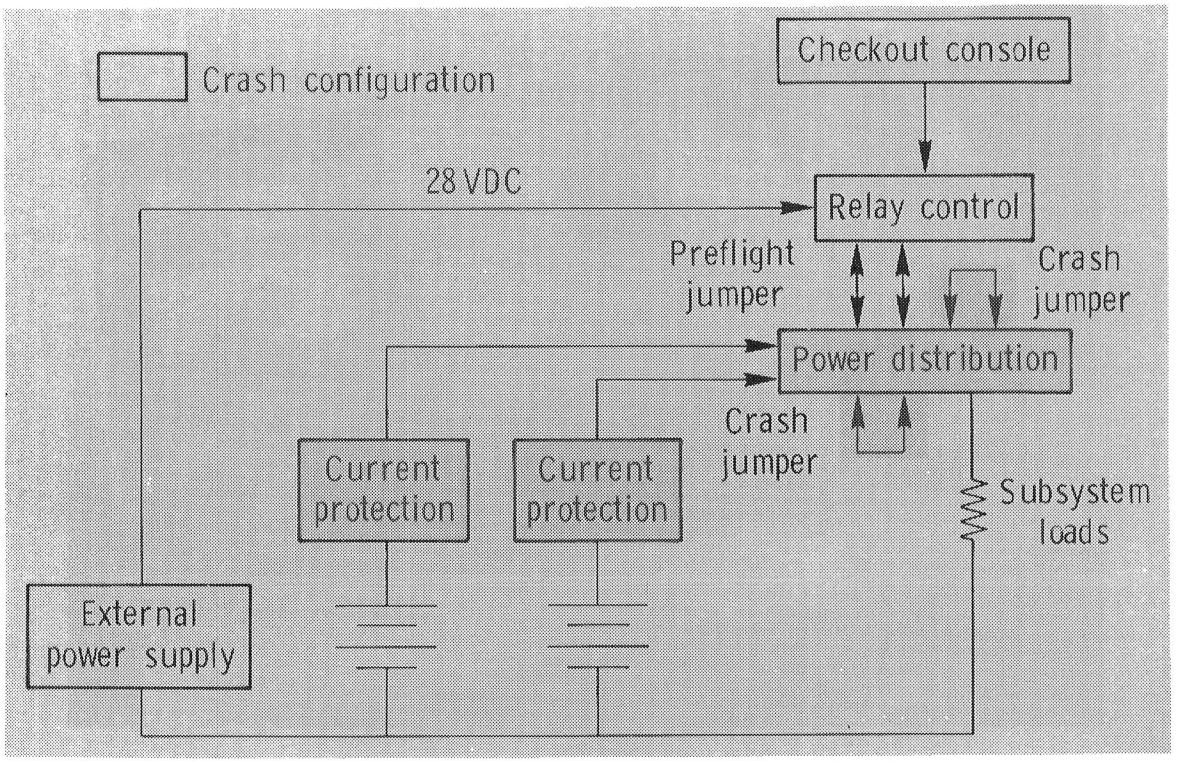


FIGURE 18

BATTERY AND DIODE BOX

A special 23 cell nicad battery was developed for this project. Unique stress release connector links were designed to increase crashworthiness. A redundant parallel fuse technique was used to increased reliability. Series diodes were used to prevent the flight batteries from reverse charging each other.

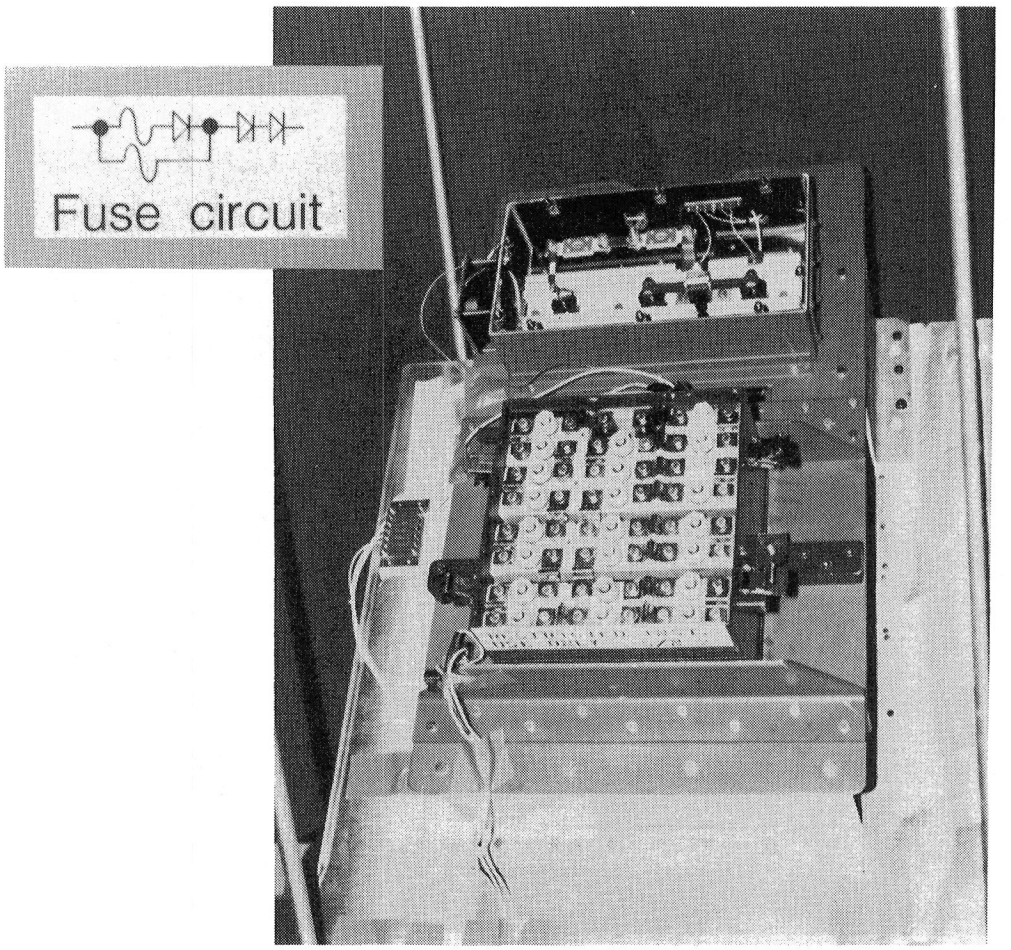


FIGURE 19

POWER DISTRIBUTION BOX

A central power distribution subsystem was developed to ensure reliable power delivery to each subsystem. The design features crashworthy techniques in the construction and the selection of electrical and mechanical components. A redundant parallel fuse technique was implemented. This technique used a unique high "G" fuse in each branch circuit. There was a screening program for each fuse that included electrical tests and X-Ray analysis.

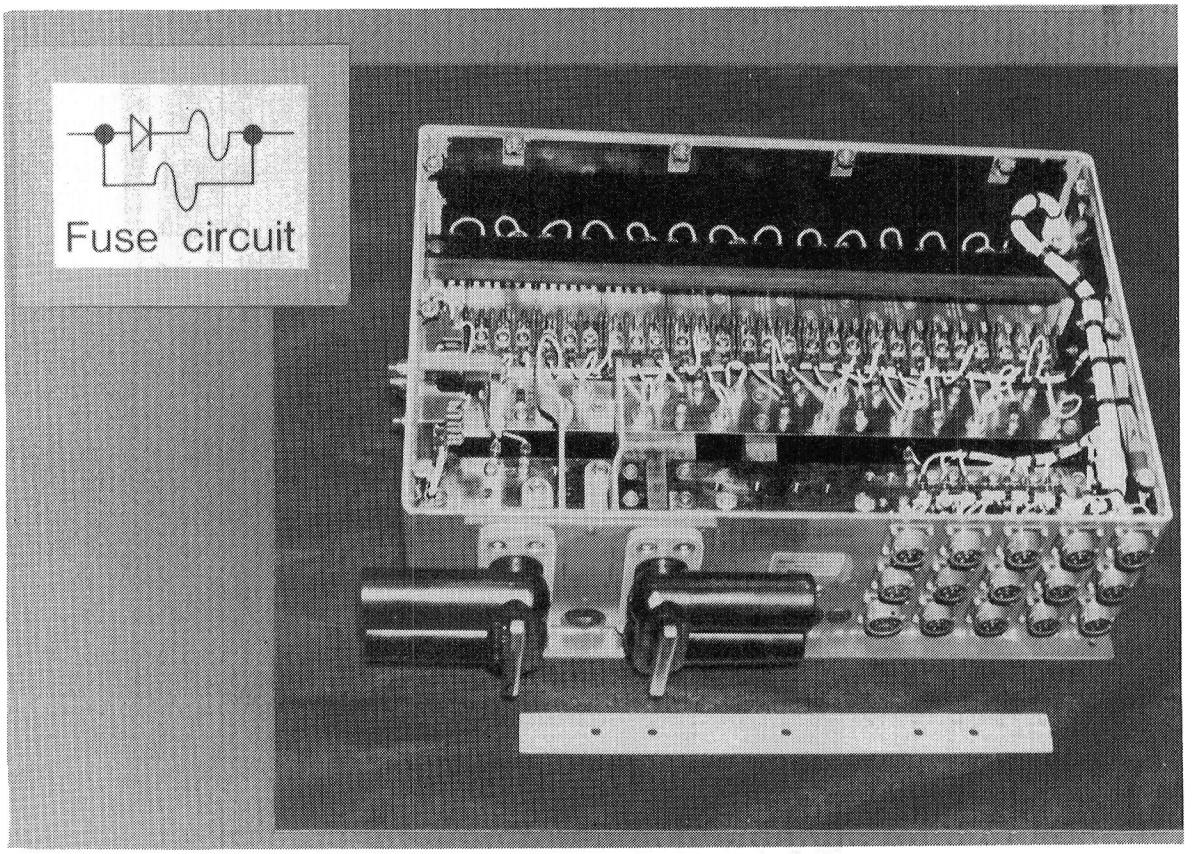


FIGURE 20

RELAY CONTROL BOX

The relay control subsystem controls power via the checkout console. High quality, high "G" components were used to perform this important function.

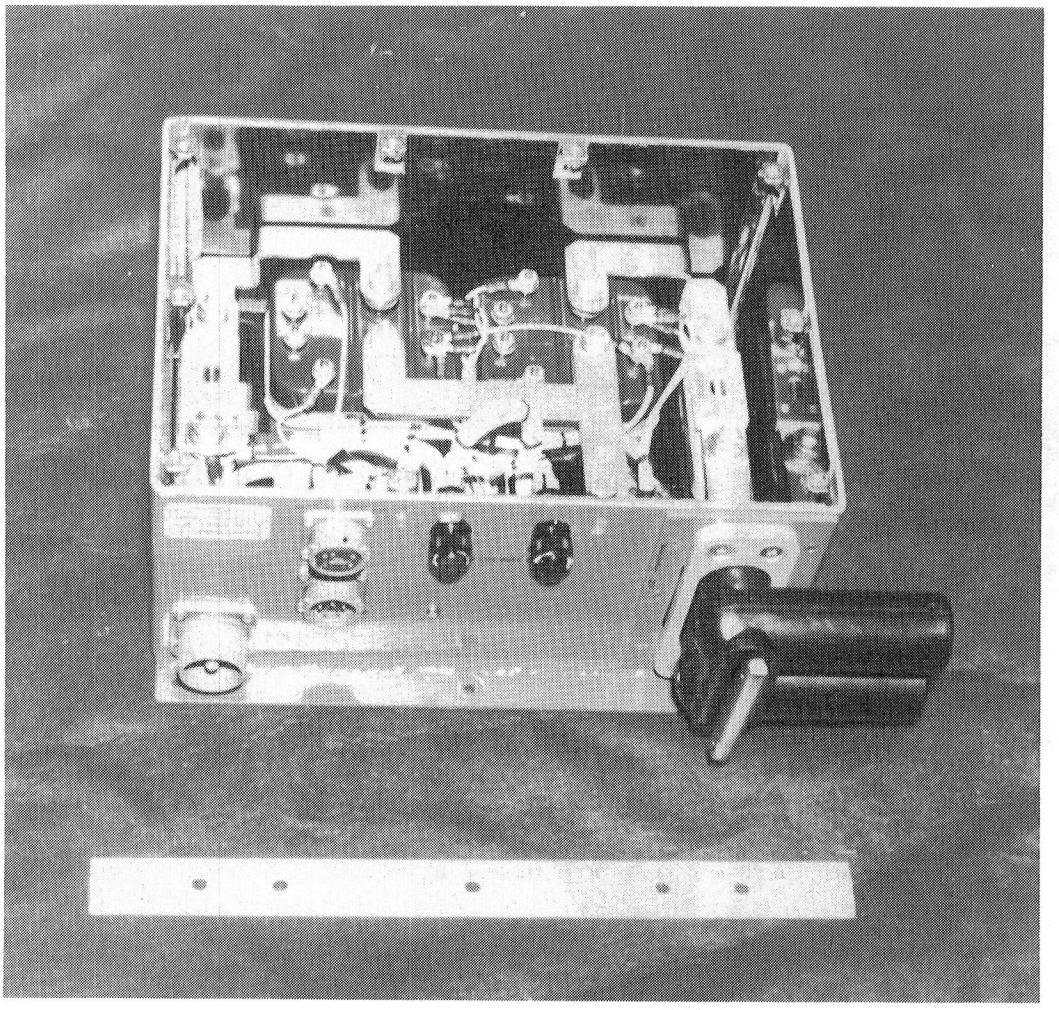


FIGURE 21

CHECKOUT SUBSYSTEM

An excellent checkout subsystem was developed to quickly assess the health of the data systems real-time. The checkout subsystem functions as a real-time monitor with quick-look capability. A checkout console/data system was used to control the data systems.

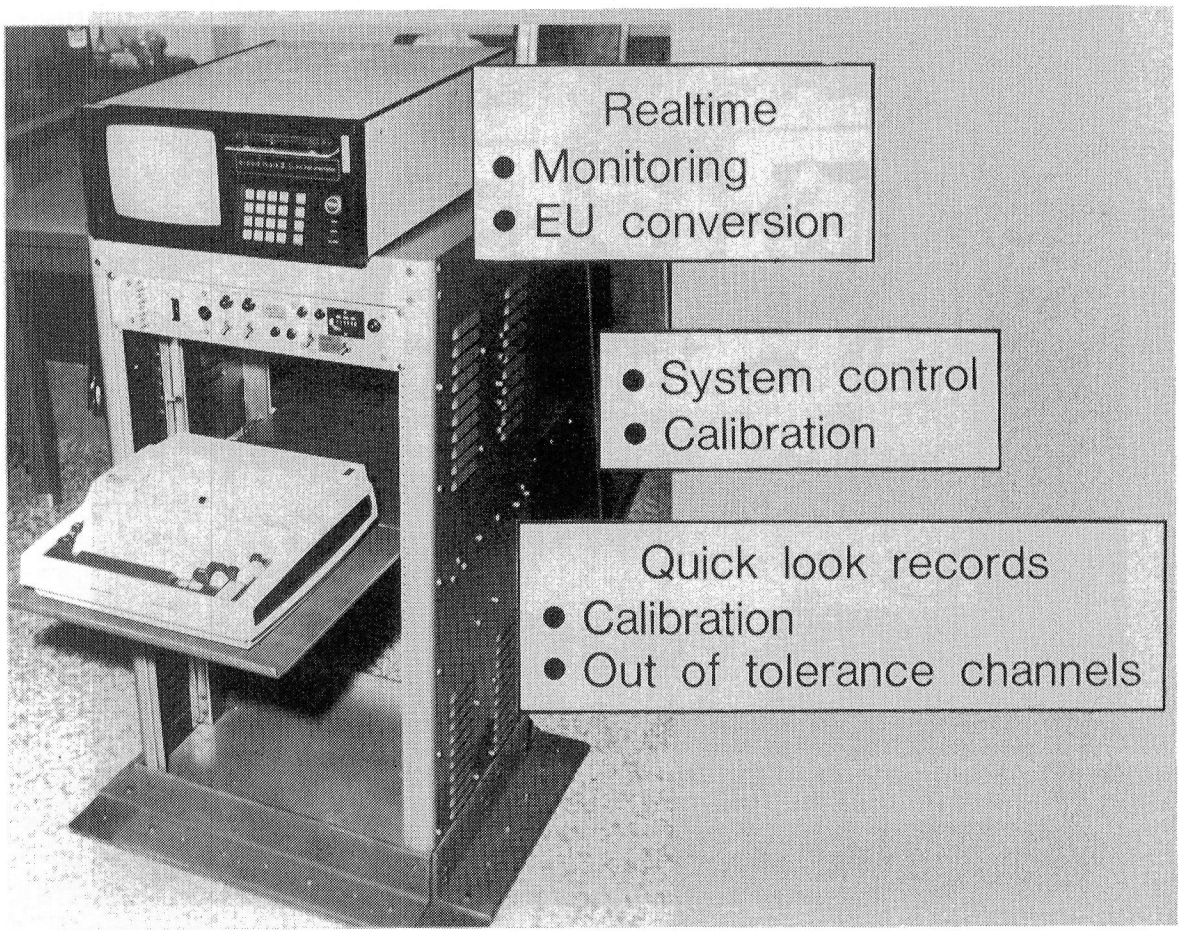


FIGURE 22

INITIAL DOWNLINK TELEMETRY SYSTEM

The initial telemetry configuration used a frequency diversity technique. This technique featured real-time selection of the best telemetry signal from the two transmitted signals per data system for on-the-ground recording.

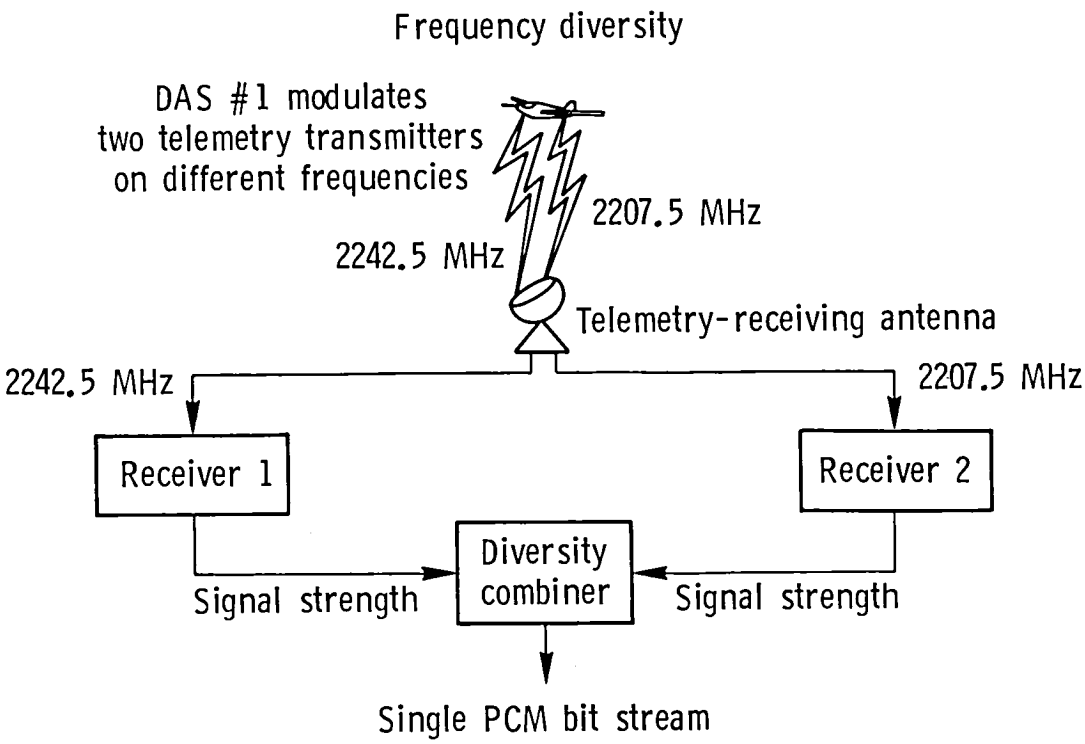


FIGURE 23

TELEMETRY PROBLEMS

The frequency diversity technique increased redundancy, but there were other problems. The most serious was the telemetry dropouts above the CID site. Another telemetry problem was the erroneous turn-on of the on-board recorders and photo instrumentation. The second problem was solved by installing diodes across the relay coils as required on other systems located in the aircraft. In addition a 1 second delay circuit was added to the uplink electronics system to eliminate erroneous turn-on by short duration spurious signals.

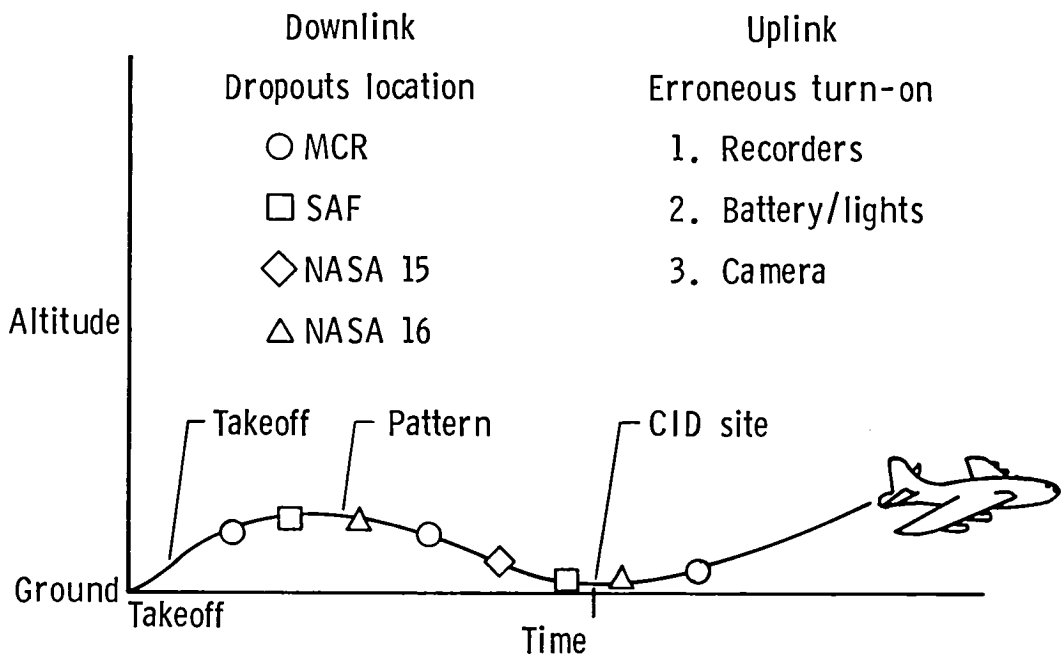


FIGURE 24

TELEMETRY REQUIREMENTS

The final telemetry configuration used a polarization diversity system. To maintain the desired redundancy two remote vans were utilized. One transmitter per data system was selected and these signals were received using the polarization technique at the ground station. The other transmitter per data system was selected and these signals were recorded by NASA 15 and NASA 16, the two mobile vans, respectively. The vans were stationed on opposite sides of the CID runway to optimize data acquisition. Two independent subsystems were activated simultaneously at 150 feet to turn on the on-board recorders and photo instrumentation. The primary activation subsystem was the uplink electronics and the secondary activation subsystem was the terminate electronics.

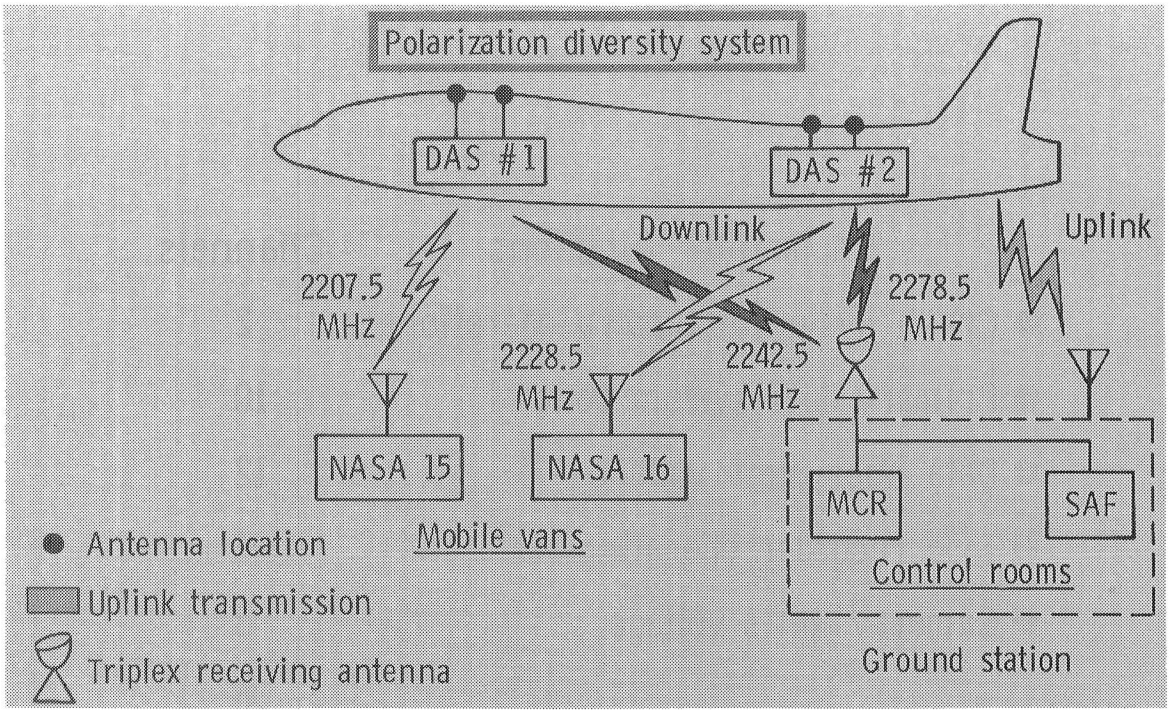


FIGURE 25

DOWNLINK REQUIREMENTS

There were 36 channels dedicated to monitoring the health of the data systems real-time in the ground station. These channels monitored subsystem voltages and currents.

TM monitor functions	Channels
● Crash system telemetry operational	2
● Primary data system power	10
● Data subsystem voltage	12
● Tape recorder operating	4
● Camera/lights voltage	8
	36

FIGURE 26

CONTROL ROOMS

There was capability to monitor data system #2 in the Spectrum Analysis Facility and data system #1 in the Main Control Room. The selected subsystem parameters and data channels were monitored real-time to establish mission readiness. There was a communication net available for communications between the control rooms and the remote vans.

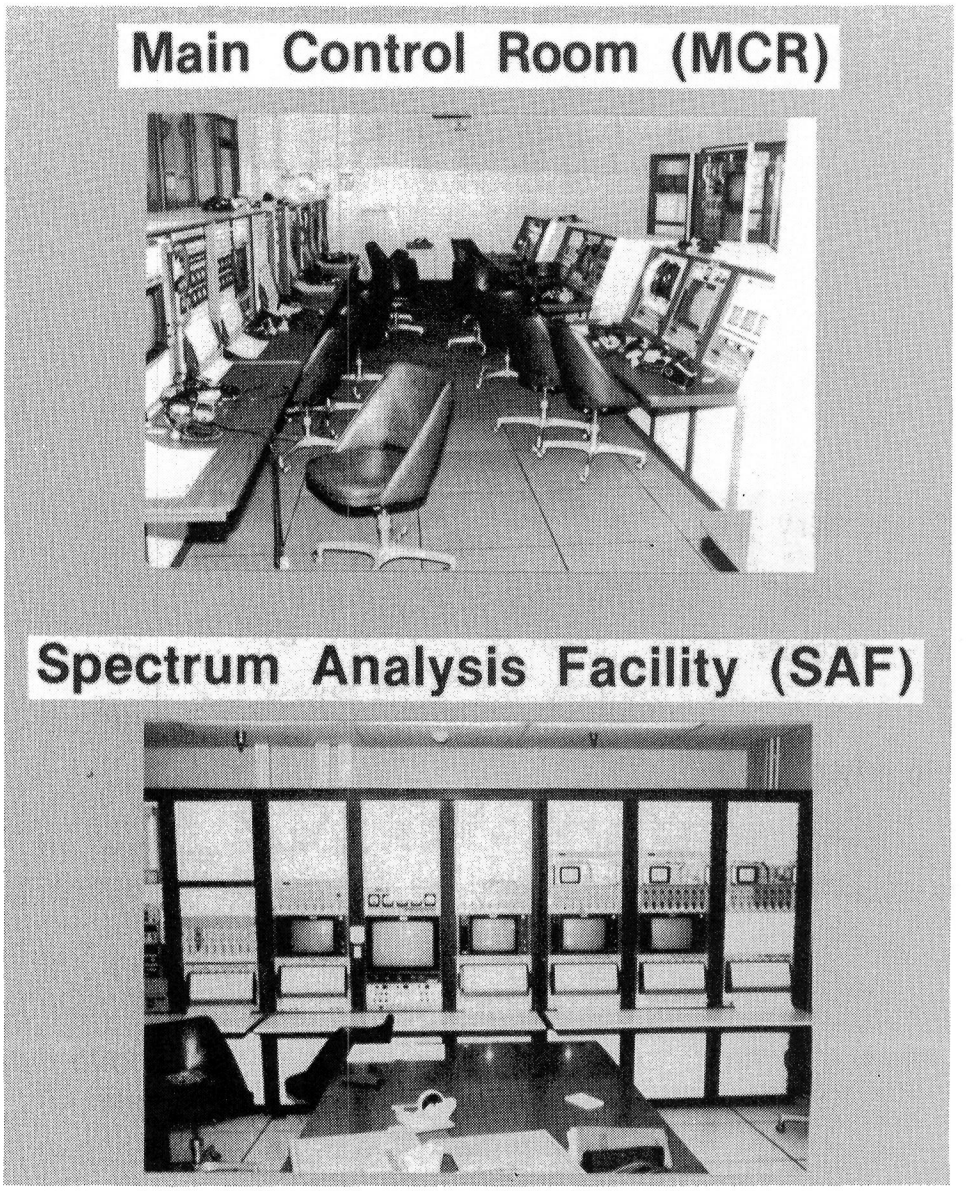


FIGURE 27

DATA SYSTEM INSTALLATION

The flight instrumentation system consisted of two autonomous data systems, DAS #1 and DAS #2, and an excellent checkout subsystem. DAS #1 was installed in the front of airplane. DAS #2 and the checkout subsystem were installed in the aft section of the airplane.

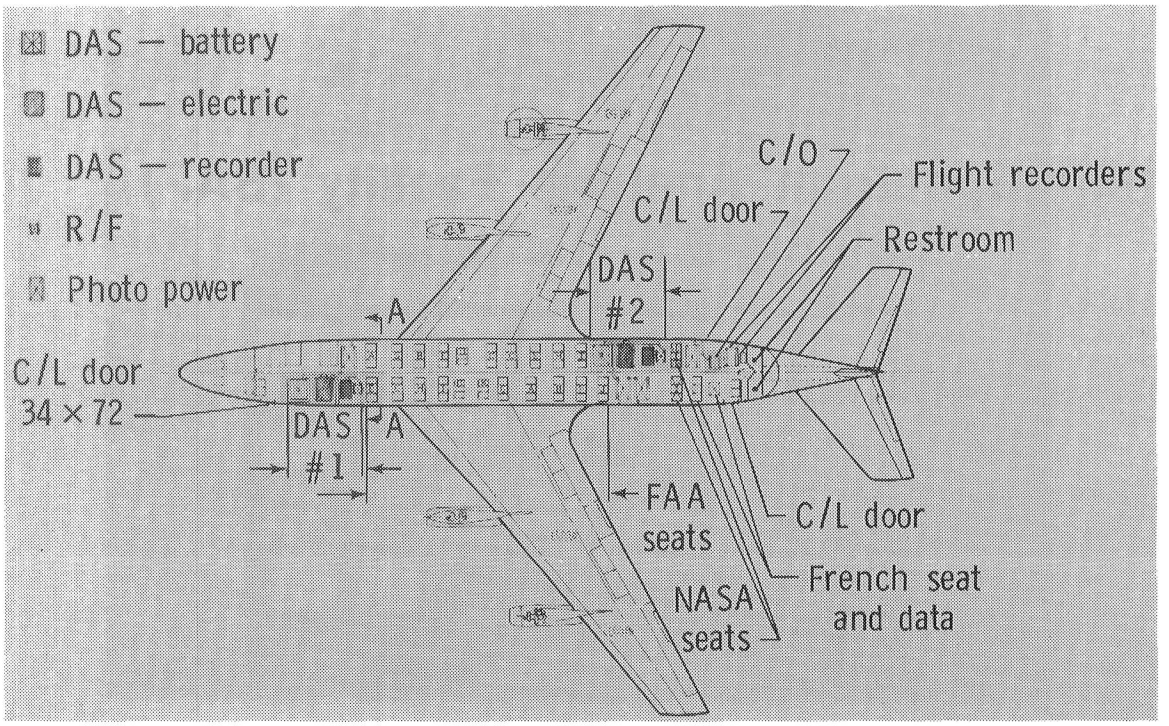


FIGURE 28

SENSOR INSTALLATIONS

Sensors were installed under the floors, in the wings, on the dummies, in the ceiling and at many other locations in the fuselage.

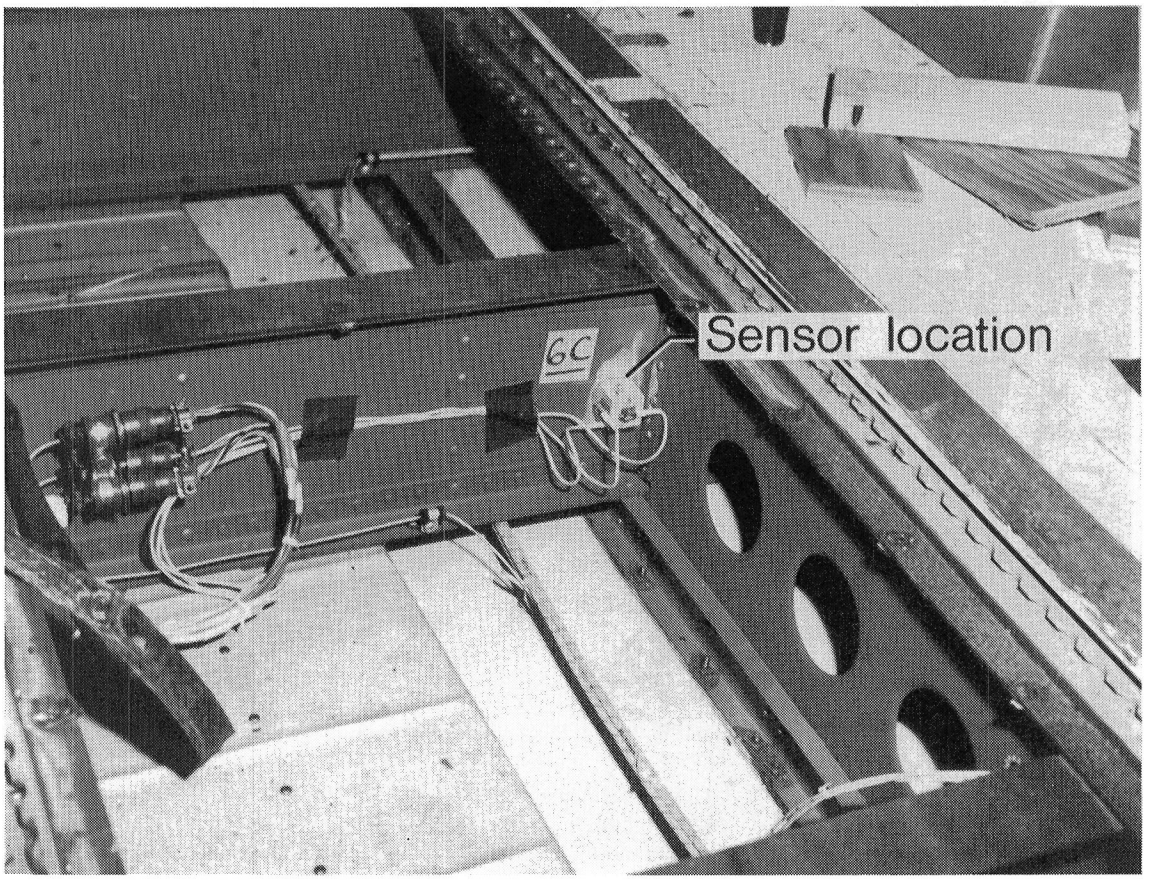


FIGURE 29

DAS #2 INSTALLATION

Each data system was partitioned into four pallets. The four pallets of DAS #2 and two of the four photo pallets are shown. There were over 800 crimp connectors installed. Solder connectors were installed on all inter-pallet cables. Special protective covers were installed to protect inter-pallet connecting cables. Thermal protective covers were developed for all the pallets.

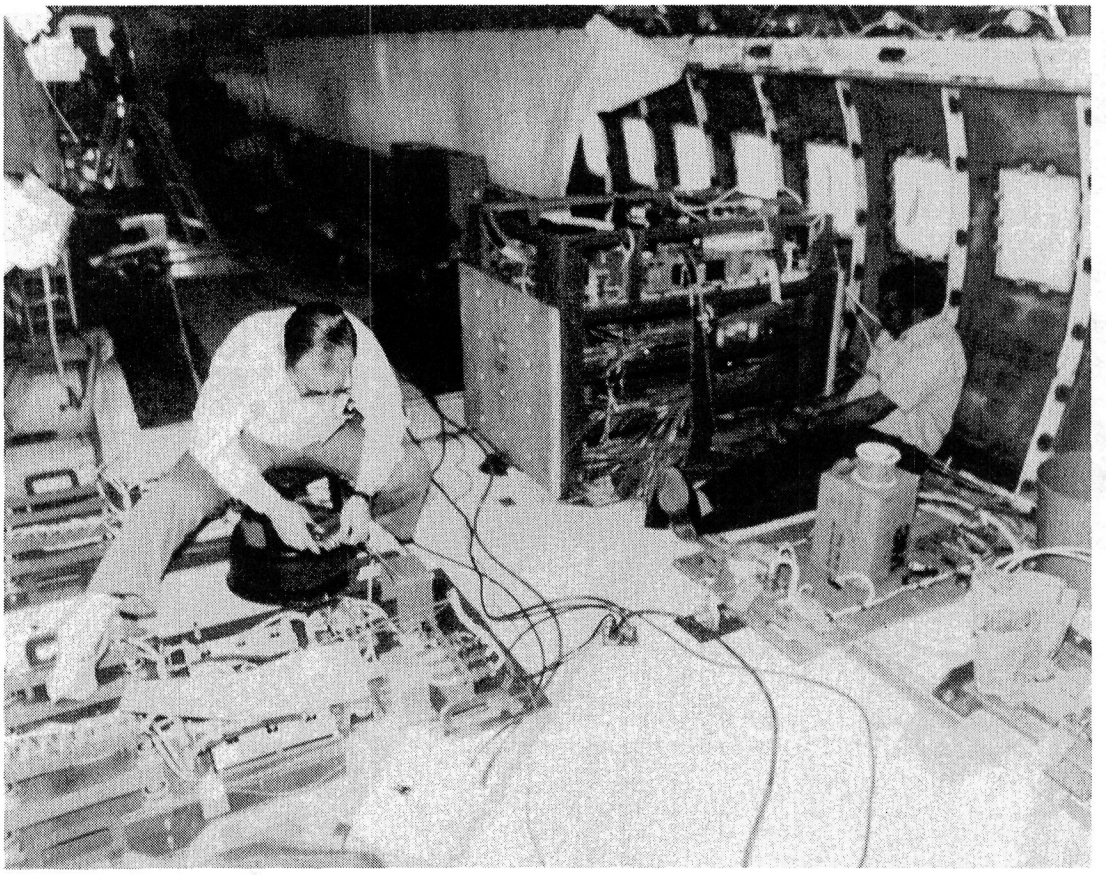


FIGURE 30

DAS #1 INSTALLATION

This photograph shows DAS #1 installation in the front section of the aircraft.

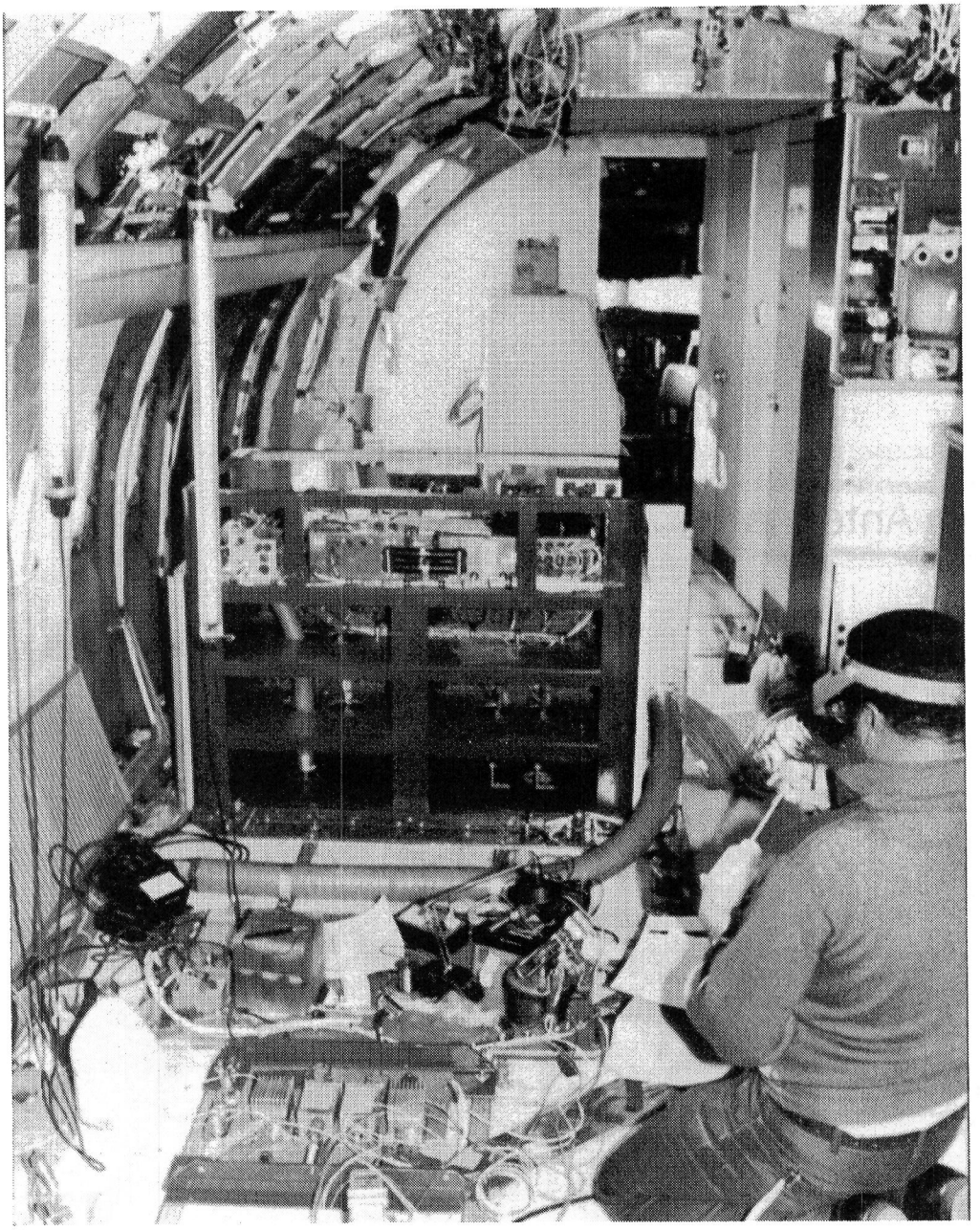


FIGURE 31

ELECTRONIC SUBSYSTEM CRASH SURVIVAL

The system's four antennas were installed in the ceiling. The telemetry signals were lost during the fire. Prior to fire, the ground recorders in the control rooms and the recorders in the remote vans successfully recorded the data during the impact sequence.

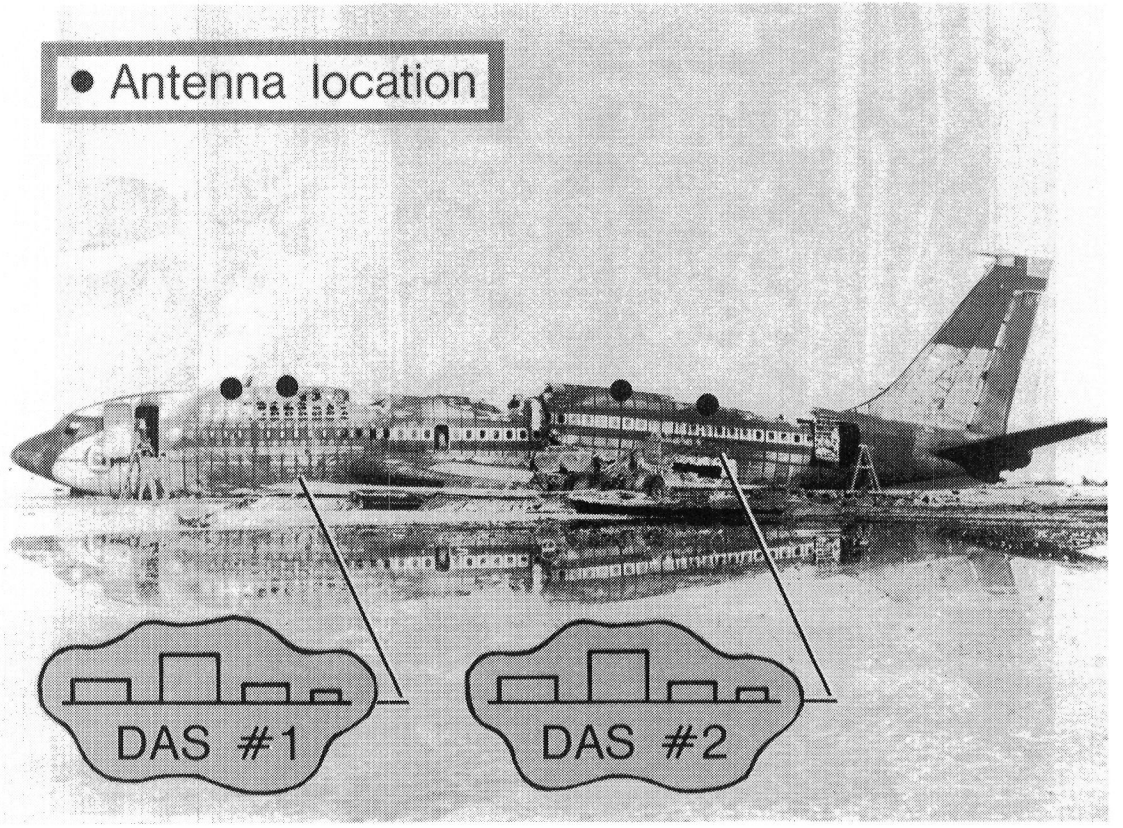


FIGURE 32

DAS #1 AFTER

All pallets were protected with thermal covers. The battery pallet is shown at the bottom of this figure. The batteries were removed from the aircraft. There was contamination on the pallet surfaces. The battery cases were externally blemished and there was a little discoloration inside the battery covers. The other pallets partially dropped below the floor level.

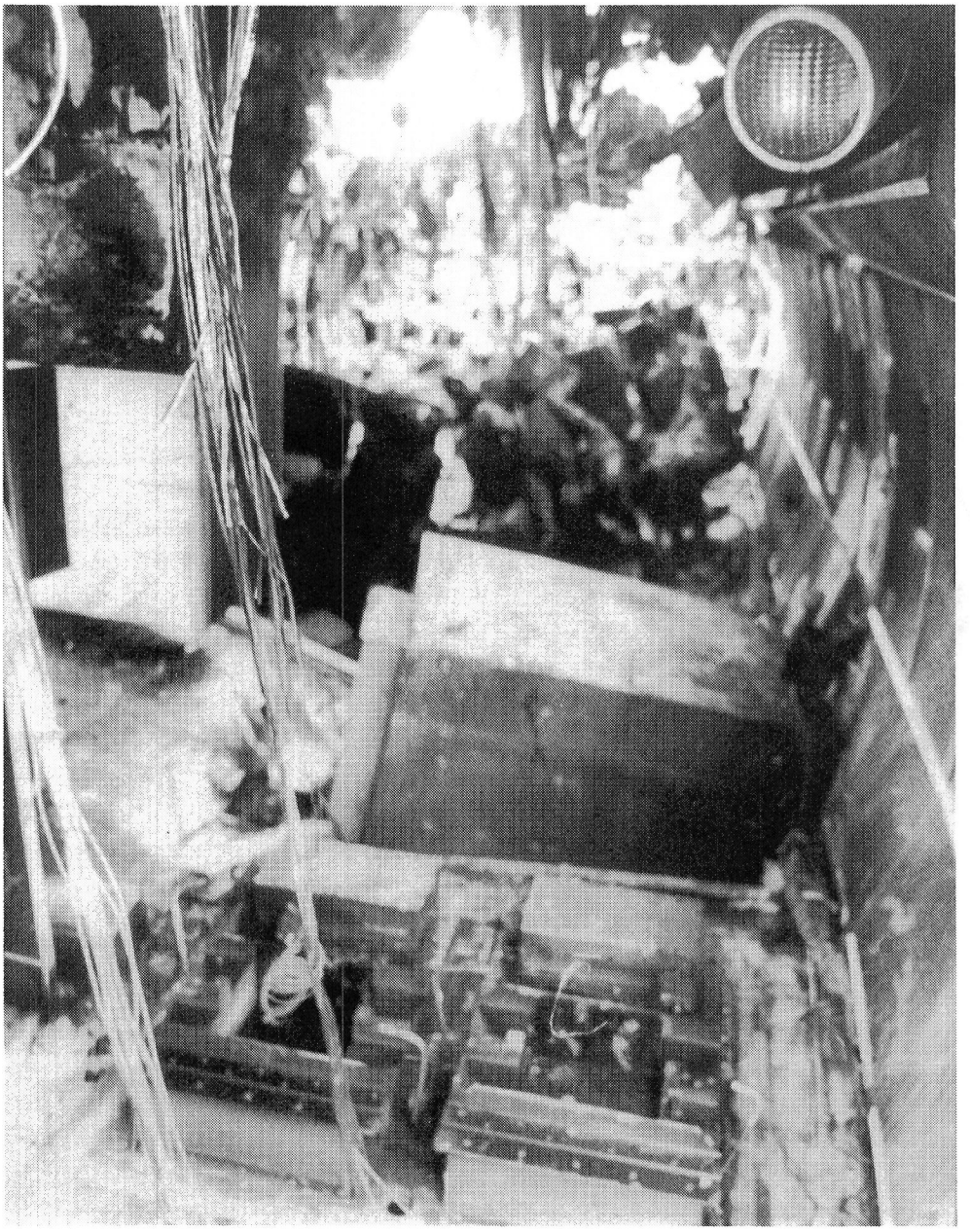


FIGURE 33

DAS MAIN PALLET

This figure shows a typical DAS main pallet before the fire.

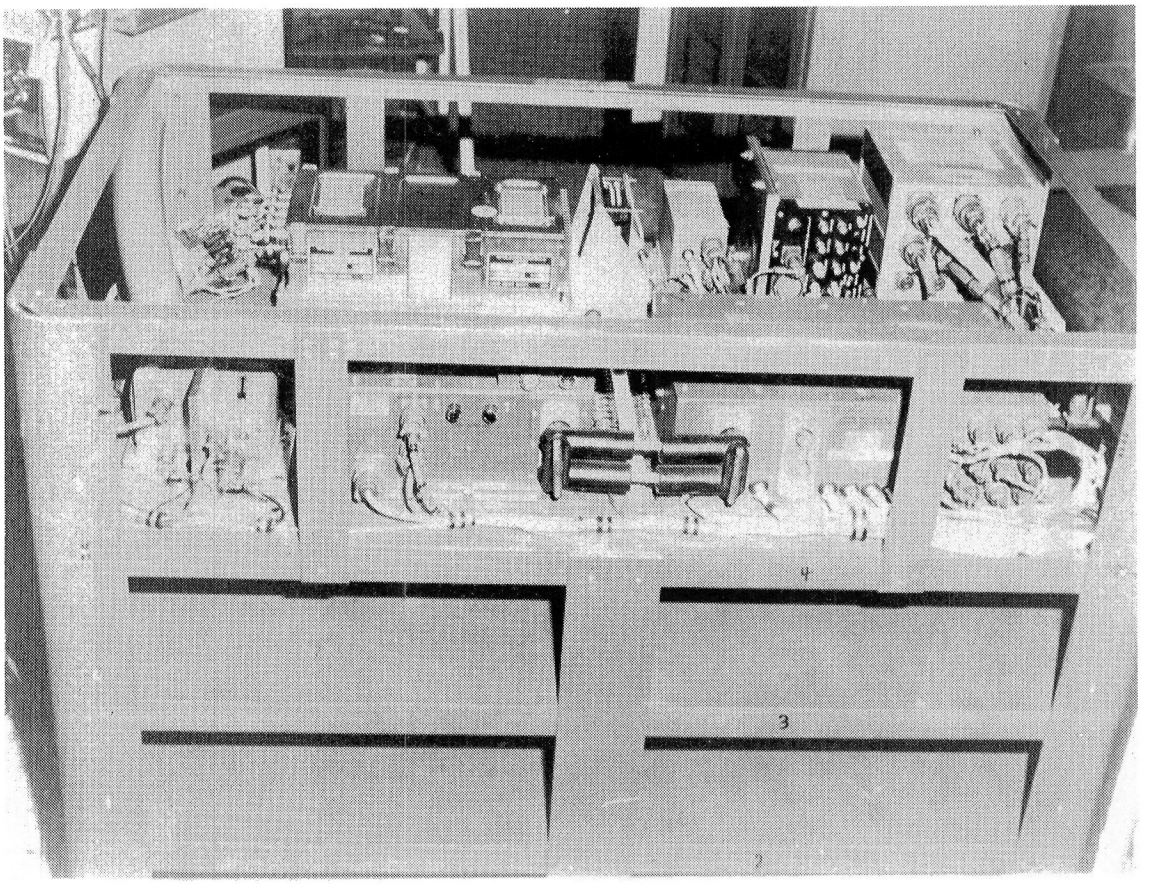


FIGURE 34

MAIN PALLET DAS #1

This figure shows DAS #1 at Langley after the fire. There was chemical residue contamination throughout the pallets' external surfaces. The residue entered all pallets via the airconditioning ducts. Further inspection revealed no signs of internal damage of any to the subsystems.

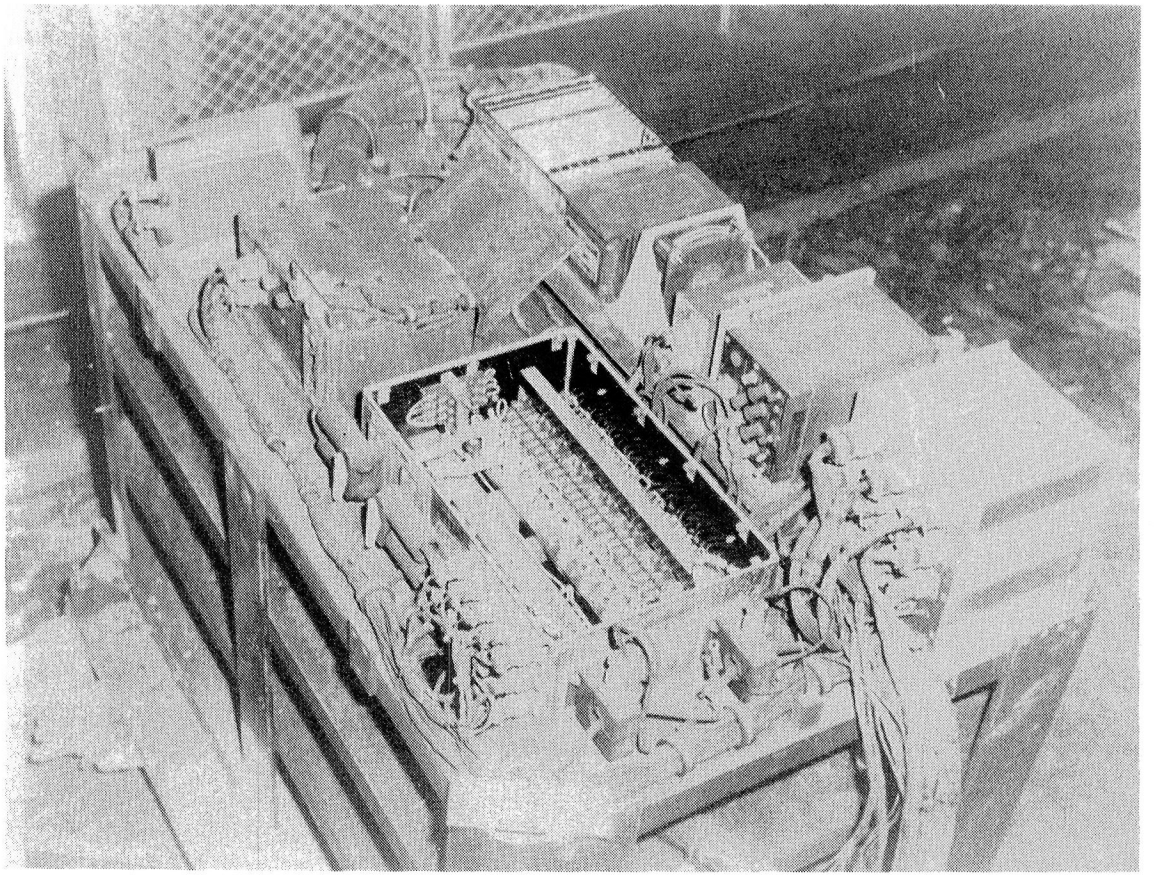


FIGURE 35

BATTERY PALLET

This figure shows a typical DAS battery pallet before the fire.

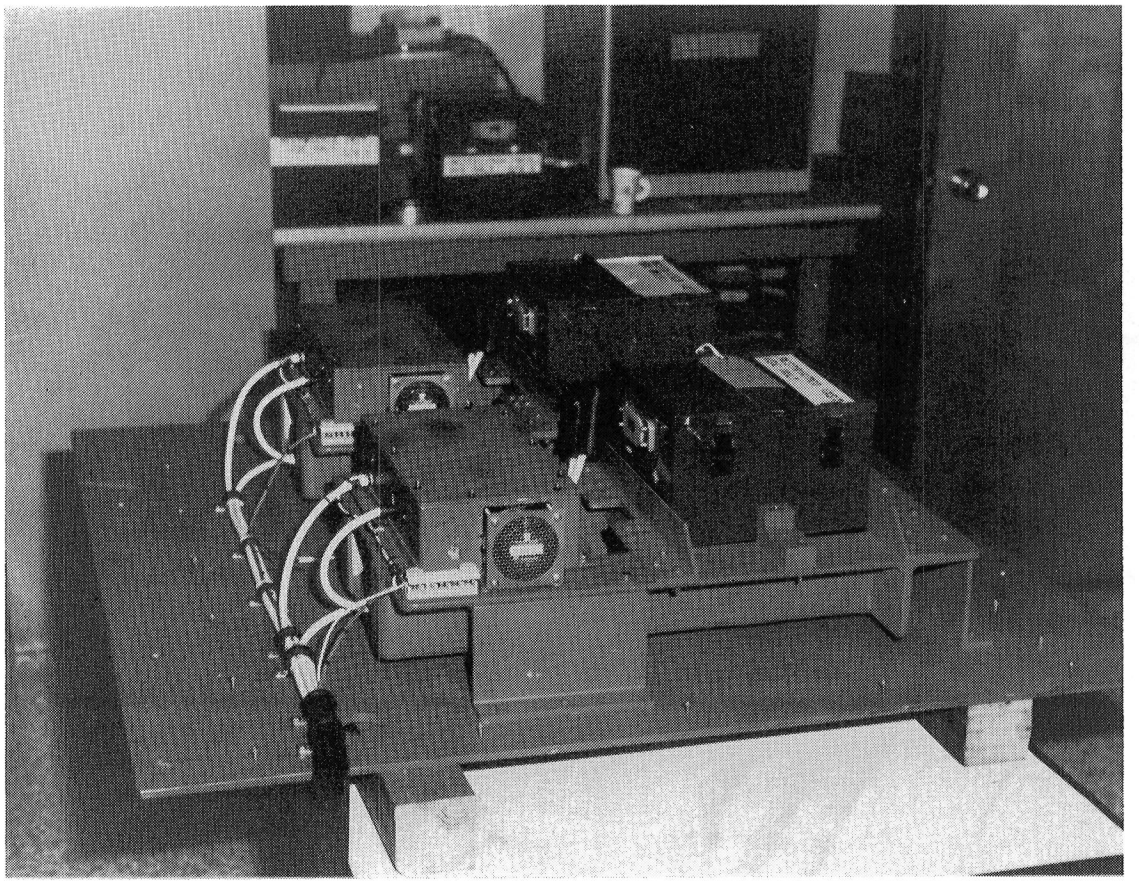


FIGURE 36

BATTERY PALLET (DAS #1)

This figure shows DAS #1's battery pallet after the fire.

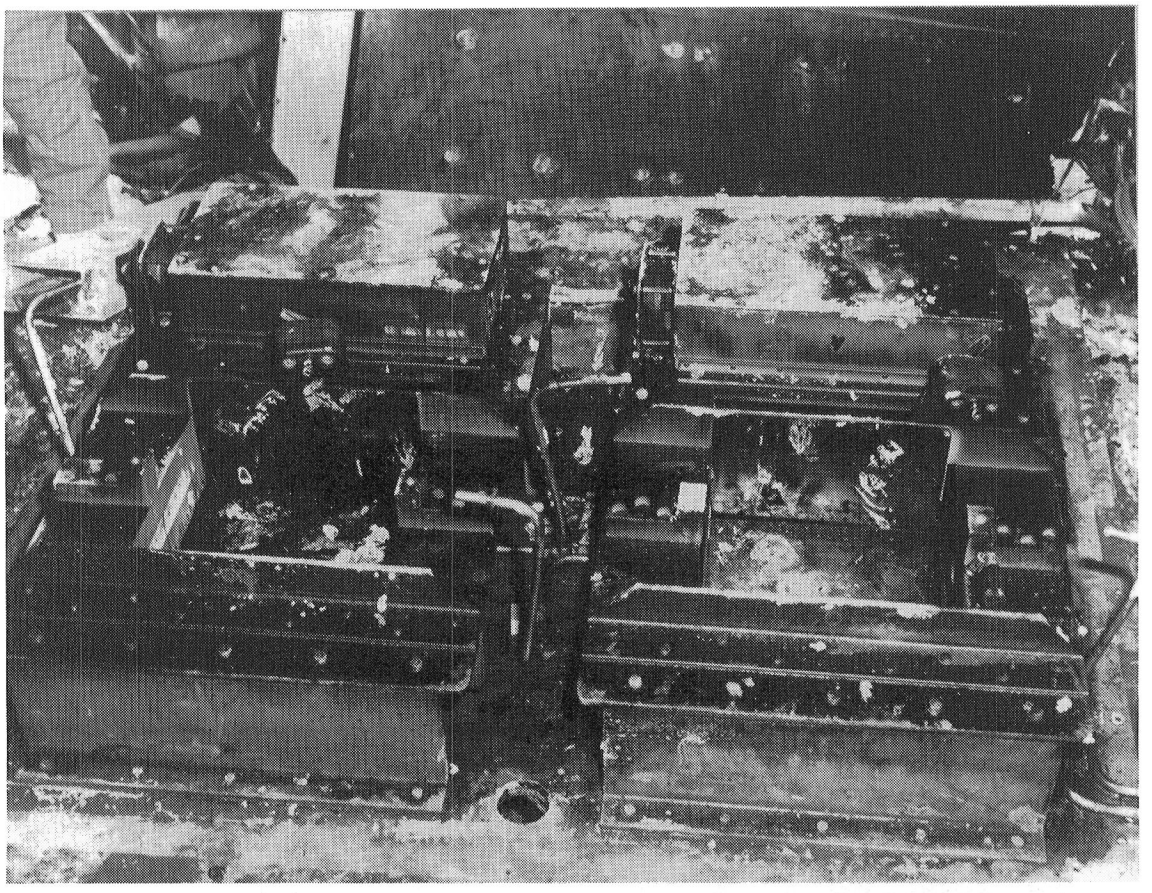


Figure 37

TRANSMITTER PALLET

This figure shows DAS #2's transmitter pallet before the fire.

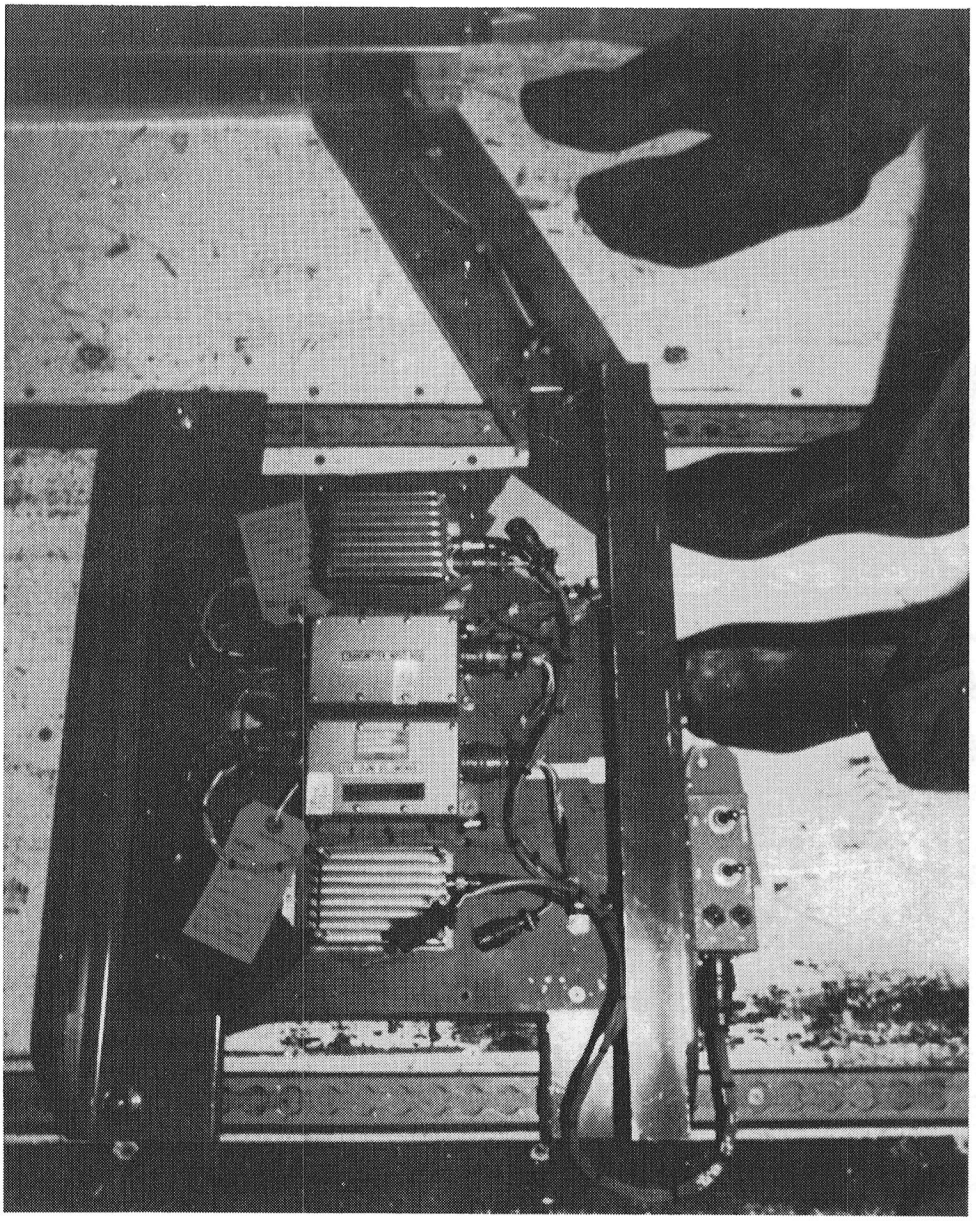


FIGURE 38

TRANSMITTER SUBSYSTEM (AFTER)

This figure shows DAS #2 transmitter pallet after the fire.

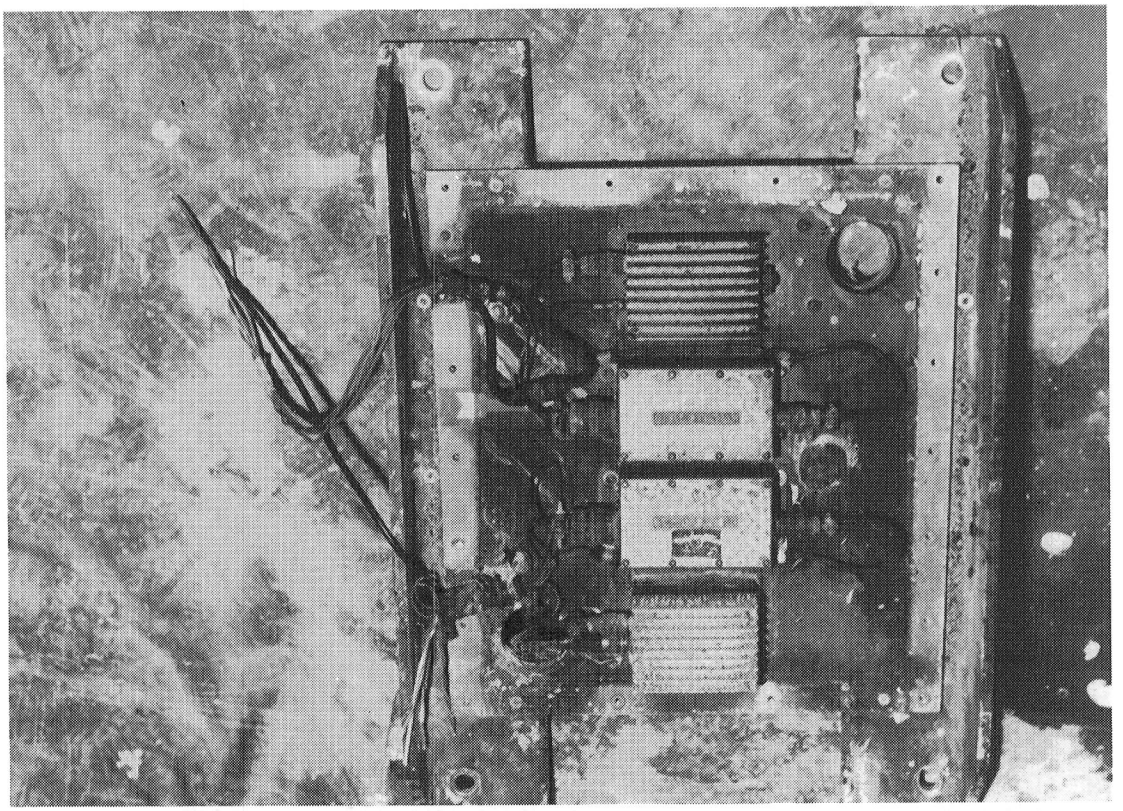


FIGURE 39

RECORDER SUBSYSTEM

This figure shows a typical recorder pallet after the fire and typical recorder before the fire.

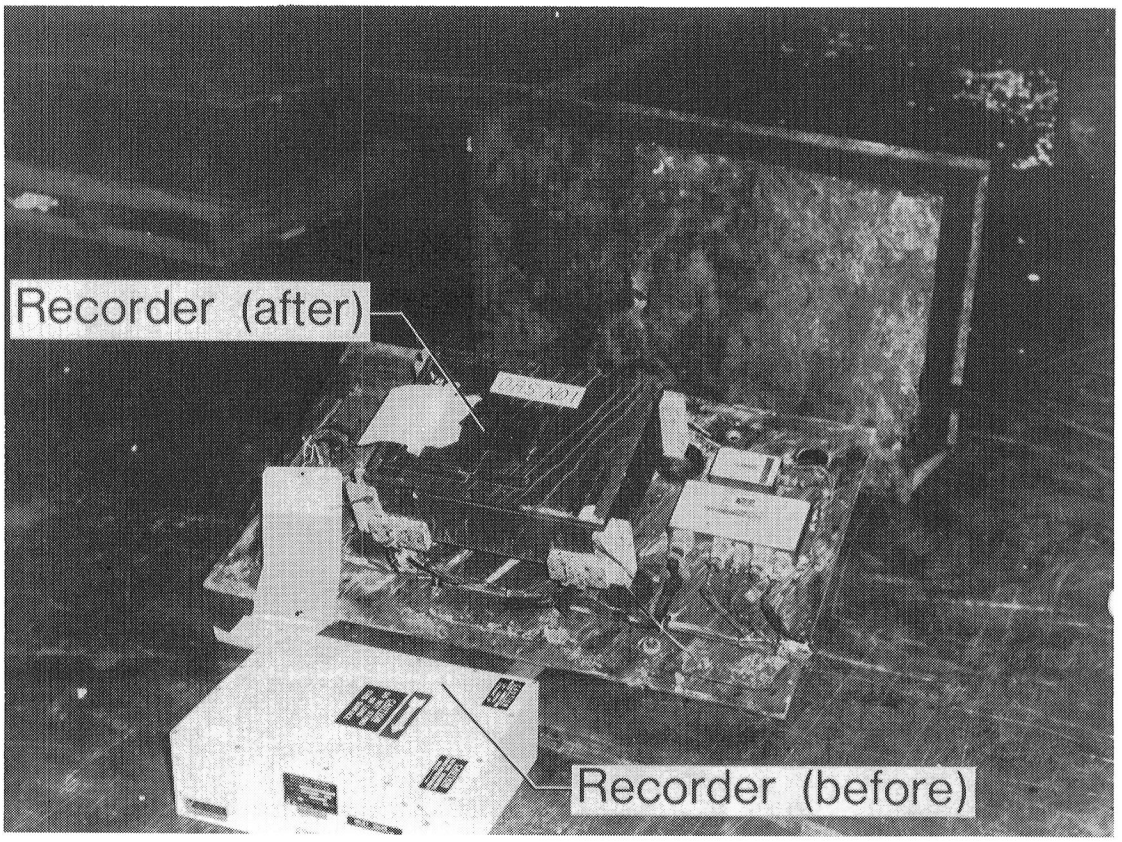


FIGURE 40

RECORDER SUBSYSTEM AND DATA TAPE (AFTER)

Both recorder pallets were externally contaminated by the chemical residues. Both recorders were started with 9 minutes of tape remaining per reel and faithfully recorded crash data until the end of tape! There were no signs of damage to either recorder internally.

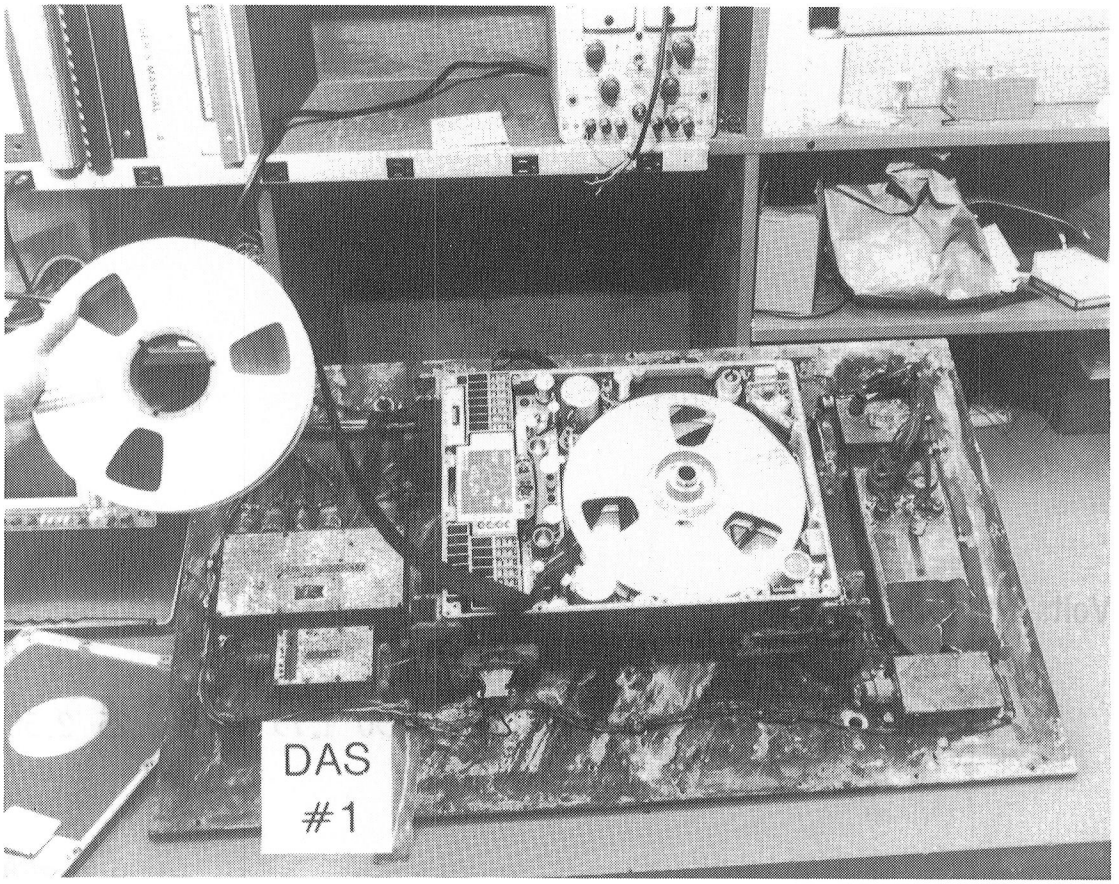


FIGURE 41

BUS VOLTAGE

The selected DAS parameters were monitored before the controlled impact and the reduced data is currently being analyzed. The battery bus voltages operated within specifications during the reduced data period. There was only one anomaly noted. Approximately two seconds after the left wing impact, there were two 40 msec spikes on the +5 volt secondary bus in signal conditioner #4. The minimum voltage during these spikes was 2.12 volts. Since this voltage was only used on the calibration card, no discernible interference on the data channels was detected.

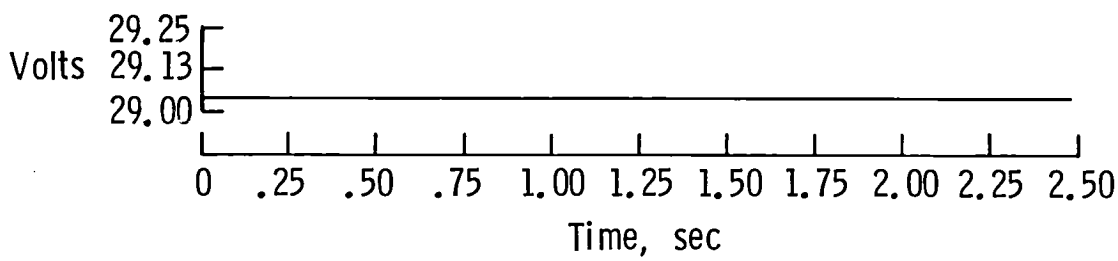


FIGURE 42

CAMERA PALLET #3 VOLTAGE (DAS #1)

There were four channels per data system dedicated to monitoring the photo pallets batteries. A typical signal is shown.

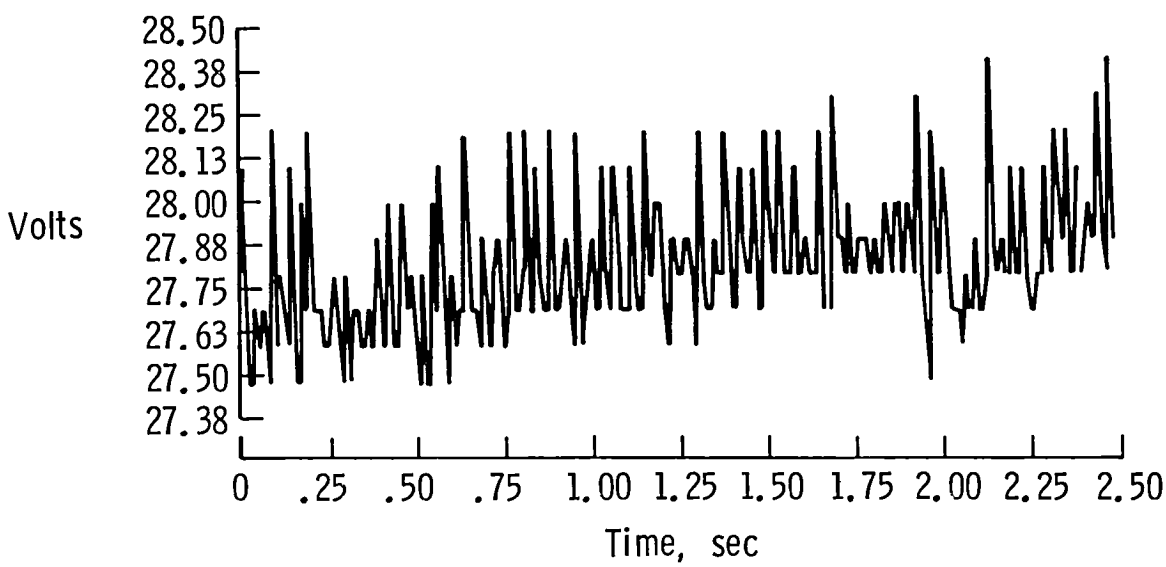


FIGURE 43

PROGRAM SCOPE

The following resources were required to develop and ship two large data systems in 18 months.

- 1.6 million dollars up front money
- Accelerated procurement priorities
- Accelerated delivery
- A dedicated work force to handle the enormous parallel efforts required
- High program priority at Langley, Dryden, and FAA

- Funding ~ 1.6 million
- Accelerated procurement and delivery
- Parallel effort and manpower commitment
- High program priority at Langley/Dryden and FAA
- Develop instrumentation within 18 months

FIGURE 44

CONCLUDING REMARKS

The highly successful data acquisition is attributed to a design approach featuring:

- HIGH RELIABILITY CONCEPTS
  - Multi-Level Redundancy
  - Fault Tolerant Design Techniques
  - Aggressive Quality Assurance Program
- HIGH ENVIRONMENT CONCEPTS
  - Shock and Vibration Isolation Techniques
  - High "G" Components
  - Thermal Protective Covers
- HIGHLY DEDICATED TEAM OF PROFESSIONALS

In addition to successfully acquiring 343 out of 352 data channels, the electronic subsystems survived the post-crash fire and are operational.

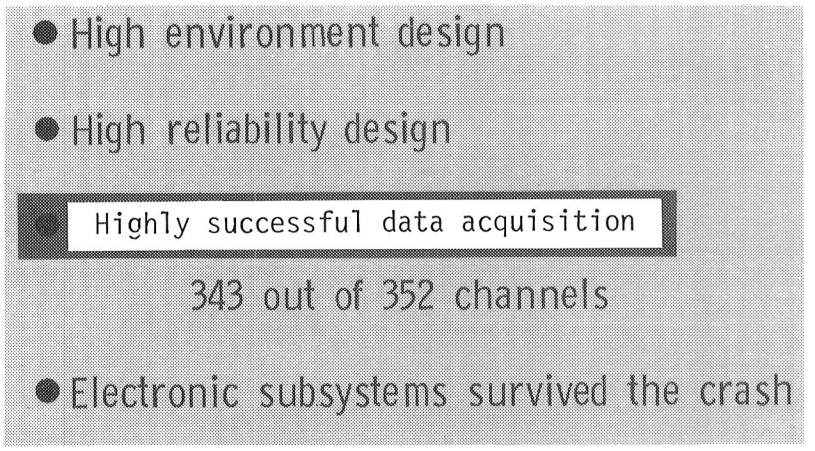


FIGURE 45

IMPACT DYNAMICS INSTRUMENTATION

Royce F. McCormick
NASA Langley Research Center
Hampton, Virginia 23665

NASA/FAA Government/Industry CID Workshop
NASA Langley Research Center
April 10, 1985

CID INSTRUMENTATION

One of the tasks specified in the NASA Langley Controlled Impact Demonstration (CID) work package was to furnish dynamic instrumentation sensors. The types of instrumentation sensors required (figure 1) were accelerometers for aircraft structural loads measurements, seat belt load cells to measure anthropomorphic dummy responses to the aircraft impact, and strain gage bending bridges to measure the aircraft fuselage and wing bending during impact.

1. Accelerometers

2. Seat belt load cells

3. Strain gage bending bridges

Figure 1

OBJECTIVES

The objective in the selection of dynamic instrumentation for the CID was to provide 352 of the highest quality transducers and remain within budget allocation. The transducers that were selected for the CID evaluation process (figure 2) were each subjected to rigorous laboratory acceptance tests and to aircraft fuselage section drop tests at the LaRC Impact Dynamics Research Facility. Data compiled from this series of tests showed the selected transducers to be best suited for the CID mission requirement.

Provide 352 data transducers for CID

1. Select transducers for evaluation

2. Evaluate selected transducers

3. Procure selected transducer on the basis of reliability-availability and costs

Figure 2

CID ACCELEROMETER

The accelerometer found to be best suited in the CID instrumentation application was the Endevco Model 7264200. A synopsis of the transducer specifications is listed in figure 3.

Range:	±200"G"
Overrange:	to ±500"G"
Sensitivity (typ):	2.0 to 2.5 mV/G
Damping ratio:	0.001 (% of critical)
Excitation:	10.00 V DC
Electrical configuration:	1/2 Wheatstone Bridge (2 active arm)

Figure 3

CID SEAT BELT LOAD CELL

Lap belt load cells used to measure lap belt forces produced at impact by the anthropomorphic dummies were from the LeBow Corporation Model 3419. Pertinent specifications are listed in figure 4.

Range:	3500 lb
Overrange:	8,000 lb
Sensitivity (nom):	±2 mV/Volt
Excitation:	10 V DC
Electrical configuration:	350 Ohm Wheatstone Bridge
Belt thickness (max):	0.1 in.
Belt width (max):	2.0 in.

Figure 4

CID STRAIN GAGES

The strain gage type selected to instrument the aircraft fuselage and wings was the Micro-Measurements Corporation type CEA-13-250-UW-350. Environmental and design characteristics of this gage make it particularly attractive for test applications on aluminum structures. Gage specifications are listed in figure 5.

Gage resistance:	350 Ohms
Gage factor:	2.11 $\pm$0.5%
K_t:	+0.1%
Temp compensation:	Self compensating
Strain limits:	30 to 50 K micro-strain (tension or compressison)
Tested on:	2024-T4 aluminum

Figure 5

CID ACCELEROMETER CONSTRUCTION

The diagram of the 7264 accelerometer (figure 6) shows the two solid-state silicone resistors that form the active elements of the transducer. The cantilevering action of the beam causes the silicone elements to vary in resistance, thereby unbalancing the bridge to produce an electrical output.

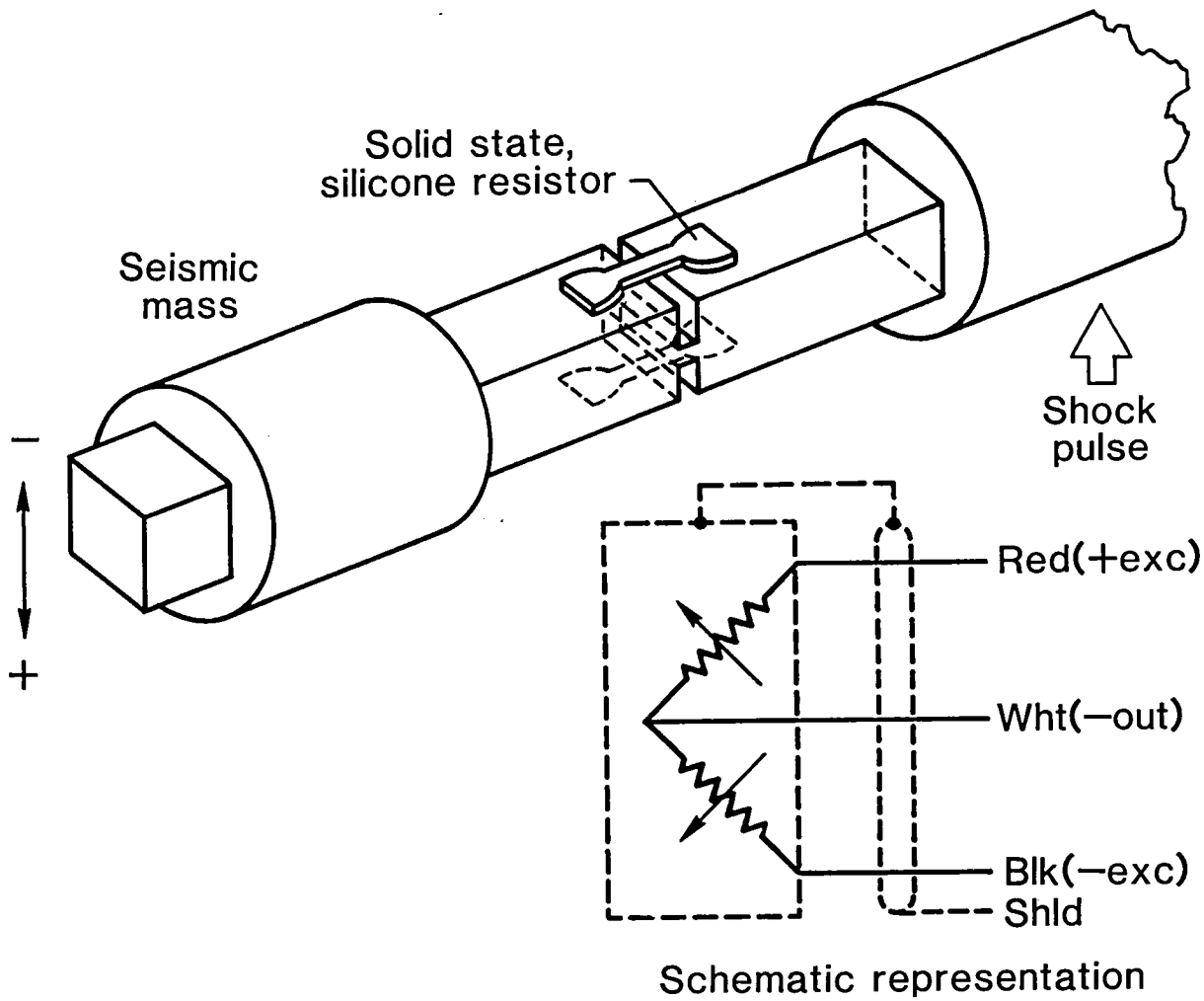


Figure 6

CID TRANSDUCER WIRING

The accelerometer plug wiring shown in figure 7 was typical of all transducers aboard the CID. All transducers being resistive bridge element type were wired in identical fashion to facilitate transducer interchange and simplify data records. Note that the accelerometer bridge completion resistors were installed in the sensor plug such that the entire bridge would be subjected to the same environmental variations.

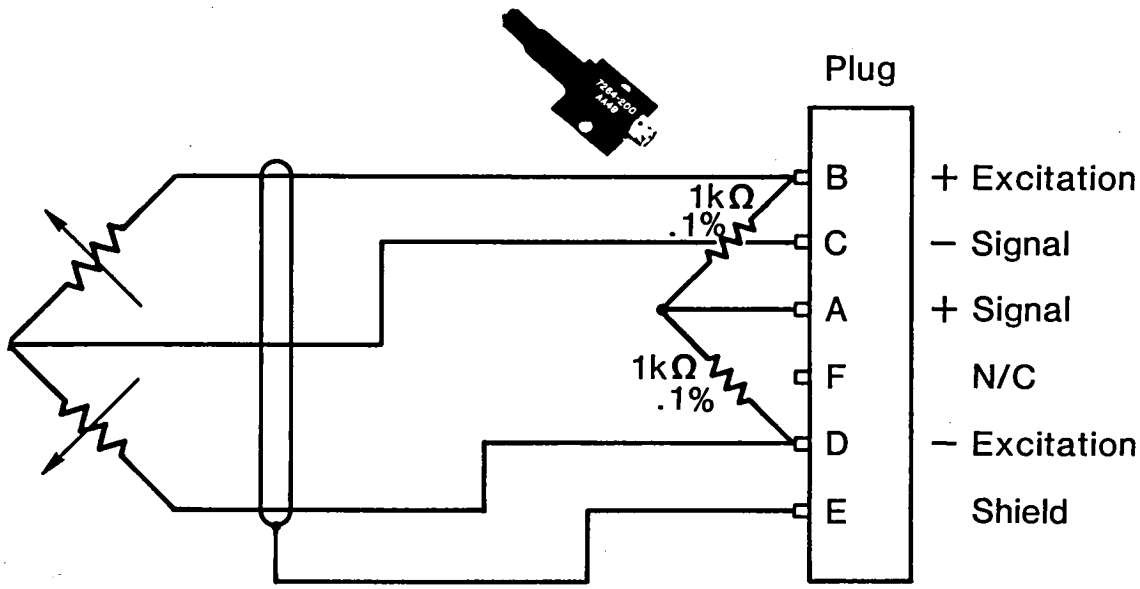


Figure 7

CID ACCELEROMETER MOUNTING

To achieve sameness with respect to specified transducer locations on the CID airframe, a one-inch cube aluminum block (figure 8) was used. This allowed all transducers in bi-axial or tri-axial clusters to measure the impact shock pulses at exactly the same airframe location thereby simplifying the task of data reduction. Scotchweld 2216 epoxy was used to affix the accelerometers and/or blocks to the airframe.

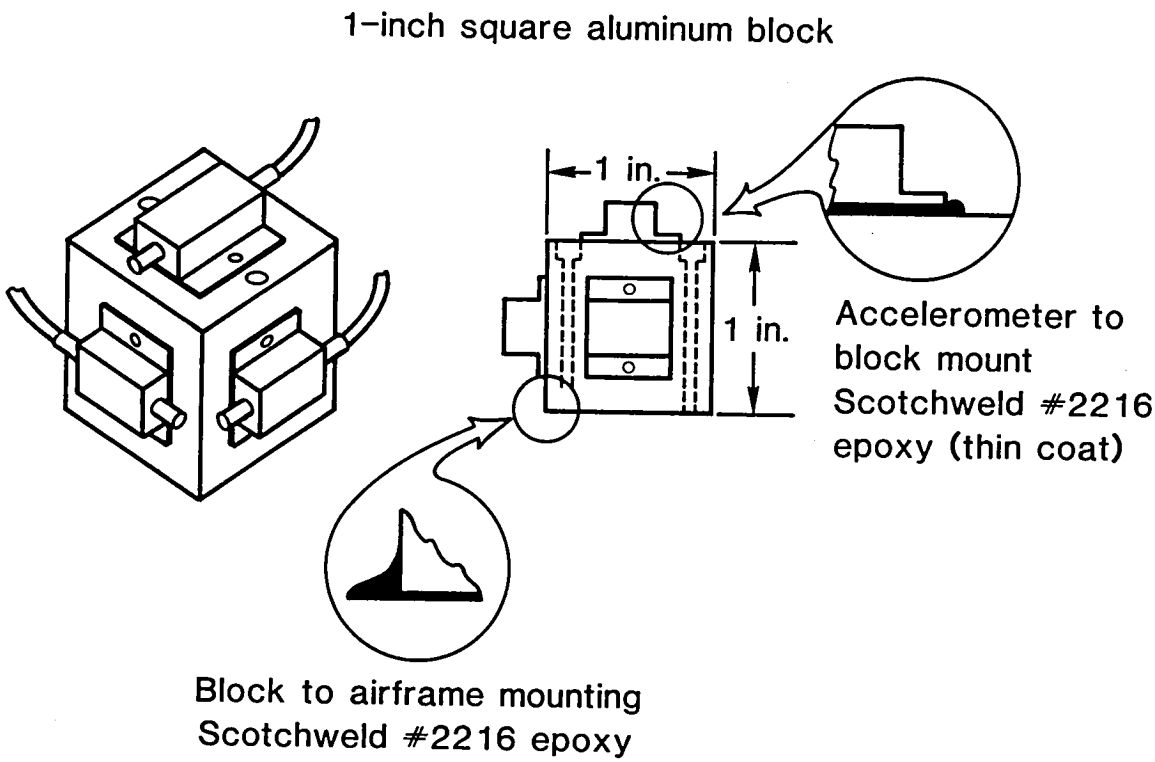


Figure 8

CID FUSELAGE CROSS SECTION
-ACCELEROMETERS-

The illustration in figure 9 depicts a typical CID aircraft fuselage ring section fully instrumented with accelerometers. Accelerometers mounted across the floor beam were used to measure the impact shock pulse input to the passenger seats.

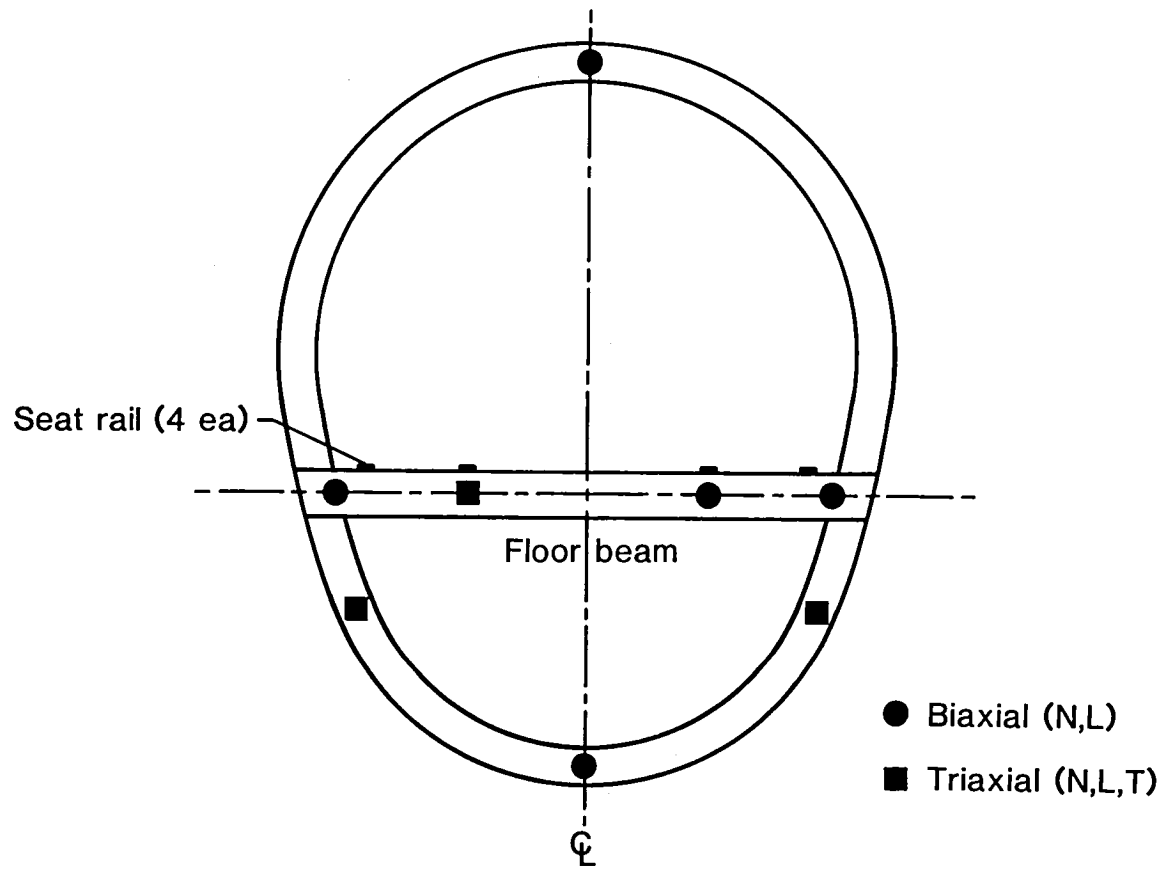


Figure 9

CID BENDING BRIDGES

The strain gage bridge representation of figure 10 describes the tension/compression configuration of the CID fuselage and wing bending bridges. This bridge gage arrangement increases the total milli-volts/volt output of the bridge by a factor of four over a single active gage bridge. Note that the connector plug wiring is compatible to that of the accelerometers wiring.

Gage type CEA-13-250-UW-350
Bending bridges - 4 active arm

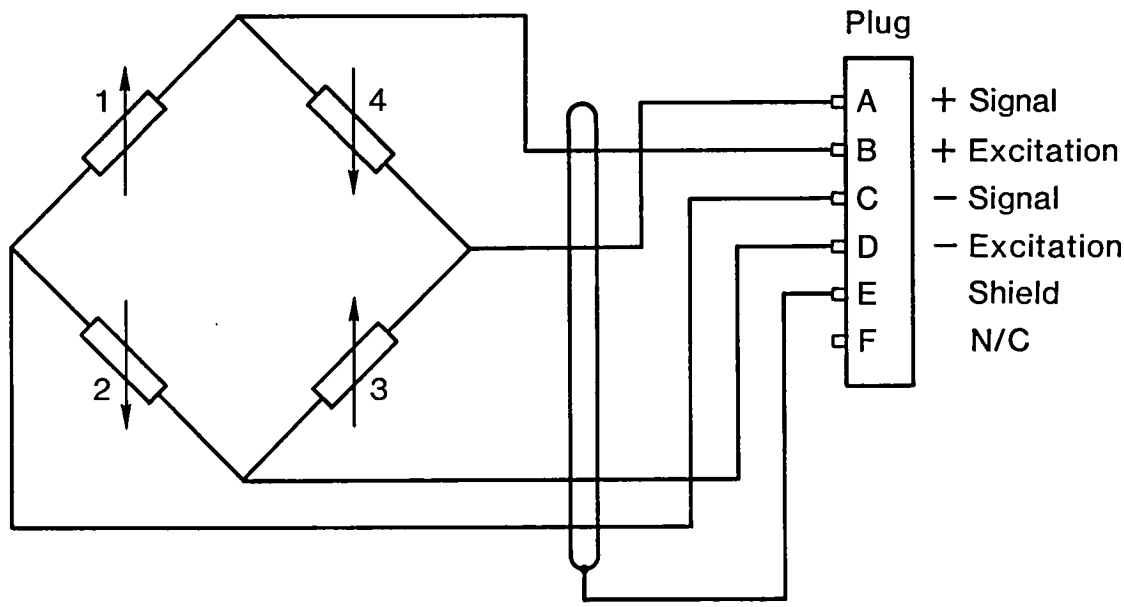


Figure 10

CID FUSELAGE CROSS SECTION
-BENDING BRIDGES-

The illustration in figure 11 depicts a typical aircraft fuselage ring section fully instrumented with strain gages. Each bending bridge location was instrumented with a primary and backup (spare) bridge. The strain gages were bonded to the structure with 610 adhesive and a weather coating applied to environmentally protect each gage.

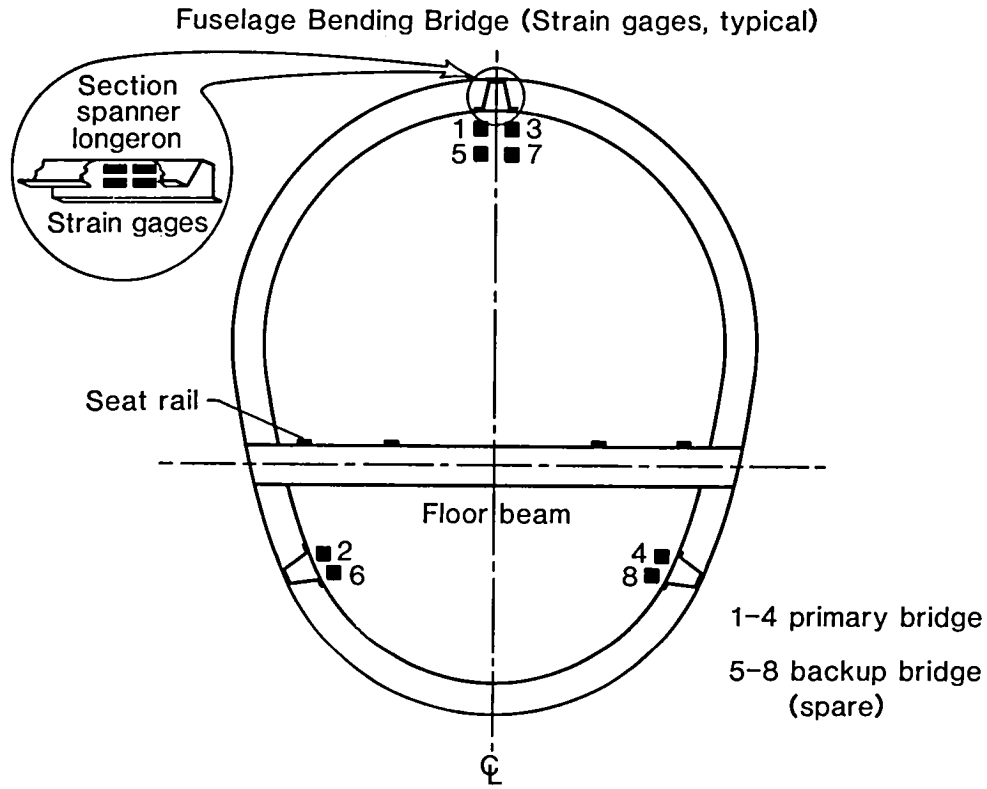


Figure 11

SUMMARY

1) The transducers installation technique on the airframe proved successful.
2) The transducer quality assurance was guaranteed through rigorous acceptance testing.
3) Data acquired was 97.0%.

CID-720 AIRCRAFT

LaRC PREFLIGHT HARDWARE TESTS:

DEVELOPMENT, FLIGHT ACCEPTANCE AND QUALIFICATION

J. D. Pride
NASA Langley Research Center
Hampton, Virginia

NASA/FAA Government/Industry CID Workshop
NASA Langley Research Center
April 10, 1985

INTRODUCTION

This paper addresses the testing conducted on LaRC-developed hardware for the CID-720 aircraft. It is divided into four major sections that first focus on the major test articles and the test environment. Other sections discuss the flight acceptance tests (FAT) and qualification tests, the fuselage vertical drop tests, and the heat shield development tests that were all performed in the LaRC test facilities.

LaRC - preflight hardware tests:
Development, flight acceptance and qualification

- Section A
  - Major test articles
  - Test environments
- Section B
  - Major test units, FAT/qualification tests
- Section C
  - Fuselage vertical drop tests
- Section D
  - Heat shield development

MAJOR TESTING TASK

To properly develop flight qualified crash systems, two environments were considered:- the aircraft flight environment with the focus on vibration and temperature effects, and the crash environment with the long pulse shock effects. Also with the large quantity of fuel in the wing tanks the possibility of fire was considered to be a threat to data retrieval and thus fire tests were included in the development test process.

Develop flight qualified crashworthy systems

Consider

- Flight environment
  - Vibration
  - Temperature
- Crash environment
  - High shock
  - Possible fire

MAJOR TEST ARTICLES

The test articles included the primary pallet subsystems of the Data Acquisition System (DAS #1 located forward in the aircraft and DAS #2 in the rear). Each DAS system included four separate subsystems as follows: main electronic pallet, recorder pallet, battery/diode pallet and R/F pallet. The photographic test units included the 4 power distribution pallets, 10 camera mounts with thermal box assemblies and 24 flood light assemblies.

The other numerous small flight units were rigorously tested at the component level and are not considered as major test articles for discussion in this paper.

- Data acquisition system #1 (located Fw'd. in A/C)
  - Main electronic pallet
  - Recorder pallet
  - Battery/diode pallet
  - R/F pallet
- Data acquisition system #2 (located rear in A/C)
  - Main electronic pallet
  - Recorder pallet
  - Battery/diode pallet
  - R/F pallet
- Photographic system
  - Power distribution pallets (4)
  - Flood light assemblies (24)
  - Camera mount/box assembly (10)

FLIGHT ENVIRONMENT

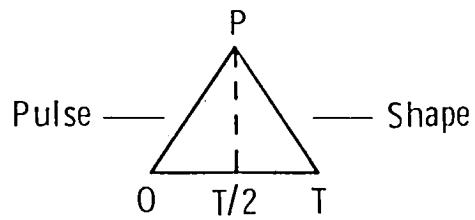
The temperature testing was divided into two phases; the operational and non-operational. The testing criteria for the operational flight phase was obtained from the "RTCA/CO-160A" document. The flight and qualification levels were combined in this case and the temperature test range was from +40°F to 120°F with a 4.0°F/minute temperature rate of change. For the nonoperational condition the temperature level was set at 160°F for a period of 30 minutes. This temperature was selected based on previous experience with inside fuselage temperatures on aircraft located on the hot lake bed at the NASA-DFRF Facility during the summer period.

The test pulse simulating the crash environment had a triangular shape with a 100 msec duration. The flight assurance test levels are 17G for the longitudinal and normal axis, while the qualification levels are 25G peak. The above levels represent a long duration pulse profile expected from the crash of typical aircraft fuselage structures at vertical descent rates of aproximately 20 ft./sec.

Temperature	Operational	Nonoperational
Combined qualification and flight	40°F to 120°F	160°F, 30 min
	$\nabla T = 4.0°F/min$	

Crash environment

Shock

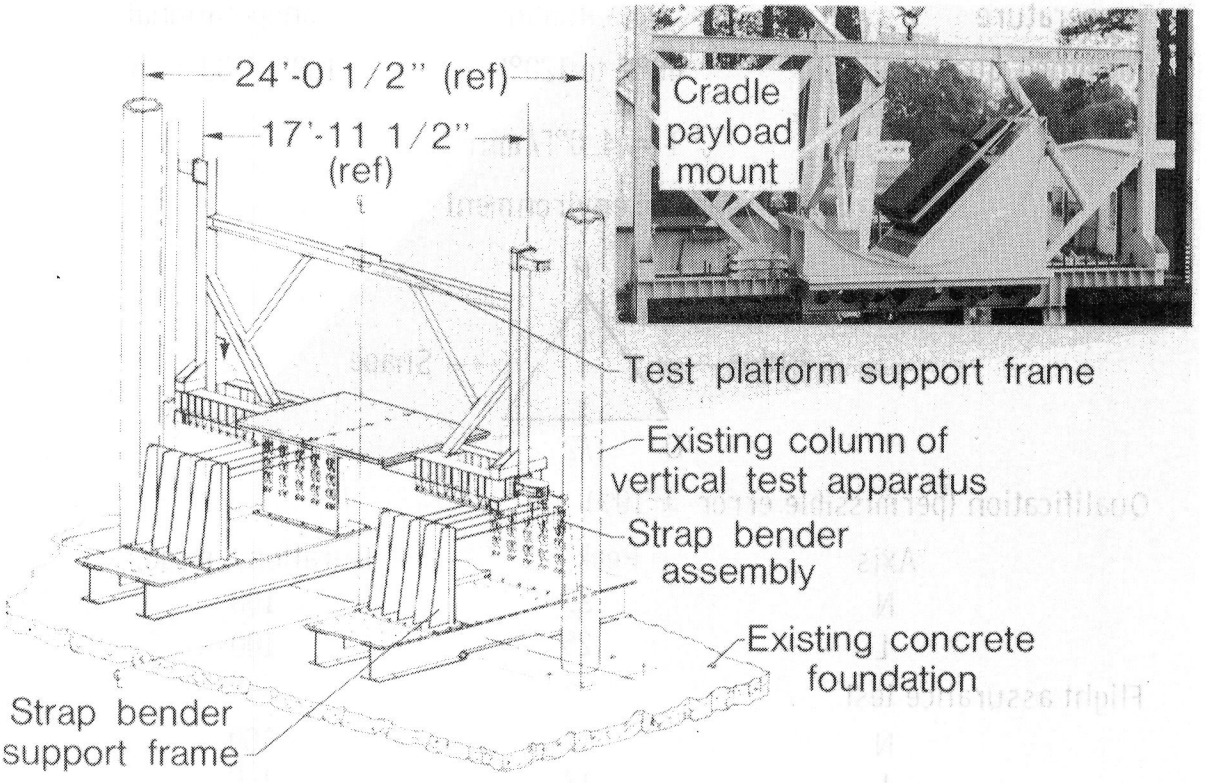


Qualification (permissible error ± 10%)

Axis	Peak, G	Duration, msec.
N	25	100
L	25	100
Flight assurance test		
N	17	100
L	17	100

PULSE GENERATOR SYSTEM FOR VERTICAL DROP TOWER

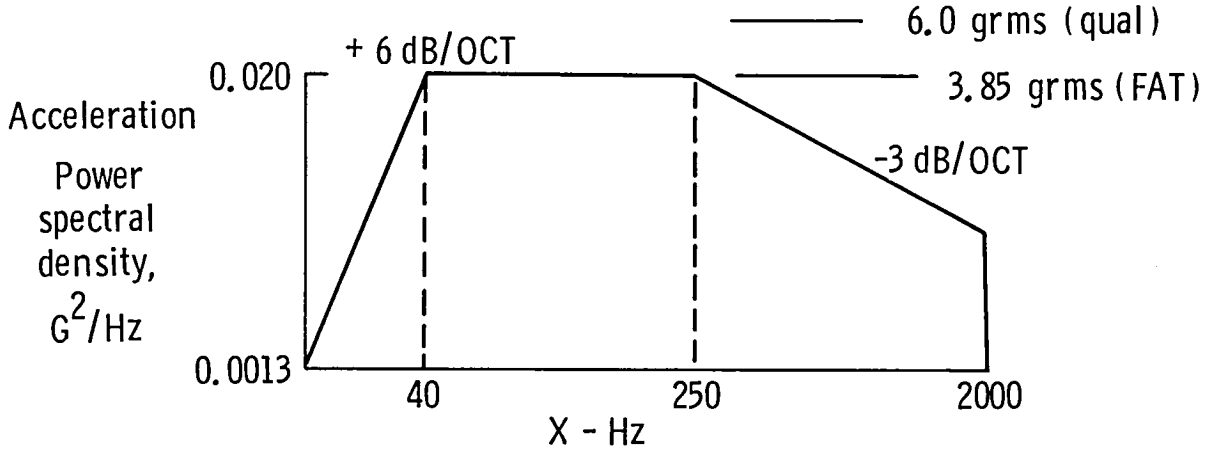
A special shock pulse generator system was installed in the LaRC 72 ft. high vertical drop tower facility. This system was designed for long duration shock pulse profiles and was ideally suited for shock qualification of the test articles. The key to this unique facility was the strap bender assembly. The technique was to extrude a wide (about 3 inches) stainless steel strap through offset rollers, thus absorbing considerable energy. A drop carriage guided on rollers impacted the selected number of straps from a calibrated drop height and total weight to give the desired pulse shape. The picture in the upper corner shows a rotatable cradle that was the interface mounting plane with the test article pallets. The cradle was positioned at 45 degrees to obtain the same shock magnitude for the normal and longitudinal axes. The payloads (test articles) in the picture depict the power distribution pallet and the 16 mm high speed camera surrounded with protective heat shield. These units were powered-up and operated successfully through the impact shock pulse.



FLIGHT ENVIRONMENT FOR AIRBORNE EQUIPMENT

The testing criteria for turbojet aircraft fuselage mounted equipment were obtained from reference 1. The vibration profile of power spectral density (G^2/Hz) versus frequency (CPS) is plotted for flight assurance (FAT) and qualification tests. The maximum level for FAT is 3.85 grms (between 40 and 250 cycles) and for qualification is 6.00 grms. The period of vibration for each axis is 3.0 minutes for FAT and 4.5 minutes for qualification. Each major test article was tested in each of the three principle axes (normal, longitudinal and transverse). The vibration test frequency range is from 0 to 2,000 cycles per second (CPS) with a high sweep rate of 6 decibels (dB) per octave from 0 to 40 (CPS). The above vibration profile was input to each major test article bolted to adapter fixtures that approximated the aircraft tie-down technique.

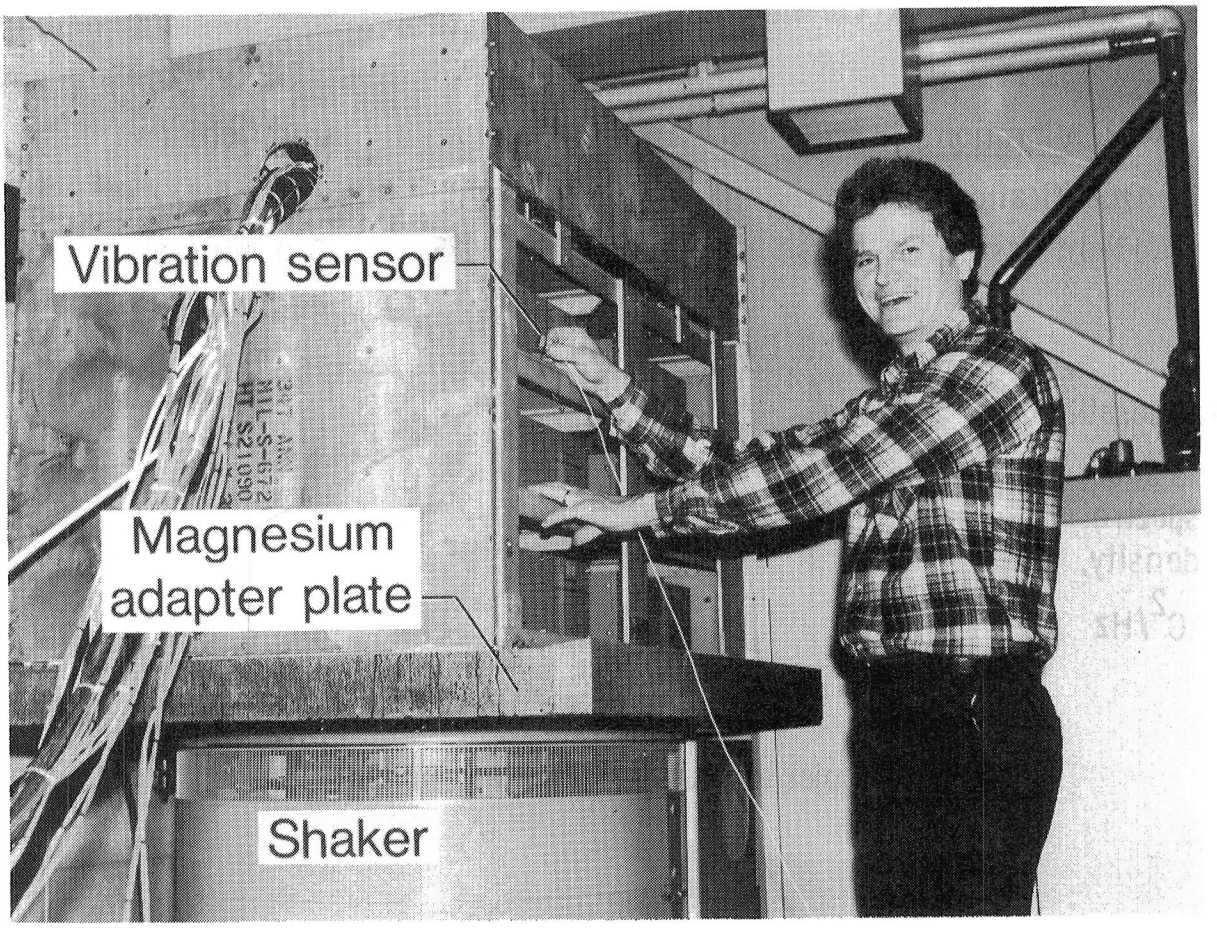
Vibration:	Axis	G (RMS)	Duration, min
Qualification tests	N, L, T	6.0	4.5 min/axis
Flight assurance tests	N, L, T	3.85	3.0 min/axis



(For turbojet aircraft-fuselage equipment)

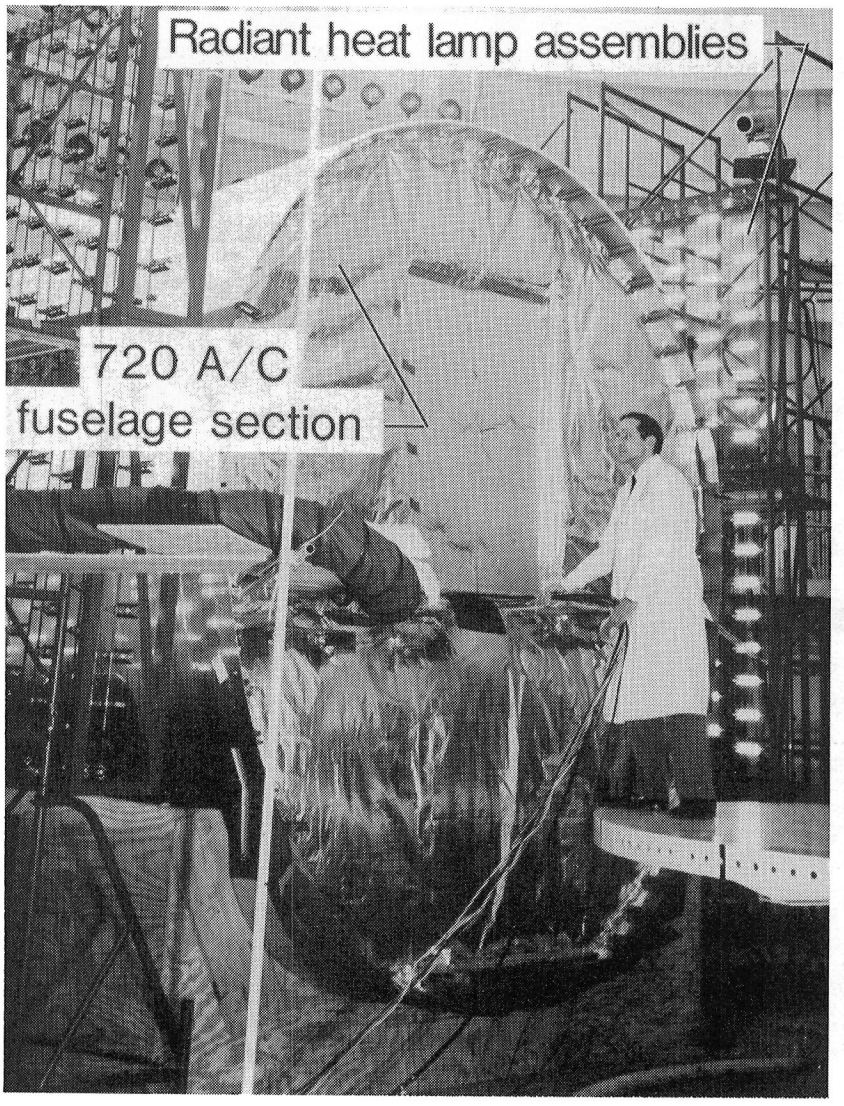
VIBRATION TEST
DAS - MAIN ELECTRONIC PALLET

The vibration test profile was input to the test article, mounted to a damped 4 inch thick magnesium adapter plate. The 17,000 force-pound shaker is shown in the vertical position with the adapter plate and approximately 900 pound DAS main electronic pallet mounted. The technician is shown placing accelerometers on each of the four shelves of the pallet unit, which has one heat shield side cover removed. The shaker was rotated 90 degrees and attached to a large slippery table for vibration of the longitudinal and transverse axes. The multicable harness was attached to the pallet components and the system was under power during the complete vibration test series. No major resonance conditions or abnormalities were evidenced during this test series.



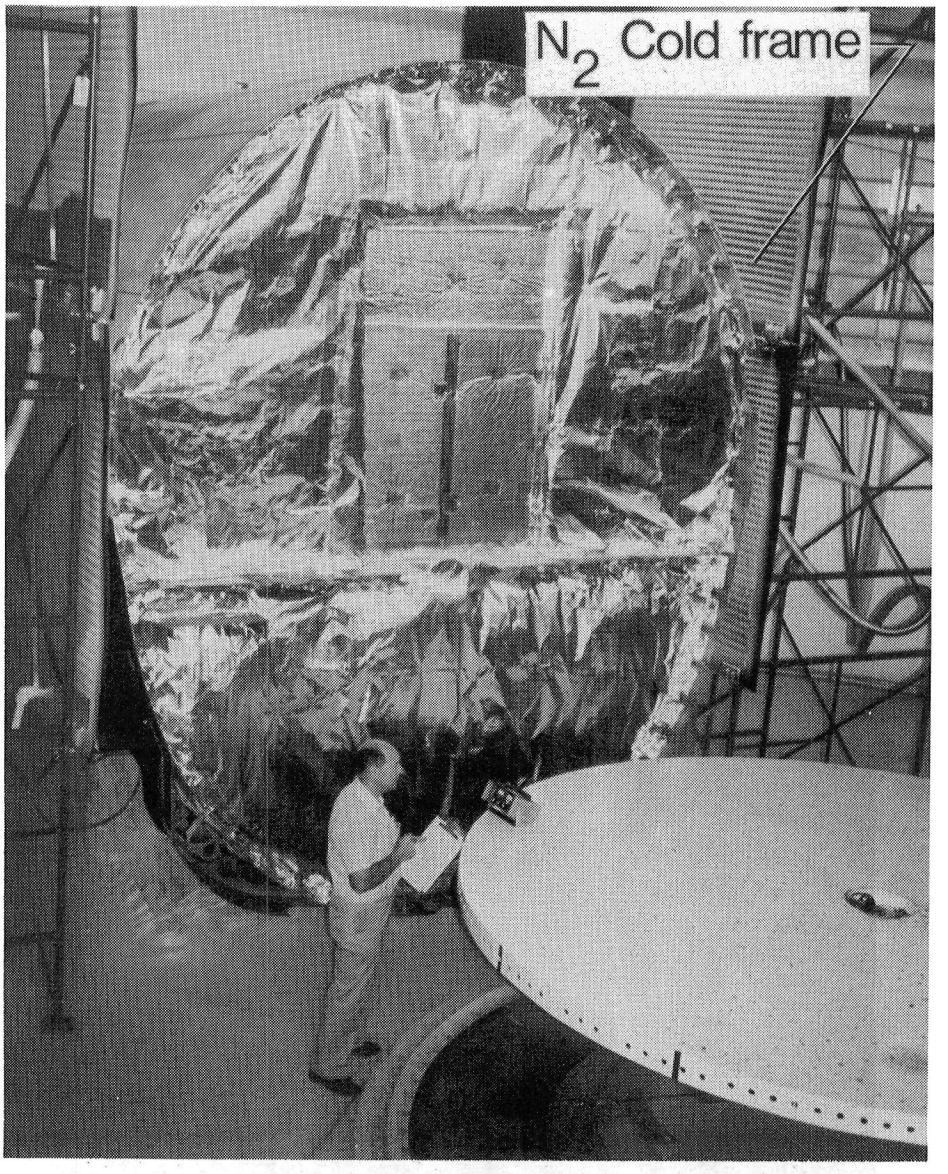
THERMAL (HOT) TEST

A full-size B-720 fuselage section was installed in the LaRC 55 ft diameter thermal vacuum facility and both ends of the section were thermally insulated. The test articles were placed inside in a typical location of the actual CID test aircraft. Large radiant heat lamp assemblies with quartz lights were positioned close to the fuselage section and powered until the inside fuselage temperature reached the desired level. All the test articles were operational through the high temperature test environment. For the nonoperational thermal (160°F) condition no power was supplied to the test units.



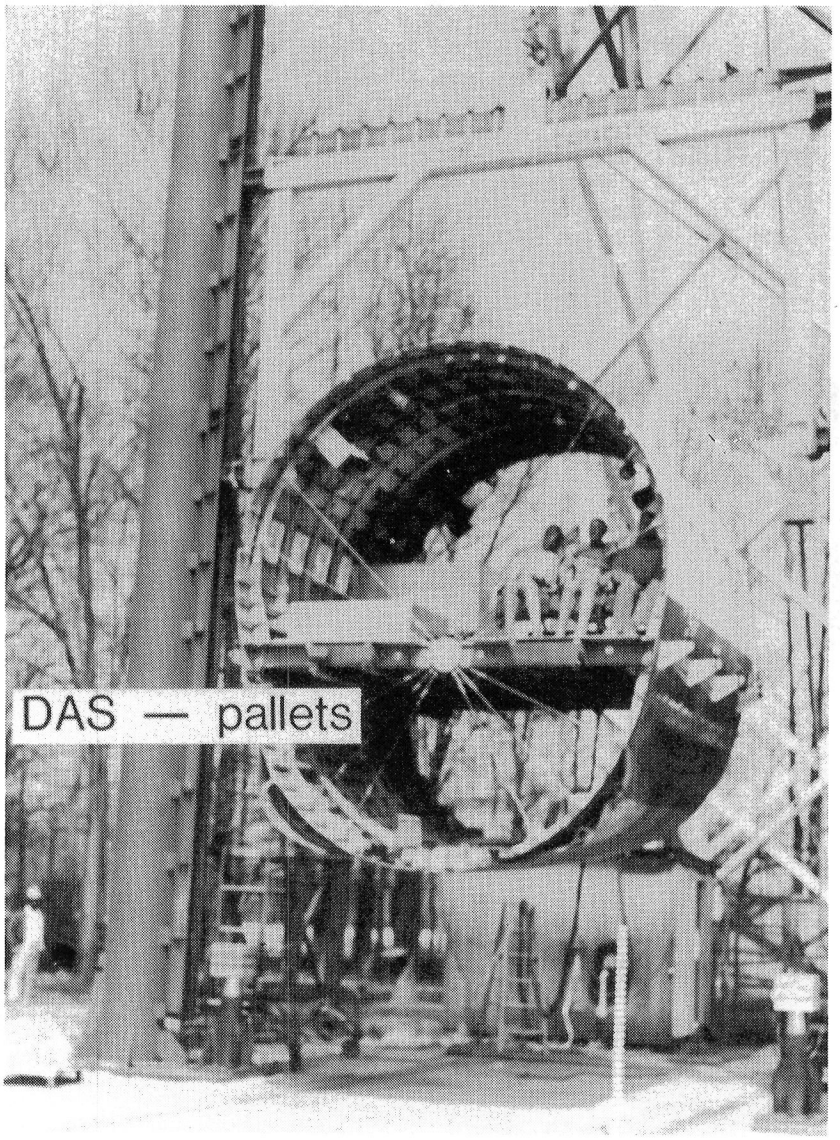
THERMAL (COLD) TEST

The full-size B-720 fuselage section was also used for the thermal (cold) test in the thermal vacuum facility. Large nitrogen cold frames were positioned adjacent to the fuselage section and temperature inside the fuselage was chilled by radiating heat away from the fuselage section to the cold frames. All of the test articles were operational through the cold temperature test environment. No major discrepancies or failures were detected throughout the thermal testing.



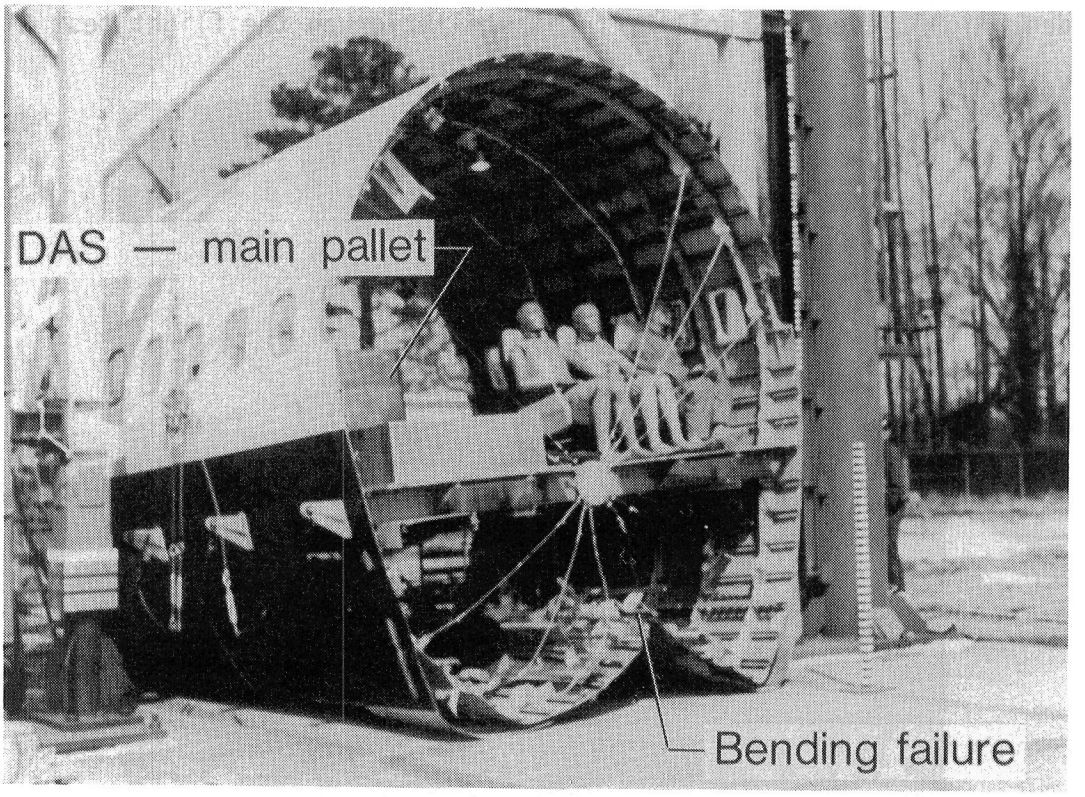
720 FUSELAGE (AFTERBODY) DROP TEST
FLIGHT SYSTEMS OPERATIONAL: QUALIFICATION

Actual fuselage sections (about 12 ft. in length) cut from a B-720 aircraft were mounted in the LaRC dynamic drop test facility for vertical drop tests. This picture shows the afterbody section (near the expected aircraft contact point) raised about 6 ft. above the concrete impact pad while being hung from the drop carriage fixture. This test unit was used to qualify the major test articles when integrated with the aircraft structure. All units were operational and data signals were telemetered at the 20 ft./sec. impact velocity. All systems performed as planned and this test was the final qualification prior to hardware shipment to NASA Dryden Flight Research Facility for installation on the flight test aircraft.



720 FUSELAGE (AFTERBODY) DROP TEST SHELL FAILURE
FLIGHT SYSTEMS OPERATIONAL

At impact, the lower fuselage shell failed where keel formers sheared and local bending occurred. A secondary bending and buckling occurred along the cargo shell sidewall. These structural failures absorbed considerable impact energy and contributed to reduced shock levels along the floor line where seats and pallets are mounted. All units were inspected after this test and shown to be qualified for flight test service.



CID-720 AIRCRAFT-FUSELAGE VERTICAL DROP TESTS - COMPARISON

Three B-720 fuselage sections were tested in the LaRC vertical drop test facility. A comparison of the accelerometer levels at the 20 ft./sec. impact velocity is shown in this table. The three test articles were taken from the forebody, centerbody, and afterbody regions of the B-720 aircraft. The acceleration levels shown are approximate maximums during the impact duration. Note that the centerbody section had very much higher levels than the other sections because it was structurally very stiff and had little structural deformation or crush at impact. The forebody and afterbody sections compared closely, especially in the levels that the dummy pelvis sustained. There was a significant structural crush (about 18 inches) in the keel/cargo bay region of these sections, which reduced the shock input to the seats and dummy passengers.

Vimpact = 20 ft/sec

Acceleration levels
(at contact) @ 60 Hz filter

Item	Fuselage section #1 (forebody)	Fuselage section #2 (centerbody)	Fuselage section #3 (afterbody)
Fuselage keel	22	High	60-100
Side frame/floor beam	10 to 12	95	10-15
Floor @ seat rails	9	70	15
Dummy pelvis	9.0	40-60	9.0-12.0
Crown	10-20	100	10

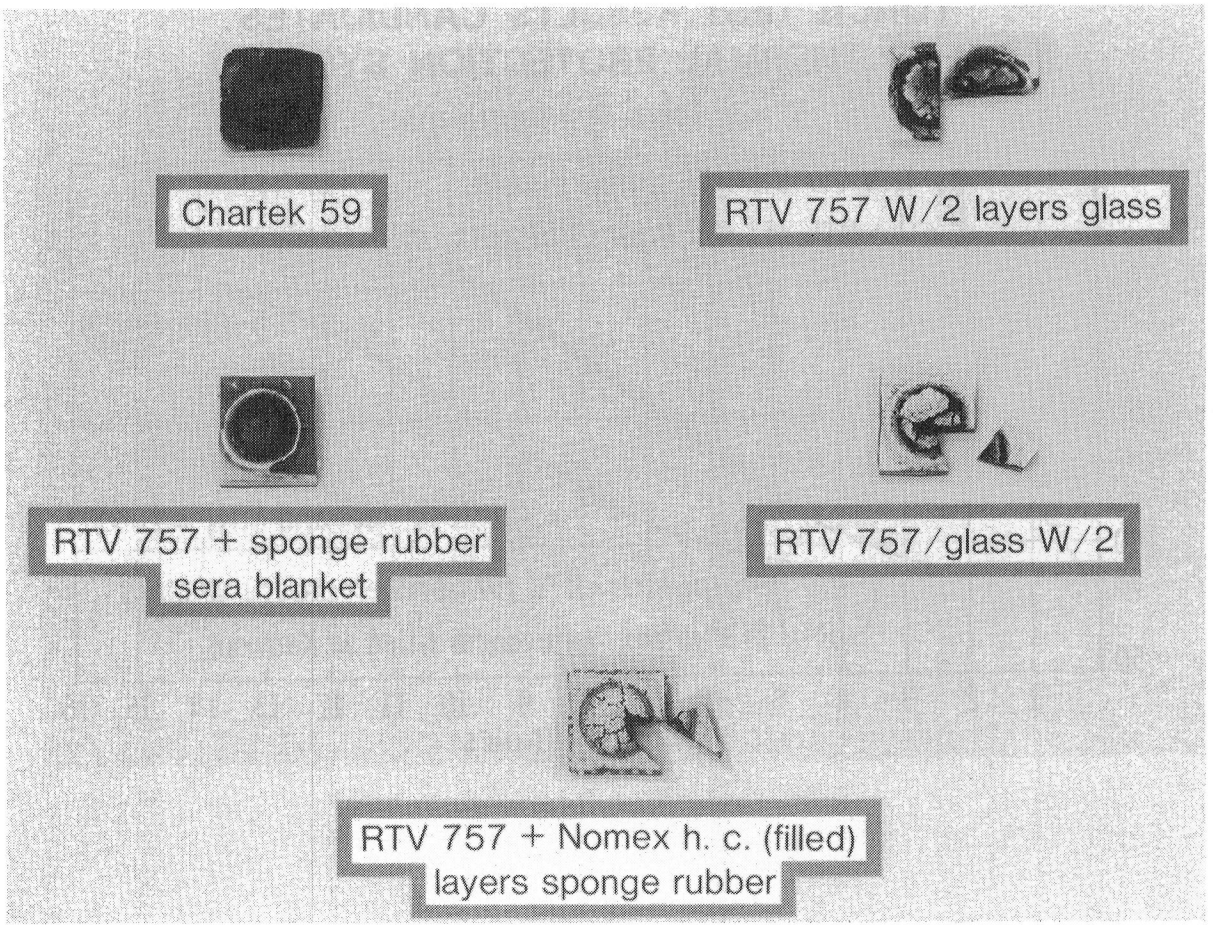
TASK

Since the CID-720 flight test aircraft carried a large quantity (about 11,000 gallons) of jet fuel in its wing tanks, a decision was made at LaRC to proceed with a protective shield development task. This development of crashworthy thermal protection shields was to provide protection for eight (8) data acquisition pallets, ten (10) photo cameras, and four (4) camera/lights power distribution pallets. The design goal was to survive an intense fuel fire for 10 minutes duration (an estimate of the minimum time to reduce an aircraft fuel fire). Also, another design goal was to survive large structural debris flying through the cabin during the crash slide-out phase.

- Development of crashworthy thermal protection shields
  - Data acquisition systems (8)
  - Photo cameras (10)
  - Camera/lights power distribution pallets (4)
- Goals
  - Survive intense fuel fire, 10 min. duration
  - Survive flying debris during crash slide-out

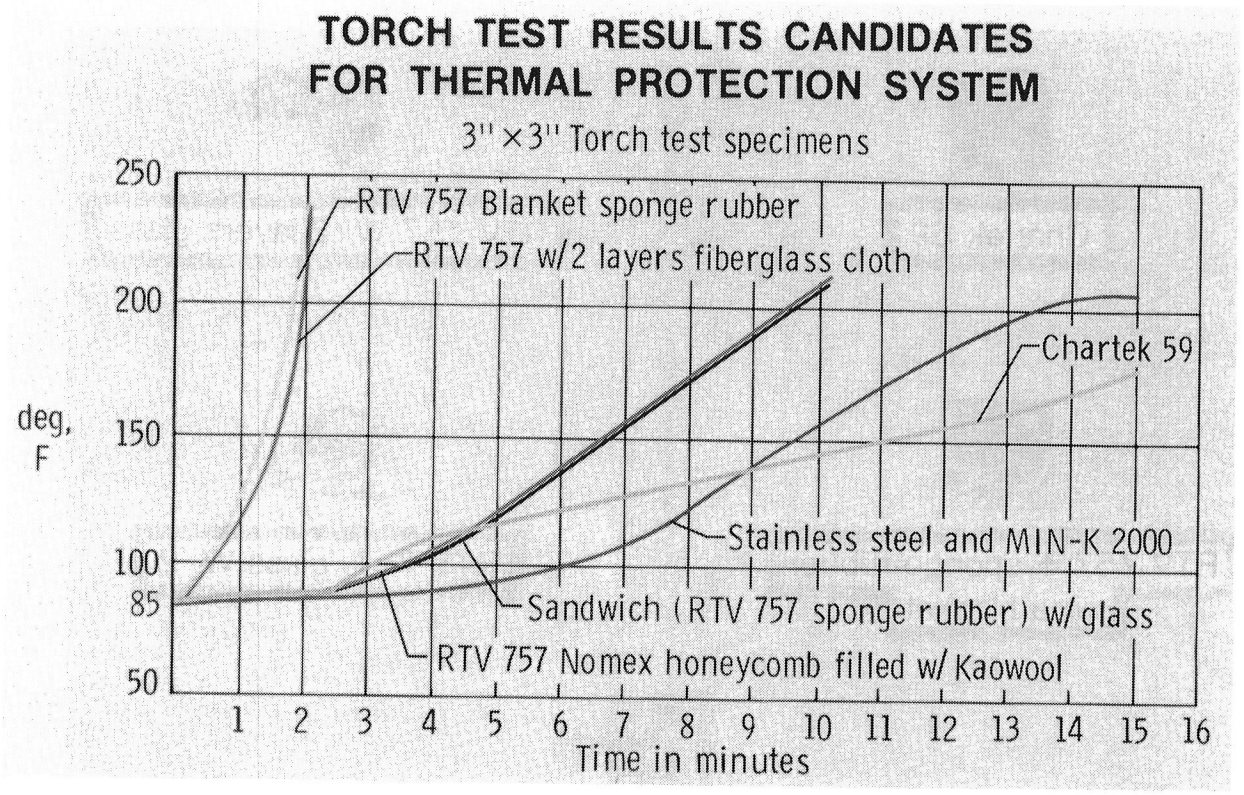
CANDIDATE FIRE PROTECTION SAMPLES
3" SQUARE TORCH TEST SPECIMEN

A screening test program of 3" square candidate fuel fire resistant samples was initiated. The five (5) samples shown in this chart represent the best combination of heat resistant materials from the total screening program. Each test sample was mounted in a ceramic holder while an acetylene torch was applied on one surface (face down) and a thermocouple/recorder showed the temperature increase with time on the back face of the sample. Another leading sample, stainless steel and MIN-K, is not shown in this chart.



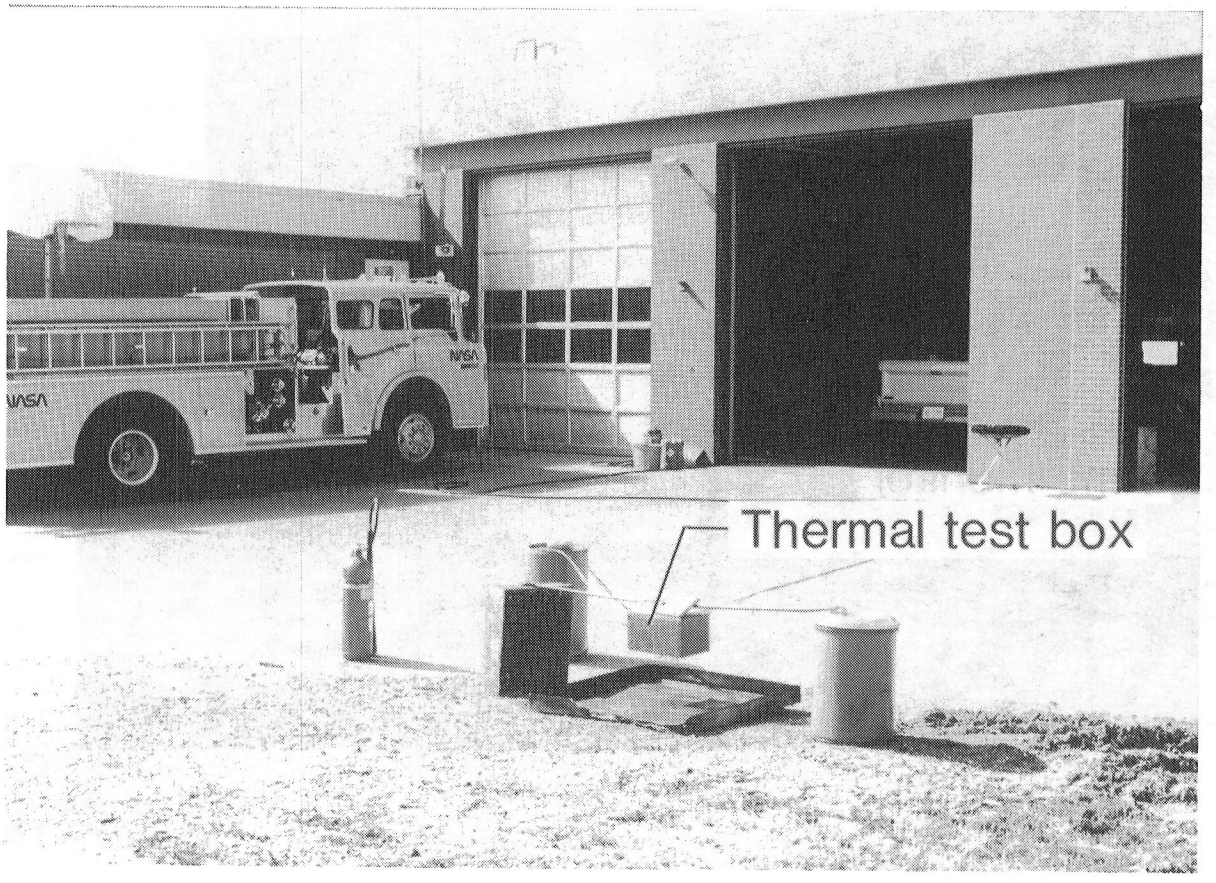
TORCH TEST RESULTS CANDIDATES FOR THERMAL PROTECTION SYSTEM

This graph shows the thermal comparisons of each of the candidate torch test specimens. The back-face temperature (degrees fahrenheit) plotted against duration of applied heat (in minutes). It shows that for the 10 minute design duration, the chartek 59 and stainless steel with MIN-K 2000 were nearly equal, but for longer times the chartek was lower in temperature rise on the back face of the specimen.



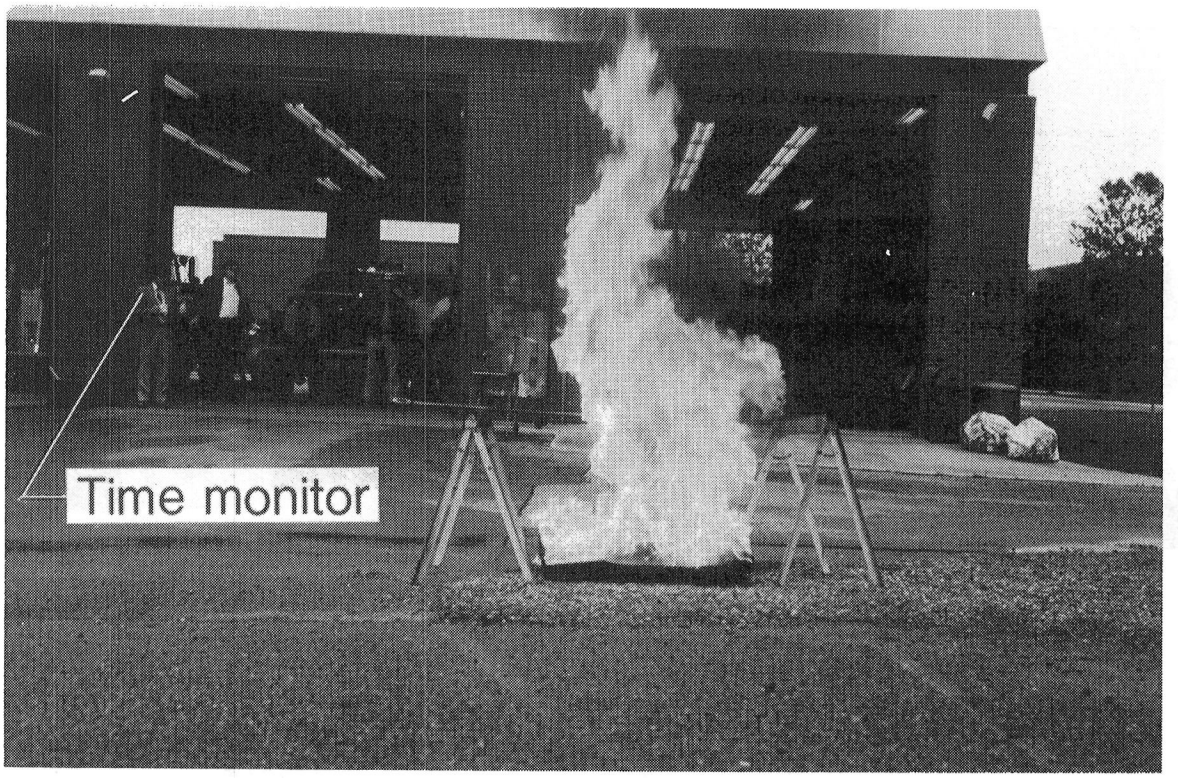
FIRE TEST SETUP

The next phase of the thermal shield development was to conduct an actual fuel-fire test with a fabricated heat shield from the best candidates of the torch screening tests. The LaRC fire department set up a quick (low budget) fire test using available equipment for an actual 10 minute gasoline fire in an uncontrolled environment. The thermal test shield was fabricated around a dummy camera and suspended by a steel rod. A large square fry pan was filled with approximately 5 gallons of gasoline. All thermocouple leads were routed to a recorder located inside the walls of the fire station.



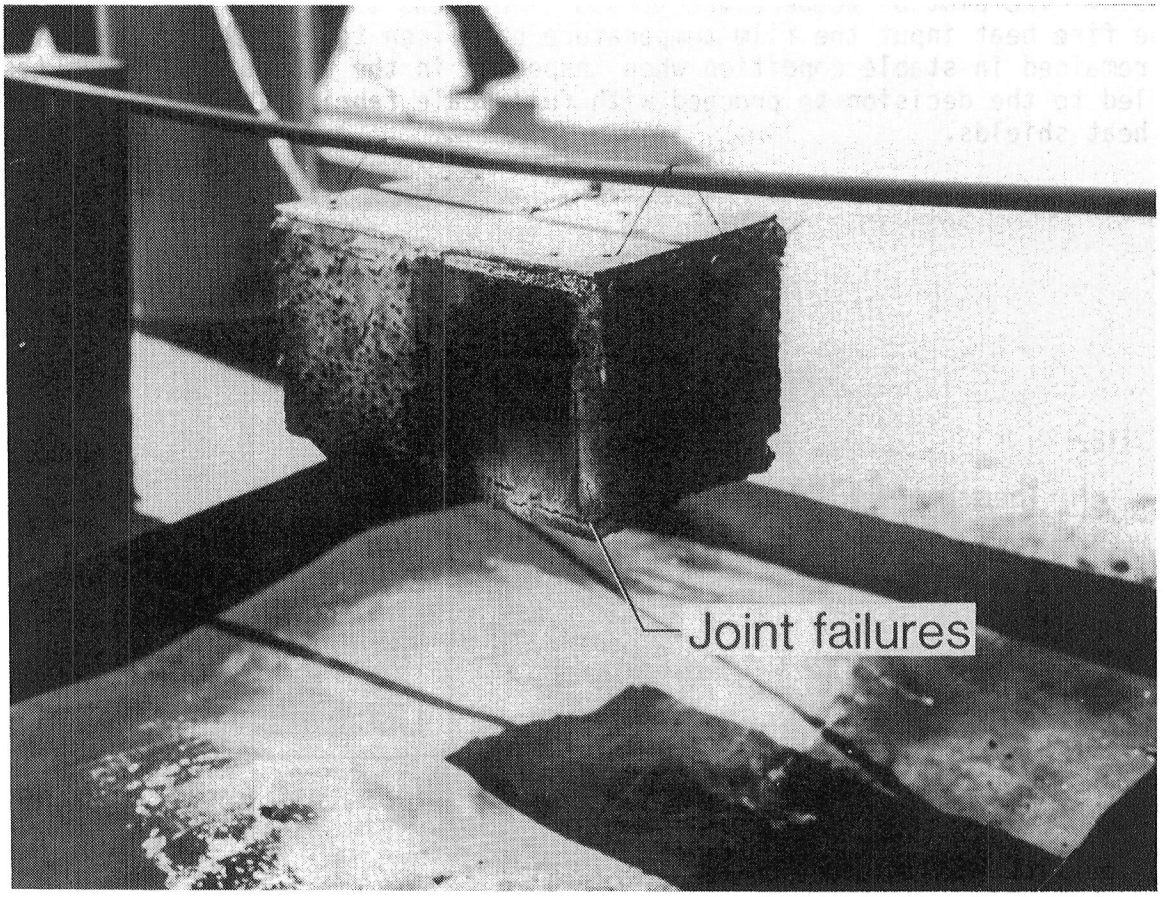
FIRE TEST - FLAME

A long handle torch was used to light the fire that enveloped the test unit for the ten (10) minute test period. The environment was uncontrolled but an attempt was made to select test periods with low wind velocity. The inside camera box temperatures were monitored with four (4) thermocouples located at critical areas. The temperature rise was indicated on a constant speed strip recorder and a backup time monitor was selected to determine the effective fire input duration.



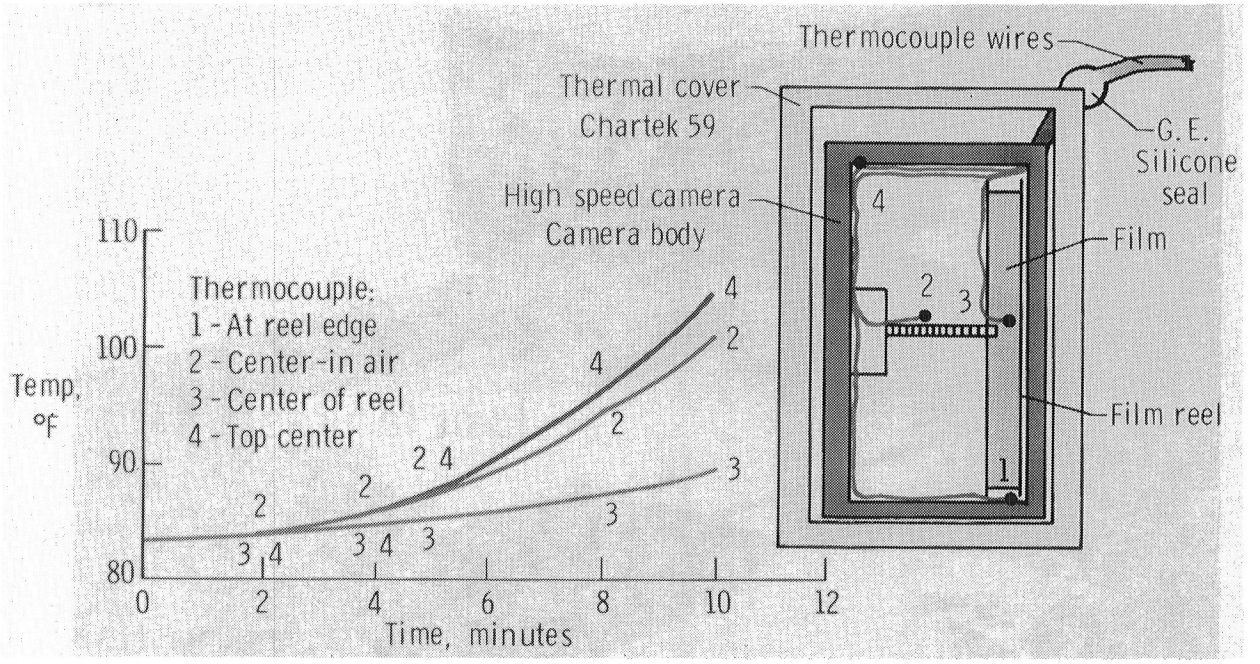
FIRE TEST - RESULTS

This initial fire test was not successful since the heat shield joints at the box corners opened and the flame entered to the metal dummy camera. All the inside thermocouples rapidly increased in only several minutes. The resulting temperatures would have destroyed any film inside the camera body.



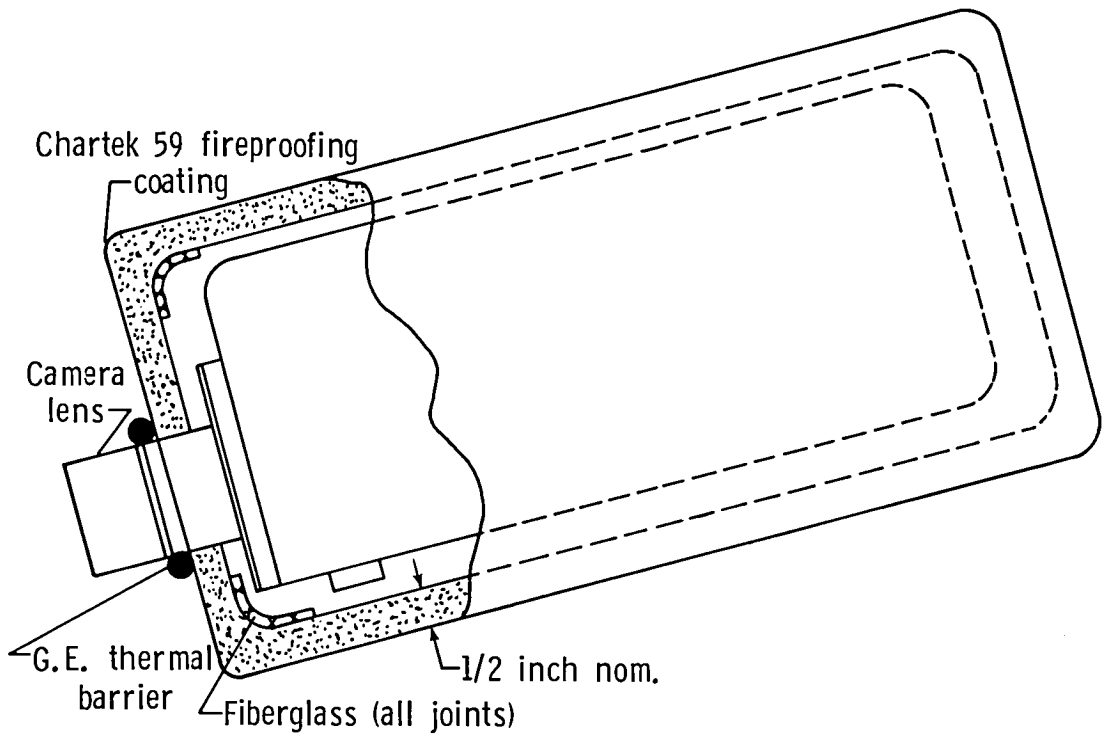
THERMAL PROTECTION

This figure shows a sketch of the last successful fire test using a chartek 59 thermal cover with fiberglass reinforced corners. The inside of the camera body included a 100 foot roll of 16 mm film that had been exposed under laboratory conditions. Thermocouple #3 was located on the film and the leads were routed out the corner of the box and sealed with a special General Electric high temperature silicone resin. The plot of temperature versus time shows that after 10 minutes gasoline fire heat input the film temperature had risen to only 90°F. The film images remained in stable condition when inspected in the laboratory. This test result led to the decision to proceed with full scale fabrication of the actual flight heat shields.



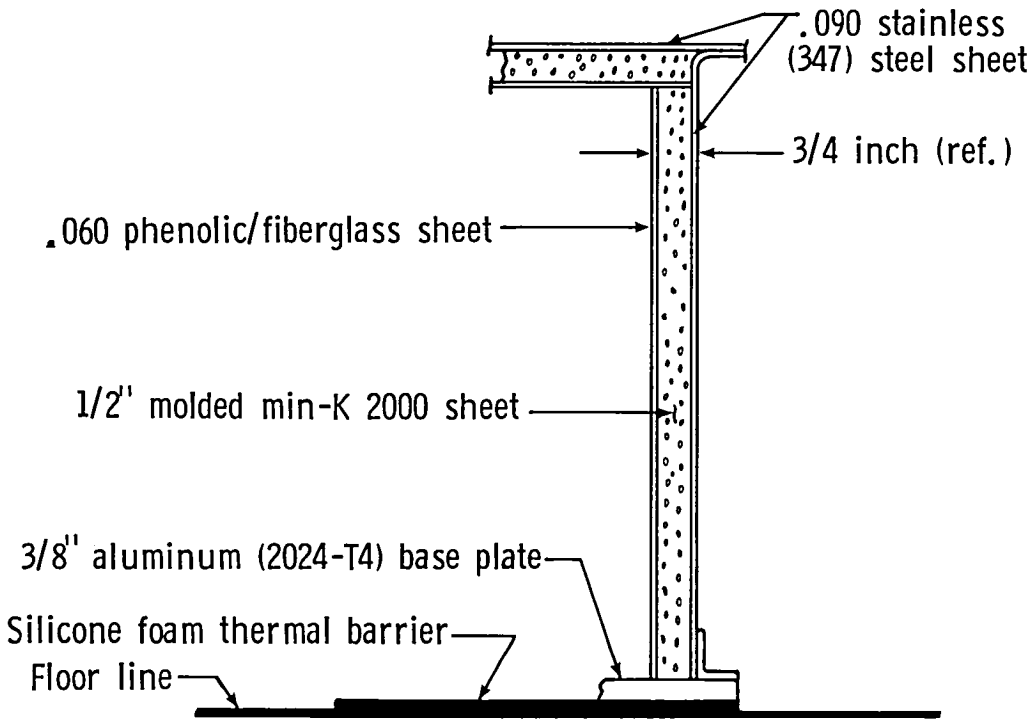
CAMERA HEAT SHIELD

This sketch shows a cutaway view of the chartek 59 fire proofing heat shield and the high speed 16 mm camera and lens. Notice the fiberglass reinforcing at the joints and the General Electric thermal barrier used to seal the port through the shield for the lens. A similar design was used at the rear of the camera where an electrical plug protruded through the heat shield. This was the fabrication technique used on the ten (10) high speed cameras mounted inside the fuselage.



DAS-RECORDER HEAT SHIELD

This sketch shows the fabrication technique for the data acquisition system-recorder heat shield. There was a 3/4 inch sandwich wall of .090 stainless steel sheet on the outside and .060 phenolic fiberglass sheet on the inside. Between the face sheets was a 1/2 inch thick molded MIN-K 2000 sheet material. The walls were attached at the 3/8 inch aluminum base plate with a sheet of foam silicone thermal barrier used to seal to the floor line of the aircraft.



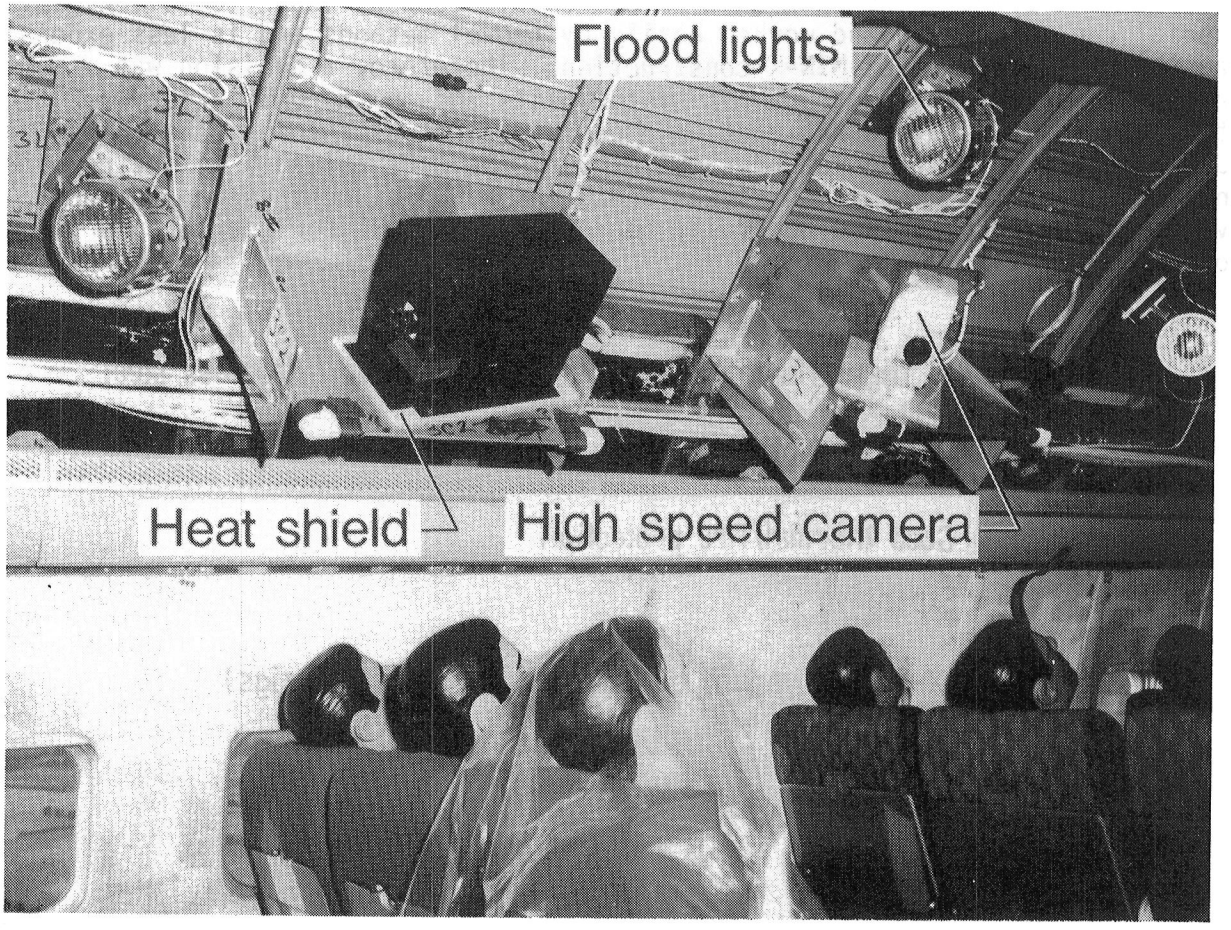
SUMMARY FINDINGS FROM FIRE DEVELOPMENT TESTS

Two protective shield concepts were selected for the LaRC developed hardware systems. The first construction technique consisted of .090 stainless steel-MIN-K 2000-phenolic fiberglass. This type of construction is similar to some advanced aircraft flight recorders with excellent penetration protection as well as good thermal/fire protection. Unfortunately, this type of construction is expensive in terms of labor and material cost. The other construction technique using the chartek 59 material had the best thermal results in the LaRC ground fire tests. Also, it is a proven fire retardant in common oil company usage (on oil rigs). This material can be handled and worked easily by trowel methods and is less expensive than the stainlesds steel MIN-K construction. Therefore, a decision was made to use chartek on all the photographic system units and on the DAS battery and telemeter pallets. These did not contain expensive electronic components. The main DAS electronic pallet and recorder pallet used the more reliable flight recorder construction concept (stainless steel and MIN-K-2000) since these units had to survive for longer periods and hopefully be returned to LaRC for use in other programs.

- Advanced flight recorder construction technique (stainless steel-MIN-K2000-Phenolic fiberglass)
  - Good penetration protection
  - Good thermal/fire protection
  - Expensive
- CHARTEX 59 - proven in oil company usage (on oil rigs)
  - Best thermal results in LaRC test
  - Less expensive

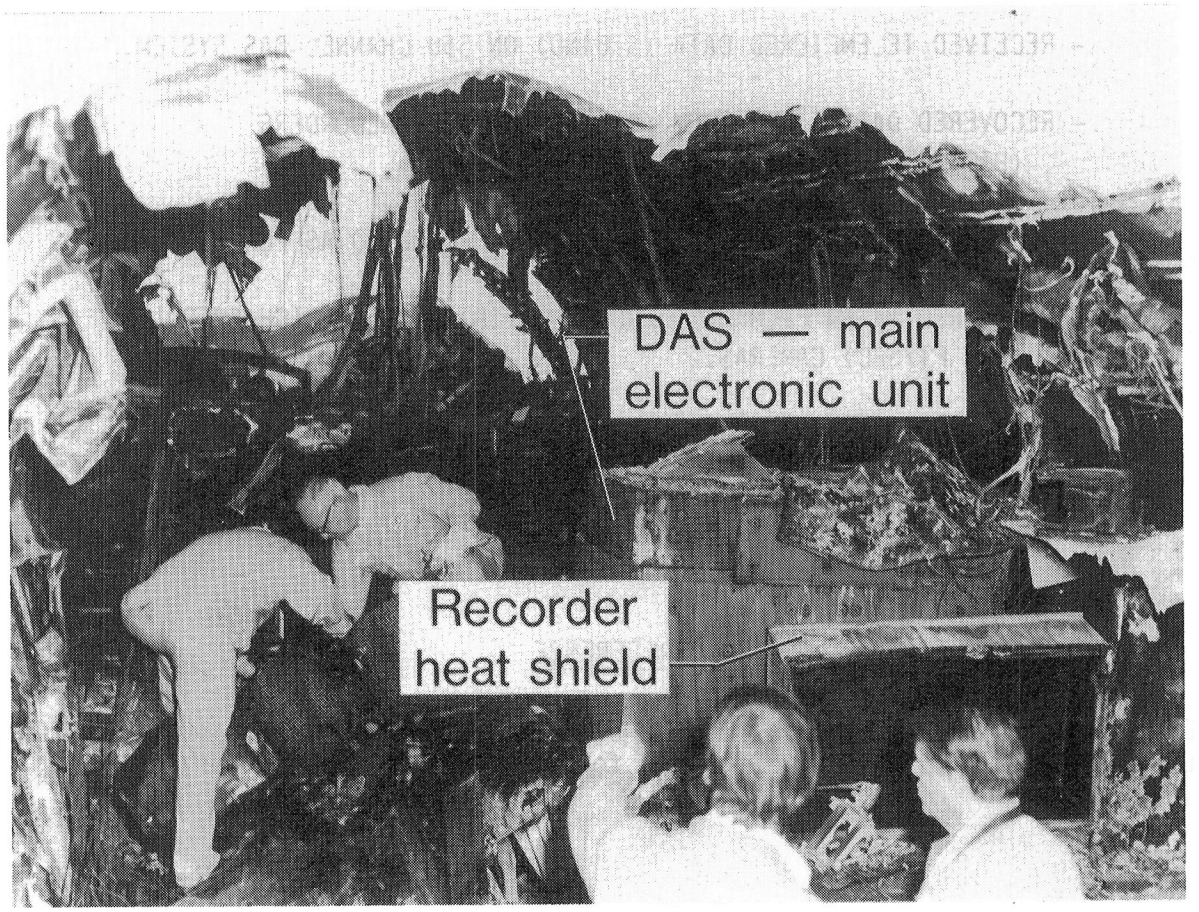
CAMERA HEAT SHIELD - INSTALLATION

This photo of the internal fuselage shows the high speed camera/mounts attached to the fuselage crown frames. Also shown are the high intensity floor lights and the dummy passengers/seats. The most rear facing camera is enclosed in the chartek 59 heat protection shield; notice the lens protruding through the box without the doughnut shaped silicone seal ring installed. The other 16 mm camera is shown mounted atop a chartek 59 insulator plate before the heat shield enclosure has been attached.



CID-720 POST-FIRE REMAINS

This photo shows the remains of the CID-720 test aircraft after the crash test with the subsequent intense fire. This is a view inside the fuselage looking forward. Shown standing rigidly in place is the DAS-main electronic unit with heat shields in place and molten aluminum metal deposited on its top from the melt down of the aircraft crown section. The DAS recorder heat shield is shown on its side after removal of the data tape from the recorder package. Both the heat shield and the data tape were in good condition. In the far right side of the photo can be seen a camera heat shield on its supporting aluminum mounting (partially melted) after removal of the 16 mm high speed camera and its spool of good film. The two technicians on the left side are inspecting the large chartek 59 heat shield that was still in excellent condition (less than 1/8 inch char layer) and the photographic power distribution system inside had performed its mission flawlessly.



SUMMARY

The CID-720 aircraft test successfully demonstrated the performance of the LaRC developed heat shields. Good telemetered data (S-band) was received during the impact and slide-out phase, and even after the aircraft came to rest. The two onboard DAS tape recorders were protected from the intense fire and high quality tape data was recovered. The complete photographic system performed as planned throughout the 40.0 sec of film supply. The four photo power distribution pallets remained in good condition and all ten onboard 16 mm high speed (400 frames/sec) cameras produced good film data.

SUCCESSFULLY DEMONSTRATED PERFORMANCE OF LaRC DESIGNED HEAT SHIELDS

- RECEIVED TELEMETERED DATA (S-BAND) ON 350 CHANNEL DAS SYSTEM.
- RECOVERED DATA TAPES FROM (2) ONBOARD TAPE RECORDERS (HIGH QUALITY DATA)
- ALL PHOTO POWER DISTRIBUTION PALLETS PERFORMED AS PLANNED.
- RECOVERED 16 MM FILM DATA FROM ALL (10) ONBOARD HIGH SPEED (400 FT/SEC) CAMERAS.

REFERENCE

1. Environmental Conditions and Test Procedures for Airborne Equipment. RTCA/DO-160A, Radio Technical Commission for Aeronautics, Washington, DC, Jan. 1980.

QUESTIONS AND ANSWERS

PRESENTATION BY ROBERT J. HAYDUK: "CID OVERVIEW"

Q: Walt Overrand, Delta

I was surprised at the interior. What was the aim and purpose in not having a full interior with carpets and so forth?

A: Bob Hayduk, NASA Langley

I would like to direct that question to John Reed after I state that the structural loads experiment was primarily concerned with the airframe and the wings and pylon and that the seat exeperiments were next in interest to us. I don't believe we had a strong materials group that was interested in filling out the complete interior of the aircraft.

A: John Reed, FAA

Needless to say, we did not plan for a fire. It was not an objective. The fire safety experiments were installed later in the preparation of the test article. Since we did not plan a fire, the interior liners were not of interest to us, either the cargo liners or the interior cabin. So there just was not any attempt in the basic experiments, from the antimisting kerosene, the crashworthiness, and the fire safety, to concern ourselves with replicating today's typical aircraft interior.

Q: Ed Widmayer, Boeing

Are you going to release the accelerations for the entire slide out?

A: Bob Hayduk, NASA Langley

We plan to release all the data that we measured as soon as the analyses are complete. At this time we have a package of about 80 channels of data for the time period of specific interest to the structural loads experiment. We have the one second after the left wing impact, and the wing cutter impact occurred after that.

PRESENTATION BY RUSS BARBER: "CID FLIGHT/IMPACT"

Q: Speaker unknown

I'd like to know what the power was on touchdown and how the airplane got so far off line.

A: Russ Barber, NASA Dryden

The aircraft had a lateral deviation at about 200 feet in altitude. We had a project guideline that once the airplane went below 150 feet, the pilot was committed to impact. We had to do that in order to ba able to activate both the on-board cameras and the cameras that were located out on the lakebed, as well as some of the other data systems. At 200 feet the airplane was slightly to the right

of the centerline, but the pilot thought he could get back. He committed at 150 feet and got rather vigorous on the controls attempting to get the airplane back, and that resulted in the trajectory you saw. The power setting at impact, as near as we can determine, can be represented by the following table.

Time	Engine no.	Engine pressure ratio	N_2*
09 22 10.980	1	1.1	76
	2	1.2	77
	3	1.2	77
	4	1.1	74

*N_2 = high-pressure compressor rotor speed in percent (97 percent = 9670 rpm = takeoff power).

Q: Speaker unknown

From your point of view, if you were going to do this over again what would you do differently?

A: Russ Barber, NASA Dryden

I would start out with an airplane that had a hydraulic control system so that we could have a redundant control capability, rather than a single string, which increased the pressure of making the impact at the earliest opportunity. I think we could make some improvements in the guidance we provided the pilot. These video guidance systems looked relatively good down to the 150-foot altitude that we were able to test them to. When you get to altitudes below that the gains get quite high on those systems, and we really weren't able to identify this on the simulator that we had developed to preanalyze our capabilities.

Q: John Clark, NTSB

What data did you use to generate the numbers you presented for sink rate, velocity, and pitch and roll attitude?

A: Russ Barber, NASA Dryden

Theodolite data.

Q: John Clark, NTSB

Looking at the cameras?

A: Russ Barber, NASA Dryden

Yes.

Q: Dave Ramage, Air Canada

What effect did the fact that you didn't hit the ground in a wings-level attitude have on the load data you got from the airplane? Did it cause any problems or did you get what you wanted?

A: Bob Hayduk, NASA Langley

We got the data we desired in terms of numbers of channels, but the left wing impact and subsequent nose impact reduced the sink rate on the fuselage, which caused the overall load levels to be substantially lower than we anticipated. However, the results that we have are still going to permit us to accomplish our major objective of having a baseline of data that we can use to validate our computer program. The data is still going to provide us with the capability to achieve what we desired to achieve.

Q: Howard Asher, Cessna

What type of ground did the fuselage actually impact on the head of the rockbed - what were the actual soil conditions?

A: Russ Barber, NASA Dryden

The lakebed is a surface that is as dense as concrete. The surface layer is softer, so you will see dust, but you could essentially conclude that it hit a surface as hard as concrete.

PRESENTATION BY E. ALFARO-BOU: "NASA EXPERIMENTS ON THE B-720 STRUCTURE AND SEATS"

Q: Gil Wittlin, Lockheed

For the pulses that you talked about in the dynamic tests, were those vertical accelerations?

A: E. Alfaro-Bou, NASA Langley

The pulse on the sled was vertical, and the pulse on the seat pan was at 45 degrees with respect to the ground.

Q: Gil Wittlin, Lockheed

What was the position of the accelerometer?

A: E. Alfaro-Bou, NASA Langley

It was normal to the wedge, which was 45 degrees to the ground.

Q: F. Clark, American Airlines

I didn't quite understand your answer; did you have a forward component of g?

A: E. Alfaro-Bou, NASA Langley

Yes, we had a forward, which we call longitudinal, and a normal component.

Q: F. Clark, American Airlines

What were the two vectors; how many g forward and how many g down?

A: E. Alfaro-Bou, NASA Langley

I only showed the normal component; the longitudinal would have been the same because it was at 45 degress. On the seat pan, it was roughly 12 g's for both normal and longitudinal components.

Q: F. Clark, American Airlines

Comparing this to the actual crash, the forward g was very small compared to the down, so this was not the same simulation when you get down to it?

A: E. Alfaro-Bou, NASA Langley

No, that was no simulation; this dynamic test was a very hard test for the seat. We wanted to make sure that the seat would survive, and we were not expecting pulses of this kind in the crash impact demonstration. The dynamic test was mostly to make sure that none of the components, the seat legs or any part of the seats, would fail.

A: Bob Hayduk, NASA Langley

That was a developmental test for the seat. We had designed the seat to begin stroking with a vertical load of 10 to 12 g's, so we exceeded that level in our developmental tests and were expecting that kind of level at that location in the aircraft. We did not achieve that level, so consequently did not get the kind of stroking we were expecting out of the seat.

Q: Dick Chandler, CAMI

On the curve showing the deceleration on the drop tower tests, I interpret the carriage input pulse to be a vertically oriented accelerometer on the carriage and the seat pan pulse to be a normal 45 degree oriented accelerometer on the seat. Wouldn't that say that if this was all a rigid ideal non-energy-absorber system, the seat pan pulse should be about 7/10 of the vertical pulse or somewhere around 10 g's? In other words, did you really get energy absorption here?

A: E. Alfaro-Bou, NASA Langley

Actually, I had not looked at it that way. In this particular test all we were concerned with at the time was making sure that all the seat components would stay put on the CID, that nothing would break. We did have a bit of a problem in a way with the energy absorber. Even though we still have one more inch of absorption left, the material from the composite tube went inside the tube and it became solid. So we did have a solid impact in there,

and that's why I didn't say much in here about energy absorption because there was a flaw in the mechanism that allowed all this material to get out of the tube. Later on we made a bigger opening on the tube so that this would not happen, but we did not do another test. So, as far as the energy absorption is concerned, this would not give you a pulse indication of what the seat can actually do. The seat still needs to be fine tuned and we never did any other tests due to lack of time. After the last testing, we just refurbished the seat and packed it and sent it back to Dryden.

Q: Dick Chandler, CAMI

When you refer to seat pan pulse, as I recall the Airest 2000 seats have a fabric seat pan. Is this really a seat frame?

A: E. Alfaro-Bou, NASA Langley

The seat pan acceleration was actually measured on the rear tube, which was on the seat frame.

PRESENTATION BY E. L. FASANELLA:

"NASA SEAT EXPERIMENT AND OCCUPANT RESPONSES"

Comment: Dick Chandler, CAMI

The DRI model, of course, is a military model and it is a simple oscillator that you can apply to virtually any measurement that you choose to apply it to. But when you begin looking at DRI versus the military ejection seat experience, it's always prudent to see what was being measured when the DRI was calculated. There is a military standard that governs testing of ejection seats and ejection capsules, and the acceleration measurements used are chest accelerations and seat pan accelerations. If the truth were known, the dummies that were in use at the time the DRI model was originated didn't even have a pelvis, let alone a place to measure pelvis acceleration. So for a number of years, we at CAMI have been trying to somehow correlate pelvis DRI with seat pan DRI. In a recent set of tests we did in cooperation with the Air Force, we had the opportunity to do this in a very closely controlled military-type of seat and restraint system, and we found that the pelvis DRI was about 1.43 times the seat pan DRI. That is the basis for the Air Force injury curves you showed. Unfortunately, the standard deviation was 0.16, so if you want to look at a confidence interval you can say it's somewhere in between 1 and 2 times as high. Even more unfortunately, when we try and do it for less well-structured seat and restraint systems, the correlation is even poorer. So I really don't know what your pelvis DRI means in terms of injury, other than I suspect that it's considerably higher than would be an indication by a true seat pan initiated DRI measurement by probably at least a factor of 1.43.

A: Ed Fasanella, Kentron

Your comment is correct. As I mentioned here earlier, there's quite a bit of controversy about human tolerance criteria and you really have to use

them with due caution. I used this model primarily as a comparison tool, so I could compare the various occupants and give you some numbers. But there's always a lot of argument among the experts in the field over how these various injury criteria are to be applied, and I think there probably will be for a number of years. (In the case of the NASA seat data that were presented, the seat pan acceleration and pelvis acceleration follow each other very closely, hence it is probable the "pelvis DRI" and "seat pan DRI" would be comparable.)

Q: Dick Coykendall, United Airlines

Had the impact been executed to plan, what were the anticipated accelerations that would have been encountered in the distribution of seats?

A: Ed Fasanella, Kentron

That's a good question. If the impact had occurred nearly flat, without roll (or yaw), I would have expected all the acceleration levels to be considerably higher. Also if the nose had been pitched up (as planned), the levels would have been higher in the rear of the airplane, which would be different than what we observed. But what the actual levels would have been in the seats is uncertain unless we repeated the test to find out.

Comment: Bob Hayduk, NASA Langley

Well, we do have some information in the section tests that we did. We had taken Boeing 707 sections and dropped them vertically at about 20 ft/s, and there we experienced acceleration levels along the floor in the neighborhood of 12 g's in the soft sections (fore and aft sections). In the hard center section that we dropped we saw acceleration levels that were in excess of 70 g's on the floor. So I think a nose-up level (no roll) impact where we would have impacted on the rear part of the aircraft would have generated much higher vertical levels throughout the aircraft.

A: Ed Fasanella, Kentron

Yes, it's true we've done quite a few section drop tests and they were very useful for studying a more controlled-type experiment where we have only a vertical velocity component. Levels in the section tests, as Bob Hayduk has said, were higher than those in the CID test, where the wing impacted first.

Q: Dan Watters, Naval Air Test Center

Is it safe to conclude from your standard NASA seat and energy absorbing seat that there's not a significant difference between the two?

A: Ed Fasanella, Kentron

No, that's not really the case. What we had here was a mild impact, especially in the rear part of the fuselage. Since the impact was mild we had no stroking of the energy absorbing seat. In that sense, since the impact was mild and there was no stroking, both seats responded about the same. But in a more severe impact, the stroking EA seat should have shown an improvement over the standard seat.

Comment: Steve Soltis, FAA

I think the point about the type of g levels you might see at higher velocities based on the section tests is that the 10 to 12 g range is usually a pretty long duration such as you saw on the CID, approximately 0.1 to 0.5 seconds. The 70 g's on the hard sections would probably be for about 10 to 30 milliseconds and the occupant might not respond to that. So the pure g level isn't really the whole criterion for a test.

A: Ed Fasanella, Kentron

That is correct; when you talk about g's, the duration is very important. You must always keep the duration in mind.

Comment: Steve Soltis, FAA

I'd just like to make one other comment with respect to this 12 g - 70 g range. I think the 12 g is probably the number I would feel you'd see on the aircraft based on some of the section drop tests and the drop test of a full-scale aircraft (Boeing 707) we saw at Laurinburg, N. C. If you just drop a section you're going to get very high levels in the hard sections because there's no crush distance when it behaves as a section. If you impact a complete aircraft you do get crushing in the hard section which will reduce the load level well below 70 g's.

PRESENTATION BY E. ALFARO-BOU: "STRUCTURAL LOADS - PRELIMINARY RESULTS"

Q: Speaker unknown

In the video tape, I thought I saw a seat attachment failure in the left side of the airplane; it looked like one was becoming detached.

A: E. Alfaro-Bou, NASA Langley

When I was talking about the seats, I was talking about the seat experiment that NASA had. NASA only had two seats and they were towards the rear in body station 1220 and we did not see any failures.

A: E. Fasanella, Kentron

I'd like to clarify the comment about seat attachments. On the NASA seats we couldn't even find the seat after the crash, so we don't even know if it was completely consumed in the fire.

PRESENTATION BY E. L. FASANELLA:

"DIGITAL FILTERING AND ACCELERATION PULSE INTERPRETATION"

Q: John Clark, NTSB

I have the delta V at 14 ft/s, but where are we looking at that velocity change?

A: Ed Fasanella, Kentron

The velocity varies according to where you're located on the plane. After the wing hit, the plane pitched over and came in nose first. You get a variation in velocity from front to rear with the velocity higher in the front. For body station 540, where I showed the trace, the actual total velocity (vertical) integrated out to be 17 to 18 ft/s. It looked like the wing lowered the vertical velocity by about 3 or 4 ft/s since the fuselage impact delta V was about 14 in the example I showed you. That's typical of a good result.

A: Bob Hayduk, NASA Langley

I think that result is also verified by the theodolite data that Dryden has.

Q: John Clark, NTSB

In one other area I noticed there were differences from 14 to 17 ft/s. Was this due to noise in the data or are there other reasons for that?

A: Ed Fasanella, Kentron

The velocity change is sensitive to various things. One problem is that if I have a zero g offset and then integrate, the velocity will be thrown off. We had to go back and correct for zero g shifts even though we were careful to do prefires. Also, the nature of the digital system which jumps essentially in 1-g increments causes errors to occur when accelerations are integrated to produce velocity changes. It's a combination of these things, so you can't quote values to the nearest decimal point.

Q: Gil Wittlin, Lockheed

I have a couple of questions. Is what you call 100 Hz defined as being something like a 3 dB dropoff at 100 Hz?

A: Ed Fasanella, Kentron

That's correct.

Q: Gil Wittlin, Lockheed

Are your cutoff and terminating frequencies (10 and 180 Hz) selected by you, or are they automatic for that type of test?

A: Ed Fasanella, Kentron

I can put anything I want in the program. I just chose those values more or less to make them fall into SAE Class 60 characteristics.

Q: Gil Wittlin, Lockheed

If your sampling rate was higher could you presumably get some higher peak data?

A: Ed Fasanella, Kentron

Yes; we had to change our filter slightly. We had to input the sample rate into the digital filter program. It does change things slightly, but not a whole lot.

Q: John Clark, NTSB

If we had this 4 ft/s velocity change when the wing impacted, how much was proportional to the #1 engine and how much to the #2 engine?

A: Ed Fasanella, Kentron

There may be a chart that tells the exact times that the #1 and #2 engines hit. You can take those times, I guess, and get an idea of the respective contributions, but I don't have those figures in my head right now.

Q: Dick Chandler, CAMI

Do I understand from your earlier comment that the resolution from your acceleration measurements was 1 g?

A: Ed Fasanella, Kentron

It depends. For an 8-bit system you have 0 to 255 (counts or divisions), essentially, and we were ranging our accelerations vertically from +150 g's to -150 g's, so we are around 1 g (resolution) vertically. The resolution goes to 1/3 g in the transverse direction. I think for longitudinal we were ranging to ±100 g's. It's less than a g per division there. It's a trade-off we had to make; i.e., number of channels, range, resolution, bit rate, etc.

Q: Dick Chandler, CAMI

I was wondering if, with the relatively low resolution in your vertical measurements and your relatively low full-scale values, you are really talking about a potential for a fairly significant error in your data?

A: Ed Fasanella, Kentron

Well, you have to be careful in interpreting the data. The levels were vey low in this case, so you have to be careful because of the resolution problem.

Q: Robert Winter, Grumman

I'm not sure I quite understand something and I'd like to get it straight. It looks like you had hardwire analog filtering on the instruments ad then processed it digitally later. Is that correct?

A: Ed Fasanella, Kentron

Yes, that's correct.

Q: Robert Winter, Grumman

Were there 60-, 100-, and 180-Hz analog filters on board and did you filter the data later on at 100 Hz?

A: Ed Fasanella, Kentron

We had some analog 60-Hz filters on board the plane, but only a very few. We bought a large number of 180-Hz analog filters initially, so when we later reduced the total number of channels we had a surplus of filters and did not buy many 60-Hz filters. It doesn't make a whole lot of sense to use an analog filter of 60 Hz and then digitally filter at 100 Hz (except for some smoothing), but there were very few acceleration channels with 60 Hz analog filters.

Q: Robert Winter, Grumman

When you present the curves that are labelled "digitally filtered" and "unfiltered," aren't the curves labelled "unfiltered" really data that were recorded with 100-Hz analog filters?

A: Ed Fasanella, Kentron

Yes, they were either 180- or 100-Hz analog filtered. But you see, the digital filter is much sharper than the analog filter. The analog filter really passes a lot of the high frequencies, but the digital filters are very sharp in comparison. You wouldn't have a hardwire type analog filter that's as sharp as the digital filter. You can compare them, but it's like comparing apples and oranges. You have to look at the response curve of the digital filter and the response curve of the analog filter to really compare them.

PRESENTATION BY RICHARD E. ZIMMERMAN: "PRELIMINARY FLOOR, SEAT, AND DUMMY DATA"

Q: Dick Coykendall, United Airlines

During a vertical acceleration such as on seat A during ground impact, the pelvis response shows a very definite double peak response that lasts something like 100 milliseconds. Is that consistent with what the theoretical dummy response would be? What is the explanation of the obstacle impact producing higher vertical accelerations?

A: Dick Zimmerman, Simula Inc.

What amplitude were you looking at?

Q: Dick Coykendall, United Airlines

The amplitude was about 6 g, but the question concerns the two-peak response with a period of about 100 milliseconds between peaks. Is that consistent with the theoretical dummy behavior?

A: Dick Zimmerman, United Airlines

It is not unusual. In response to your second question, why we got the vertical response in the obstacle impact when the aircraft was obviously just sliding along the ground, I can't really explain. All I could offer would be conjecture. There were things happening to the aircraft, such as those obstacles tearing the structure underneath it. The landing gear was coming up underneath, pushing up on the floor. Perhaps the airframe climbed up on these obstacles a bit. That would be about the only reason you would see a vertical acceleration in that impact.

A: Bob Hayduk, NASA Langley

As further verification, those obstacles were very strong ones, built out of heavy steel. When they impacted the fuselage there was a pretty strong upward load on the fuselage due to the fuselage trying to come up over the top of the wing openers. I believe that the explanation for the substantial vertical load is the fact that they were so rigidly planted in the ground.

A: John Clark, NTSB

Basically, it was the heavy center structure impacting the wing cutters that produced the vertical load. However, in conjuction with that keel beam, is that why one chart shows the peak floor acceleration below seat F at 120? Is that still g's or is that a different scale?

A: Ed Fasanella, Kentron

I think I would disregard that trace entirely. I think it is bad data.

A: Dick Zimmerman, Simula, Inc.

The data for the channel at seat F was consistent with all other channels during ground impact. Somewhere as the aircraft was sliding along the ground something happened to that data channel. I can't tell you what happened to it that made it increase in amplitude like that but I also think it's wrong.

This morning Ed Fasanella was talking about validating this data. I showed you the number of channels we had for the seats and I said we only lost 10 of them. There are other channels that will have to be looked at very hard and validated, as Ed said. One of the checks, as he pointed out, is to integrate the data and see if the velocity checks out. For seat F it does not; the velocity is much too high. I think that data shows something about what was going on there, but it is not the right amplitude.

Q: John Clark, NTSB

When the cutters ripped through the fuselage, the no. 1 cutter sliced through and hit the main gear right under that seat with the high output. There was a lot of damage. It took out the keel beam just ahead and went into the left gear strut and knocked it completely out of the airplane. That was right under the seat where the data is, where we got that 120 g. That may be part of the problem. Part of the vertical acceleration could also have come from the plane trying to rise up on the gravel. There is about a 6 to 8 inch very gradual lift and that is also consistent with the total depth and crush that we had at the initial contact, so that could be a source of vertical loading. The whole airplane had to rise 6 inches when it slid across the gravel. What I would like to know is how the overhead bins fared, whether they stayed in place.

A: Dick Zimmerman, Simula, Inc.

They burned up on the ground.

Q: John Clark, NTSB

How were they loaded? What kind of luggage was put in, and did the latch stay closed during the sequence?

A: Dick Zimmerman, Simula, Inc.

They were loaded with a 60-lb mass bolted to the door.

Q: John Clark, NTSB

Was this the placarded weight of the bin or was it a lighter load? Was this a Boeing wide-body bin?

A: Roger Lloyd, RMS Technologies

It came out of a Boeing 707.

PRESENTATION BY LEO J. GARODZ: "CONTROLLED IMPACT DEMONSTRATION FLIGHT DATA RECORDERS/COCKPIT VOICE RECORDERS"

Q: Dick Tobiason, RMS Technologies

Am I correct in saying that the foil recorder behaved as you expected it to behave, and three digital recorders malfunctioned for 5 to 7 seconds after touching?

A: Leo Garodz, FAA

I can't answer that on the foil recorder. I don't know what might have happened afterwards if we had added electrical power to the unit. This system was tied into the airplane's electrical power unit. It was not tied into my inverter and battery pack.

Q: Speaker unknown

Could you amplify a little more on the digital flight recorder response - the 5 to 7 seconds of malfunction? You made a statement that the three digital flight recorders had a 5- to 7-second malfunction time after impact, and they were on standby independent power with your inverter and battery pack.

A: Leo Garodz, FAA

Some of them started to operate again properly; however, we lost certain transducers during the impact with the wing openers. For example, we lost our triaxial accelerometer. It was in a keel section which was ripped out immediately. But we continued to get the pitch and roll signals on the three flight data recorders.

Q: Speaker unknown

The slideout was about 10 or 11 seconds. Are you saying that you have 3 to 4 seconds worth of data after touchdown after that malfunction period?

A: Leo Garodz, FAA

Yes.

PRESENTATION BY J. D. PRIDE: "LARC PREFLIGHT HARDWARE TESTS"

Q: Speaker unknown

What was behind your decision for your high-temperature environmental test of 120°F operational and 160°F nonoperational?

A: Joe Pride, NASA Langley

The operational comes out of the TRCA 106A document for turbojet aircraft for thermal. The 160°F nonoperational came from conversations with NASA Dryden about their experience with aircraft sitting out on the hot lakebed during the summer. Because the aircraft was not air conditioned over the weekends, we designed the system to survive these temperatures.

1. Report No.	2. Government Accession No.	3. Recipient's Catalog No.
NASA CP-2395		

4. Title and Subtitle	5. Report Date
FULL-SCALE TRANSPORT CONTROLLED IMPACT DEMONSTRATION	January 1986
	6. Performing Organization Code 505-33-53-05

7. Author(s)	8. Performing Organization Report No.
Robert J. Hayduk, Compiler	L-16048
	10. Work Unit No.

9. Performing Organization Name and Address	11. Contract or Grant No.
NASA Langley Research Center Hampton, VA 23665	
	13. Type of Report and Period Covered
12. Sponsoring Agency Name and Address	Conference Publication
National Aeronautics and Space Administration Washington, DC 20543	14. Sponsoring Agency Code

15. Supplementary Notes

16. Abstract

The Full-Scale Transport Controlled Impact Demonstration (C.I.D.) took place on December 1, 1984, crashing at a prepared site on Rogers Dry Lakebed, Edwards Air Force Base, California. Ninety-seven percent of the sensors on the fuselage and wing structure, seats, dummies, restraint systems, galley, and bins were active at impact. A wealth of sensor data was collected from this once-in-a-lifetime research test. The flight data recorder experiments on board were also generally successful. Because of the significance of the test to the crashworthiness of future aircraft, NASA Langley Research Center conducted a workshop to release the preliminary structural loads data to the industry, other government agencies, and academia. The NASA/FAA Government/Industry C.I.D. Workshop was held April 10, 1985, at NASA Langley Research Center, Hampton, Virginia. Seventy-four participants attended the 1-day workshop. The attendees were equally divided between industry and governmental agencies. Only one university researcher attended. Four foreign countries were represented among 13 foreign attendees. This publication contains the technical presentations made at the workshop plus the ensuing discussions. Additional questions forwarded to the Chairman either before or after the workshop are also included.

17. Key Words (Suggested by Author(s))	18. Distribution Statement
Transport Crash damage Impact test Crash dynamics Crashworthiness	Unclassified - Unlimited Subject category 39

19. Security Classif. (of this report)	20. Security Classif. (of this page)	21. No. of Pages	22. Price
Unclassified	Unclassified	352	A16

For sale by the National Technical Information Service, Springfield, Virginia 22161

NASA-Langley, 1986

National Aeronautics and
Space Administration
Code NIT-4

Washington, D.C.
20546-0001

Official Business
Penalty for Private Use, $300

SPECIAL FOURTH CLASS MAIL
BOOK

Postage and Fees Paid
National Aeronautics and
Space Administration
NASA-451



NASA

POSTMASTER: If Undeliverable (Section 158 Postal Manual) Do Not Return